

Universidad de Málaga

Escuela Técnica Superior de Ingeniería de Telecomunicación

Programa de Doctorado en Ingeniería de Telecomunicación



TESIS DOCTORAL

On the Performance of Terrestrial Free-Space Optical (FSO)  
Links under the Presence of Generalized Pointing Errors

Autor:

RUBÉN BOLUDA RUIZ

Director:


ANTONIO GARCÍA ZAMBRANA

2017



UNIVERSIDAD  
DE MÁLAGA

AUTOR: Rubén Boluda Ruiz

 <http://orcid.org/0000-0002-1843-3467>

EDITA: Publicaciones y Divulgación Científica. Universidad de Málaga



Esta obra está bajo una licencia de Creative Commons Reconocimiento-NoComercial-SinObraDerivada 4.0 Internacional:

<http://creativecommons.org/licenses/by-nc-nd/4.0/legalcode>

Cualquier parte de esta obra se puede reproducir sin autorización pero con el reconocimiento y atribución de los autores.

No se puede hacer uso comercial de la obra y no se puede alterar, transformar o hacer obras derivadas.

Esta Tesis Doctoral está depositada en el Repositorio Institucional de la Universidad de Málaga (RIUMA): [riuma.uma.es](http://riuma.uma.es)





## Autorización para lectura de la Tesis Doctoral.

Por la presente, Dr. D. Antonio García Zambrana, profesor doctor del Departamento de Ingeniería de Comunicaciones de la Universidad de Málaga, certifica que el doctorando Rubén Boluda Ruiz Ingeniero de Telecomunicación, ha realizado en el Departamento de Ingeniería de Comunicaciones de la Universidad de Málaga bajo su dirección, el trabajo de investigación correspondiente a su TESIS DOCTORAL titulada:

### "On the Performance of Terrestrial Free-Space Optical (FSO) Links under the Presence of Generalized Pointing Errors"

En dicho trabajo se han propuesto aportaciones originales dentro del análisis de las prestaciones de los sistemas de comunicaciones ópticas atmosféricas. Los resultados expuestos han dado lugar a las siguientes publicaciones en revistas y congresos que no han sido utilizadas en tesis anteriores.

1. R. Boluda-Ruiz, A. García-Zambrana, B. Castillo-Vázquez, and C. Castillo-Vázquez, "On the effect of correlated sways on generalized misalignment fading for terrestrial FSO links," *Photonics Journal, IEEE*, 9(3), 1-13, 2017.
2. R. Boluda-Ruiz, A. García-Zambrana, C. Castillo-Vázquez, B. Castillo-Vázquez, and Steve Hranilovic, "Outage Performance of Exponentiated Weibull FSO Links Under Generalized Pointing Errors," *J. of Lightwave Technol., IEEE*, vol. 35, no. 9, pp. 1605-1613, 2017.
3. R. Boluda-Ruiz, A. García-Zambrana, C. Castillo-Vázquez, and B. Castillo-Vázquez, "Novel approximation of misalignment fading modeled by Beckmann distribution on free-space optical links," *Opt. Express* 24(20), 22635–22649, 2016.
4. R. Boluda-Ruiz, A. García-Zambrana, B. Castillo-Vázquez, and C. Castillo-Vázquez, "Impact of nonzero boresight pointing error on ergodic capacity of MIMO FSO communication systems," *Opt. Express* 24(4), 3513–3534, 2016.
5. R. Boluda-Ruiz, A. García-Zambrana, B. Castillo-Vázquez, and C. Castillo-Vázquez, "On the capacity of MISO FSO systems over gamma-gamma and misalignment fading channels," *Opt. Express* 23(17), 22371–22385, 2015.
6. R. Boluda-Ruiz, A. García-Zambrana, B. Castillo-Vázquez, and C. Castillo-Vázquez, "Ergodic capacity analysis for DF strategies in cooperative FSO systems," *Opt. Express* 23(17), 21565–21584, 2015.
7. R. Boluda-Ruiz, A. García-Zambrana, B. Castillo-Vázquez, and C. Castillo-Vázquez, "Ergodic capacity analysis of decode-and-forward relay-assisted FSO systems over alpha-mu fading channels considering pointing errors," *Photonics Journal, IEEE*, 8(1), 1-11, 2016.
8. R. Boluda-Ruiz, A. García-Zambrana, B. Castillo-Vázquez, and C. Castillo-Vázquez, "Evaluating pointing errors on ergodic capacity of DF relay-assisted FSO communication systems", *IEEE 82th Vehicular Technology Conference (VTC-Fall September 6-9, 2015, Boston, USA)*.
9. R. Boluda-Ruiz, A. García-Zambrana, B. Castillo-Vázquez, and C. Castillo-Vázquez, "Análisis de la capacidad ergódica en sistemas cooperativos de comunicaciones ópticas no guiadas," *XXX Simposium Nacional de la Unión Científica Internacional de Radio (URSI septiembre 2-4, 2015, Pamplona, España)*.

Por todo ello, considera que esta Tesis es apta para su presentación al Tribunal que ha de juzgarla. Y para que conste a efectos de lo establecido, AUTORIZA la presentación de esta Tesis en la Universidad de Málaga.

Director y tutor de Tesis

Fdo.: Dr. D. Antonio García Zambrana

En Málaga a 5 de junio de 2017





UNIVERSIDAD  
DE MÁLAGA

**UNIVERSIDAD DE MÁLAGA**  
**ESCUELA TÉCNICA SUPERIOR DE INGENIERÍA DE**  
**TELECOMUNICACIÓN**

Reunido el tribunal examinador en el día de la fecha, constituido por:

Presidente: Dr. D. \_\_\_\_\_

Secretario: Dr. D. \_\_\_\_\_

Vocal: Dr. D. \_\_\_\_\_

para juzgar la Tesis Doctoral titulada *On the Performance of Terrestrial Free-Space Optical (FSO) Links under the Presence of Generalized Pointing Errors* realizada por D. Rubén Boluda Ruiz y dirigida por el Prof. Dr. D. Antonio García Zambrana, acordó por

\_\_\_\_\_ otorgar la calificación de

\_\_\_\_\_ y para que conste,

se extiende firmada por los componentes del tribunal la presente diligencia.

Málaga a \_\_\_\_\_ de \_\_\_\_\_ del \_\_\_\_\_

El Presidente:

El Secretario:

El Vocal:

Fdo.: \_\_\_\_\_

Fdo.: \_\_\_\_\_

Fdo.: \_\_\_\_\_



UNIVERSIDAD  
DE MÁLAGA

To my family and Noelia  
for their firm and unconditional support.



UNIVERSIDAD  
DE MÁLAGA



# Acknowledgments

It has been a period of intense learning for me both personally and professionally over the years. Writing this thesis has had a significant impact on me. To be honest, this thesis could not have been finished without the great support that I have received from so many people. I wish to offer my most affective thanks to the following people.

First of all, I would like to sincerely thank my advisor, Dr. Antonio García-Zambrana, for giving me the opportunity to start this adventure and participate in his research group. I also want to thank him for his excellent guidance and patience, for providing me with an excellent atmosphere for doing research and for helping me regardless of the time of day. Additionally, I would like to thank the Optics Communications Group members for making the environment pretty nice to work.

I would like to express my most sincere gratitude to Noelia for her unconditional love, for her inexhaustible patience and for making me look at life with greater enthusiasm. She was always there cheering me up and standing by me through the good and not so good times.

I would also like to thank my parents and my brothers for their unconditional support. They were always there for me.

Last but not the least, I would like to thank my friends and the rest of my family for their support during the development of this thesis.

I wish to acknowledge the financial support given by the Spanish Ministry of Economy and Competitiveness (MINECO) under FPI grant BES-2013-062689 and the research project TEC2012-32606, and the Junta de Andalucía (research group: TIC-0102).



UNIVERSIDAD  
DE MÁLAGA

# Contents

<b>List of Figures</b>	<b>vii</b>
<b>List of Tables</b>	<b>xi</b>
<b>Abstract</b>	<b>xiii</b>
<b>Resumen</b>	<b>xv</b>
<b>Acronyms</b>	<b>xvii</b>
<b>1 Introduction</b>	<b>1</b>
1.1 Motivation . . . . .	1
1.2 Challenges and Aims . . . . .	4
1.3 Thesis Outlines . . . . .	7
1.4 Thesis Contributions . . . . .	8
<b>2 Fundamentals of FSO Systems</b>	<b>11</b>
2.1 General Overview . . . . .	11
2.1.1 Transmitter . . . . .	11
2.1.2 Receiver . . . . .	12
2.1.3 Channel Model . . . . .	13
2.2 Optical Turbulence Theory . . . . .	15
2.2.1 Introduction . . . . .	15
2.2.2 Wave Propagation Modes . . . . .	16
2.2.3 Irradiance Fluctuations . . . . .	17
2.2.4 Atmospheric Turbulence Statistical Models . . . . .	20
2.3 FSO Channel Modeling . . . . .	23
2.3.1 Atmospheric Attenuation . . . . .	23
2.3.2 Dynamic Misalignment Statistical Model . . . . .	24
2.3.3 Composite Fading Channel . . . . .	25
2.4 Performance of FSO Communication Systems . . . . .	27
2.4.1 Bit Error-Rate (BER) Performance Analysis . . . . .	28
2.4.2 Outage Performance Analysis . . . . .	29



2.4.3	Ergodic Capacity Analysis . . . . .	30
2.5	Summary . . . . .	31
<b>3</b>	<b>Ergodic Capacity Analysis</b>	<b>33</b>
3.1	Motivation . . . . .	33
3.2	Related Work . . . . .	34
3.3	Structure . . . . .	35
3.4	Ergodic Capacity of MISO FSO Systems . . . . .	35
3.4.1	System Model . . . . .	36
3.4.2	Performance Analysis . . . . .	36
3.4.3	Numerical Results and Discussion . . . . .	39
3.5	Ergodic Capacity of MIMO FSO Systems . . . . .	44
3.5.1	System Model . . . . .	46
3.5.2	Performance Analysis . . . . .	48
3.5.3	Numerical Results and Discussion . . . . .	51
3.6	Ergodic Capacity of DF Strategies . . . . .	58
3.6.1	General Background on Cooperative Communication . . . . .	58
3.6.2	System Model . . . . .	60
3.6.3	Performance Analysis . . . . .	62
3.6.4	Numerical Results and Discussion . . . . .	68
3.7	Summary . . . . .	72
<b>4</b>	<b>Generalized Misalignment Fading Model</b>	<b>75</b>
4.1	Motivation and Related Work . . . . .	75
4.2	Statistical Background . . . . .	76
4.3	Structure . . . . .	78
4.4	An MGF-based approach . . . . .	78
4.4.1	System and Channel Models . . . . .	79
4.4.2	Performance Analysis . . . . .	81
4.4.3	Numerical Results and Discussion . . . . .	83
4.5	Approximation of Generalized Pointing Errors . . . . .	89
4.5.1	System and Channel Models . . . . .	90
4.5.2	Performance Analysis . . . . .	93
4.5.3	Numerical Results and Discussion . . . . .	93
4.6	Impact of Correlated Sways on Pointing Errors . . . . .	101
4.6.1	Statistical Background . . . . .	102
4.6.2	System and Channel Models . . . . .	105
4.6.3	Performance Analysis . . . . .	105
4.6.4	Numerical Results and Discussion . . . . .	106
4.7	Summary . . . . .	111

<b>5</b>	<b>Conclusions and Future Work</b>	<b>115</b>
5.1	Conclusions . . . . .	115
5.2	Future Work . . . . .	117
<b>A</b>	<b>Special Functions</b>	<b>119</b>
A.1	Gamma Function . . . . .	119
A.2	Macdonald Function . . . . .	119
A.3	Meijer's G-Function . . . . .	120
	A.3.1 Relation to Other Functions . . . . .	120
	A.3.2 Definite Integrals . . . . .	120
A.4	Digamma Function . . . . .	121
A.5	H-Fox Function . . . . .	122
A.6	Generalized Bivariate Meijer's G-Function . . . . .	122
A.7	Mellin Transform . . . . .	122
	A.7.1 Derivation of $I_{LB} = \prod_{k=1}^M I_k$ in Ergodic Capacity Analysis of MISO FSO Systems . . . . .	123
	A.7.2 Derivation of $I_T^{LB} = I_{SD}I_{RD}$ in Ergodic Capacity Analysis of Coop- erative FSO Systems . . . . .	124
A.8	Other Relations . . . . .	124
A.9	Other Definite Integrals . . . . .	124
A.10	Impact of Pointing Errors on Ergodic Capacity . . . . .	125
<b>B</b>	<b>Derivation of the Correcting Factors</b>	<b>127</b>
B.1	Correcting Factor for MISO FSO Systems . . . . .	127
B.2	Correcting Factor for MIMO FSO Systems . . . . .	127
B.3	Correcting Factor for the BDF Cooperative Protocol . . . . .	128
B.4	Correcting Factor for the ADF Cooperative Protocol . . . . .	129
<b>C</b>	<b>Correlated Sways</b>	<b>131</b>
<b>D</b>	<b>Publications and Projects</b>	<b>133</b>
D.1	Publications . . . . .	133
D.2	Projects . . . . .	135
D.3	Research Fellowship . . . . .	136
<b>E</b>	<b>Summary (Spanish)</b>	<b>137</b>
E.1	Introducción . . . . .	137
	E.1.1 Motivación . . . . .	137
	E.1.2 Objetivos . . . . .	138
E.2	El Canal Óptico Atmosférico . . . . .	139
E.3	Análisis de la Capacidad Ergódica . . . . .	140
	E.3.1 Motivación . . . . .	140
	E.3.2 Capacidad Ergódica de Sistemas MISO FSO . . . . .	140

E.3.3	Capacidad Ergódica de Sistemas MIMO FSO . . . . .	145
E.3.4	Capacidad Ergódica de Sistemas Cooperativos FSO . . . . .	148
E.3.5	Comunicaciones Cooperativas . . . . .	148
E.4	Modelado de Errores por Desapuntamiento Generalizado . . . . .	152
E.4.1	Motivación . . . . .	152
E.4.2	Aproximación para Modelar Desapuntamiento Generalizado . . . . .	155
E.4.3	Impacto de Ejes Correlados . . . . .	156
E.4.4	Resultados Numéricos . . . . .	158
E.5	Conclusiones y Líneas Futuras . . . . .	159
E.5.1	Conclusiones . . . . .	159
E.5.2	Líneas Futuras . . . . .	161
	<b>References</b>	<b>163</b>

# List of Figures

1.1	Some of the most typical OWC applications depending on the transmission distance. . . . .	2
1.2	FSO system topology as a solution for the last-mile connectivity problem and backhaul for cellular systems. . . . .	4
1.3	Thesis flow-chart. . . . .	10
2.1	Block diagram of laser beam propagation through the atmosphere. . . . .	12
2.2	Kolmogorov cascade theory of turbulence. . . . .	15
2.3	Scintillation index for different receiver aperture diameters. . . . .	19
3.1	Block diagram of the considered MISO FSO communications system. . . . .	36
3.2	Ergodic capacity for a S-D link distance of $d_{SD} = 3$ km under different weather conditions. Different normalized beam width and normalized jitter values of $(\omega_z/a, \sigma_s/a) = (5, 1)$ and $(\omega_z/a, \sigma_s/a) = (10, 2)$ are assumed. . . . .	40
3.3	Gain for different weather conditions when a normalized beam width value of $\omega_z/a = 7$ and different normalized jitter values of $\sigma_s/a = \{1, 3, 4\}$ are assumed. . . . .	42
3.4	Ergodic capacity for a S-D link distance of $d_{SD} = 3$ km under different weather conditions. A normalized beam width value of $\omega_z/a = 7$ and different normalized jitter values of $\sigma_s/a = \{1, 3\}$ are assumed. . . . .	43
3.5	Block diagram of the considered MIMO FSO communications system. . . . .	46
3.6	Different geometric arrangement for the receiver from the juxtaposition of equilateral triangles. . . . .	47
3.7	Asymptotic ergodic capacity of MIMO FSO systems when (a) LN and (b) GG atmospheric turbulence models are assumed for different normalized beam width and normalized jitter values of $(\omega_z/a, \sigma_s/a) = \{(5, 1), (10, 2)\}$ as well as different normalized spacing values among receive apertures of $d'/a = \{6, 8\}$ . . . . .	52
3.8	Asymptotic ergodic capacity of MIMO FSO systems over EW atmospheric turbulence for different normalized beam width and normalized jitter values of $(\omega_z/a, \sigma_s/a) = \{(5, 1), (10, 2)\}$ . . . . .	53
3.9	Receive apertures. . . . .	55



3.10	Comparison among different geometric arrangements for the receiver over EW atmospheric turbulence when different spacing values among receive apertures of $d' = \{12 \text{ mm}, 24 \text{ mm}\}$ are considered. . . . .	56
3.11	(a) $Loss_{AB}[\text{dB}]$ as a function of the horizontal displacement of the normalized additional boresight error when different normalized beam width and normalized jitter values of $(\omega_z/a, \sigma_s/a) = \{(5, 1), (10, 2)\}$ are considered and, (b) performance over GG atmospheric turbulence. . . . .	57
3.12	Block diagram of the considered 3-way FSO communication system, where $d_{SD}$ is the S-D link distance and $(x_R, y_R)$ represents the location of the relay node. . . . .	61
3.13	Ergodic capacity for a S-D link distance of $d_{SD} = 3 \text{ km}$ when different weather condition and different normalized beam width and normalized jitter values of $(\omega_z/a, \sigma_s/a) = (5, 1)$ and $(\omega_z/a, \sigma_s/a) = (5, 3)$ are assumed. . . . .	70
3.14	Gain, $G[\text{dB}]$ , for a S-D link distance of $d_{SD} = 3 \text{ km}$ when different weather conditions and different normalized beam width and normalized jitter values of $(\omega_z/a, \sigma_s/a) = (5, 1)$ and $(\omega_z/a, \sigma_s/a) = (5, 3)$ are assumed. . . . .	71
4.1	Beam footprint with generalized pointing errors on the receiver aperture plane. . . . .	77
4.2	Outage performance for a 10 cm receiver aperture together with a beam width value of $\omega_z = 200 \text{ cm}$ when different jitter values of $(\sigma_x, \sigma_y) = \{(35, 35), (30, 15), (10, 5)\} \text{ cm}$ are assumed under different atmospheric turbulence conditions. . . . .	84
4.3	$Loss_{pe}[\text{dB}]$ for moderate atmospheric turbulence and strong atmospheric turbulence when a 10 cm receiver aperture together with a beam width value of $\omega_z = 200 \text{ cm}$ are considered under different nonzero boresight error values. . . . .	86
4.4	Optimum beam width, $\omega_{zopt}$ , versus horizontal jitter, $\sigma_x$ , when different vertical jitter values, $\sigma_y$ , are assumed in FSO links over EW atmospheric turbulence together with a S-D link distance of $d_{SD} = 3 \text{ km}$ for a 10 cm receiver aperture. . . . .	87
4.5	Outage performance for a 10 cm receiver aperture together with jitter values of $(\sigma_x, \sigma_y) = (5, 20) \text{ cm}$ when different beam width values of $\omega_z = \{100, 150, 200\} \text{ cm}$ are assumed under different atmospheric turbulence conditions. . . . .	88
4.6	Outage performance over GG atmospheric turbulence and generalized misalignment fading channels when different weather conditions (a) $C_n^2 = 1.7 \times 10^{-14} \text{ m}^{-2/3}$ and (b) $C_n^2 = 8 \times 10^{-14} \text{ m}^{-2/3}$ are assumed for a S-D link distance of $d_{SD} = 3 \text{ km}$ . . . . .	94
4.7	BER performance over GG atmospheric turbulence and generalized misalignment fading channels when different weather conditions (a) $C_n^2 = 1.7 \times 10^{-14} \text{ m}^{-2/3}$ and (b) $C_n^2 = 8 \times 10^{-14} \text{ m}^{-2/3}$ are assumed for a S-D link distance of $d_{SD} = 3 \text{ km}$ . . . . .	95



4.8	Accuracy metric $M_{OP}$ as a function of $q$ for the outage probability when (a) a S-D link distance of $d_{SD} = 3$ km is assumed, and when (b) a S-D link distance of $d_{SD} = 5$ km is assumed. . . . .	98
4.9	$Loss_{pe}$ [dB] as a function of $q$ for a S-D link distance of $d_{SD} = 3$ km and different normalized boresight error values. . . . .	99
4.10	Impact of nonzero boresight error as a function of the normalized horizontal boresight error $\mu_x/a$ for a S-D link distance of $d_{SD} = 3$ km under different normalized vertical boresight error values of $\mu_y/a = \{1, 2, 3\}$ . . . . .	100
4.11	Minimum normalized beam width as a function of $q$ for a S-D link distance of $d_{SD} = 3$ km and different normalized boresight error values. . . . .	101
4.12	Effect of correlation on normalized jitters as a function of the correlation coefficient $\rho$ for a S-D link distance of $d_{SD} = 3$ km. . . . .	104
4.13	Outage diversity $O_d$ as a function of the correlation coefficient $\rho$ for a S-D link distance of $d_{SD} = 3$ km and different normalized boresight error values when a normalized beam width value of $\omega_z/a = 60$ is assumed. . . . .	108
4.14	Outage performance over GG atmospheric turbulence and generalized misalignment fading channels with correlated sways, when different weather conditions (a) $C_n^2 = 2 \times 10^{-14} m^{-2/3}$ and (b) $C_n^2 = 8 \times 10^{-14} m^{-2/3}$ are assumed for a S-D link distance of $d_{SD} = 3$ km and different correlation values. . . . .	110
4.15	$Loss$ [dB] as a function of the correlation coefficient for a S-D link distance of $d_{SD} = 3$ km and different jitter variances and normalized boresight error values. . . . .	111
E.1	Diagrama de bloques del sistema MISO FSO bajo estudio. . . . .	141
E.2	Capacidad ergódica para una distancia de enlace FSO de $d_{SD} = 3$ km cuando se adoptan diferentes condiciones climáticas. También se asumen diferentes valores de ancho de haz normalizado y <i>jitter</i> normalizado de $(\omega_z/a, \sigma_s/a) = (5, 1)$ y $(\omega_z/a, \sigma_s/a) = (10, 2)$ . . . . .	144
E.3	Diagrama de bloques del sistema MIMO FSO bajo estudio. . . . .	145
E.4	Comportamiento asintótico de la capacidad ergódica de sistemas MIMO FSO para turbulencia atmosférica GG ante diferente severidad de errores por desapuntamiento. . . . .	148
E.5	Diagrama de bloques del sistema cooperativo FSO considerado en este estudio donde $d_{SD}$ es la distancia fuente-destino (S-D), y $(x_R, y_R)$ representa la ubicación del nodo <i>relay</i> . . . . .	150
E.6	Capacidad ergódica para una distancia S-D de $d_{SD} = 3$ km, y ante diferente severidad de errores por desapuntamiento usando valores de ancho de haz y <i>jitter</i> normalizado de $(\omega_z/a, \sigma_s/a) = (5, 1)$ y $(\omega_z/a, \sigma_s/a) = (5, 3)$ . . . . .	153
E.7	Probabilidad de <i>outage</i> sobre canales con turbulencia atmosférica GG para una distancia de enlace 3 km en dos escenarios diferentes: (a) turbulencia moderada $C_n^2 = 2 \times 10^{-14} m^{-2/3}$ , y (b) turbulencia fuerte $C_n^2 = 8 \times 10^{-14} m^{-2/3}$ . . . . .	160





UNIVERSIDAD  
DE MÁLAGA

# List of Tables

2.1	Values of $q$ for different visibility conditions. . . . .	24
3.1	Weather conditions for atmospheric turbulence. . . . .	39
4.1	SISO FSO system configuration. . . . .	83
4.2	Weather conditions for EW atmospheric turbulence. . . . .	83
4.3	Expressions for pointing error parameters with correlated sways. . . . .	103
4.4	FSO communication system settings. . . . .	106
E.1	Condiciones climáticas del enlace FSO. . . . .	143
E.2	Expresiones para desapuntamiento con ejes correlados. . . . .	157
E.3	Configuración del sistema FSO. . . . .	159





UNIVERSIDAD  
DE MÁLAGA

# Abstract

Recently, the interest in optical wireless communication (OWC) has increased for terrestrial, space and underwater links since this technology is capable of providing high-data rates with low power and mass requirement. Particularly, the use of technology based on free-space optical (FSO) communication has been demonstrated to be a very competitive solution for establishing the terrestrial high-capacity wireless links that are demanded by the new wide-band telecommunication services, whose objectives are defined in Horizon 2020 programme of the European Union. Also, it is expected that these communication systems assume a noticeable role in the development of 5G infrastructure, thus efficiently contributing to overcome the important challenge caused by the radio-frequency (RF) spectrum scarcity. Furthermore, this technology is able to provide immunity to RF interferences and robustness to eavesdropping. However, FSO communication systems are not without drawbacks such as atmospheric turbulence, pointing errors and heavy fog, which can deteriorate the performance considerably, among others. This thesis investigates and analyses the performance of terrestrial FSO links over gamma-gamma (GG) atmospheric turbulence channels with generalized pointing errors in terms of the bit error-rate (BER), outage probability and ergodic capacity.

On the one hand, the ergodic capacity is carefully analyzed for multiple-input/single-output (MISO), single-input/multiple-output (SIMO), multiple-input/multiple-output (MIMO), and cooperative FSO systems over atmospheric turbulence channels with different severity of pointing errors. New approximate closed-form expressions for the ergodic capacity of these systems have been found which allow us to compute the capacity over the whole signal-to-noise ratio (SNR) range. In addition, the effect of nonzero boresight pointing errors is a new feature in the study of ergodic capacity of FSO systems based on receiver diversity.

On the other hand, the study of ergodic capacity of MIMO FSO systems has allowed us to assume a more generic pointing error model that takes into account the effect of nonzero boresight errors and, hence, to establish a second research line. This one is related to the study of performance of FSO links under generalized misalignment fading channels. In this generalized model, the effect of different jitters for the elevation and the horizontal displacement, nonzero boresight errors and the effect of correlated sways are taken into consideration. In addition, an accurate and useful approximation of the well-known Beck-



mann distribution is proposed to efficiently include such effects in FSO system design. This approximation is used to evaluate both the BER and the outage probability. Finally, the developed expressions for these performance metrics are used to find optimum beam widths that minimize the impact of pointing error effects in a variety of atmospheric turbulence conditions.

# Resumen

Los sistemas de comunicaciones ópticas en espacio libre (FSO, *Free-Space Optical*) para aplicaciones terrestres se presentan en la actualidad como una solución muy interesante para solventar el importante reto provocado por la escasez del espectro RF (*Radio-Frequency*) disponible. Además, los sistemas FSO se configuran como una seria alternativa frente a otras tecnologías de acceso y transporte como los sistemas de RF debido a las altas tasas de señalización potencialmente muy superiores que se pueden conseguir. Estas ventajas, entre otras, han intensificado la investigación en estos sistemas en las últimas décadas. Por tanto, el análisis de sus prestaciones en términos de probabilidad de error de bit (BER, *Bit Error-Rate*), probabilidad de *outage* y capacidad ergódica es de interés relevante, siendo estas altamente afectadas por la turbulencia atmosférica, los errores por desapuntamiento entre transmisor y receptor así como por la niebla densa. En esta tesis, el análisis de las prestaciones de los sistemas FSO ha sido abordado, presentando novedosos resultados para la comunidad científica e investigadora. Dicho análisis de prestaciones se ha dividido en dos grandes áreas de investigación: análisis de la capacidad ergódica, y modelado de errores por desapuntamiento generalizado entre transmisor y receptor.

Las contribuciones realizadas dentro del análisis de la capacidad ergódica están divididas en dos grupos: por un lado, el análisis de la capacidad de sistemas FSO avanzados basados en diversidad espacial tales como los sistemas MISO (*Multiple-Input/Single-Output*), SIMO (*Single-Input/Multiple-Output*) y MIMO (*Multiple-Input/Multiple-Output*) FSO; por otro lado, el análisis de la capacidad de sistemas cooperativos basados en retransmisión DF (*Detect-and-Forward*). En ambos grupos se han obtenido expresiones matemáticas en forma cerrada que permiten evaluar la capacidad en todo el rango de valores de SNR (*Signal-to-Noise Ratio*) en algunos casos y, en otros, solo ha sido posible obtener su comportamiento asintótico debido a la dificultad matemática que presentaba el análisis.

En el caso de las contribuciones realizadas en el modelado de errores por desapuntamiento generalizado, los cuales siguen una distribución Beckmann, podemos destacar la aproximación propuesta en esta tesis que nos permite incluir de una forma eficiente y sencilla dichos errores por desapuntamiento al análisis de prestaciones de cualquier sistema de comunicaciones FSO. Dicha aproximación es utilizada para estudiar la BER y la probabilidad de *outage* sobre canales afectados por la turbulencia atmosférica.



UNIVERSIDAD  
DE MÁLAGA



# Acronyms

4G	<i>Fourth Generation</i>
5G	<i>Fifth Generation</i>
ADF	<i>Adaptive Detect-and-Forward</i>
AF	<i>Amplify-and-Forward</i>
AM	<i>Arithmetic Mean</i>
APD	<i>Avalanche Photodiode</i>
AWGN	<i>Additive White Gaussian Noise</i>
BER	<i>Bit Error-Rate</i>
BDF	<i>Bit-Detect-and-Forward</i>
CDF	<i>Cumulative Density Function</i>
CSI	<i>Channel State Information</i>
D	<i>Destination</i>
DD	<i>Direct Detection</i>
DF	<i>Detect-and-Forward</i>
EGC	<i>Equal Gain Combining</i>
EW	<i>Exponentiated Weibull</i>
FCC	<i>Federal Communications Commission</i>
FOV	<i>Field of View</i>
FSO	<i>Free-Space Optical</i>
FTTH	<i>Fiber-to-the-Home</i>
GBMGF	<i>Generalized Bivariate Meijer's G-Function</i>
GM	<i>Geometric Mean</i>
GG	<i>Gamma-Gamma</i>
HD	<i>High-Definition</i>
IM	<i>Intensity Modulation</i>
IR	<i>Infrared</i>
ITU	<i>International Telecommunication Union</i>
IoT	<i>Intenert of Things</i>
LAN	<i>Local area network</i>
LD	<i>Laser Diode</i>
LED	<i>Light-Emitting Diode</i>



LN	<i>Log-Normal</i>
LB	<i>Lower Bound</i>
LOS	<i>Line-of-Sight</i>
M-PAM	<i>M-ary Pulse Amplitude Modulation</i>
MAN	<i>Metropolitan Area Network</i>
MAP	<i>Maximum a Posteriori</i>
MGF	<i>Moment Generating Function</i>
MmWave	<i>Millimeter-Wave</i>
MIMO	<i>Multiple-Input/Multiple-Output</i>
MISO	<i>Multiple-Input/Single-Output</i>
ML	<i>Maximum-Likelihood</i>
MRC	<i>Maximum Ratio Combining</i>
NMSE	<i>Normalized mean-squared Error</i>
NRZ	<i>Non-Return-to-Zero</i>
OOK	<i>On-Off Keying</i>
OWC	<i>Optical Wireless Communication</i>
PDF	<i>Probability Density Function</i>
R	<i>Relay</i>
RC	<i>Repetition Coding</i>
RF	<i>Radio-Frequency</i>
RV	<i>Random Variable</i>
S	<i>Source</i>
SI	<i>Scintillation Index</i>
SIM	<i>Sub-carrier Intensity Modulation</i>
SIMO	<i>Single-Input/Multiple-Output</i>
SISO	<i>Single-Input/Single-Output</i>
SNR	<i>Signal-to-Noise Ratio</i>
STBC	<i>Space-Time Block Coding</i>
STTC	<i>Space-Time Trellis Code</i>
TEM	<i>Transverse Electromagnetic</i>
UV	<i>Ultraviolet</i>
UOC	<i>Underwater Optical Communication</i>
VHF	<i>Very High Frequency</i>
WDM	<i>Wavelength-Division Multiplexing</i>

# Chapter 1

## Introduction

This chapter gives a general overview of this thesis. Then, the motivation, challenges and aims as well as the thesis outlines are presented. Finally, the publications obtained during the development of this thesis are summarized.

### 1.1 Motivation

Today, the proliferation of wireless communications continues being one of the biggest events in the recent history of telecommunication. The overall traffic volume in wireless communication networks has grown tremendously in recent years, mainly due to the increase in mobile broadband [1, 2]. This trend is expected to continue growing in the near future with the evolution of wireless communications standards into the fourth generation (4G) and, specially, fifth generation (5G) networks [3]. We are all active participants in the development of new information and communication technologies, such as ultra-broadband Internet access, the Internet of Things (IoT), streamed multimedia applications, high-definition (HD) television services, among others.

In our present-day society, the wireless term is widely used to refer radio-frequency (RF) technology as a result of the deployment and utilization of wireless RF devices and systems. As the number of users and data traffic increase, the demand for RF spectrum is already a critical issue due to a severe congestion that this band of the electromagnetic spectrum is experiencing at this moment. Additionally, this technology presents the inconvenience of the license fees that have to be paid for use. In the last few years, new devices, such as tablets and smart-phones have landed in our life creating new types of demands and constraints on broadband wireless access. Consequently, new data services and applications are appearing to improve the mobile broadband experience [4]. In order to be able to transport an increasing amount of data to users and to deal with this variety of applications,

considering other potential options for wireless communication networks by using the upper parts of the electromagnetic spectrum is taking shape.

Lately, the interest in optical wireless communication (OWC) has increased for terrestrial, space and underwater links since this technology is capable of providing high-data rates with low power and mass requirement. The term OWC refers to transmission in unguided propagation media using optical carriers in the visible, infrared (IR) and ultraviolet (UV) spectral range. According to [2], OWC systems can be classified into five categories depending on the transmission distance. In this way, different technologies can be studied such as chip-to-chip communication, underwater optical communication (UOC), indoor IR, visible light communication (VLC), free-space optical (FSO) communication, inter-satellite links, among others. In Fig. 1.1, we can see these categories with some examples. In this

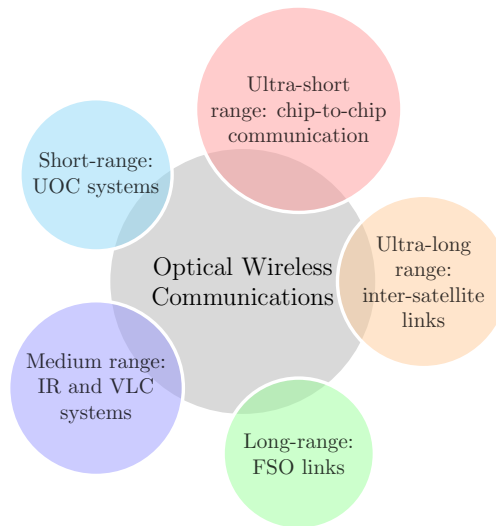


Figure 1.1: Some of the most typical OWC applications depending on the transmission distance.

thesis, we only focus on terrestrial OWC links, which are commonly called FSO links by the research and photonics community. Current terrestrial FSO links operate in the near-IR wavelengths, i.e., at wavelengths of 850 nm, 1300 nm and 1550 nm which correspond to the first, second and third optical transmission windows, respectively.

According to recent advances in FSO communication systems, it has been demonstrated that this technology is quite a competitive solution for establishing the terrestrial high-capacity wireless links that are demanded by the new wide-band telecommunication services, whose objectives are defined in Horizon 2020 programme of the European Union. Also, it is expected that these communication systems assume a noticeable role in the development of 5G infrastructure, thus efficiently contributing to overcome the important challenge caused

by the RF spectrum scarcity. Furthermore, this technology is able to provide immunity to RF interferences and robustness to eavesdropping.

Traditionally, FSO communication systems have generated attention as an efficient solution for the last-mile problem to bridge the gap between the fiber optic infrastructure and the end user in urban area applications as an alternative solution to the RF links. This problem arises at the network terminals due to the need for connecting buildings, companies and other ones to the fiber optic network using a high speed carrier. This problem continues being the bottle-neck in the current networks since RF technology limits the data rates delivered by the fiber optic network, operating at rates on the order of 10-100 Mbps. Although, fiber-to-the-home (FTTH) installations are fairly frequent, this kind of services is only suitable for large urban areas. Despite the high cost, fiber optic is the best solution from reliability and rate approaches. Among many possible wireless technologies, both millimeter-wave (mmWave) communication [5] and FSO communication are becoming strong alternatives to fiber optic infrastructure since they allow to transmit data with high-bandwidth requirements. Each of them has its own challenges and benefits. In the case of mmWave communication, this one is in the frequency band between 30-300 GHz, known as very high frequency (VHF) by the International Telecommunications Union (ITU). It must be noted that most of the communication links are used in the range of 60-92 GHz, which require a license from the Federal Communications Commission (FCC). However, these bands are beginning to be congested in a number of countries [6]. Operating at 60 GHz has gained much attention for short-range data links due to the license-free operation allowed by the FCC [7, 8]. Despite these systems are capable of providing Gbps data rates, the cost and the high atmospheric attenuation can reduce the range and strength of the wave and, furthermore, these links are susceptible to interference, increased latency, and require a high signal-to-noise ratio (SNR) [9]. All these effects in combination with rain and humidity are the main challenges of this kind of communication systems [5]. On the contrary, FSO technology has the potential to provide license-free links above 300 GHz. Unlike mmWave and RF links in general, an FSO link presents smaller attenuation in rain and immunity to interference due to the used narrow beam between transmitter and receiver. At the same time, FSO technology also presents a lower cost of installation and maintenance in comparison with fiber optic systems [10].

With regard to the field of application, FSO systems can be used in a significant number of applications such as metropolitan area network (MAN) extension, local area network (LAN)-to-LAN connectivity, high data-rate links between buildings, next generation wireless broadband networks and back-haul for wireless cellular networks, among others. Back-haul for cellular systems are specially useful for cases where fiber optic infrastructure is expensive or difficult to deploy, allowing much higher throughput. Some of the mentioned applications can be seen in Fig. 1.2 in order to make this read more understandable.

From a commercial point of view, there are a great deal of private companies in the world that provide this kind of systems. Among the most highlighted companies are fSONA Inc.

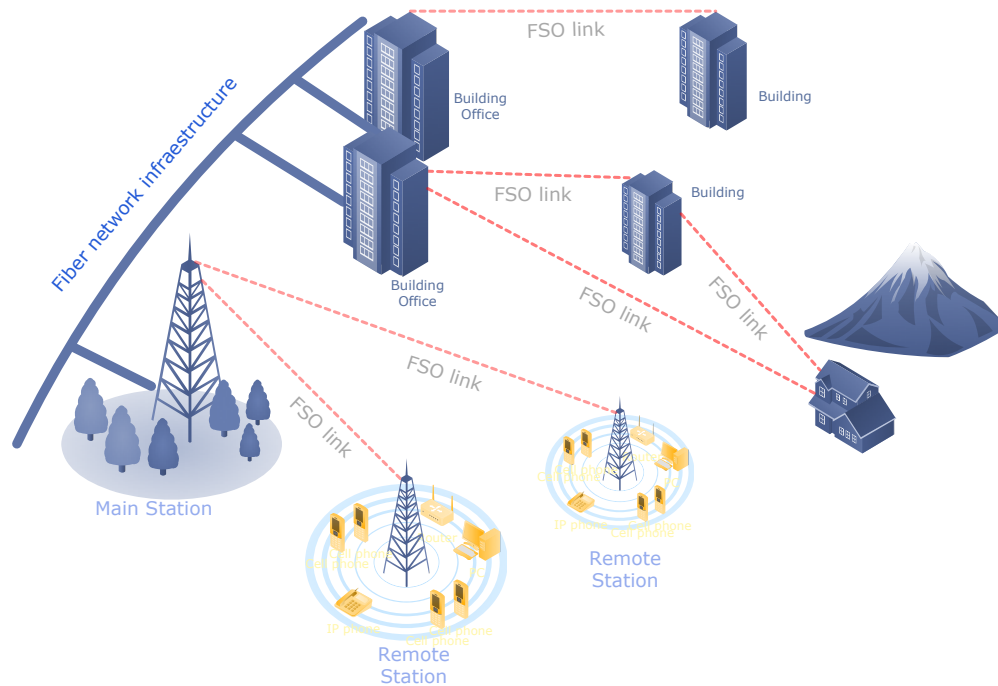


Figure 1.2: FSO system topology as a solution for the last-mile connectivity problem and backhaul for cellular systems.

(Canada) and LightPointe Communications Inc. (the United States, U.S.), which can offer capacities in the range of 100 Mbps to 2.5 Gbps [9, 11]. Moreover, it is expected that these systems are capable of providing speeds of 10 Gbps using wavelength-division multiplexing (WDM) in the near future. All these applications and advantages make FSO technology become a potential candidate for the future and the present of wireless communication networks.

## 1.2 Challenges and Aims

Despite the advantages and applications of FSO communication systems mentioned in the previous section, this technology presents some critical issues and limitations that must be commented. FSO is a line-of-sight (LOS) technology and, hence, transmitter and receiver must be free from physical obstructions. In other words, they must see each other. In addition, this technology must be designed to combat changes in the atmosphere that can deteriorate the performance.

One of the major challenges in FSO communication systems is the weather-dependent performance where heavy fog may result in a link outage due to the fact that fog can modify

the light characteristics. Rain and snow have little effect on FSO communication systems. Another one is to mitigate the combined effect of atmospheric turbulence and dynamic misalignment to increase the distance, rate and reliability. The atmospheric turbulence produces random fluctuations in the irradiance, also known as *scintillation*, beam spreading, beam wander, among others effects, as a result of variations in the refractive index along the communication link. The *scintillation* process produces random fluctuations in both the amplitude and the phase of the received optical signal; the effect of beam spreading is related to a loss of power at the receiver side caused by diffraction; and the effect of beam wander is related to an angular deviation of the beam from LOS [12, 13]. Atmospheric turbulence along with absorption and scattering are considered as the three basic processes that affect optical wave propagation in the literature. Absorption and scattering refer to wavelength- and weather-dependent attenuation of optical wave. In addition to the effect of atmospheric turbulence, FSO communication links are strongly affected by pointing errors, resulting in serious misalignment of fixed-position laser communication systems.

Other challenges in FSO systems are related to safety and physical obstructions. Due to eye safety regulations, FSO systems are limited in the transmitted optical power since this technology uses lasers for transmission [10]. Physical obstructions such as birds, tree limbs, or other factors can temporarily or permanently block the laser LOS.

Finally, another challenge in FSO communication is to find the maximum reliable data rates, i.e., average channel capacity. As a fundamental step to achieve this, an accurate optical channel model is required for the atmospheric turbulence model and dynamic misalignment.

In general, the main objective of this thesis is to present advances in the field of FSO communication systems in order to cope with these challenges. This thesis is aimed at investigating the performance of advanced FSO communication systems with the goal of analyzing their benefits and limitations from a practical point of view. Therefore, the analysis and design of these communication systems are carried out, developing new results in two major areas:

- (a) Ergodic capacity analysis.
- (b) Generalized misalignment fading model for terrestrial FSO links.

On the one hand, the study of ergodic capacity represents the first research area of this thesis in which we analyze not only the ergodic capacity of FSO communication systems based on spatial diversity such as multiple-input/single-output (MISO), single-input/multiple-output (SIMO) and multiple-input/multiple-output (MIMO) FSO systems, but also the ergodic capacity of cooperative FSO systems based on detect-and-forward (DF) relaying. Hence, the objective of this research area is twofold: firstly, to develop new closed-form expressions that allow us to compute the ergodic capacity over the whole range of SNR values, as well as to study how this one is deteriorated by the effect of atmospheric turbulence and,

furthermore, how this one is also enhanced in relation to the ergodic capacity obtained by a single-input/single-output (SISO) FSO system; secondly, to include the effect of pointing errors in the study of the ergodic capacity (this effect has not been taken into account in the literature), as well as to include the effect of nonzero boresight pointing errors on SIMO and MIMO FSO systems, i.e., systems with more than one receiver aperture. The use of a more sophisticated pointing error model for the study of the ergodic capacity of SIMO and MIMO FSO systems has led to a second line of research that is focused on the modeling of generalized pointing errors.

On the other hand, the second research area of this thesis is the modeling of generalized pointing errors. Over the last decade, different statistical models have been proposed in the literature to model pointing errors. These models have been used in a large number of research articles with the goal of adding this effect to different studies, and giving them a higher degree of realism. Incorporating the effect of pointing errors results in an added difficulty in developing new closed-form expressions for the performance evaluation of FSO communication systems. Therefore, including such effect in the performance analysis is not only to give a greater degree of realism to the performance analysis, but also represents a great challenge from a mathematical point of view. In the general case, pointing errors are distributed according to the Beckmann distribution which is the focus of this research line.

In order to achieve all this, a number of research objectives have been set, which are outlined as follows:

1. Review the fundamental aspects of terrestrial FSO links and the statistical models that describe the atmospheric turbulence and dynamic misalignment. At the same time, understanding the limits and range of validity of each of the statistical models.
2. Investigate either approximate or exact closed-form expressions for the bit error-rate (BER), outage probability and ergodic capacity in order to evaluate the performance of FSO communication systems over atmospheric turbulence channels with pointing error effects. Moreover, all the theoretical studies derived from this thesis for the performance are verified by using Monte Carlo simulation.
3. Investigate the ergodic capacity of MISO, SIMO, MIMO and cooperative systems based on DF for FSO communication. The study of the ergodic capacity represents one of the great challenges of this thesis.
4. Investigate a new statistical model for generalized pointing errors that can be used in an easy way to study more complex FSO scenarios. In the general case, generalized pointing errors are modeled by the Beckmann distribution which is intractable from a mathematical point of view due to the fact that its density function appears in integral-form. This is another great challenge of this thesis, i.e, finding out an efficient way of including generalized pointing errors in FSO system design.



## 1.3 Thesis Outlines

To make this read much easier, this thesis is organized in five chapters. The remainder of this thesis is organized as follows.

**Chapter 1** gives a general overview of this thesis, describing the motivation, challenges and aims.

**Chapter 2** presents basic fundamentals of FSO technology related to the system and channel models, and the performance metrics used in this thesis such as BER, outage probability and ergodic capacity which are evaluated for a SISO FSO system. In addition to this, this chapter also introduces the zero boresight pointing error model which is considered as a cornerstone of pointing error models and under which the proposed generalized pointing error model is based. This chapter is essential to establish the theoretical fundamentals of FSO technology and, hence, this knowledge is required to make this read more fruitful.

Next, the following two chapters represent the most important part of this thesis, i.e., the contributions of the work developed during this thesis. At the beginning of each chapter, a deep insight into each research area is given with the goal of introducing the reader to the contribution. At the same time, a mind map which details the relations among these subjects can be seen in Fig. 1.3 at the end of this chapter.

**Chapter 3** is related to the ergodic capacity analysis of FSO communication systems. This chapter evaluates the ergodic capacity of MISO, MIMO and SIMO FSO communication systems, and DF-based cooperative FSO systems. The study of ergodic capacity of MIMO FSO systems has allowed us to assume a more generic pointing error model that takes into account the effect of nonzero boresight errors and, hence, to establish the second research area.

**Chapter 4** is related to the study of performance of FSO links under generalized misalignment fading channels. In this generalized model, the effect of different jitters for the elevation and the horizontal displacement, nonzero boresight errors and the effect of correlated sways are taken into account.

**Chapter 5** presents conclusions and future work.

In order to make this read more pleasant, some appendices have been added with useful information but not essential to understand the main core of this thesis. Thus, a compound of some special functions and definite integrals involved in the derivation of metrics such as BER, outage probability and ergodic capacity is given in Appendix A which are needed in

this thesis specially in Chapters 3 and 4. At the same time, some calculus related to Chapters 3 and 4 are performed in greater detail in Appendix B and Appendix C, respectively. In Appendix D, a complete list of all the publications obtained during the development of this thesis is given. Finally, a summary of this thesis in Spanish is also included in Appendix E.

## 1.4 Thesis Contributions

In this section, the following publications have been produced as a result of this thesis which are summarized as follows:

- [14] R. Boluda-Ruiz, A. García-Zambrana, B. Castillo-Vázquez, and C. Castillo-Vázquez, "On the effect of correlated sways on generalized misalignment fading for terrestrial FSO links," *Photonics Journal, IEEE*, **9**(3), 1–13, 2017 (Impact factor 2.177, 60/257 Engineering, Electrical and Electronic Q1 JCR 2015).
- [15] R. Boluda-Ruiz, A. García-Zambrana, C. Castillo-Vázquez, B. Castillo-Vázquez, and Steve Hranilovic, "Outage Performance of Exponentiated Weibull FSO Links Under Generalized Pointing Errors," *J. of Lightwave Technol., IEEE/OSA*, vol. 35, no. 9, pp. 1605–1613, 2017. (Impact factor 2.567, 20/90 Optics Q1 JCR 2015).
- [16] R. Boluda-Ruiz, A. García-Zambrana, C. Castillo-Vázquez, and B. Castillo-Vázquez, "Novel approximation of misalignment fading modeled by Beckmann distribution on free-space optical links," *Opt. Express* **24**(20), 22635–22649, 2016 (Impact factor 3.148, 14/90 Optics Q1 JCR 2015).
- [17] R. Boluda-Ruiz, A. García-Zambrana, B. Castillo-Vázquez, and C. Castillo-Vázquez, "Impact of nonzero boresight pointing error on ergodic capacity of MIMO FSO communication systems," *Opt. Express* **24**(4), 3513–3534, 2016 (Impact factor 3.148, 14/90 Optics Q1 JCR 2015).
- [18] R. Boluda-Ruiz, A. García-Zambrana, B. Castillo-Vázquez, and C. Castillo-Vázquez, "On the capacity of MISO FSO systems over gamma-gamma and misalignment fading channels," *Opt. Express* **23**(17), 22371–22385, 2015 (Impact factor 3.488, 9/86 Optics Q1 JCR 2013).
- [19] R. Boluda-Ruiz, A. García-Zambrana, B. Castillo-Vázquez, and C. Castillo-Vázquez, "Ergodic capacity analysis for DF strategies in cooperative FSO systems," *Opt. Express* **23**(17), 21565–21584, 2015 (Impact factor 3.488, 9/86 Optics Q1 JCR 2013).
- [20] R. Boluda-Ruiz, A. García-Zambrana, B. Castillo-Vázquez, and C. Castillo-Vázquez, "Ergodic capacity analysis of decode-and-forward relay-assisted FSO systems over alpha-mu fading channels considering pointing errors," *Photonics Journal, IEEE*,

8(1), 1–11, 2016 (Impact factor 2.177, 60/257 Engineering, Electrical and Electronic Q1 JCR 2015).

- R. Boluda-Ruiz, A. García-Zambrana, B. Castillo-Vázquez, and C. Castillo-Vázquez, “Evaluating pointing errors on ergodic capacity of DF relay-assisted FSO communication systems”, IEEE 82th Vehicular Technology Conference (VTC-Fall September 6-9, 2015, Boston, USA).
- R. Boluda-Ruiz, A. García-Zambrana, B. Castillo-Vázquez, and C. Castillo-Vázquez, “Análisis de la capacidad ergódica en sistemas cooperativos de comunicaciones ópticas no guiadas,” XXX Symposium Nacional de la Unión Científica Internacional de Radio (URSI September 2-4, 2015, Pamplona, España).

Other publications by the author which have also been achieved in the context of FSO communication systems are summarized as follows:

- R. Boluda-Ruiz, A. García-Zambrana, B. Castillo-Vázquez, and C. Castillo-Vázquez, “MISO relay-assisted FSO systems over gamma-gamma fading channels with pointing errors,” *Photonics Technology Letters, IEEE* **28**(3), 229–232, 2016 (Impact factor 2.110, 56/249 Electrical and Electronic Engineering Q1 JCR 2013).
- A. García-Zambrana, R. Boluda-Ruiz, C. Castillo-Vázquez, and B. Castillo-Vázquez, “Novel space-time trellis codes for free-space optical communications using transmit laser selection,” *Opt. Express* **23**(19), 24195–24211, 2015 (Impact factor 3.488, 9/86 Optics Q1 JCR 2013).
- C. Castillo-Vázquez, R. Boluda-Ruiz, B. del Castillo-Vázquez, and A. García-Zambrana, “Outage performance of DF relay assisted FSO communications using time-diversity,” *Photonics Technology Letters, IEEE* **27**(11), 1149–1152, 2015 (Impact factor 2.110, 56/249 Electrical and Electronic Engineering Q1 JCR 2013).
- R. Boluda-Ruiz, A. García-Zambrana, B. Castillo-Vázquez, and C. Castillo-Vázquez, “Impact of relay placement on diversity order in adaptive selective DF relay-assisted FSO communications,” *Opt. Express* **23**(3), 2600–2617, 2015 (Impact factor 3.488, 9/86 Optics Q1 JCR 2013).
- A. García-Zambrana, R. Boluda-Ruiz, C. Castillo-Vázquez, and B. Castillo-Vázquez, “Transmit alternate laser selection with time diversity for FSO communications,” *Opt. Express* **22**(20), 23,861–23,874, 2014 (Impact factor 3.488, 9/86 Optics Q1 JCR 2013).
- R. Boluda-Ruiz, A. García-Zambrana, C. Castillo-Vázquez, and B. Castillo-Vázquez, “Adaptive selective relaying in cooperative free-space optical systems over atmospheric turbulence and misalignment fading channels,” *Opt. Express* **22**(13), 16,629–16,644, 2014 (Impact factor 3.488, 9/86 Optics Q1 JCR 2013).

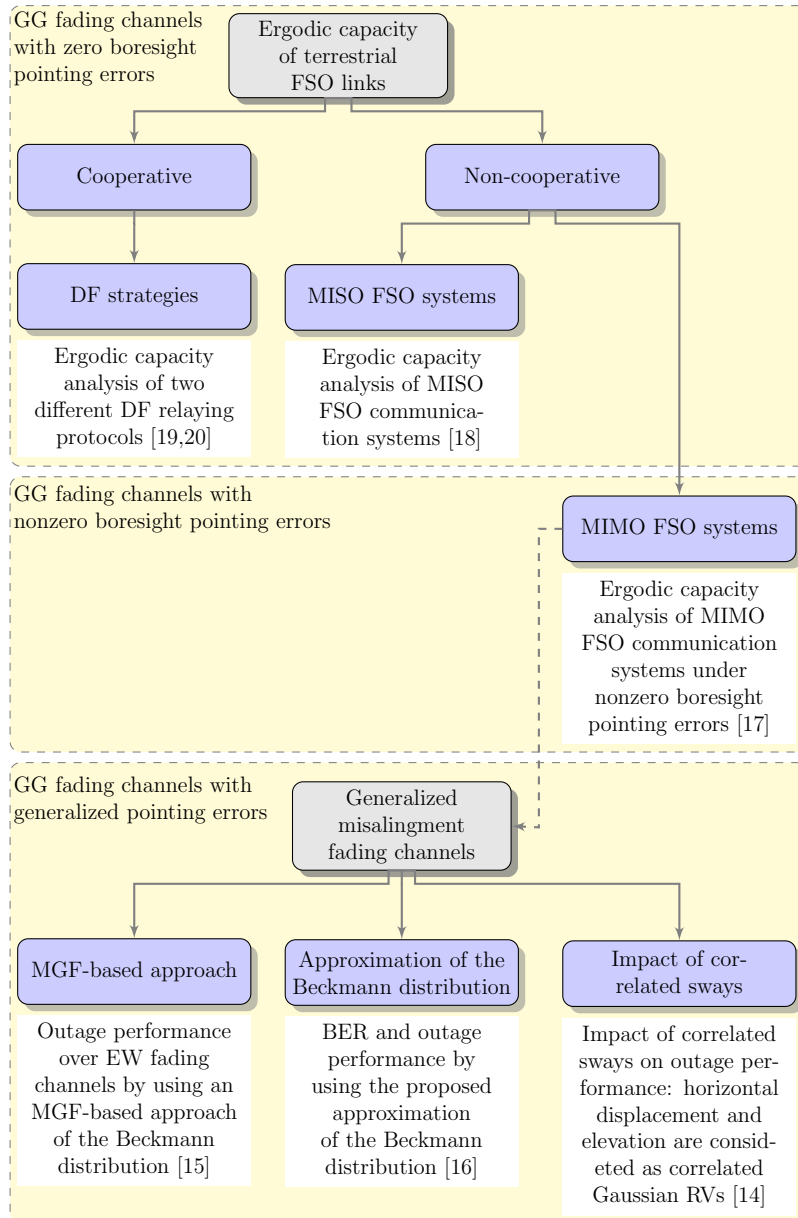


Figure 1.3: Thesis flow-chart.

## Chapter 2

# Fundamentals of FSO Systems

In this chapter, a complete review of the current theory of FSO communication through atmosphere is presented.

### 2.1 General Overview

Most commercial FSO systems are based on intensity-modulation and direct-detection (IM/DD) schemes due to their lower implementation complexity and cost. Intensity-modulation (IM) means that an FSO transmitter transmits information by modulating the instantaneous power of the carrier, in response to an input electrical signal. The information sent on this FSO channel is not contained in the amplitude, phase or frequency of the transmitted optical wave, but in the intensity of the transmitted signal. It is said that the most practical down-conversion technique is direct-detection (DD), in which a photodetector produces a current proportional to the received instantaneous power, i.e., proportional to the square of the received electric field [10, 21].

Basically, the modeling of FSO channels with IM/DD consists of three subsystems: transmitter, channel and receiver, as shown in Fig. 2.1. The transmitter is responsible for preparing and sending the information on an optical carrier. The channel is the medium between transmitter and receiver, i.e., the atmosphere. Finally, the receiver is responsible for collecting the transmitted optical field and recovering the information.

#### 2.1.1 Transmitter

The transmitter prepares and sends the information on an optical carrier and consists of an encoder, an optical source and a modulator. The electro-optical conversion process is

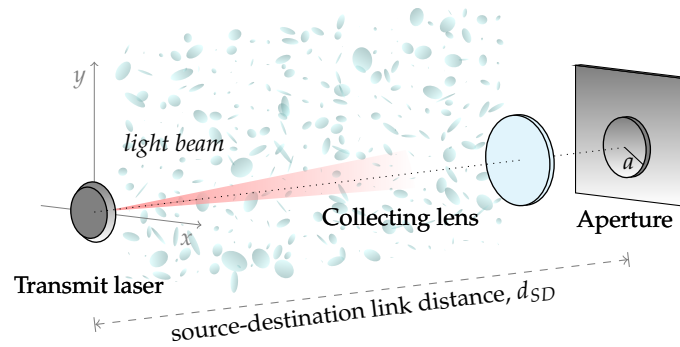


Figure 2.1: Block diagram of laser beam propagation through the atmosphere.

performed by an optical source through a semiconductor laser diode (LD) or a light-emitting diode (LED) [10].

Commercial FSO systems operate in the near-IR-wavelength range between 750-850 nm, 1520-1600 nm, with some systems being developed to operate at IR wavelength of 10000 nm [13, 22]. The choice of the wavelength depends on some factors such as price, transmitted power and component availability. Due to the combination of low attenuation and component availability in the range between 1520-1600 nm, the deployment of FSO communication links using this range is more convenient despite this one is even more expensive than the range between 750-850 nm. In addition, much power can be sent at 1520-1600 nm than can be sent at 780-850 nm for the same eye safety regulation [22] and, hence, it may be possible to overcome some situations under bad weather conditions such as heavy fog.

### 2.1.2 Receiver

The receiver is responsible for collecting the transmitted optical beam and recovering the information. A receiver can be classified into two classes based on detection type: coherent detection and non-coherent detection. In this thesis, non-coherent detection is assumed. Unlike coherent detection, the intensity of the emitted light is used to transmit the information in non-coherent detection, and the photodetector directly detects changes in the light intensity without the need for a local oscillator. In other words, a non-coherent receiver detects only the amplitude of the optical wave and is used in applications when no use is made of the phase of the optical wave [13].

A typical optical receiver consists of a photodetector that converts the focused optical field into an output current (opto-electrical conversion), and a lens that has the role of collecting and focusing the received beam onto the photodetector. Thus, the photodetector produces an output electrical current which is proportional to the integral over the photodetector surface of the total instantaneous optical power.

In all FSO communication systems, the determination of noise sources at the input of the receiver is a critical issue in determining performance since the transmitted optical signal is always detected in the presence of different noise sources. In this way, background radiation such as sun and blackbody radiation, among others, is collected by the receiving lens and focused onto the photodetector along with the transmitted optical signal. Background radiation can be eliminated by optical filtering or treated as an additive noise to the desired signal. In most practical FSO systems, the received SNR is limited by high-intensity shot noise caused by the photodetection process itself and/or by thermal noise in the processing electronics following the photodetector [13]. As a result, the noise at the receiver can be modeled with high accuracy as additive, white Gaussian noise (AWGN) and independent of the transmitted signal with zero mean and variance  $\sigma_n^2$ .

Regarding the photodetector, P-i-N (PIN) and avalanche photodiodes (APD) are the most commonly used photodetectors in terrestrial FSO links. In this way, PIN diodes are usually used for FSO link distances up to a few kilometers, and the receiver becomes thermal noise-limited. For longer distances, APDs are mostly used [?].

### 2.1.3 Channel Model

The channel is the atmosphere, but the combined effect of atmospheric turbulence, dynamic misalignment and atmospheric path loss is really the limiting factor in performance of FSO systems. The modeling of random fluctuations of an optical wave propagating through atmosphere will be carefully reviewed in Section 2.2.

A mathematical model for an FSO communications system in baseband is given by

$$y(t) = Ri(t)x(t) + z(t), \quad (2.1)$$

where  $y(t) \triangleq Y$  is the output electrical current in the photodetector,  $R$  is the detector responsivity,  $I \triangleq i(t)$  is the channel gain that represents the random fluctuations due to the propagation medium,  $X \triangleq x(t)$  is the transmitted optical power, and  $Z \triangleq z(t)$  is AWGN with zero mean and variance  $\sigma_n^2 = N_0/2$ , i.e.  $Z \sim N(0, N_0/2)$ , independent of whether the received bit is On or Off. In this case, we assume a shot-noise limited receiver since background radiation is ignored. The detector responsivity is measured in amperes per watts (A/W) and represents the conversion factor from optical to electrical domain at the receiver. The detector responsivity is defined as  $R = \eta e/h\nu$ , where  $\eta$  is the detector quantum efficiency in electrons/photon,  $e$  is the electric charge in coulombs,  $h$  is the Planck's constant ( $h = 6.63 \times 10^{-34}$  joule-second), and  $\nu$  is optical frequency in hertz [10, 13]. Without loss of generality, the detector responsivity is assumed hereinafter to be the unity.

Since the channel input  $x(t)$  represents instantaneous optical power, the channel is nonnegative and, hence,  $x(t)$  must satisfy  $\forall t, x(t) \geq 0$ . Due to eye and skin safety regulations, the transmitted optical power is limited and, hence, the average amplitude of  $X$  is also

limited [10, 21]. According to [21], the average transmitted optical power  $P_t$  is given by

$$P_t = \lim_{T \rightarrow \infty} \frac{1}{2T} \int_{-T}^T x(t) dt. \quad (2.2)$$

Here, it is used that  $Y$ ,  $I$ ,  $X$ , and  $Z$  represent random variables (RVs), and  $y(t)$ ,  $i(t)$ ,  $x(t)$ , and  $z(t)$  their corresponding realizations. In this case, a simple discrete representation for an FSO link is given by

$$Y = IX + Z. \quad (2.3)$$

In this model,  $I$  represents the optical intensity fluctuations, i.e. the irradiance or channel gain, which is due to three different factors: atmospheric path loss ( $L$ ), atmospheric turbulence ( $I_a$ ), and geometric spread and pointing errors ( $I_p$ ). The channel gain is expressed as follows

$$I = L \cdot I_a \cdot I_p, \quad (2.4)$$

where  $L$  is a deterministic factor, and  $I_a$  and  $I_p$  are both RVs as will be seen in the next section.

Regarding modulation, the most commonly modulation scheme in FSO communication systems is on-off keying (OOK) due to its simplicity and low cost, which is considered as a special case of the M-ary pulse amplitude modulation (M-PAM) when the parameter  $M = 2$ . OOK signaling is a popular modulation scheme not only in FSO links, but also in a wide variety of data communication applications. This modulation scheme is also known as non-return-to-zero (NRZ) encoding. Assuming that the channel is distortionless, the ideal maximum-likelihood (ML) receiver for OOK in AWGN channels consists of a continuous-time filter matched to the transmitted pulse shape, followed by a sampler and threshold detector set midway between the “low” and “high” pulse amplitudes [21].

In OOK signaling, the modulation process is represented by the presence or absence of a light pulse in each bit interval. The transmitted symbols consist of constant intensities of zero or  $2P_t$  through the symbol time. The signal can be represented by the basis function for OOK,  $\Phi(t)$ . This function is defined as  $\Phi(t) = g(t)/\sqrt{T_b}$ , where  $T_b$  is the bit period, and  $g(t) = \text{rect}(t/T_b)$  represents a rectangular pulse shape satisfying the non-negativity constraint, with  $0 \leq g(t) \leq 1$  in the bit period and 0 otherwise. In this way, an expression for the transmitted optical signal can be written as

$$x(t) = \sum_{k=-\infty}^{\infty} a_k 2P_t \sqrt{T_b} \Phi(t - kT_b), \quad (2.5)$$

where the RV  $a_k$  follows a Bernoulli distribution with parameter  $p = 1/2$ , taking values of 0 for the bit “0” and 1 for the bit “1”. From this expression, it is known that the average optical power transmitted is  $P_t$ , defining a constellation of two equiprobable points whose Euclidean distance is given by  $d_E = 2P_t \sqrt{T_b}$ .



## 2.2 Optical Turbulence Theory

As mentioned in Chapter 1, the *scintillation* process produces random fluctuations in both the amplitude and the phase of the received optical signal, i.e., channel fading. This result is due to variations in the refractive-index along the FSO link. In [13], a comprehensive analysis of the theory of atmospheric turbulence applied to optical communications in general was developed. In this thesis, most of the concepts related to turbulence modeling for terrestrial FSO links are drawn from therein.

### 2.2.1 Introduction

In the atmosphere, the temperature is constantly changing leading to temporal and spatial temperature gradients. These temperature fluctuations in the presence of dynamic wind results in index-of-refraction fluctuations, commonly called as optical turbulence or atmospheric turbulence. This is one of the most important phenomena in optical wave propagation.

For a better understanding of the structure of atmospheric turbulence, the energy cascade theory of turbulence reported in [23] is usually adopted. According to this theory, turbulent air motion represents a set of eddies (air masses) of various scale size. This scale size ranges from a large or outer scale  $L_0$  of turbulence to a small or inner scale  $l_0$  of turbulence. Under the influence of inertial forces, large eddies break up into smaller ones, forming a continuous cascade of scale sizes between  $L_0$  and  $l_0$ . Scale sizes smaller than the inner scale  $l_0$  are dissipated as heat, as shown in Fig. 2.2.

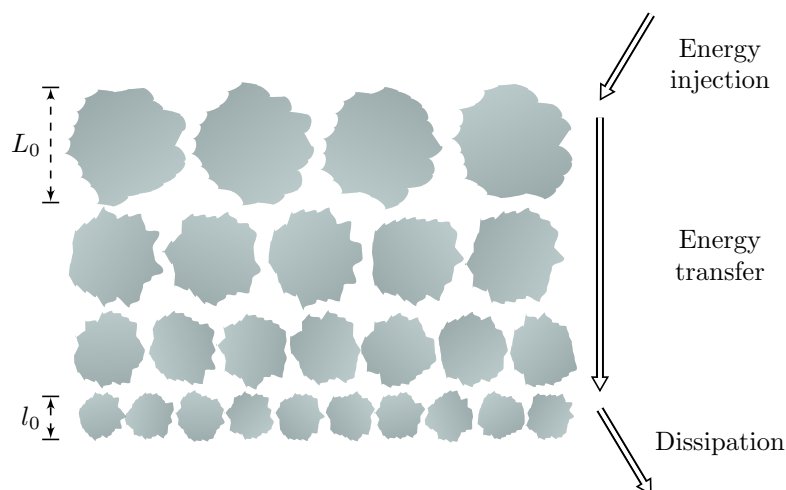


Figure 2.2: Kolmogorov cascade theory of turbulence.

The energy distribution of the eddies is well described by the Kolmogorov spectrum, who suggested that this set of eddies has a degree of statistical consistency and, furthermore, points in the atmosphere separated certain scale size show statistical homogeneity and isotropy, allowing a handy mathematical analysis [13]. Without going in too much details of this theory, it is said that fluctuations in the refractive index are related to variations in temperature and pressure. In particular, refractive-index fluctuations for optical wave propagation are mainly caused by variations in temperature, considering variation in pressure neglected. Regarding turbulence strength, on the one hand, strong turbulence has smaller inner scale than weak turbulence. On the other hand, increase or decrease of the large scale is directly related to turbulence strength. In [13, Chapter 3], the whole optical turbulence theory is examined in greater detail and, hence, final results are only presented here. In this way, the corresponding associated power spectral density for refractive-index fluctuations is defined by Kolmogorov under the assumption of a statistical homogeneous and isotropic atmosphere as follows

$$\Phi_n(\kappa) = 0.033C_n^2\kappa^{-11/3}, \quad 1/L_0 < \kappa < 1/l_0 \quad (2.6)$$

where  $\kappa = 2\pi/\lambda$  is the number of wave,  $\lambda$  is the wavelength, and  $C_n^2$  is the refractive-index structure parameter, which is the most significant parameter that determines the turbulence strength. The above equation plays a fundamental role in the description of atmospheric turbulence. The refractive-index structure parameter  $C_n^2$  is a height-dependent parameter, being specially important in both vertical and slant links, such as inter-satellite links. Also,  $C_n^2$  depends on the local conditions such as terrain type, geographic location, cloud cover, and time of day [24]. The parameter  $C_n^2$  is typically within the range  $10^{-17}$ - $10^{-13} \text{ m}^{-2/3}$ , i.e., from weak to strong turbulence [12, 13]. Values of  $C_n^2$  can be considered as a constant for horizontal links such as terrestrial FSO links. Many authors have tried to describe the behavior of this parameter for vertical and slant links, and various experimental models have been proposed. In this thesis, the corresponding value of the refractive-index structure parameter is considered as a constant value since only terrestrial FSO links are studied.

Notice that the Kolmogorov spectrum is widely used in theoretical studies but it is limited in relation to the wavelength. Other models of the spectrum for index-refractive fluctuations are required when effects corresponding to the outer scale and inner scale cannot be ignored, such as Tatarskii and Kármán models [13]. However, it is usually assumed that the outer scale is infinity and the inner scale is zero.

### 2.2.2 Wave Propagation Modes

The optical wave propagation modes can be classified into three categories such as plane wave, spherical wave and Gaussian-beam wave. Despite most theoretical treatments of optical wave propagation have concentrated on plane wave and spherical wave, a Gaussian-beam wave model is more convenient to characterize propagation of the optical wave, particularly

when some characteristics such as focusing and diverging are of interest. The Gaussian-beam wave model used most often is the lowest-order transverse electromagnetic (TEM<sub>00</sub>) wave, i.e., we assume that the laser beam has an ideal Gaussian intensity profile. Note that, when the Gaussian beam has a relatively large divergence, the corresponding wavefronts are close to the case of a point source and, hence, both plane and spherical waves are perfectly applicable to FSO communication systems. Limiting cases of the TEM<sub>00</sub> Gaussian-beam wave led to the plane wave and spherical wave models [13]. In addition, for the sake of modeling simplicity, we consider plane wave propagation.

### 2.2.3 Irradiance Fluctuations

A monochromatic optical wave propagating through a random medium, i.e. atmosphere, can be analyzed mathematically by solving the following partial differential equation

$$\nabla^2 \mathbf{E} + \kappa^2 n^2(\mathbf{R}) \mathbf{E} = \mathbf{0}, \quad (2.7)$$

where  $\nabla$  is Laplacian operator,  $\mathbf{E}$  is the field of the electromagnetic wave, and  $\mathbf{R}$  is a point in space. The above equation can be simplified into three scalar equations. One of the components that is transverse to the direction of propagation along the positive z-axis,  $U$ , is expressed by the scalar stochastic Helmholtz equation as follows

$$\nabla^2 U + \kappa^2 n^2(\mathbf{R}) U = 0, \quad (2.8)$$

where the refractive index can be expressed as  $n(\mathbf{R}) = 1 + n_1(\mathbf{R})$ , being  $n_1(\mathbf{R})$  the random deviation with zero mean, representing the changes caused by atmospheric turbulence. It is noteworthy to mention that  $n_1(\mathbf{R})$  depends on time, but under the Taylor frozen turbulence hypothesis, the time dependence is neglected. Several approaches have been proposed to solve the scalar stochastic Helmholtz equation by using different assumptions and approximations. For instance, Born and Rytov approximations have traditionally been used to solve the above equation under extremely weak turbulence and weak turbulence, respectively. Mainly, the Rytov approximation has successfully been used to predict all relevant statistical parameters in weak turbulence regime. An extension of the Rytov approximation was needed to study such effect in strong turbulence regime.

Next, some important parameters and concepts are introduced. Firstly, one of the most important parameters is the Rytov variance  $\sigma_R^2$  which is used to differentiate between weak and strong turbulence to classify the turbulence strength [13, eqn. (5.15)]:

$$\sigma_R^2 = 1.23 C_n^2 \kappa^7 d_m^{11/6}, \quad (2.9)$$

where  $d_m$  is the link distance. Physically, the Rytov variance is the irradiance fluctuations for an infinite plane wave. Traditionally, weak turbulence corresponds to  $\sigma_R < 1$ , moderate turbulence corresponds to  $\sigma_R^2 \sim 1$ , and strong turbulence corresponds to  $\sigma_R^2 > 1$ .

Secondly, the irradiance fluctuations can be quantified by computing the variance of the irradiance fluctuations scaled of the square of the mean irradiance, i.e., by computing the scintillation index (SI). This parameter is defined as follows

$$\sigma_{I_a}^2 = \frac{\mathbb{E}[I_a^2] - \mathbb{E}[I_a]^2}{\mathbb{E}[I_a]^2} = \frac{\mathbb{E}[I_a^2]}{\mathbb{E}[I_a]^2} - 1, \quad (2.10)$$

with  $\mathbb{E}[\cdot]$  denoting expectation. Depending on the wave propagation mode, different expressions for SI can be found in [13]. In the case of plane wave propagation mode, SI is expressed as

$$\sigma_{I_a}^2 = \sigma_R^2 = 1.23C_n^2 \kappa^{7/6} d_m^{11/6}, \quad \sigma_R^2 < 1 \quad (2.11a)$$

$$\sigma_{I_a}^2 = \exp \left( \frac{0.49\sigma_R^2}{\left(1 + 1.11\sigma_R^{12/5}\right)^{7/6}} + \frac{0.51\sigma_R^2}{\left(1 + 0.69\sigma_R^{12/5}\right)^{5/6}} \right) - 1, \quad \sigma_R^2 > 1 \quad (2.11b)$$

One of the best ways to mitigate the effect of scintillation on performance of FSO communication systems is to use a larger receiver aperture to collect as much light as possible. A receiver aperture size smaller than the correlation length or correlation width  $\rho_c$ , i.e.  $D \leq \rho_c$ , acts as a point-like receiver, while a receiver aperture size larger than the correlation length, i.e.  $D \geq \rho_c$ , can collect much more light. This phenomenon is called aperture averaging and is defined as follows

$$AA = \frac{\sigma_{I_a}^2(D)}{\sigma_{I_a}^2(0)}, \quad (2.12)$$

where  $\sigma_{I_a}^2(0)$  is the SI for a point-like receiver given in Eq. (2.11), and  $\sigma_{I_a}^2(D)$  is the SI for a receiver aperture with diameter  $D$ . In the case of plane wave propagation mode,  $\sigma_{I_a}^2(D)$  is expressed under both weak and strong turbulence as

$$\begin{aligned} \sigma_{I_a}^2(D) &= \exp \left( \frac{0.49\sigma_R^2}{\left(1 + 0.65\xi^2 + 1.11\sigma_R^{12/5}\right)^{7/6}} \right) \\ &\times \exp \left( \frac{0.51\sigma_R^2 \left(1 + 0.69\sigma_R^{12/5}\right)^{-5/6}}{1 + 0.9\xi^2 + 0.62\xi^2\sigma_R^{12/5}} \right) - 1, \end{aligned} \quad (2.13)$$

where  $\xi^2 = \frac{D^2\kappa}{4d_m}$ . For weak turbulence,  $AA$  can be approximated by

$$AA = \left(1 + 1.06\xi^2\right)^{7/6}, \quad \sigma_R^2 < 1. \quad (2.14)$$

Note that the lowest possible value of  $AA$  is desirable in order to average out signal fluctuations due to atmospheric turbulence.

In Fig. 2.3 a plot of the scintillation index is shown, where different receiver aperture diameters as well as a wavelength value of 1550 nm and an FSO link distance of 3 km are

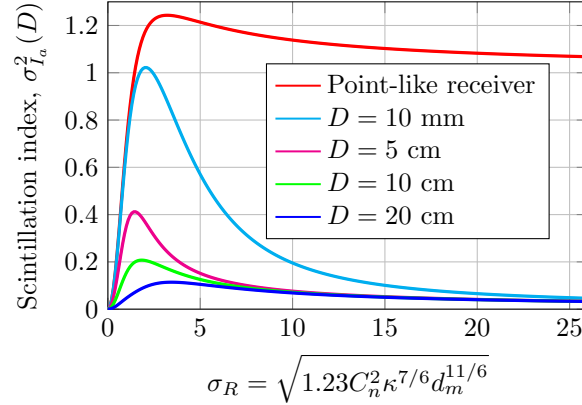


Figure 2.3: Scintillation index for different receiver aperture diameters.

considered to compute Eq. (2.13). From Fig. 2.3, we can see three different zones. In the first one, the scintillation index increases as Rytov variance also increases until it reaches a maximum value. This point is known as the strongest effect. In the second one, once the maximum SI value is reached, the so-called the saturation regime starts to become established, decreasing slightly the effect of atmospheric turbulence. Qualitatively, saturation occurs because multiple scattering causes the optical wave to become increasingly less coherent as it propagates [26].

The correlation length  $\rho_c$  is defined as the width of the irradiance covariance function at  $1/e^2$  of its peak value. In other words, the correlation length describes the average speckle size at the receiver. This parameter is particularly useful in determining the size of the receiver aperture needed to mitigate the effect of atmospheric turbulence, mainly in strong turbulence. Note that  $\rho_c$  depends on both the weather and the link distance. The correlation length of irradiance fluctuations is determined by the Fresnel zone  $\sqrt{d_m/\kappa}$  under weak turbulence, whereas the correlation length of irradiance fluctuations is defined by the spatial coherence radius  $\rho_0$  under strong turbulence [26]. The plane wave coherence radius  $\rho_0$  is smaller than the Fresnel Zone under strong turbulence conditions. In this way, when the refractive index structure parameter  $C_n^2$  is treated as constant, i.e., horizontal FSO link, the plane wave coherence radius  $\rho_0$  is defined as

$$\rho_0 = 0.79 (C_n^2 \kappa^2 d_m)^{-3/5}, \quad (2.15)$$

in both weak and strong turbulence conditions. The well-known Fried's parameter or atmospheric coherence length is related to the plane wave spatial coherence radius by  $r_0 = 2.1\rho_0$ . The atmospheric coherence length can be used to determine the minimum spacing among transmitters at the transmitter side in a multiple transmitters system, or among receiver apertures at the receiver side in a multiple receivers system and, hence, to consider uncorrelated fading.

As previously commented in Chapter 1, the performance of FSO communication systems can be studied in terms of the BER, outage probability and channel capacity, among others. These metrics can be evaluated using atmospheric turbulence statistical models. In the following section, a detailed discussion is given for modeling the density function of irradiance under weak and strong turbulence conditions.

## 2.2.4 Atmospheric Turbulence Statistical Models

In order to describe from a statistical point of view the effect of atmospheric turbulence, different statistical models have been proposed in the literature. On the one hand, these statistical models must be capable of validating the practical measurements. On the other hand, an easy mathematical treatment is required in order to obtain simple analytical expressions.

Early probability density function (PDF) models developed for the irradiance were the modified Rician distribution, which is obtained from the Born approximation, and the log-normal (LN) model, which is based on the first Rytov approximation and was proposed several decades ago in [12, 13]. Both of them are suitable for weak turbulence. However, the modified Rician distribution is used under extremely weak fluctuations [27]. The LN turbulence model is widely used to study the performance under weak turbulence conditions. However, it is well known that the LN turbulence model is not appropriate for moderate-to-strong turbulence conditions in agreement with experimental data [12, 13, 28]. For that reason, a number of statistical models were developed to address this problem in strong turbulence regime.

Most statistical models are based on heuristic arguments and observed experimental data and, hence, they show good agreement with experimental data under certain conditions. One of the early models that gained wide acceptance for strong turbulence was the K distribution [29, 30], which was originally proposed as a model for non-Rayleigh sea clutter. One extension of the K distribution was the I-K distribution, which was presented in [31] to also cover weak turbulence. Later, other statistical models were arising such as lognormally modulated exponential distribution [32], and the more general lognormal-Rician distribution [33], also known as the Beckmann distribution. The Beckmann distribution was presented for the first time in [34]. These models, like K and I-K distributions, present the inconvenience of not being able to relate their statistical parameters to atmospheric conditions. Another atmospheric turbulence model is the gamma-gamma (GG) distribution [12, 13, 28], which has gained a wide acceptance by the research community since the parameters involved in this distribution can be measured directly from the channel. This density function has been extensively utilized in the literature to evaluate the FSO system performance since it provides a close agreement with measurement data. In addition, this distribution can be used to study the performance in a wide range of turbulence conditions, i.e., from moderate-to-strong. However, the GG turbulence model does not provide a good fit to simulation data

in moderate to strong turbulence regimes when  $D \geq \rho_c$ , i.e., when aperture averaging takes place [35, 36]. In Subsection 2.2.4, a brief description of this atmospheric turbulence model is given since GG density function is the most used statistical model in this thesis.

Over the years, many attempts have been conducted to propose atmospheric turbulence statistical models that can be used under all turbulence conditions, i.e, from weak to strong. A universal model able to characterize different turbulence strengths is one of the main concerns. A number of authors have proposed universal statistical channel models, such as the Málaga ( $\mathcal{M}$ )-distributed atmospheric turbulence [37], the double GG generalized fading channels [38, 39], and the exponentiated Weibull (EW) turbulence model [40–43]. The EW model provides a good fit between simulation and experimental data under moderate to strong aperture averaging conditions [40–43]. It should be noted that the EW distribution offers an excellent fit to simulation and experimental data under all aperture averaging conditions  $D \geq \rho_c$ , from weak to strong [40, 41]. Indeed, this atmospheric turbulence model has been used in a significant number of research articles in order to study the performance of FSO communication systems [44–51].

### Log-Normal (LN) Model

The LN turbulence model is the most widely accepted model under weak turbulence conditions, which was proposed several decades ago in [12, 13]. The corresponding PDF of LN model is given by

$$f_{I_a}(i) = \frac{1}{i\sqrt{8\pi\sigma_X^2}} \exp\left(-\frac{(\ln(i) + 2\sigma_X^2)^2}{8\sigma_X^2}\right), \quad i \geq 0 \quad (2.16)$$

where  $\sigma_X^2$  is the log-amplitude variance given by  $\sigma_X^2 \approx \sigma_R^2/4$ . The SI is related to the log-amplitude variance according to

$$\sigma_{I_a}^2 = \exp(4\sigma_X^2) - 1. \quad (2.17)$$

### Gamma-Gamma (GG) Model

In the GG statistical model, the irradiance  $I_a$  is expressed as a product of two independent gamma RVs, i.e.,  $I_a = I_L \cdot I_S$ . These RVs represent the irradiance fluctuations from large ( $I_L$ ) and small ( $I_S$ ) scale turbulence, whose PDF is given by

$$f_{I_a}(i) = \frac{2(\alpha\beta)^{(\alpha+\beta)/2}}{\Gamma(\alpha)\Gamma(\beta)} i^{((\alpha+\beta)/2)-1} K_{\alpha-\beta}\left(2\sqrt{\alpha\beta i}\right), \quad i \geq 0 \quad (2.18)$$

where  $\Gamma(\cdot)$  is the well-known Gamma function (See Appendix A.1),  $K_\nu(\cdot)$  is the  $\nu$ th-order modified Bessel function of the second kind (See Appendix A.2), and the parameters  $\alpha$  and

$\beta$  represent the effective numbers of large and small scale turbulence cells according to

$$\alpha = \frac{1}{\sigma_{I_L}^2} = \frac{1}{\exp\left(\sigma_{\ln I_L}^2\right) - 1}, \quad (2.19a)$$

$$\beta = \frac{1}{\sigma_{I_S}^2} = \frac{1}{\exp\left(\sigma_{\ln I_S}^2\right) - 1}. \quad (2.19b)$$

The parameters  $\alpha$  and  $\beta$  can be selected to achieve a good agreement between Eq. (2.18) and measurement data [28]. Expressions for  $\alpha$  and  $\beta$  for plane, spherical and Gaussian-beam wave are given in [13], which are all expressed in terms of Rytov variance. In the case of plane wave propagation,  $\alpha$  and  $\beta$  can be expressed as follows

$$\alpha = \left[ \exp\left(\frac{0.49\sigma_R^2}{(1 + 0.65\xi^2 + 1.11\sigma_R^{12/5})^{7/6}}\right) - 1 \right]^{-1}, \quad (2.20a)$$

$$\beta = \left[ \exp\left(\frac{0.51\sigma_R^2(1 + 0.69\sigma_R^{12/5})^{-5/6}}{(0.62\xi^2\sigma_R^{12/5} + 0.9\xi^2 + 1)^{5/6}}\right) - 1 \right]^{-1}. \quad (2.20b)$$

It must be emphasized that parameters  $\alpha$  and  $\beta$  cannot arbitrarily be chosen in FSO applications since both parameters are related to Rytov variance. The SI can be computed as

$$\sigma_{I_a}^2 = \frac{1}{\alpha} + \frac{1}{\beta} + \frac{1}{\alpha\beta}. \quad (2.21)$$

It must be noted that the PDF in Eq. (2.18) contains other statistical atmospheric turbulence models adopted in strong turbulence such as the K distribution ( $\beta = 1$  and  $\alpha > 0$ ) and the negative exponential distribution ( $\beta = 1$  and  $\alpha \rightarrow \infty$ ). From the scintillation index point of view, it is easy to deduce the fact that the strength of atmospheric turbulence represented by the GG turbulence model with channel parameters  $\beta = 1$  and increasing  $\alpha$  tends to be closer and closer to 1, i.e., the corresponding SI of the negative exponential atmospheric turbulence model.

### Exponentiated Weibull (EW) Model

Atmospheric turbulence is also modeled using the EW distribution in order to consider a wide range of turbulence conditions (weak-to-strong) as well as aperture averaging conditions i.e., when the condition  $D \geq \rho_c$  holds. The corresponding PDF was derived in [40, eqn. (7)] as follows

$$f_{I_a}(i) = \frac{m_1 m_2}{m_3} \left(\frac{i}{m_3}\right)^{m_2-1} \times \exp\left(-\left(\frac{i}{m_3}\right)^{m_2}\right) \left\{1 - \exp\left(-\left(\frac{i}{m_3}\right)^{m_2}\right)\right\}^{m_1-1}, \quad i \geq 0 \quad (2.22)$$



where  $m_2 > 0$  is a shape parameter related to the SI,  $m_3 > 0$  is a scale parameter related to the mean value of the irradiance, and  $m_1 > 0$  is an extra shape parameter that is strongly dependent on the receiver aperture size. By fitting the EW turbulence model to simulated or experimental PDF data, several specific values of the parameters  $m_1$ ,  $m_2$  and  $m_3$  as well as some expressions for evaluating these parameters have been obtained in [40, 41]. In this thesis, expressions obtained in [41, eqs. (20)-(22)] are used for moderate-to-strong turbulence conditions. The corresponding expressions of the EW parameters are given as a function of the SI as follows

$$m_1 = \frac{7.220\sigma_{I_a}^{2/3}}{\Gamma\left(2.487\sigma_{I_a}^{2/6}\right) - 0.104}, \quad (2.23a)$$

$$m_2 = 1.012(m_1\sigma_{I_a}^2)^{-13/25} + 0.142, \quad (2.23b)$$

$$m_3 = \frac{1}{m_1\Gamma\left(1 + 1/m_2\right)g_1(m_1, m_2)}, \quad (2.23c)$$

where  $g_n(m_1, m_2)$  is defined as follows

$$g_n(m_1, m_2) = \sum_{k=0}^{\infty} \frac{(-1)^k \Gamma(m_1)}{k!(k+1)^{1+n/m_2} \Gamma(m_1 - k)}. \quad (2.24)$$

It must be noted that the above expressions are valid when  $AA < 0.9$  [41]. At the same time, we can express the SI as a function of the EW parameters as

$$\sigma_{I_a}^2 = \frac{\Gamma\left(1 + \frac{2}{m_2}\right)g_2(m_1, m_2)}{a\left(\Gamma\left(1 + \frac{1}{m_2}\right)g_1(m_1, m_2)\right)^2} - 1. \quad (2.25)$$

## 2.3 FSO Channel Modeling

### 2.3.1 Atmospheric Attenuation

The atmospheric turbulence along with absorption and scattering are the three basic processes that affect optical wave propagation. The two phenomena that produce optical power attenuation in optical wave propagation are absorption and scattering. Both of them are wavelength and weather dependent. During the absorption process, atmospheric molecules absorb energy from incident photons. Scattering is the result of photons colliding with atmospheric particles [12, 13]. Unlike the absorption process, there is no loss of energy during the scattering process, only a directional redistribution of energy that may result in a significant reduction in beam intensity for longer distances. There are two kinds of scattering according to the physical size: Rayleigh scattering and Mie scattering. The first one is produced by haze and air molecules that are smaller than wavelength, and the second one is produced by particles that present a size quite similar to wavelength. Note that the atmospheric effects

Table 2.1: Values of  $q$  for different visibility conditions.

Visibility	$q$
$V > 50$ km	1.6
$6$ km $< V < 50$ km	1.3
$V < 6$ km	$0.585V^{-1/3}$

are a consequence of using shorter wavelengths. The atmospheric attenuation has been well studied in the literature.

The attenuation of laser power through atmosphere is determined by the exponential Beers-Lambert law as follows

$$L(d_m) = \frac{P(d_m)}{P(0)} = \exp(-\Phi d_m), \quad (2.26)$$

where  $L(d_m)$  is the loss over a propagation link of length  $d_m$ ,  $P(0)$  is the laser power at the transmitter,  $P(d_m)$  is the laser power at a distance  $d_m$ , and  $\Phi$  is the atmospheric attenuation coefficient described in [52]. The path loss is considered as a deterministic factor that depends on size and distribution of the atmosphere particles and wavelength. Furthermore, this factor is expressed in terms of the visibility, which can be measured directly from the atmosphere. A formula to compute the attenuation coefficient is given in [52]:

$$\Phi = \frac{3.91}{V} \left( \frac{\lambda}{550 \times 10^{-9}} \right)^{-q}, \quad (2.27)$$

where  $V$  is the visibility, and  $q$  is the size distribution of the particles related to visibility as can be seen in Table 2.1.

### 2.3.2 Dynamic Misalignment Statistical Model

FSO communication links are strongly affected by pointing errors, resulting in serious misalignment of fixed-position laser communication systems. An accurate alignment between transmitter and receiver is required [10, 22, 53]. Pointing accuracy is a critical issue in determining link performance and reliability and they can be arisen due to many different factors such as building sway and mechanical errors. Firstly, building sway is due to wind loads, differential heating and cooling, or ground motion over time that can result in an important misalignment error [24, 54]; secondly, mechanical errors are due to errors in tracking systems or mechanical vibrations present in the FSO system [55]. Due to the narrowness of the optical beam and the fact that aperture receivers have a limited field of view (FOV), building sway can even lead to link outages [22]. Hence, pointing errors play an important role in channels fading characteristics.

Statistical modeling of the pointing errors have been studied in the literature. In this thesis, a general misalignment fading model given in [53] by Farid and Hranilovic is used as the cornerstone of pointing error models, where the effect of beam width, detector size and jitter variance is considered. In this way, the attenuation due to geometric spread and pointing errors can be approximated, as in [53], by

$$I_p(r; z) \approx A_0 \exp\left(-\frac{2r^2}{\omega_{zeq}^2}\right), \quad r \geq 0, \quad (2.28)$$

where  $v = \sqrt{\pi}a/\sqrt{2}\omega_z$ ,  $A_0 = [\text{erf}(v)]^2$  is the fraction of the collected power at  $r = 0$ ,  $a = D/2$  is the radius of a circular detection aperture, and  $\omega_{zeq}^2 = \omega_z^2 \sqrt{\pi} \text{erf}(v)/2v \exp(-v^2)$  is the equivalent beam width. The beam width  $\omega_z$  can be approximated by  $\omega_z = \theta z$ , where  $\theta$  is the transmit divergence angle describing the increase in beam radius with distance from the transmitter. The approximation in Eq. (2.28) is in good agreement with the exact value when the beam width  $\omega_z > 6a$ , as shown in [53, appendix]. The approximate expression for  $I_p$  can even be used when  $\omega_z < 6a$  but obtaining a normalized mean-squared error (NMSE)  $\text{NMSE} > 10^{-3}$ .

The radial displacement  $r$  at the receiver plane can be expressed as  $r^2 = x^2 + y^2$ , where  $x$  and  $y$  represent the horizontal displacement and the elevation, respectively. Moreover, the radial displacement is distributed according to a Rayleigh distribution when  $x$  and  $y$  are modeled as independent Gaussian RVs with zero means and same jitters for the horizontal displacement and the elevation, i.e.  $x \sim N(0, \sigma_s)$  and  $y \sim N(0, \sigma_s)$ , whose PDF is given by

$$f_r(r) = \frac{r}{\sigma_s^2} \exp\left(-\frac{r^2}{2\sigma_s^2}\right), \quad r \geq 0. \quad (2.29)$$

Thus, combining Eq. (2.28) and Eq. (4.28), the corresponding PDF of the irradiance  $I_p$  is obtained as follows

$$f_{I_p}(i) = \frac{\varphi^2}{A_0 \varphi^2} i^{\varphi^2-1}, \quad 0 \leq i \leq A_0 \quad (2.30)$$

where  $\varphi = \omega_{zeq}/2\sigma_s$  is the ratio between the equivalent beam radius at the receiver and the pointing error displacement standard deviation (jitter) at the receiver. This pointing error model and its corresponding derivation can be seen in greater detail in [53].

Note that this pointing error model does not take into account the effect of nonzero boresight, which will be addressed later. In that model, the radial displacement  $r$  at the receiver follows a lognormal-Rice distribution, and it was presented in [56]. This effect and other ones such as different jitters for the horizontal displacement and the elevation and correlated sways will take into consideration in Chapter 4.

### 2.3.3 Composite Fading Channel

Before computing the probability distribution of the channel  $I$ , some comments about considering atmospheric turbulence and pointing errors statistically independent are required.

As we know well, pointing errors are due to building sway and, hence, the correlation time is on the order of a few seconds [57], which is bigger than correlation time of the atmospheric turbulence (10-100 ms). Hence, both effects can be considered to be statistically independent.

The probability distribution of the channel  $I = L \cdot I_a \cdot I_p$  can be expressed as follows

$$f_I(i) = \int_{i/A_0L}^{\infty} f_{I|I_a}(i|i_a) f_{I_a}(i_a) di_a, \quad (2.31)$$

where  $f_{I|I_a}(i|i_a)$  is the conditional probability given an atmospheric turbulence state,  $f_{I_a}(i_a)$  is the corresponding PDF of atmospheric turbulence, and  $L$  acts as a scaling factor. In this way, the conditional probability is expressed as

$$\begin{aligned} f_{I|I_a}(i|i_a) &= \frac{1}{L \cdot i_a} f_{I_p} \left( \frac{i}{L \cdot i_a} \right) \\ &= \frac{\varphi^2}{(Li_a)A_0^{\varphi^2}} \left( \frac{i}{L \cdot i_a} \right)^{\varphi^2-1}, \quad 0 \leq i \leq A_0Li_a \end{aligned} \quad (2.32)$$

The integral in Eq. (2.32) can be computed by substituting the corresponding statistical model of atmospheric turbulence. In GG atmospheric turbulence, we can substitute Eq. (2.18) and Eq. (2.32) into Eq. (2.31), resulting in

$$f_I(i) = \frac{\varphi^2 2(\alpha\beta)^{\frac{\alpha+\beta}{2}}}{(LA_0)^{\varphi^2} \Gamma(\alpha)\Gamma(\beta)} i^{\varphi^2-1} \int_{i/A_0L}^{\infty} i_a^{\frac{\alpha+\beta}{2}-\varphi^2-1} K_{\alpha-\beta} \left( 2\sqrt{\alpha\beta i_a} \right) di_a. \quad (2.33)$$

In order to solve the above integral, we can express the function  $K_\nu(\cdot)$  in terms of the Meijer's G-function (See Appendix A.3.1) and, then, we can use [58, eqn. (07.34.21.0085.01)] (See Appendix A.3.2) to obtain the corresponding closed-form expression of the combined PDF of  $I$  as follows

$$f_I(i) = \frac{\varphi^2 i^{-1}}{\Gamma(\alpha)\Gamma(\beta)} G_{1,3}^{3,0} \left( \frac{\alpha\beta}{A_0L} i \left| \begin{array}{c} \varphi^2 + 1 \\ \varphi^2, \alpha, \beta \end{array} \right. \right), \quad i \geq 0 \quad (2.34)$$

where  $G_{p,q}^{m,n}[\cdot]$  is the Meijer's G-function (See Appendix A.3). The corresponding cumulative distribution function (CDF) is given by

$$F_I(i) = \text{Prob}(I \leq i) = \int_0^i f_I(x) dx = \frac{\varphi^2}{\Gamma(\alpha)\Gamma(\beta)} \int_0^i i^{-1} G_{1,3}^{3,0} \left( \frac{\alpha\beta}{A_0L} i \left| \begin{array}{c} \varphi^2 + 1 \\ \varphi^2, \alpha, \beta \end{array} \right. \right) di. \quad (2.35)$$

The above integral can be derived by using [59, eqn. (1.16.2.1)] (See Appendix A.3.2) as follows

$$F_I(i) = \frac{\varphi^2}{\Gamma(\alpha)\Gamma(\beta)} G_{2,4}^{3,1} \left( \frac{\alpha\beta}{A_0L} i \left| \begin{array}{c} 1, \varphi^2 + 1 \\ \varphi^2, \alpha, \beta, 0 \end{array} \right. \right), \quad i \geq 0. \quad (2.36)$$

It must be noted that the above equations appear to be cumbersome to use in order to obtain simple closed-form expressions in the analysis of FSO communication systems, resulting in

numerical solutions that obscure the impact of channel and FSO system parameters on performance. To overcome this inconvenience, the PDF in Eq. (2.34) can be approximated by using the first term of the Taylor expansion at  $i = 0$  as  $f_I(i) = ai^{b-1} + O(i^b)$  [60], which can provide a deeper insight on how atmospheric turbulence and pointing errors deteriorate the performance of FSO communication systems. In this way, the PDF in Eq. (2.34) is approximated by a single polynomial term as follows

$$f_I(i) \doteq ai^{b-1}, \quad i \geq 0 \quad (2.37)$$

based on the fact that the asymptotic behavior of the system performance is dominated by the behavior of the PDF near the origin, i.e.  $f_I(i)$  at  $i \rightarrow 0$  determines high SNR performance [60]. The parameter  $a$  is a positive constant, and the parameter  $b$  quantifies the order of smoothness of  $f_I(i)$  at the origin. The high SNR approximations are especially useful for performance analysis of FSO communication systems, where severe fading renders necessary a large SNR for achieving a target in terms of the BER and outage probability. Hence, we can obtain the following asymptotic expression for the PDF of GG atmospheric turbulence model in Eq. (2.34) as

$$f_I(i) \doteq ai^{b-1} = \begin{cases} \frac{\varphi^2(\alpha\beta)^{\min(\alpha,\beta)}\Gamma(|\alpha-\beta|)}{(A_0L)^{\min(\alpha,\beta)}\Gamma(\alpha)\Gamma(\beta)(\varphi^2-\min(\alpha,\beta))} i^{\min(\alpha,\beta)-1}, & \varphi^2 > \min(\alpha,\beta) \\ \frac{\varphi^2(\alpha\beta)\varphi^2\Gamma(\alpha-\varphi^2)\Gamma(\beta-\varphi^2)}{(A_0L)^{\varphi^2}\Gamma(\alpha)\Gamma(\beta)} i^{\varphi^2-1}. & \varphi^2 < \min(\alpha,\beta) \end{cases} \quad (2.38)$$

It is noteworthy to mention that the above asymptotic expression is dominated by  $b-1$ , i.e.,  $\min(\alpha,\beta,\varphi^2)-1$ . Hence, different expressions for  $a$  and  $b$  are derived in Eq. (2.38) depending on the relation between  $\varphi^2$  and  $\min(\alpha,\beta)$ . In plane wave propagation, it is demonstrated that the relation  $\alpha > \beta$  is always satisfied and, hence,  $\beta$  is lower bounded above 1 as turbulence strength increases [61]. In this case, the asymptotic expression given in Eq. (2.38) is dominated by  $\min(\beta,\varphi^2)-1$ . The corresponding asymptotic CDF is obtained as follows

$$F_I(i) = \int_0^i f_I(x)dx \doteq \frac{a}{b}i^b, \quad i \geq 0. \quad (2.39)$$

The asymptotic behavior has been applied to the combined effect of atmospheric turbulence (GG in this case) and pointing errors ( $I$ ), but this procedure can directly be applied to atmospheric turbulence ( $I_a$ ) as long as this one can always be expanded into Maclaurin series. For instance, both GG and EW atmospheric turbulence can be expanded into Maclaurin series, among others. In the case of GG atmospheric turbulence,  $I_a$  can be expressed as

$$f_{I_a}(i) \doteq ai^{b-1} = \frac{(\alpha\beta)^{\min(\alpha,\beta)}\Gamma(|\alpha-\beta|)}{\Gamma(\alpha)\Gamma(\beta)} i^{\min(\alpha,\beta)-1}, \quad i \geq 0. \quad (2.40)$$

## 2.4 Performance of FSO Communication Systems

The measurement of the performance in FSO communication systems has always been a subject of real interest. The SNR is a common measure of system performance, but

there are other metrics, which are able to provide a better performance in communications, such as probability of error, outage probability and channel capacity. The performance of FSO communication systems is usually quantified in terms of the BER. At the same time, outage probability is another performance metric that is defined as the probability that SNR falls below a certain specified threshold. Finally, the performance of FSO communication systems is measured in terms of ergodic capacity, which basically provides information about the limiting error-free information rate that can be achieved. Unlike outage probability and ergodic capacity, the BER is the only metric that depends on the modulation scheme employed by the FSO communications system.

The main difficulties when evaluating these performance metrics lie on the fact that the PDF of the irradiance might not be known in closed-form when a generalized pointing errors model is assumed. In this way, there are no available closed-form expressions for the BER, outage probability and ergodic capacity. The performance analysis is restricted to the numerical evaluation.

In this section, the performance of an FSO link over GG atmospheric turbulence channels with zero boresight pointing errors is analyzed in terms of the BER, outage probability and ergodic capacity in order to establish the baseline performance.

### 2.4.1 Bit Error-Rate (BER) Performance Analysis

The BER of IM/DD systems with OOK modulation in the presence of AWGN and assuming perfect channel state information (CSI) at the receiver is given by

$$P_b(e|i) = P_b(0)P_b(e|0) + P_b(1)P_b(e|1), \quad (2.41)$$

where  $P_b(0)$  and  $P_b(1)$  are the probabilities of sending 0 and 1 bits, respectively, and  $P_b(e|0)$  and  $P_b(e|1)$  denote the conditional bit error probability when the transmitted bit is 0 and 1, respectively. Assuming each bit is equally likely, the conditional BER at the receiver is given by

$$P_b(e|i) = Q\left(\frac{d_E}{2\sigma_n}i\right) = Q\left(\frac{2P_t\sqrt{T_b}}{2\sqrt{N_0/2}}i\right) = Q\left(\sqrt{\frac{2P_t^2T_b}{N_0}}i\right) = Q\left(\sqrt{2\gamma}i\right), \quad (2.42)$$

where  $Q(\cdot)$  is the Gaussian  $Q$ -function defined as  $Q(x) = (1/2\pi) \int_x^\infty \exp(-t^2/2) dt$ , and  $\gamma = P_t^2T_b/N_0$  is the received electrical SNR in absence of turbulence. Hence, the average BER  $P_b$  can be obtained by averaging  $P_b(e|i)$  over the combined PDF  $f_I(i)$  as follows

$$P_b = \int_0^\infty Q\left(\sqrt{2\gamma}i\right) f_I(i) di, \quad (2.43)$$

where  $f_I(i)$  is given by Eq. (2.37). To evaluate the integral in Eq. (2.43), we can use that the  $Q$ -function is related to the complementary error function  $\text{erfc}(\cdot)$  by  $\text{erfc}(x) = 2Q(\sqrt{2}x)$  [62,

eqn. (6.287)] and, then, we can use [62, eqn. (6.281)] (See Appendix A.9), obtaining an asymptotic closed-form expression for a generic average BER as follows

$$P_b \doteq \left[ \left( \frac{a\Gamma((b+1)/2)}{2b\sqrt{\pi}} \right)^{-\frac{2}{b}} \cdot \gamma \right]^{-\frac{b}{2}}, \quad (2.44)$$

where the parameters  $a$  and  $b$  depend on the atmospheric turbulence and pointing errors. Interestingly, it is straightforward to show that the average BER behaves asymptotically as

$$P_b \doteq (G_c\gamma)^{-G_d}, \quad (2.45)$$

where  $G_d$  and  $G_c$  denote diversity order and coding gain, respectively [60]. At high SNR, the diversity order determines the slope of the BER versus average SNR curve in a log-log scale, and the coding gain (in decibels) determines the shift of the curve in SNR.

It can be observed that the diversity order is independent of pointing errors when the relation  $\varphi^2 > \min(\alpha, \beta)$  holds, i.e., atmospheric turbulence is the dominant effect in relation to pointing errors. In other words, the diversity order only depends on atmospheric turbulence when larger amounts of misalignment are not assumed. It can be shown that most practical terrestrial FSO systems operate under the condition of atmospheric turbulence is the dominant effect. It must also be mentioned that a much higher diversity order can be achieved under this condition and, hence, a much better BER performance is obtained. As a result, the adoption of the transmitter with accurate control of their beam width is especially important here to satisfy this desired FSO scenario in order to maximize the diversity order.

### 2.4.2 Outage Performance Analysis

The outage probability,  $P_{\text{out}}$ , can be defined as the probability that the instantaneous combined SNR,  $\gamma_T$ , falls below a certain specified threshold,  $\gamma_{th}$ , that is

$$P_{\text{out}} := P(\gamma_T \leq \gamma_{th}) = \int_0^{\gamma_{th}} f_{\gamma_T}(i) di, \quad (2.46)$$

where  $\gamma_T$  is the resulting received electrical SNR given by

$$\gamma_T(i) = \frac{1}{2} \frac{d_E^2}{N_0/2} i^2 = \frac{4P_t^2 T_b}{N_0} i^2 = 4\gamma i^2. \quad (2.47)$$

By using Eq. (2.46), the outage probability can be written as

$$P_{\text{out}} = P(4\gamma i^2 \leq \gamma_{th}) = \int_0^{\sqrt{\gamma_{th}/4\gamma}} f_I(i) di = F_I \left( \sqrt{\frac{\gamma_{th}}{4\gamma}} \right), \quad (2.48)$$

where  $P_{\text{out}}$  represents the exact closed-form solution for the outage probability. In the case of GG atmospheric turbulence,  $F_I \left( \sqrt{\frac{\gamma_{th}}{4\gamma}} \right)$  is expressed according to Eq. (2.36). Similar to

BER,  $P_{\text{out}}$  can also be expressed in terms of its asymptotic behavior by using Eq. (2.37) as follows

$$P_{\text{out}} \doteq \int_0^{\sqrt{\gamma_{\text{th}}/4\gamma}} ai^{b-1} di = \left[ \left( \frac{a}{b2^b} \right)^{-\frac{2}{b}} \cdot \frac{\gamma}{\gamma_{\text{th}}} \right]^{-\frac{b}{2}}. \quad (2.49)$$

In this way, the outage probability also behaves asymptotically as

$$P_{\text{out}} \doteq (O_c \gamma)^{-O_d}, \quad (2.50)$$

where  $O_d$  and  $O_c$  denote outage diversity and coding gain, respectively [60]. As in BER performance, the outage diversity determines at high SNR the slope of the outage probability versus average SNR curve in a log-log scale and the coding gain (in decibels) determines the shift of the curve in SNR. Note that the same conclusions drawn from the BER performance about diversity order can be applied to outage diversity.

### 2.4.3 Ergodic Capacity Analysis

Assuming instantaneous CSI at the receiver, the ergodic capacity of FSO links in bps is given by Shannon's well-known expression [63]

$$C = \frac{B}{2 \ln(2)} \int_0^\infty \ln(1 + 4\gamma i^2) f_I(i) di, \quad (2.51)$$

where  $B$  is the channel bandwidth,  $\ln(\cdot)$  is the natural logarithm [62, eqn. (1.511)], and  $f_I(i)$  is the combined PDF of atmospheric turbulence and pointing errors. It should be noted that the factor  $1/2$  in Eq. (2.51) is because the transmitter is assumed to operate in half-duplex mode and, hence, we consider a transmission in one direction at a time. By other hand, this analysis can be extended to full-duplex transmission, i.e., both directions simultaneously. Now, we solve the integral in Eq. (2.51) for GG atmospheric turbulence as given in Eq. (2.34). This integral can be solved using [59, eqn. (8.4.6.5)] in order to express the natural logarithm in terms of the Meijer's G-function (See Appendix A.3.1) and, then, we can use [58, eqn. (07.34.21.0013.01)]. Hence, the closed-form expression for the ergodic capacity of an FSO link in bits/s/Hz is given by

$$C/B = \frac{\varphi^2 2^{\alpha+\beta-4}}{\pi \ln(2) \Gamma(\alpha) \Gamma(\beta)} G_{8,4}^{1,8} \left( \frac{64 A_0^2 L^2 \gamma}{\alpha^2 \beta^2} \left| \begin{array}{c} 1, 1, \frac{1-\alpha}{2}, \frac{2-\alpha}{2}, \frac{1-\beta}{2}, \frac{2-\beta}{2}, \frac{1-\varphi^2}{2}, \frac{2-\varphi^2}{2} \\ 1, 0, -\frac{\varphi^2}{2}, \frac{1-\varphi^2}{2} \end{array} \right. \right). \quad (2.52)$$

An asymptotic analysis can be performed in order to obtain a simpler closed-form expression for the ergodic capacity of FSO links. An asymptotic expression at high SNR is easily and accurately lower-bounded due to the fact that  $\ln(1+z) \approx \ln(z)$  when  $z \rightarrow \infty$  as follows

$$C/B \doteq \frac{1}{\ln(4)} \int_0^\infty \ln(4\gamma i^2) f_I(i) di. \quad (2.53)$$

By applying the following identity:  $\ln(a \cdot b) = \ln(a) + \ln(b)$  in Eq. (2.53) as

$$\ln(4\gamma i^2) = \ln(4\gamma) + 2 \ln(i), \quad (2.54)$$



the integral in Eq. (2.53) can be written as follows

$$C/B \doteq \frac{\ln(4\gamma)}{\ln(4)} + \frac{1}{\ln(2)} \int_0^\infty \ln(i) f_I(i) di. \quad (2.55)$$

Another way of obtaining the ergodic capacity of FSO communication systems at high SNR is via utilizing moments method which was presented for the first time in [64, Eqs. (8) and (9)]. Knowing that atmospheric turbulence and pointing errors are statistically independent, the integral in Eq. (2.55) can be rewritten as follows

$$\begin{aligned} \int_0^\infty \ln(i) f_I(i) di &= \int_0^\infty \int_0^{A_0} \ln(L \cdot i_a \cdot i_p) f_{I_a}(i_a) f_{I_p}(i_p) di_a di_p = \ln(L) \\ &+ \underbrace{\int_0^\infty \ln(i_a) f_{I_a}(i_a) di_a}_{INT_1} + \underbrace{\int_0^{A_0} \ln(i_p) f_{I_p}(i_p) di_p}_{INT_2} = \ln(L) + INT_1 + INT_2. \end{aligned} \quad (2.56)$$

To evaluate the integral  $INT_1$  for GG atmospheric turbulence, we can use that the function  $K_\nu(\cdot)$  is related to the function  $J_\nu(\cdot)$  and, then, we can also use that the function  $J_\nu(\cdot)$  is related to the function  $I_\nu(\cdot)$  (See Appendix A.8). Next, using [62, eqn. (6.771)] (See Appendix A.9) and, performing some algebraic manipulations, we can express  $INT_1$  as follows

$$INT_1 = \ln\left(\frac{1}{\alpha\beta}\right) + \psi(\alpha) + \psi(\beta), \quad (2.57)$$

where  $\psi(\cdot)$  is the psi (digamma) function (See Appendix A.4). Secondly,  $INT_2$  is obtained as follows (See Appendix A.10)

$$INT_2 = \int_0^{A_0} \ln(i_p) f_{I_p}(i_p) di_p = \ln(A_0) - \frac{1}{\varphi^2}. \quad (2.58)$$

Finally, the asymptotic expression for the corresponding ergodic capacity of an FSO link in bits/s/Hz is expressed as

$$C/B \doteq \frac{\ln(4\gamma)}{\ln(4)} + \frac{1}{\ln(2)} \left( \ln(L) + \ln\left(\frac{1}{\alpha\beta}\right) + \psi(\alpha) + \psi(\beta) + \ln(A_0) - \frac{1}{\varphi^2} \right). \quad (2.59)$$

The above expression is identical to the asymptotic expression obtained in [65, eqn. (24)] by applying the moments method. Similar to BER and outage performance, some comments can be drawn from this asymptotic analysis. Firstly, it can be deduced from the asymptotic analysis at high SNR that the shift of the ergodic capacity versus SNR is more relevant than the slope of the curve in SNR compared with BER and outage probability. This shift can be interpreted as an improvement on ergodic capacity in order to maintain the same performance in terms of capacity with less SNR.

## 2.5 Summary

In this chapter, we have reviewed the theory of optical wave propagation through a random media, i.e. atmosphere, as well as the mathematical tools used in the performance analysis

of SISO FSO communication systems. These mathematical tools will be used in the following chapters to study the ergodic capacity of MISO, SIMO, MIMO and cooperative FSO systems in Chapter 3 as well as the effect of generalized pointing errors on BER and outage performance in Chapter 4.

On the one hand, we have introduced some concepts and assumptions that will be assumed throughout the thesis. The channel model of any FSO link is given in Eq. (2.4) where the irradiance is considered to be a product of three factors: atmospheric path loss, atmospheric turbulence, and pointing errors. Different statistical models for atmospheric turbulence have been presented where GG distribution is the main model assumed in this thesis. Other models such as LN and EW distributions will also be assumed in some specific cases. At the same time, a zero boresight pointing error model has also been presented where the effect of beam width, detector size and jitter variance are considered. This statistical model will be used to develop a generalized pointing error model in Chapter 4.

On the other hand, performance metrics such as BER, outage probability and ergodic capacity have been analyzed in detail for a SISO FSO system over GG atmospheric turbulence channels with zero boresight pointing errors. The FSO channel is based on IM/DD schemes and OOK modulation, and the parameters related to atmospheric turbulence are computed by assuming plane wave propagation.

Finally, to check the validity of the analytical expressions obtained in this thesis, Monte Carlo simulation results have always been included. Generally, the simulation of a communication system requires the generation of sampled values of all input RVs to estimate the system performance from the output samples [66]. Nevertheless, Monte Carlo simulations involve the generation and processing of large numbers of samples and, hence, computational efficiency of random number generators is extremely important. In this way, quasianalytical Monte Carlo simulation methods are widely used to reduce the simulation time, where not all input processes into the system are simulated explicitly, providing a complete curve of BER as a function of SNR. In applying a quasianalytical technique, we can make use of the idea of an equivalent noise source. In this way, a simulation model for FSO communication systems to estimate BER performance is stated as follows. The random binary source follows a Bernoulli distribution, i.e. each bit occurs with probability of  $1/2$ , at a rate of  $1/T_b$  bits per second. Next, an OOK modulator is implemented in order to generate the corresponding waveform where a rectangular shape pulse is used. In baseband modulation, the output waveform takes predefined values corresponding to a 1 or 0, i.e., either 0 or  $2P_t$ . The FSO channel is modeled according to Eq. (2.4). At the receiver side, the transmitted signal is detected using a matched filter whose impulse response matched to the considered pulse shape. This filter is optimal in the sense of maximizing the sampled SNR. The best decision rule to use, in the sense of minimizing the probability of symbol error, is the ML detector.

## Chapter 3

# Ergodic Capacity Analysis

The study of ergodic capacity for terrestrial FSO links is addressed in this chapter. New results are derived in the fields of MISO, SIMO and MIMO FSO communication and cooperative FSO systems, presenting novel approximate closed-form expressions for the capacity over GG fading channels mainly with pointing errors.

### 3.1 Motivation

Over the last decade, a remarkable variety of works have been reported wherein the ergodic capacity is analyzed over different statistical models to describe the irradiance of FSO links and under the presence of pointing error effects [65, 67–72]. Ergodic capacity, also known as average channel capacity, defines the maximum data rate that can be sent over the channel with asymptotically small error probability, without any delay or complexity constraints [73].

The study of ergodic capacity for terrestrial FSO links has generated considerable controversy in the literature due to the physical characteristics of atmospheric turbulence. It is commonly known that atmospheric turbulence channels are well described as slow fading or block fading channels and, hence, outage capacity becomes a more realistic measure of channel capacity than ergodic capacity in FSO systems. However, ergodic capacity can be perfectly applied to terrestrial FSO links when some aspects related to the information theory are considered:

- (a) The FSO channel is assumed to be memoryless, stationary and ergodic, with independent and identically distributed intensity fast fading statistics. In spite of scintillation is a slow time varying process relative to typical symbol rates of an FSO system, having a coherence time on the order of milliseconds, this approach is valid because temporal correlation can in practice be overcome by means of long interleavers [67, 74–77]. This

assumption has to be considered like an ideal scenario where the latency introduced by the interleaver is not an inconvenience for the required application.

- (b) Ergodic capacity is also applicable to slowly varying (block-fading) channels, i.e. terrestrial FSO links, when the message is long enough to reveal long-term ergodic properties of the turbulence process [78]. This fact was taken into account in [79] in the context of FSO communication systems.
- (c) The ergodic capacity for terrestrial FSO links based on IM/DD systems represents a lower bound as given in [80] by Lapidoth.
- (d) The effect of atmospheric turbulence is studied along with pointing error effects, which typically lead to an increase in the signal fluctuation rate. Additionally, the ergodic capacity analysis is a great challenge.

### 3.2 Related Work

Ergodic capacity analysis has attracted a notable interest in both cooperative and non-cooperative FSO communication systems. It is well known that both MISO, SIMO and MIMO structures can be employed to reduce scintillation and therefore improve FSO channel capacity. To the best of our knowledge, just a few works have studied the ergodic capacity in the context of MISO, SIMO and MIMO FSO communication systems only taking into account the effect of atmospheric turbulence, i.e., without considering the effect of pointing errors [81–85]. In [81], a closed-form expression for the average capacity of MIMO FSO systems with equal gain combining (EGC) reception is obtained over LN fading channels without pointing errors. In [82], the ergodic capacity of MIMO FSO systems is investigated over strong turbulence channels by using a single GG approximation [86]. In [83], closed-form expressions for the average capacity of MIMO FSO channels with EGC and maximum ratio combining (MRC) reception are obtained over GG fading channels without pointing errors. In [84], the effect of MIMO FSO systems under aperture averaging conditions on the ergodic capacity over GG fading channels is studied and compared for different weather conditions. In [85], the ergodic capacity of MIMO FSO systems with EGC reception is studied over GG fading channels without pointing errors by using the  $\alpha$ - $\mu$  distribution [87]. However, to the best of our knowledge, the combined effect of atmospheric turbulence and misalignment fading has not been taken into account on the ergodic capacity analysis of MISO, SIMO and MIMO FSO communication systems.

Regarding cooperative FSO systems, a few researchers have addressed the study of the ergodic capacity in this regard [88–93]. In [88], the end-to-end ergodic capacity of dual-hop FSO system employing amplify-and-forward (AF) relaying is evaluated over GG fading channels with pointing errors by approximating the PDF of the end-to-end SNR by the  $\alpha$ - $\mu$  distribution. In [89], a cooperative FSO system is analyzed where an approximate

expression for the ergodic capacity is obtained over LN and GG fading channels when the best user is selected. In [90], the channel capacity of a DF-based dual-hop FSO system is studied over GG fading channels with pointing errors. In [91, 92], the capacity performance of a subcarrier intensity modulation (SIM)-based dual-hop FSO system with DF and AF relaying is evaluated over GG fading channels with pointing errors. The results are obtained in terms of special function known as generalized bivariate Meijer's G-function (GBMGF). In [93], a relay system over asymmetric links composed of both Nakagami-m and GG fading is studied where a closed-form expression for the ergodic capacity is also presented in terms of the GBMGF.

In the light of the related work, on the one hand, there are no closed-form expressions that study the ergodic capacity of MISO, SIMO and MIMO FSO systems under the presence of pointing errors. On the other hand, there are no reported works that study the ergodic capacity of cooperative FSO systems based on DF relaying when LOS is available.

### 3.3 Structure

The remainder of this chapter is organized as follows. In Section 3.4 the analysis of the ergodic capacity of MISO FSO systems is carried out over GG atmospheric turbulence channels with zero boresight pointing errors. In Section 3.5 the analysis of the ergodic capacity of SIMO and MIMO FSO systems is performed over different atmospheric turbulence channels such as GG, LN and EW distributions with nonzero boresight pointing errors. The nonzero boresight pointing error model is briefly reviewed at the beginning of that section, highlighting some differences with respect to the zero boresight pointing error model. In Section 3.6 the analysis of the ergodic capacity of two different DF relaying schemes is also performed over GG atmospheric turbulence channels with zero boresight pointing errors. Finally, this chapter is concluded in Section 3.7.

### 3.4 Ergodic Capacity of MISO FSO Systems

In this section, the ergodic capacity of MISO FSO systems is studied. To the best of our knowledge, the study of the ergodic capacity of MISO FSO systems was never taken into account in the literature. In this way, this research problem is addressed in this thesis, presenting new results for the optics community. The ergodic capacity is analyzed over GG atmospheric turbulence channels with zero boresight pointing errors.

### 3.4.1 System Model

Let us adopt a MISO FSO system with  $M$  transmitters or laser sources ( $M \geq 1$ ), and a single receiver, as shown in Fig. 3.1.

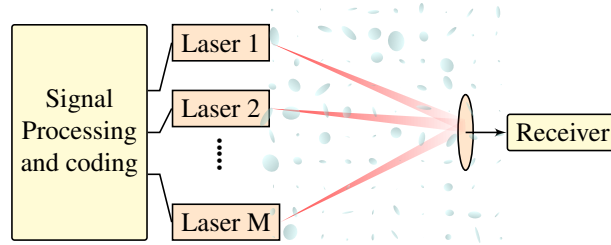


Figure 3.1: Block diagram of the considered MISO FSO communications system.

Before starting the analysis, some assumptions must be commented:

- (a) The receiver is assumed to be centered at the origin. In addition, the laser sources and the receiver are physically situated so that all transmitters are simultaneously observed by the receiver.
- (b) The laser sources are separated by a fixed distance so that uncorrelated fading can be considered. The latter is due to the fact that diversity techniques are most efficient under the condition of uncorrelated fading. It is assumed that the spacing among transmitters is sufficiently larger than the atmospheric coherence length  $r_0$ , then uncorrelated fading can be considered [94, 95]. In contrast to spatial diversity for RF systems, spatial diversity for FSO systems is readily deployed since the atmospheric coherence length is of the order of centimeters.
- (c) The EGC reception technique is adopted due to its lower implementation complexity even maintaining a relevant performance in FSO links [96, 97].

### 3.4.2 Performance Analysis

In this section, the ergodic capacity of MISO FSO systems is evaluated over GG fading channels with zero boresight pointing errors. When the EGC reception is used, the statistical channel model can be written as

$$Y = X \frac{1}{M} \sum_{k=1}^M I_k + Z, \quad Z \sim N(0, N_0/2), \quad (3.1)$$

where  $I_k$  represents the equivalent irradiance through the optical channel between the  $k$ th transmit aperture and the photodetector. Here, the division by  $M$  is considered in Eq. (3.1)

to maintain the average optical power in the air at a constant level of  $P_t$ , being transmitted by each laser an average optical power  $P_t/M$ . In this way, the total transmit power is the same as in an FSO system with no transmit diversity, i.e. direct path link or SISO FSO system. The resulting received electrical SNR  $\gamma_{\text{MISO}}$  can be defined as follows

$$\gamma_{\text{MISO}} = \frac{1}{2} \frac{(2P_t\sqrt{T_b}/M)^2}{N_0/2} \left( \sum_{k=1}^M I_k \right)^2 = \frac{4P_t^2 T_b}{M^2 N_0} I_T^2 = \frac{4\gamma}{M^2} I_T^2, \quad (3.2)$$

where  $I_T$  is the total channel gain. Assuming instantaneous CSI at the receiver, the ergodic capacity of the considered MISO FSO system in bits/s/Hz can be obtained as in Eq. (2.51) as follows

$$C_{\text{MISO}}/B = \frac{1}{2\ln(2)} \int_0^\infty \ln \left( 1 + \frac{4\gamma}{M^2} i^2 \right) f_{I_T}(i) di, \quad (3.3)$$

where  $f_{I_T}(i)$  is the PDF of the sum of  $M$  GG with zero boresight pointing errors variates which are statistically independent but not necessarily identically distributed, i.e.,  $I_T = I_1 + I_2 + \dots + I_M$ . It should be noted that obtaining the PDF of  $I_T$  is remarkably tedious and not easily tractable due to the difficulty in finding its statistics. Hence, a lower bound (LB) for this sum can be obtained by using the well-known inequality between arithmetic mean (AM) and geometric mean (GM) given by

$$AM \geq GM, \quad (3.4)$$

where  $AM = (1/M) \sum_{k=1}^M I_k$  and  $GM = \sqrt[M]{\prod_{k=1}^M I_k}$  are the arithmetic and geometric means, respectively. Therefore, a lower bound for the sum of  $M$  GG with pointing errors variates is obtained as

$$I_T = \sum_{k=1}^M I_k \geq M \sqrt[M]{F \cdot \prod_{k=1}^M I_k} = M \sqrt[M]{F \cdot I_{LB}}. \quad (3.5)$$

Note that the PDF of the product of  $M$  GG with pointing errors variates  $f_{I_{LB}}(i)$ , i.e. the PDF of  $I_{LB}$ , is mathematically more tractable than  $f_{I_T}(i)$  and can efficiently be applied to the analysis of the ergodic capacity of MISO FSO communication systems. From Eq. (3.5), it can easily be deduced that the mathematical expectation in both sides of the inequality takes different values and, hence, a correcting factor  $F$  must be added to the inequality in order to maintain the same value in both sides. In fact, the correcting factor  $F$  is added to Eq. (3.5) in order to obtain a strict approximation of this ergodic capacity. The correcting factor  $F$  can be derived from Eq. (3.5) as follows

$$F = \frac{\mathbb{E} \left[ \sum_{k=1}^M I_k \right]^M}{M^M \cdot \mathbb{E} \left[ \sqrt[M]{\prod_{k=1}^M I_k} \right]^M}. \quad (3.6)$$

In addition,  $F$  only depends on channel parameters (See Appendix B.1). Substituting Eq. (3.5) into Eq. (3.3) and, after performing some algebraic manipulations, the ergodic

capacity of MISO FSO systems can be accurately approximated as follows

$$C_{\text{MISO}/B} \approx \frac{1}{\ln(4)} \int_0^\infty \ln \left( 1 + 4\gamma (i \cdot F)^{\frac{2}{M}} \right) f_{I_{LB}}(i) di. \quad (3.7)$$

The PDF  $f_{I_{LB}}(i)$  can be derived in closed-form via inverse Mellin transform, which is an essential tool in studying the distribution of products and quotients of independent RVs (See Appendix A.7). The importance of the Mellin transform in probability theory lies in the fact that if  $I_k$  for  $k = \{1, 2, \dots, M\}$  are  $M$  independent RVs, then the Mellin transform of their product is equal to the product of the Mellin transforms of  $I_k$  for  $k = \{1, 2, \dots, M\}$  [98]. Hence, a closed-form expression for the PDF of  $I_{LB}$  can be expressed in terms of the Meijer's G-function by employing the definition of the Mellin transform as follows (See Appendix A.7.1)

$$f_{I_{LB}}(i) = \frac{i^{-1} \prod_{k=1}^M \varphi_k^2 G_{M,3M}^{3M,0} \left( \prod_{k=1}^M \frac{\alpha_k \beta_k}{A_{0_k} L_k} i \left| \begin{array}{c} \varphi_1^2 + 1, \dots, \varphi_M^2 + 1 \\ \varphi_1^2, \alpha_1, \beta_1, \dots, \varphi_M^2, \alpha_M, \beta_M \end{array} \right. \right)}{\prod_{k=1}^M \Gamma(\alpha_k) \Gamma(\beta_k)}. \quad (3.8)$$

The integral in Eq. (3.7) can be solved with the help of [59, eqn. (8.4.6.5)] in order to express the natural logarithm in terms of the Meijer's G-function (See Appendix A.3.1) and, then, we can obtain the approximate closed-form expression for the ergodic capacity of MISO FSO systems by using [58, eqn. (07.34.21.0012.01)] (See Appendix A.3.2) as follows

$$C_{\text{MISO}/B} \doteq \frac{\prod_{k=1}^M \varphi_k^2 H_{2+3M,2+M}^{1,2+3M} \left( 4\gamma \sqrt[M]{F} \left( \prod_{k=1}^M \frac{A_{0_k} L_k}{\alpha_k \beta_k} \right)^{\frac{2}{M}} \left| \begin{array}{c} (1, 1), (1, 1), \xi_1 \\ (1, 1), \xi_2, (0, 1) \end{array} \right. \right)}{\ln(4) \prod_{k=1}^M \Gamma(\alpha_k) \Gamma(\beta_k)}, \quad (3.9)$$

where  $\xi_1 = \{(1 - \varphi_1^2, \frac{2}{M}), (1 - \alpha_1, \frac{2}{M}), (1 - \beta_1, \frac{2}{M}), \dots, (1 - \varphi_M^2, \frac{2}{M}), (1 - \alpha_M, \frac{2}{M}), (1 - \beta_M, \frac{2}{M})\}$ ,  $\xi_2 = \{(-\varphi_1^2, \frac{2}{M}), \dots, (-\varphi_M^2, \frac{2}{M})\}$ , and  $H_{p,q}^{m,n}[\cdot]$  is the H-Fox function (See Appendix A.5). A computer program in Mathematica for the efficient implementation of the H-Fox function is given in [99, Appendix A] since this function is not available in software packages such as Maple<sup>TM</sup> and Wolfram Mathematica<sup>TM</sup>. Note that the above expression reduces to Eq. (2.52) when  $M$  is set to 1 and, hence,  $F$  is also equal to 1. Nevertheless, results obtained via H-Fox function will be checked through Monte Carlo simulation.

In order to observe how atmospheric turbulence and pointing errors impact on the ergodic capacity of MISO FSO communication systems, an asymptotic expression is derived to provide a deeper insight. It should be mentioned that an asymptotic ergodic expression can be derived from Eq. (3.9) by using the corresponding series expansion of the H-Fox function [100, Chapter 1]. However, this ergodic capacity analysis might not result in a closed-form expression and, hence, we cannot always obtain an asymptotic expression from its corresponding approximate closed-form expression. Within this context, from Eq. (3.7) and knowing that  $I_{LB} = I_1 \cdot I_2 \dots I_M$ , an asymptotic expression at high SNR can be readily



Table 3.1: Weather conditions for atmospheric turbulence.

Weather	Visibility (km)	$C_n^2 \times 10^{-14} \text{ m}^{-2/3}$
Haze	4	1.7 (Moderate turb.)
Clear	16	8 (Strong turb.)

and accurately lower-bounded due to the fact that  $\ln(1+z) \approx \ln(z)$  when  $z \rightarrow \infty$  as follows

$$C_{\text{MISO}/B}^H \doteq \frac{\ln(4\gamma)}{\ln(4)} + \frac{\ln(F)}{M \ln(2)} + \frac{1}{M \ln(2)} \sum_{k=1}^M \int_0^\infty \ln(i_k) f_{I_k}(i_k) di_k. \quad (3.10)$$

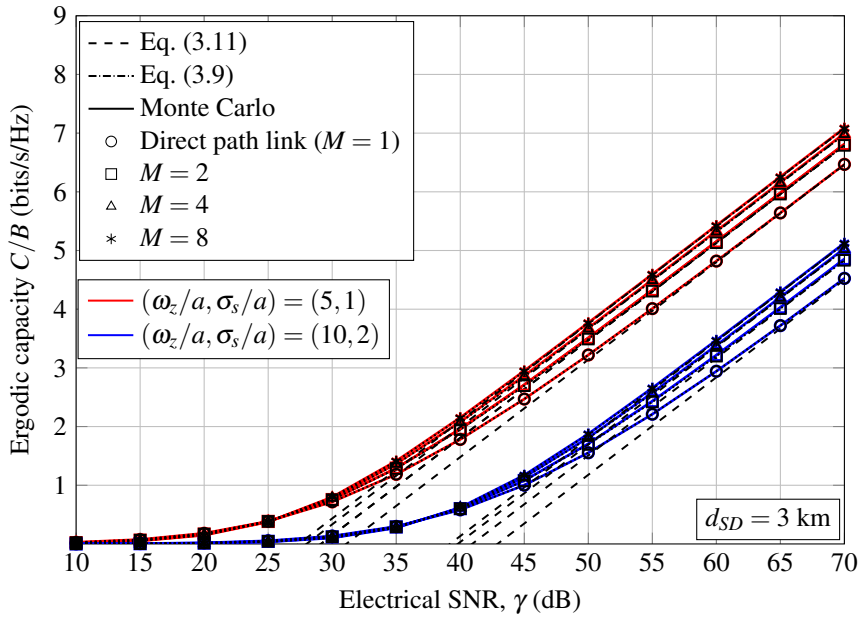
Note that the integral in Eq. (3.10) was resolved in Eq. (2.55) by applying that atmospheric turbulence and pointing errors are statistically independent. Therefore, the asymptotic closed-form expression for the ergodic capacity of MISO FSO systems can be seen in

$$C_{\text{MISO}/B}^H \doteq \frac{\ln(4\gamma)}{\ln(4)} + \frac{\ln(F)}{M \ln(2)} + \frac{1}{M \ln(2)} \times \sum_{k=1}^M \ln(L_k) + \ln\left(\frac{1}{\alpha_k \beta_k}\right) + \psi(\alpha_k) + \psi(\beta_k) + \ln(A_{0_k}) - \frac{1}{\varphi_k^2}. \quad (3.11)$$

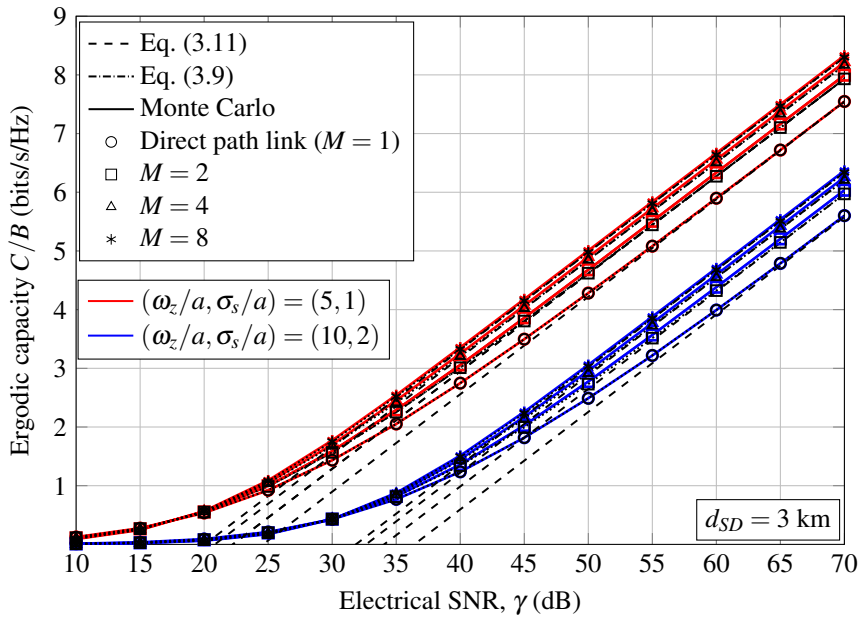
### 3.4.3 Numerical Results and Discussion

For the sake of simplicity, the numerical results have been computed for independent and identically distributed (i.i.d.) GG and misalignment fading channels. Due to the fact that the distance between lasers and the photodetector is several orders of magnitude the spacing among lasers, the MISO FSO channel can be considered as i.i.d, obtaining the similar results as in i.n.i.d. fading channels. At this point, it should, however, be noted that obtained expressions are for i.n.i.d. fading channels, and the subscripts are retained in order to present more general expressions which are totally valid for i.i.d. fading channels.

The corresponding results of this ergodic capacity analysis are depicted in Fig. 3.2 when different values of  $M = \{2, 4, 8\}$  are considered for a S-D link distance of  $d_{SD} = 3$  km. Additionally, we also include the performance analysis for the direct path link in order to establish the baseline performance that was analyzed in Chapter 2. Different weather conditions are adopted as shown in Table 3.1. Note that a spacing of 2.94 cm among the lasers is required under moderate turbulence as well as 1.16 cm under strong turbulence for plane wave propagation in order to consider uncorrelated fading in this analysis. Both spacing among the lasers at the transmitter are perfectly feasible in this MISO FSO communications system in order to consider that fading is approximately independent of one another. Pointing errors are present here assuming normalized beam width and normalized jitter



(a) Moderate turbulence.



(b) Strong turbulence.

Figure 3.2: Ergodic capacity for a S-D link distance of  $d_{SD} = 3$  km under different weather conditions. Different normalized beam width and normalized jitter values of  $(\omega_z/a, \sigma_s/a) = (5, 1)$  and  $(\omega_z/a, \sigma_s/a) = (10, 2)$  are assumed.

values of  $(\omega_z/a, \sigma_s/a) = (5, 1)$  and  $(\omega_z/a, \sigma_s/a) = (10, 2)$ . Monte Carlo simulation results are furthermore included as a reference. In addition, this figure shows a high accuracy of the asymptotic results based on the logarithm approximation at high SNR as given in Eq. (3.11). It is noteworthy to mention that the obtained results provide an excellent match between the analytical and the respective simulated results, which verify the high accuracy of the proposed approximation. In addition to this, it must be highlighted that the analytical ergodic capacity given in Eq. (3.9) is very precise in the entire SNR regime, i.e., from low to high SNR. As expected, the ergodic capacity of MISO FSO systems is proportional to the number of lasers, achieving a greater capacity as this number increases. Note that this improvement is no longer meaningful when the number of lasers is greater than four. At the same time, this capacity is decreased as pointing errors increase.

From previous results, the asymptotic ergodic capacity analysis can be extended in order to obtain a point where the expression in Eq. (3.11) intersects with the  $\gamma$ -axis ( $C/B = 0$  bits/s/Hz). This point can be understood as a SNR threshold, i.e.  $\gamma_{\text{MISO}}^{\text{th}}$ , in which the ergodic capacity of MISO FSO systems starts increasing. From Eq. (3.11), the corresponding expression of  $\gamma_{\text{MISO}}^{\text{th}}$  can be derived as

$$\begin{aligned} \gamma_{\text{MISO}}^{\text{th}}[dB] &= \frac{-20}{\ln(10)} \\ &\times \left( \frac{\ln(F)}{M} + \ln(2) + \frac{1}{M} \sum_{k=1}^M \psi(\alpha_k) + \psi(\beta_k) - \ln \left( \frac{\alpha_k \beta_k}{A_{0_k} L_k} \right) - \frac{1}{\varphi_k^2} \right). \end{aligned} \quad (3.12)$$

Similar to Eq. (3.12), we can also obtain the corresponding SNR threshold of the direct path link  $\gamma_{\text{DL}}^{\text{th}}$  when the parameter  $M$  is set to 1 as follows

$$\gamma_{\text{DL}}^{\text{th}}[dB] = \frac{-20}{\ln(10)} \left( \ln(2) + \psi(\alpha_{\text{DL}}) + \psi(\beta_{\text{DL}}) - \ln \left( \frac{\alpha_{\text{DL}} \beta_{\text{DL}}}{A_{0_{\text{DL}}} L_{\text{DL}}} \right) - \frac{1}{\varphi_{\text{DL}}^2} \right), \quad (3.13)$$

where  $\alpha_{\text{DL}}$ ,  $\beta_{\text{DL}}$ ,  $\varphi_{\text{DL}}^2$ ,  $A_{0_{\text{DL}}}$  and  $L_{\text{DL}}$  are the corresponding parameters of the direct path link. Next, taking into account that the shift of the ergodic capacity versus SNR is more relevant than the slope of the curve in SNR, this shift is interpreted as an improvement on ergodic capacity in order to maintain the same performance in terms of capacity with less SNR, as commented in Chapter 2. From Eqs. (3.12) and (3.13), we can obtain the improvement or gain of this MISO FSO system for i.i.d. fading channels in relation to the direct path link, i.e.  $G_{\text{MISO}}[dB]$ , as follows

$$G_{\text{MISO}}[dB] = \gamma_{\text{DL}}^{\text{th}}[dB] - \gamma_{\text{MISO}}^{\text{th}}[dB] = \frac{20 \ln(F)}{M \ln(10)}. \quad (3.14)$$

The expression in Eq. (3.14) has been derived for i.i.d. fading channels in order to observe the impact of the number of lasers on MISO FSO systems. For a better understanding of the impact of  $G_{\text{MISO}}[dB]$  on MISO FSO systems, this gain is plotted in Fig. 3.3 as a function of the S-D link distance when a normalized beam width value of  $\omega_z/a = 7$  and normalized jitter values of  $\sigma_s/a = \{1, 3, 4\}$  are considered along with different values of  $M = \{2, 6\}$ . As

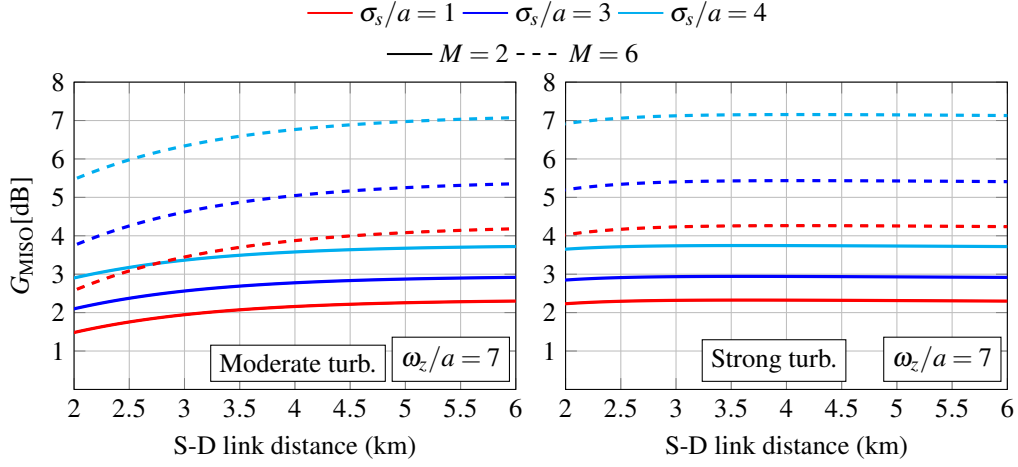


Figure 3.3: Gain for different weather conditions when a normalized beam width value of  $\omega_z/a = 7$  and different normalized jitter values of  $\sigma_s/a = \{1, 3, 4\}$  are assumed.

expected, the ergodic capacity of MISO FSO systems not only depends on the number of laser sources, but also on the severity of pointing errors. The ergodic capacity is significantly increased as the number of lasers increases. Furthermore, a greater gain can be achieved as normalized jitter values increase, showing an excellent robustness against pointing errors and atmospheric turbulence. It must also be commented that the gain is less vulnerable as the S-D link distance increases under strong turbulence conditions.

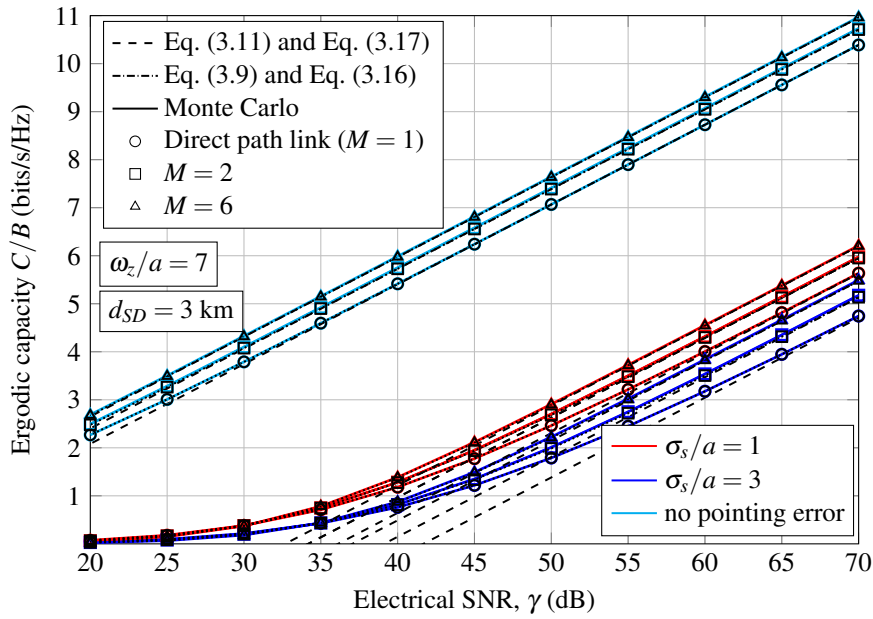
These results show a relevant impact of pointing errors on the ergodic capacity of MISO FSO systems. Knowing that the impact of pointing errors in our analysis can be suppressed by assuming  $A_0 \rightarrow 1$  and  $\varphi^2 \rightarrow \infty$  [53], the corresponding ergodic capacity expression with no pointing errors is derived from Eq. (3.9). This expression can easily be obtained from the definition of the H-Fox function (See Appendix A.5) by using the following property  $z\Gamma(z) = \Gamma(z+1)$  (See Appendix A.1) as

$$\prod_{k=1}^M \lim_{\varphi_k^2 \rightarrow +\infty} \frac{\Gamma(\varphi_k^2 + 1) \Gamma(\varphi_k^2 - \frac{2s}{M})}{\Gamma(\varphi_k^2) \Gamma(1 + \varphi_k^2 - \frac{2s}{M})} = \prod_{k=1}^M \lim_{\varphi_k^2 \rightarrow +\infty} \frac{M\varphi_k^2}{M\varphi_k^2 - 2s} = 1. \quad (3.15)$$

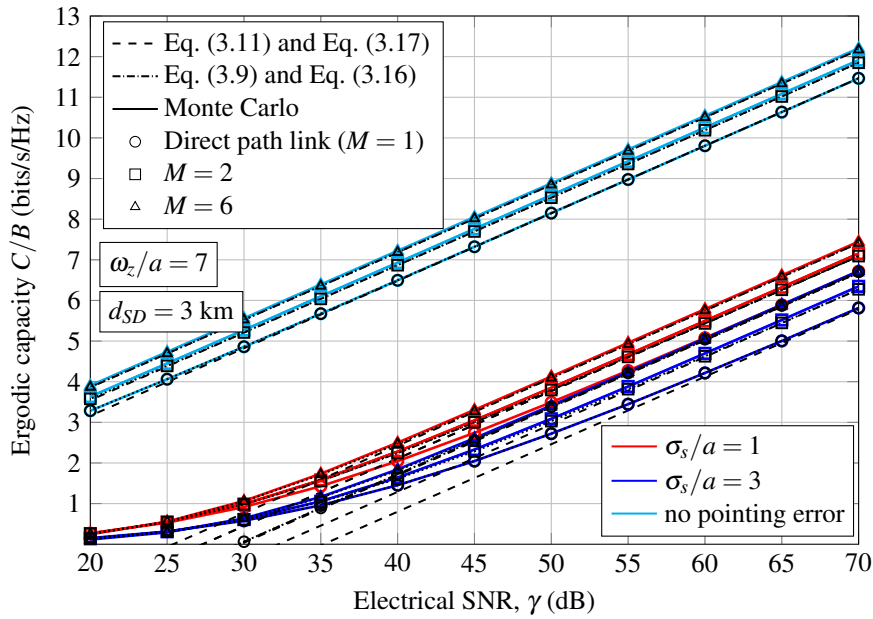
Hence, the approximate closed-form expression for the ergodic capacity of MISO FSO systems with no pointing errors  $C_{\text{MISO}}^{\text{npe}}$  is obtained as

$$C_{\text{MISO}}^{\text{npe}}/B \approx \frac{H_{2+2M,2}^{1,2+2M} \left( 4\gamma \sqrt{F^{\text{npe}}} \left( \prod_{k=1}^M \frac{L_k}{\alpha_k \beta_k} \right)^{\frac{2}{M}} \middle| \begin{matrix} (1,1), (1,1), \xi_3 \\ (1,1), (0,1) \end{matrix} \right)}{\ln(4) \prod_{k=1}^M \Gamma(\alpha_k) \Gamma(\beta_k)}, \quad (3.16)$$

where  $\xi_3 = \{(1 - \alpha_1, \frac{2}{M}), (1 - \beta_1, \frac{2}{M}), \dots, (1 - \alpha_M, \frac{2}{M}), (1 - \beta_M, \frac{2}{M})\}$  and  $F^{\text{npe}}$  is the correcting factor when pointing error effects are suppressed (See Appendix B.1). Similar to



(a) Moderate turbulence.



(b) Strong turbulence.

Figure 3.4: Ergodic capacity for a S-D link distance of  $d_{SD} = 3$  km under different weather conditions. A normalized beam width value of  $\omega_z/a = 7$  and different normalized jitter values of  $\sigma_s/a = \{1, 3\}$  are assumed.

Eq. (3.11), we can also obtain the asymptotic ergodic capacity expression of MISO FSO systems with no pointing errors as follows

$$C_{\text{MISO}}^{H_{\text{nppe}}}/B \doteq \frac{\ln(4\gamma)}{\ln(4)} + \frac{\ln(F^{\text{nppe}})}{M \ln(2)} + \frac{1}{M \ln(2)} \sum_{k=1}^M \psi(\alpha_k) + \psi(\beta_k) - \ln\left(\frac{\alpha_k \beta_k}{L_k}\right). \quad (3.17)$$

At the same time, we can derive the corresponding SNR threshold of MISO FSO systems with no pointing errors  $\gamma_{\text{MISO}}^{\text{th}_{\text{nppe}}}$  as in Eq. (3.12) as follows

$$\gamma_{\text{MISO}}^{\text{th}_{\text{nppe}}}[dB] = \frac{-20}{\ln(10)} \left( \frac{\ln(F^{\text{nppe}})}{M} + \ln(2) + \frac{1}{M} \sum_{k=1}^M \psi(\alpha_k) + \psi(\beta_k) - \ln\left(\frac{\alpha_k \beta_k}{L_k}\right) \right). \quad (3.18)$$

Conclusions obtained in Fig. 3.2 are contrasted in Fig. 3.4, where the effect of misalignment on the ergodic capacity of MISO FSO systems is evaluated when different values of  $M = \{2, 6\}$  are considered for a S-D link distance of  $d_{SD} = 3$  km. Here, the performance analysis for the direct path link is also included as well as the results when pointing errors are not considered. Pointing errors are present assuming a normalized beam width value of  $\omega_z/a = 7$  and normalized jitter values of  $\sigma_s/a = \{1, 3\}$ . It can be observed that the ergodic capacity of this MISO FSO system is dramatically decreased as normalized jitter values increase. Finally, from Eqs. (3.12) and (3.18), the impact of pointing error effects translates into a loss  $Loss_{pe}[dB]$  relative to this MISO FSO system without misalignment fading given by

$$\begin{aligned} Loss_{pe}[dB] &\triangleq \gamma_{\text{MISO}}^{\text{th}}[dB] - \gamma_{\text{MISO}}^{\text{th}_{\text{nppe}}}[dB] \\ &= \frac{20}{M \ln(10)} \left( \ln\left(\frac{F^{\text{nppe}}}{F}\right) + \sum_{k=1}^M \frac{1}{\varphi_k^2} - \ln(A_{0_k}) \right). \end{aligned} \quad (3.19)$$

The expression in Eq. (3.19) can be simplified for i.i.d. fading channels as

$$Loss_{pe}[dB] \triangleq \frac{20}{\ln(10)} \left( M \ln\left(\frac{M\varphi^2}{M\varphi^2 + 1}\right) + \ln\left(\frac{\varphi^2 + 1}{\varphi^2}\right) + \frac{1}{\varphi^2} - \ln(A_0) \right). \quad (3.20)$$

The above expression only depends on the number of laser sources and pointing error parameters. According to Eq. (3.20), it can be seen in Fig. 3.4 that a loss of 28.65 dB is achieved for  $M = \{2, 6\}$  when normalized beam width and normalized jitter values of  $(\omega_z/a, \sigma_s/a) = (7, 1)$  are assumed for moderate turbulence, and a loss of 33 dB is achieved for  $M = \{2, 6\}$  when normalized beam width and normalized jitter values of  $(\omega_z/a, \sigma_s/a) = (7, 3)$  are assumed for strong turbulence.

### 3.5 Ergodic Capacity of MIMO FSO Systems

In order to generalize the results obtained in the previous section, the ergodic capacity analysis is carried out for SIMO and MIMO FSO systems over different atmospheric turbulence

models and under the presence of nonzero boresight pointing errors. The effect of nonzero boresight is a new feature of this study. To the best of our knowledge, there are no reported works that take into consideration the effect of nonzero boresight pointing errors on the performance of SIMO and MIMO FSO systems. So far, the effect of nonzero boresight pointing error was only considered for FSO links, i.e., SISO FSO systems in [50, 72, 101]. Next, the nonzero boresight pointing error model is briefly reviewed.

### Nonzero Boresight Pointing Error Model

The effect of pointing errors consists of three essential parameters: beam width, jitter and boresight displacement. The beam width represents the beam waist (radius computed at  $e^{-2}$ ), the jitter represents the random offset of the beam center at receive aperture plane and the boresight represents the fixed displacement between beam center and the alignment point.

Regarding boresight displacements, there are two kinds of boresight displacements: the inherent boresight displacement and the additional boresight error.

**Inherent boresight displacement** This inherent boresight displacement is related to the spacing among receive apertures at the receiver. This inherent boresight displacement represents a fixed distance, i.e., the distance between each receive aperture and the corresponding alignment point.

**Additional boresight error** The additional boresight error is due to the thermal expansion of the building, which was defined in [56].

Although an FSO communication system can be installed with an additional boresight error close to zero or even negligible, the inherent boresight displacement must necessarily always be taken into account at the receiver when more than one receive aperture is assumed in order to increase the performance by using receive-diversity. The latter is due to the fact that each laser can be aligned with only one receive aperture and, hence, there is an inherent boresight displacement that depends on the spacing among receive apertures, the corresponding alignment point as well as the geometric arrangement of the receive apertures.

We use a model of misalignment fading given in [53] and commented in Chapter 2, which was extended in [56] to take into account the boresight displacement at the receiver. Therefore, assuming a Gaussian spatial intensity profile of beam waist radius  $\omega_z$  on the receiver plane at distance  $z$  from the transmitter and a circular receive aperture of radius  $a$ , the PDF of nonzero boresight pointing errors was derived in [56] as

$$f_{I_p}(i) = \frac{\varphi^2 i^{\varphi^2-1}}{A_0^{\varphi^2}} \exp\left(-\frac{s^2}{2\sigma_s^2}\right) I_0\left(\frac{s}{\sigma_s} \sqrt{-2\varphi^2 \ln\left(\frac{i}{A_0}\right)}\right), \quad 0 \leq i \leq A_0 \quad (3.21)$$

where  $s$  is the boresight displacement, and  $I_0(\cdot)$  is the modified Bessel function of the first kind with order zero [62, eqn. (8.431.1)]. The rest of parameters are the same ones as commented in Chapter 2. Note that the PDF in Eq. (3.21) reduces to the pointing errors model proposed in [53] when zero boresight pointing error is considered, i.e.  $s = 0$ , as follows

$$f_{I_p}(i) = \frac{\varphi^2}{A_0 \varphi^2} i^{\varphi^2 - 1}, \quad 0 \leq i \leq A_0. \quad (3.22)$$

### 3.5.1 System Model

Let us adopt a MIMO FSO communications system with  $M$  transmitters or laser sources and  $N$  receive apertures, and EGC reception at the receiver. An example of a MIMO FSO system with  $M = 2$  and  $N = 5$  is depicted in Fig. 3.5. In that figure, all lasers are aligned with the centroid (alignment point located in  $p_c = (x_c, y_c) = (0, 0)$ ) of the geometric arrangement (trapezium) of the receive apertures. It must be noted that all receive apertures

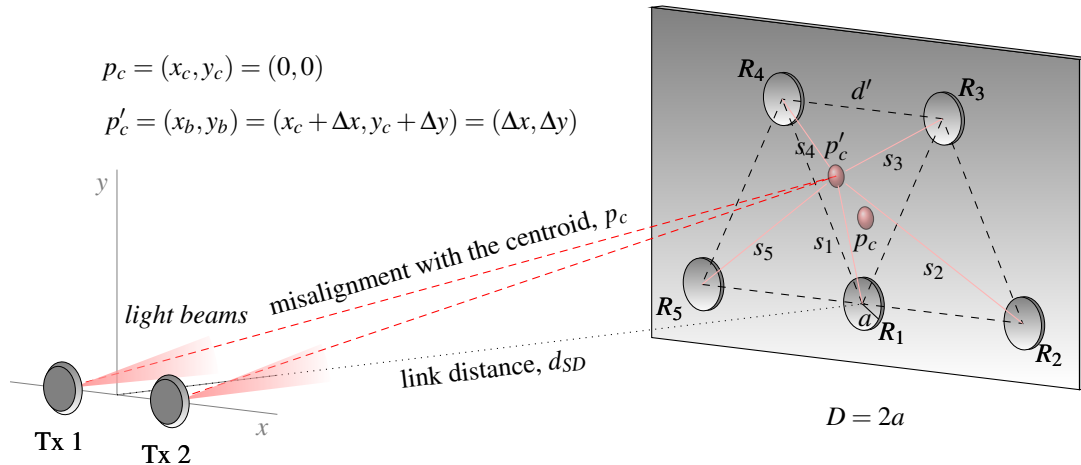


Figure 3.5: Block diagram of the considered MIMO FSO communications system.

are separated by a fixed distance equals  $d'$  (as shown in Fig. 2.1 in black dashed line) in order to consider uncorrelated fading, which depends on the atmospheric coherence length  $r_0$ . On the one hand, the minimum value of the spacing among receive apertures is equal to  $d' = r_0$  to assume uncorrelated fading as long as this spacing is technically feasible for potential FSO applications. On the other hand, a greater spacing among receive apertures leads to an increase in the inherent boresight displacement at the receiver plane. Additionally, the laser sources are separated by a fixed distance so that uncorrelated fading can also be considered at the transmitter [94, 95]. Before evaluating the corresponding expression of the total boresight displacement, i.e. taking into account both the inherent boresight displacement and the additional boresight error, we firstly obtain the expression of the inherent boresight displacement assuming that the additional boresight error equals zero. In other words,



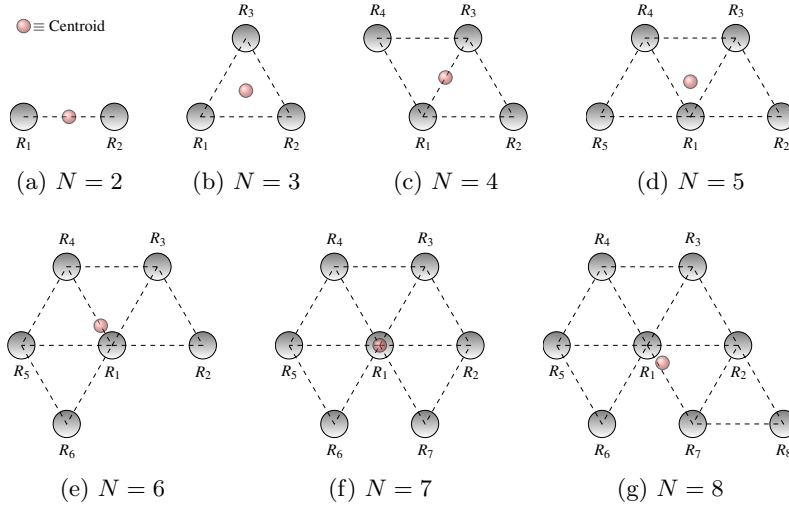


Figure 3.6: Different geometric arrangement for the receiver from the juxtaposition of equilateral triangles.

assuming that  $p_c = p'_c$ . In this case, the inherent boresight displacement is equal to the Euclidean distance between each receive aperture and the corresponding alignment point, i.e. the centroid  $p_c$ , which is defined as  $d_{R_k-p_c}$  for  $k = 1 \dots N$ . Hence, the boresight displacement is given by  $s_k = d_{R_k-p_c}$ . In order to add the additional boresight error to this analysis, we have to rewrite the expression of  $s_k$  but considering a nonzero additional boresight error. When there is a nonzero additional boresight error, the alignment point becomes  $p'_c$  instead of  $p_c$ . Hence, knowing that  $p'_c = (x_c + \Delta x, y_c + \Delta y) = (\Delta x, \Delta y)$ , it can easily be deduced that the corresponding expression of the total boresight displacement of each receiver aperture when all lasers are aligned with the centroid is given by

$$s_k = \sqrt{d_{R_k-p_c}^2 + \Delta x^2 + \Delta y^2 - 2(\Delta x \cdot x_k + \Delta y \cdot y_k)}, \quad k = 1 \dots N \quad (3.23)$$

where  $(x_k, y_k)$  represents the corresponding receive aperture location of  $R_k$  for  $k = 1 \dots N$ . The additional boresight error ( $s_{AB}$ ) is given by the Euclidean distance between  $p_c$  and  $p'_c$ , i.e.  $s_{AB} = \sqrt{\Delta x^2 + \Delta y^2}$ .

### Analysis of the Proposed Geometric Arrangement for the Receiver

With the goal of reducing the effect of the inherent boresight displacement, we propose an interesting solution for the geometric arrangement at the receiver, as shown in Fig. 3.6, from the juxtaposition of equilateral triangles, and considering the centroid of each figure as an alignment point in order to balance the distance between the alignment point and each receive aperture. Firstly, we start with the easiest case, i.e. the case of two receive

apertures, which are separated by a distance equals  $d'$ , as shown in Fig. 3.6(a). Note that the distance  $d'$  should sufficiently be larger than the atmospheric coherence length in order to assume uncorrelated fading. In order to add one more receive aperture to the geometric arrangement, the next formed figure should be an equilateral triangle, where all receive apertures are at the same distance as shown in Fig. 3.6(b), and, hence, the inherent boresight displacement is reduced. The following formed figure is a diamond, as shown in Fig. 3.6(c), which is generated from the juxtaposition of two equilateral triangles. It is noteworthy to mention that the total area formed by all receive apertures is also reduced. And the next one is a trapezium, as shown in Fig. 3.6(d), when there are five receive apertures at the receiver. This method consists of adding receive apertures to the receiver always around the centroid of the formed geometric arrangement, and so on.

### 3.5.2 Performance Analysis

In this section, the ergodic capacity of MIMO FSO systems is evaluated over LN, GG and EW fading channels with nonzero boresight pointing errors. As in MISO FSO systems, EGC reception is used at the receiver and, hence, the statistical channel model can be written, as in [102], as

$$Y = \frac{X}{MN} \sum_{k=1}^M \sum_{l=1}^N I_{kl} + Z_{\text{EGC}}, \quad Z_{\text{EGC}} \sim N(0, N_0/2), \quad (3.24)$$

where  $I_{kl}$  represents the equivalent irradiance through the optical channel between the  $k$ th transmit aperture and the  $l$ th receive aperture. Here, the division by  $M$  is also considered in Eq. (3.24) to maintain the average optical power in the air at a constant level of  $P_t$ , being transmitted by each laser an average optical power  $P_t/M$  as in MISO FSO systems. Furthermore, the division by  $N$  is considered to ensure that the area of the receive aperture in SISO FSO systems has the same size as in the sum of  $N$  receive aperture areas [103]. The resulting received electrical SNR  $\gamma_{\text{MIMO}}$  can be defined as follows

$$\gamma_{\text{MIMO}} = \frac{1}{2} \frac{(2P_t \sqrt{T_b}/MN)^2}{N_0/2} \left( \sum_{k=1}^M \sum_{l=1}^N I_{kl} \right)^2 = \frac{4\gamma}{M^2 N^2} \left( \sum_{k=1}^M \sum_{l=1}^N I_{kl} \right)^2 = \frac{4\gamma}{M^2 N^2} I_T^2, \quad (3.25)$$

where  $I_T$  is the total channel gain. Assuming instantaneous CSI at the receiver, the ergodic capacity of the considered MIMO FSO system in bits/s/Hz can be obtained as in Eq. (2.51) as follows

$$C_{\text{MIMO}}/B = \frac{1}{\ln(4)} \underbrace{\int_0^\infty \cdots \int_0^\infty}_{\text{MN-fold}} \ln \left( 1 + \frac{4\gamma}{M^2 N^2} \left( \sum_{k=1}^M \sum_{l=1}^N i_{kl} \right)^2 \right) \prod_{k=1}^M \prod_{l=1}^N f_{I_{kl}}(i_{kl}) di_{kl}, \quad (3.26)$$

where  $f_{I_{kl}}(i_{kl})$  represents the combined PDF of the equivalent irradiance through the optical channel between the  $k$ th transmit aperture and the  $l$ th receive aperture. It must be noted that deriving the PDF of  $I_T = \sum_{k=1}^M \sum_{l=1}^N I_{kl}$  is tedious, if not impossible, and not readily

tractable due to the difficulty in finding its statistics. Hence, a lower bound for this sum can also be obtained here by using the inequality between AM and GM as in the previous section, i.e.  $AM \geq GM$ , where  $AM = (1/MN) \sum_{k=1}^M \sum_{l=1}^N I_{kl}$  and  $GM = \sqrt[MN]{\prod_{k=1}^M \prod_{l=1}^N I_{kl}}$  are the arithmetic and geometric means, respectively. Therefore, a lower bound for the sum of  $MN$  RVs can be obtained as

$$\sum_{k=1}^M \sum_{l=1}^N I_{kl} \geq MN \sqrt[MN]{F \cdot \prod_{k=1}^M \prod_{l=1}^N I_{kl}}. \quad (3.27)$$

As in previous section, a correcting factor  $F$  is also used here in order to obtain a good approximation of the ergodic capacity analysis of MIMO FSO systems. The correcting factor  $F$  can be derived from Eq. (3.27) as follows

$$F = \frac{\mathbb{E} \left[ \sum_{k=1}^M \sum_{l=1}^N I_{kl} \right]^{MN}}{(MN)^{MN} \cdot \mathbb{E} \left[ \sqrt[MN]{\prod_{k=1}^M \prod_{l=1}^N I_{kl}} \right]^{MN}}, \quad (3.28)$$

and can be seen in more detail in Appendix B.2. Note that Eq. (3.28) reduces to Eq. (3.6) when the number of receiver apertures equals one, i.e,  $N = 1$ . Now, substituting Eq. (3.27) into Eq. (3.26) and, after performing some algebraic manipulations, the ergodic capacity of MIMO FSO systems can accurately be approximated as follows

$$C_{\text{MIMO}}/B \approx \frac{1}{\ln(4)} \times \underbrace{\int_0^\infty \cdots \int_0^\infty}_{\text{MN-fold}} \ln \left( 1 + 4\gamma F^{\frac{2}{MN}} \left( \prod_{k=1}^M \prod_{l=1}^N i_{kl} \right)^{\frac{2}{MN}} \right) \prod_{k=1}^M \prod_{l=1}^N f_{I_{kl}}(i_{kl}) di_{kl}. \quad (3.29)$$

To the best of our knowledge, the integral in Eq. (3.29) is highly complex to find an exact solution even might not be expressed in closed-form. For this reason, an asymptotic analysis is carried out and, hence, simple closed-form expressions are derived for MIMO FSO systems. An asymptotic expression at high SNR can be readily and accurately lower-bounded due to the fact that  $\ln(1+z) \approx \ln(z)$  when  $z \rightarrow \infty$  as follows

$$C_{\text{MIMO}}/B \doteq \frac{1}{\ln(4)} \underbrace{\int_0^\infty \cdots \int_0^\infty}_{\text{MN-fold}} \ln \left( 4\gamma F^{\frac{2}{MN}} \left( \prod_{k=1}^M \prod_{l=1}^N i_{kl} \right)^{\frac{2}{MN}} \right) \prod_{k=1}^M \prod_{l=1}^N f_{I_{kl}}(i_{kl}) di_{kl}. \quad (3.30)$$

We can rewrite the above integral as follows

$$C_{\text{MIMO}}/B \doteq \frac{\ln(4\gamma_0)}{\ln(4)} + \frac{\ln(F)}{MN \ln(2)} + \frac{1}{MN \ln(2)} \sum_{k=1}^M \sum_{l=1}^N \underbrace{\int_0^\infty \ln(i_{kl}) f_{I_{kl}}(i_{kl}) di_{kl}}_{\text{INT}}. \quad (3.31)$$

Knowing that atmospheric turbulence and pointing errors are statistically independent, the integral  $INT$  in Eq. (3.31) can be rewritten as follows

$$\begin{aligned}
INT &= \int_0^\infty \ln(i_{kl}) f_{I_{kl}}(i_{kl}) di_{kl} \\
&= \int_0^\infty \int_0^{A_{0kl}} \ln(L_{kl} \cdot i_{kl}^a \cdot i_{kl}^p) f_{I_{kl}^a}(i_{kl}^a) f_{I_{kl}^p}(i_{kl}^p) di_{kl}^a di_{kl}^p \\
&= \ln(L_{kl}) + \underbrace{\int_0^\infty \ln(i_{kl}^a) f_{I_{kl}^a}(i_{kl}^a) di_{kl}^a}_{INT_1} + \underbrace{\int_0^{A_{0kl}} \ln(i_{kl}^p) f_{I_{kl}^p}(i_{kl}^p) di_{kl}^p}_{INT_2} \\
&= \ln(L_{kl}) + INT_1 + INT_2.
\end{aligned} \tag{3.32}$$

Firstly, we derive  $INT_2$  in Eq. (3.32) (See Appendix A.10) as follows

$$INT_2 = \int_0^{A_{0kl}} \ln(i_{kl}^p) f_{I_{kl}^p}(i_{kl}^p) di_{kl}^p = \ln(A_{0kl}) - \frac{1}{\varphi_{kl}^2} - \frac{s_{kl}^2}{2\sigma_{s_{kl}}^2 \varphi_{kl}^2}. \tag{3.33}$$

Secondly, we solve the integral  $INT_1$  in Eq. (3.32) for each atmospheric turbulence model considered in the analysis of MIMO FSO systems, i.e., LN, GG and EW. In the case of GG model, this one was already solved in Eq. (2.57). Hence, the asymptotic closed-form expression for the ergodic capacity of MIMO FSO systems over GG fading channels with nonzero boresight pointing errors can be expressed as

$$\begin{aligned}
C_{\text{MIMO}/B}^{\text{GG}} &\doteq \frac{\ln(4\gamma)}{\ln(4)} + \frac{\ln(F)}{MN \ln(2)} + \frac{1}{MN \ln(2)} \\
&\times \sum_{k=1}^M \sum_{l=1}^N \ln\left(\frac{L_{kl}}{\alpha_{kl}\beta_{kl}}\right) + \psi(\alpha_{kl}) + \psi(\beta_{kl}) + \ln(A_{0kl}) - \frac{1}{\varphi_{kl}^2} - \frac{s_{kl}^2}{2\sigma_{s_{kl}}^2 \varphi_{kl}^2}.
\end{aligned} \tag{3.34}$$

In the case of LN model, by making a change of variable  $t = \ln(x)$ , it can easily be deduced that the result of integral  $INT_1$  is  $INT_1 = -\sigma_{R_{kl}}^2/2$ . Hence, the asymptotic closed-form expression for the ergodic capacity of MIMO FSO systems over LN fading channels with nonzero boresight pointing errors can be expressed as

$$\begin{aligned}
C_{\text{MIMO}/B}^{\text{LN}} &\doteq \frac{\ln(4\gamma)}{\ln(4)} + \frac{\ln(F)}{MN \ln(2)} + \frac{1}{MN \ln(2)} \\
&\times \sum_{k=1}^M \sum_{l=1}^N \ln(L_{kl}) - \frac{\sigma_{R_{kl}}^2}{2} + \ln(A_{0kl}) - \frac{1}{\varphi_{kl}^2} - \frac{s_{kl}^2}{2\sigma_{s_{kl}}^2 \varphi_{kl}^2}.
\end{aligned} \tag{3.35}$$

In the case of EW model, we write the corresponding integral  $INT_1$  as follows

$$\begin{aligned}
INT_1 &= \frac{m_1 m_2}{m_3} \\
&\times \int_0^\infty \ln(i) \left(\frac{i}{m_3}\right)^{m_2-1} \exp\left(-\left(\frac{i}{m_3}\right)^{m_2}\right) \left\{1 - \exp\left(-\left(\frac{i}{m_3}\right)^{m_2}\right)\right\}^{m_1-1} di.
\end{aligned} \tag{3.36}$$

By using the corresponding series expansion of  $(1 + e^x)^\alpha$  as follows

$$(1 + e^x)^\alpha = \sum_{k=1}^{\infty} \frac{\Gamma(\alpha + 1)e^{xk}}{k!\Gamma(\alpha - k + 1)}, \quad (3.37)$$

we can rewrite the integral in Eq. (3.36) as

$$\begin{aligned} INT_1 &= \frac{m_2 \Gamma(m_1 + 1)}{m_3^{m_2}} \\ &\times \sum_{k=0}^{\infty} \frac{(-1)^k}{k! \Gamma(m_1 - k)} \int_0^{\infty} \ln(i) i^{m_2 - 1} \exp\left(- (k + 1) \left(\frac{i}{m_3}\right)^{m_2}\right) di. \end{aligned} \quad (3.38)$$

To evaluate the above integral, we can make a change of variable  $x = i^{m_2}$  and, then, we can use [62, eqn. (4.352.1)] (See Appendix A.9) to derive the following expression

$$\begin{aligned} INT_1 &= g(m_{1_{kl}}, m_{2_{kl}}, m_{3_{kl}}) \\ &= \frac{\Gamma(m_{1_{kl}} + 1)}{m_{2_{kl}}} \sum_{i=0}^{\infty} \frac{(-1)^i \left(\psi(1) - \ln\left((i + 1) \left(\frac{1}{m_{3_{kl}}}\right)^{m_{2_{kl}}}\right)\right)}{\Gamma(i + 2) \Gamma(m_{1_{kl}} - i)}, \end{aligned} \quad (3.39)$$

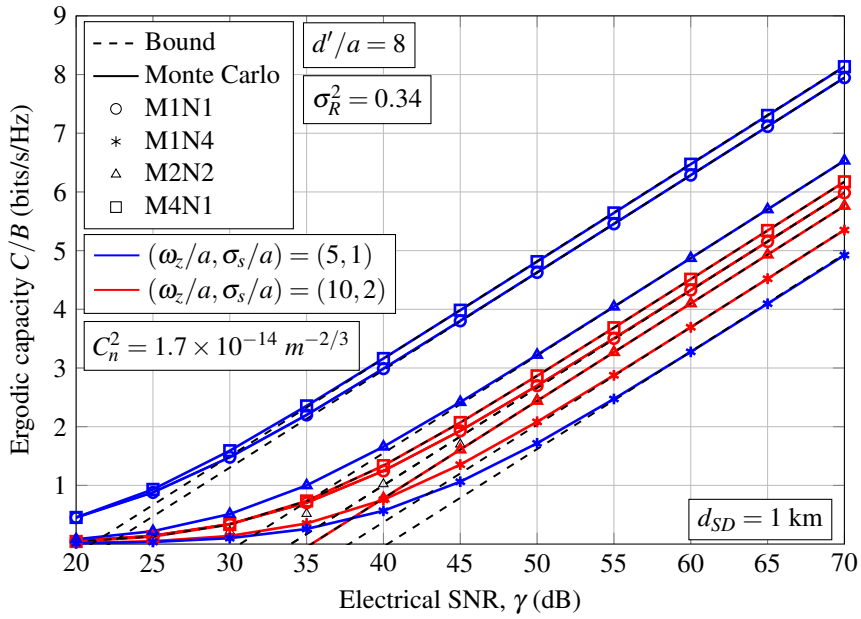
where  $-\psi(1)$  is the Euler's constant. Note that Eq. (3.39) can easily be computed as the series converges fast, and usually as much as 20 terms or less are sufficient for the series to converge. Now, substituting Eq. (3.39) into Eq. (3.31), we can obtain the corresponding asymptotic closed-form expression for the ergodic capacity of MIMO FSO systems over EW fading channels with nonzero boresight pointing errors as

$$\begin{aligned} C_{\text{MIMO}}^{\text{EW}}/B &\doteq \frac{\ln(4\gamma)}{\ln(4)} + \frac{\ln(F)}{MN \ln(2)} + \frac{1}{MN \ln(2)} \\ &\times \sum_{k=1}^M \sum_{l=1}^N \ln(L_{kl}) + g(m_{1_{kl}}, m_{2_{kl}}, m_{3_{kl}}) + \ln(A_{0_{kl}}) - \frac{1}{\varphi_{kl}^2} - \frac{s_{kl}^2}{2\sigma_{s_{kl}}^2 \varphi_{kl}^2}. \end{aligned} \quad (3.40)$$

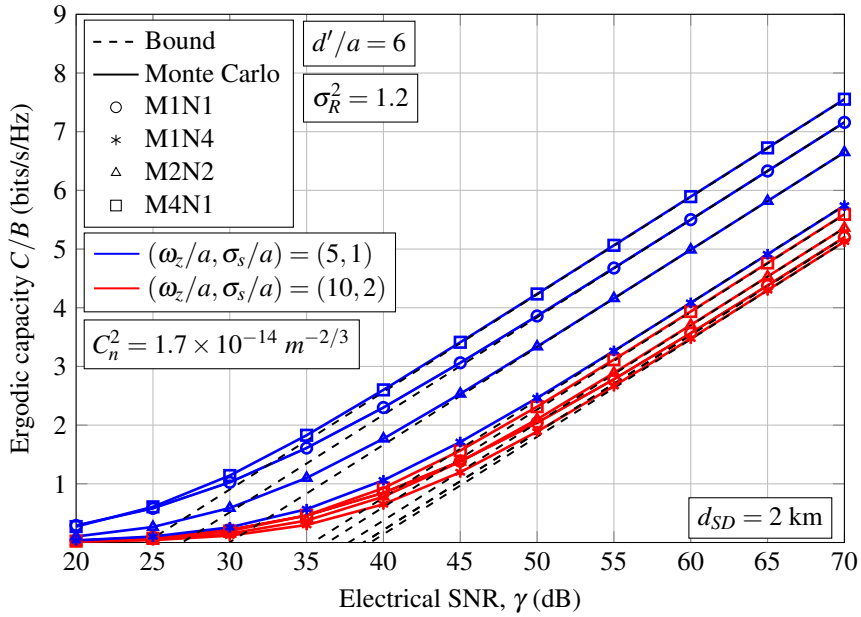
### 3.5.3 Numerical Results and Discussion

As in MISO FSO systems, the numerical results are evaluated for i.i.d. atmospheric turbulence channels with pointing errors but considering nonzero inherent boresight displacement and zero additional boresight error, i.e.  $(\Delta x, \Delta y) = (0, 0)$ . In other words, the alignment point is  $p_c = p'_c$  as shown in Fig. 3.5. The impact of nonzero additional boresight error will be studied at the end of this subsection.

As an illustration of the obtained expressions, numerical results over LN, GG and EW fading channels are depicted in Figs. 3.7(a), 3.7(b) and 3.8, respectively. Without loss of generality, we consider some scenarios as case study of MISO, SIMO and MIMO FSO systems when all transmit lasers are aligned with the centroid of the geometric arrangement at the receiver. In this way, different values of  $M$  and  $N$  are taken into account in order to

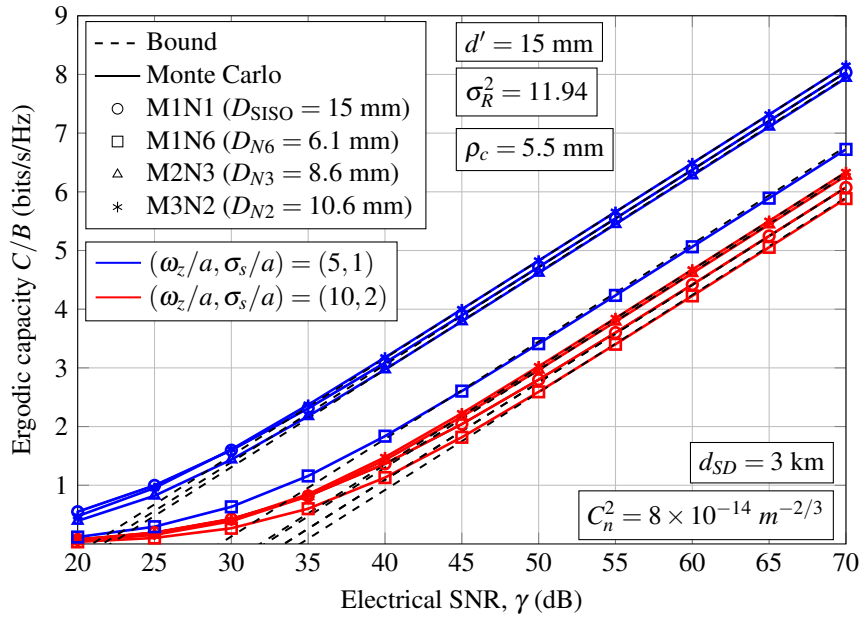


(a) LN atmospheric turbulence.

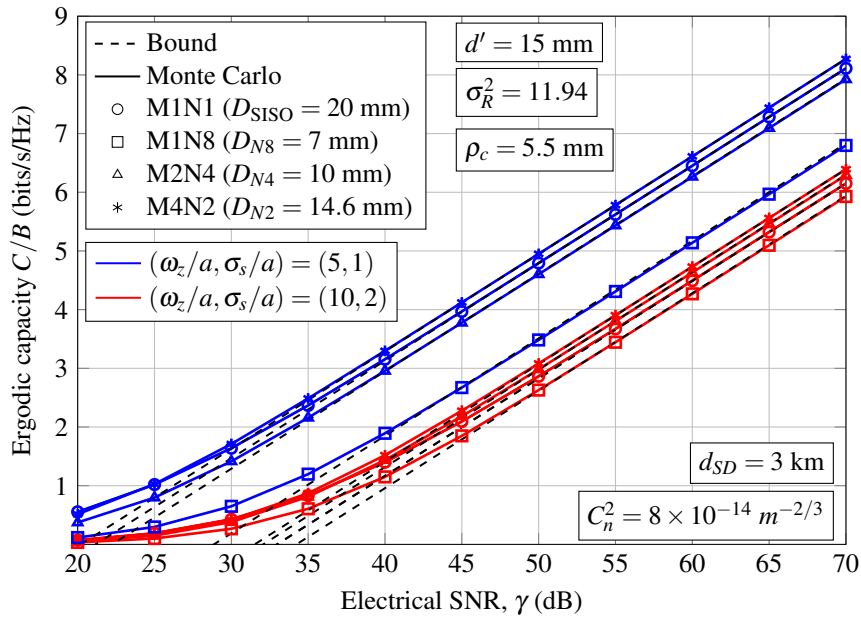


(b) GG atmospheric turbulence.

Figure 3.7: Asymptotic ergodic capacity of MIMO FSO systems when (a) LN and (b) GG atmospheric turbulence models are assumed for different normalized beam width and normalized jitter values of  $(\omega_z/a, \sigma_s/a) = \{(5, 1), (10, 2)\}$  as well as different normalized spacing values among receive apertures of  $d'/a = \{6, 8\}$ .



(a) EW atmospheric turbulence.



(b) EW atmospheric turbulence.

Figure 3.8: Asymptotic ergodic capacity of MIMO FSO systems over EW atmospheric turbulence for different normalized beam width and normalized jitter values of  $(\omega_z/a, \sigma_s/a) = \{(5, 1), (10, 2)\}$ .

analyze how the effect of nonzero inherent boresight pointing errors impacts on the ergodic capacity of SIMO and MIMO FSO systems when point-like receiver apertures are considered for LN and GG atmospheric turbulence, i.e.,  $D \leq \rho_c$  and, when aperture averaging takes place for EW, i.e.,  $D \geq \rho_c$ . Different weather conditions are adopted as shown in Table 3.1. Pointing errors are present assuming normalized beam width and normalized jitter values of  $(\omega_z/a, \sigma_s/a) = (5, 1)$  and  $(\omega_z/a, \sigma_s/a) = (10, 2)$ . A S-D link distance of  $d_{SD} = 1$  km and a normalized spacing value among receiver apertures of  $d'/a = 8$  as well as a S-D link distance of  $d_{SD} = 2$  km and a normalized spacing value among receiver apertures of  $d'/a = 6$  are considered for LN and GG atmospheric turbulence, respectively. Analogously, a S-D link distance of  $d_{SD} = 3$  km as well as a spacing value among receiver apertures of  $d' = 15$  mm are considered when the diameter  $D_{\text{SISO}}$  of the receive aperture corresponding to the SISO FSO system is set to 15 mm and 20 mm for EW atmospheric turbulence. The corresponding radius of SIMO and MIMO FSO systems is equal to  $D_N = D_{\text{SISO}}/\sqrt{N}$ . As can be observed, the aperture averaging always takes place since the condition  $D \geq \rho_c$  always holds for EW model. These aperture sizes can be used for commercial FSO applications that requires high speed optical detectors [104]. Additionally, we also include the performance analysis for the direct path link in order to establish the baseline performance. Monte Carlo simulation results are furthermore included as a reference.

It is noteworthy to mention that the obtained results provide an excellent match between the analytical and the respective Monte Carlo simulation results, which are obtained from Eq. (3.26), and, hence, verifying the high accuracy of the proposed approximation. As can be seen in Fig. 3.7, a MISO FSO system present a much better performance than SIMO and MIMO FSO systems in terms of the ergodic capacity, keeping the product  $M \cdot N = 4$  and not considering the additional boresight error. It must be noted that both SIMO and MIMO present a nonzero inherent boresight displacement, which depends on the distance between the alignment point and each receive aperture and, hence, the obtained performance is significantly reduced. Therefore, an FSO system with multiple receive apertures can improve the capacity of the direct path link when the spacing among receive apertures is not too large in order to reduce the effect of nonzero inherent boresight. Alternatively, the obtained performance of SISO and MISO FSO systems depend on the additional boresight error which will be studied at the end of this subsection. These conclusions are totally valid for EW atmospheric turbulence in Fig. 3.8. Alternatively, the effect of beam width and jitter is also discussed. As expected, as the normalized beam width increases, i.e. from  $\omega_z/a = 5$  to  $\omega_z/a = 10$ , the performance decreases. As a result, an increase in the normalized beam width leads to a greater deterioration in performance.

### Comparison among Different Geometric Arrangements at the Receiver

Now, we examine different geometric arrangements for the receiver in order to make a fair comparison between the proposed method and other more typical geometric arrangements,



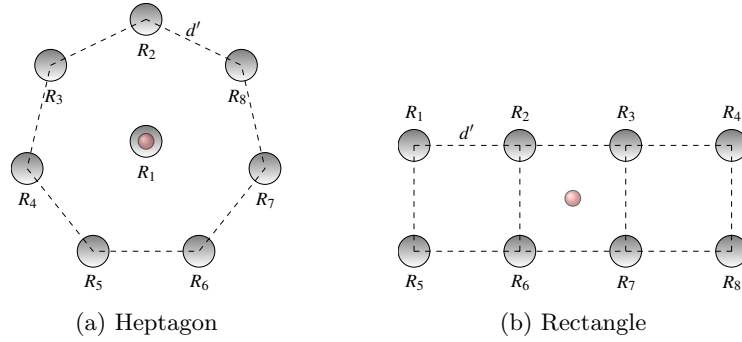


Figure 3.9: Receive apertures.

as shown in Fig. 3.9. In this way, we compare three different configurations when  $M$  and  $N$  are equal to 1 and 8, respectively, i.e a SIMO FSO system with eight receive apertures. In Fig. 3.9(a), an heptagon is depicted where one receive aperture is located at the center and the rest ones are equally spaced around a circle ( $d'$ ), whose radius is equal to  $d'/2 \sin(\pi/7)$ . In Fig. 3.9(b), a rectangle is depicted wherein all receive apertures are separated by a distance equals  $d'$ . In both geometric arrangements, their corresponding centroid is the alignment point.

From Eq. (3.33), we can see that the effect of nonzero boresight appears as a sum of squares ( $\sum_{k=1}^M \sum_{l=1}^N s_{kl}^2$ ) and, hence, the methodology based on the juxtaposition of triangle equilaterals is able to minimize this sum respect to the receiver configurations depicted in Fig. 3.9. It is deduced that the corresponding sum of squares ( $s_{kl}^2$ ) of Fig. 3.6(g) is equal to  $8.68d'^2$  while Figs. 3.9(a) and 3.9(b) are equal to  $9.29d'^2$  and  $12d'^2$ , respectively. This conclusion is corroborated in Fig. 3.10. However, it should be noted that this methodology does not provide the optimal performance due to the fact that finding the best method can be time-consuming and is often technically difficult to perform.

As can be seen in Fig. 3.10, a S-D link distance of  $d_{SD} = 4$  km as well as some spacing values among receiver apertures of  $d' = 12$  mm and  $d' = 24$  mm are considered when the diameter  $D_{SISO}$  of the corresponding receiver aperture of the SISO FSO system is set to 30 mm for EW atmospheric turbulence. As commented before, depending on the distance among receive apertures, the effect of nonzero inherent boresight displacement can be more severe. It should be highlighted that the proposed geometric arrangement for the receiver is able to achieve a better performance than other more typical geometric arrangements such as Figs. 3.9(a) and 3.9(b).

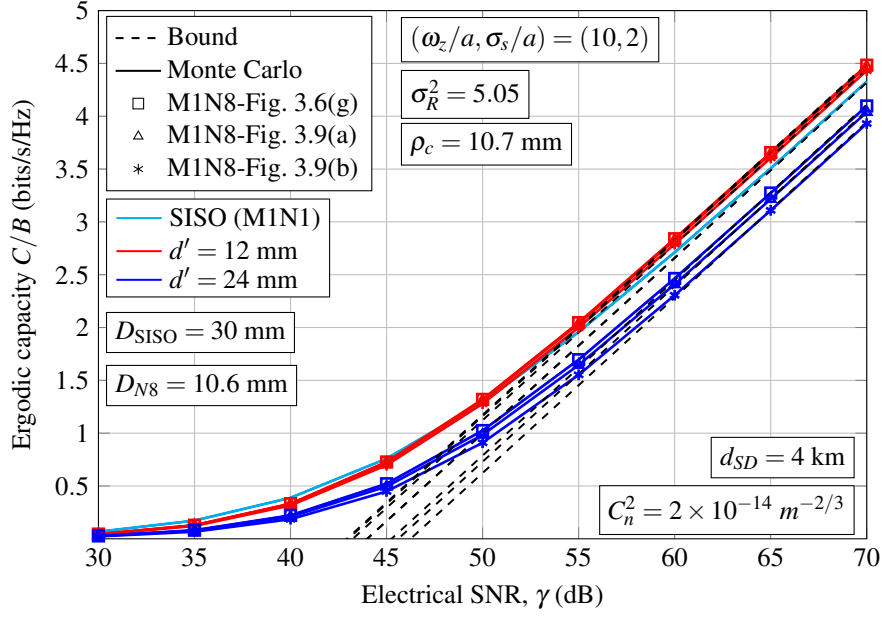


Figure 3.10: Comparison among different geometric arrangements for the receiver over EW atmospheric turbulence when different spacing values among receive apertures of  $d' = \{12 \text{ mm}, 24 \text{ mm}\}$  are considered.

### Impact of Nonzero Additional Boresight Error

The impact of nonzero additional boresight error ( $s_{AB}$ ) on the ergodic capacity of MIMO FSO systems is also analyzed, which depends on the number of receive apertures and pointing error parameters such as beam width, boresight error and alignment point. From the asymptotic ergodic capacity analysis carried out in this section, we can obtain the loss in decibels between considering and not considering nonzero additional boresight error. To do this, we perform the same process as in MISO FSO systems, i.e., we obtain a point where the asymptotic ergodic capacity intersects with the  $\gamma$ -axis. Hence, the corresponding expression of  $\gamma_{\text{MIMO}}^{\text{th}}$  in terms of the channel parameters can be derived as follows

$$\gamma_{\text{MIMO}}^{\text{th}}[dB] = \frac{-20}{\ln(10)} \times \left( \frac{\ln(F)}{MN} + \ln(2) + \frac{1}{MN} \sum_{k=1}^M \sum_{l=1}^N \ln(L_{kl}) + INT_1 + \ln(A_{0_{kl}}) - \frac{1}{\varphi_{kl}^2} - \frac{s_{kl}^2}{2\sigma_{s_{kl}}^2 \varphi_{kl}^2} \right), \quad (3.41)$$

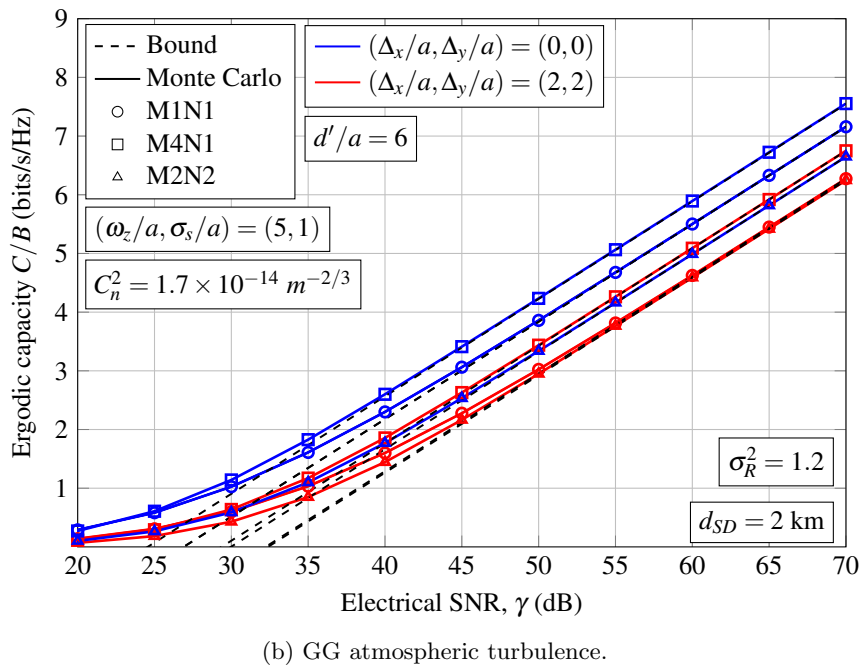
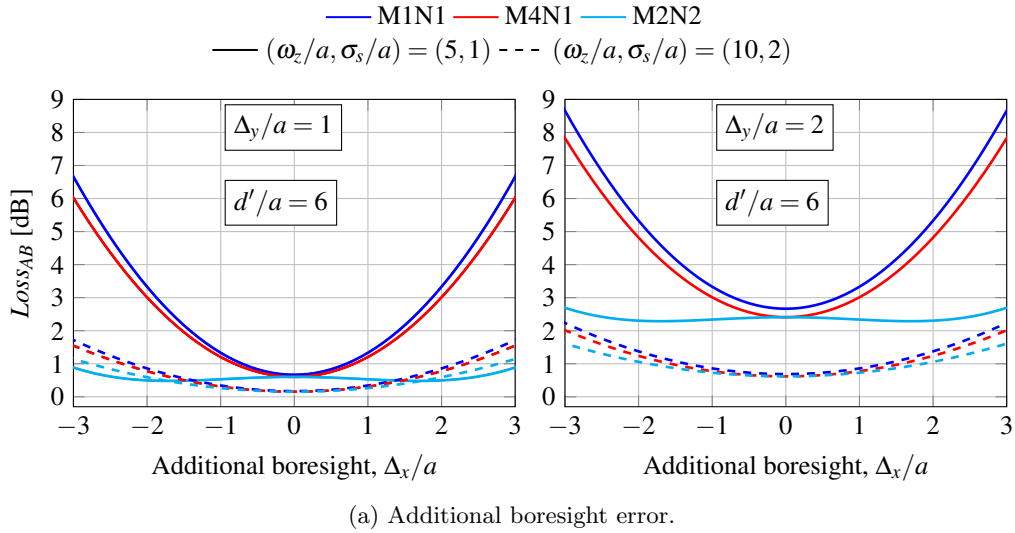


Figure 3.11: (a)  $Loss_{AB}$ [dB] as a function of the horizontal displacement of the normalized additional boresight error when different normalized beam width and normalized jitter values of  $(\omega_z/a, \sigma_s/a) = \{(5, 1), (10, 2)\}$  are considered and, (b) performance over GG atmospheric turbulence.

where  $INT_1$  depends on the selected atmospheric turbulence model, i.e., LN (Eq. (3.35)), GG (Eq. (3.34)) and EW (Eq. (3.40)). This loss can be written as

$$\begin{aligned} Loss_{AB}[dB] = \gamma_{th}^{AB}[dB] - \gamma_{th}^{IB}[dB] = & \frac{20 \ln(F^{IB}/F^{AB})}{MN \ln(10)} \\ & + \frac{10}{MN \ln(10) \sigma_s^2 \varphi^2} \sum_{k=1}^M \sum_{l=1}^N s_{AB}^2 - 2(\Delta x \cdot x_{kl} + \Delta y \cdot y_{kl}), \end{aligned} \quad (3.42)$$

where  $F^{IB}$  represents the correcting factor taking into account the inherent boresight displacement and  $F^{AB}$  represents both the inherent boresight displacement and the additional boresight error. It should be noted that the above expression does not depend on the atmospheric turbulence. This expression not only depends on the pointing error parameters but also on the geometric arrangements of the receive apertures at the receiver.

In this way, this loss is depicted in Fig. 3.11(a) as a function of the horizontal displacement of the normalized additional boresight error  $\Delta_x/a$  for different vertical displacements of the normalized boresight error of  $\Delta_y/a = \{1, 2\}$ . Normalized beam width and normalized jitter values of  $(\omega_z/a, \sigma_s/a) = \{(5, 1), (10, 2)\}$  as well as different values of  $M$  and  $N$  are also considered. As expected, the effect of nonzero additional boresight error can dramatically reduce the ergodic capacity of FSO systems with  $N = 1$ , i.e., SISO and MISO FSO systems. In addition to this, the performance has not been so affected by the presence of a nonzero additional boresight error when the parameter  $N > 1$ , i.e. MIMO and SIMO FSO systems. This latter is owing to the robustness provided by the centroid as an alignment point. Finally, Fig. 3.11(b) is added to this study in order to contrast some values of  $Loss_{AB}[dB]$  considering the same scenario as in Fig. 3.7(b). It can be seen in this figure that losses of 5.32 dB, 4.81 dB and 2.3 dB are obtained for SISO, MISO and MIMO FSO systems, respectively, when normalized beam width and normalized jitter values of  $(\omega_z/a, \sigma_s/a) = (5, 1)$  are assumed.

## 3.6 Ergodic Capacity of DF Strategies

The purpose of this study is to analyze and comprehend the ergodic capacity in the context of cooperative FSO systems when LOS is available. Motivated by the fact that the performance of cooperative FSO systems has been widely analyzed in terms of the BER and outage probability, we focus on the study of the ergodic capacity for two different DF relaying strategies over GG atmospheric turbulence channels with zero boresight pointing errors.

### 3.6.1 General Background on Cooperative Communication

According to the literature, cooperative communications were initially proposed as an interesting proposal to achieve spatial diversity in the context of RF systems.

In general, a cooperative FSO system consists of at least three terminals or nodes: a source node (S), a destination node (D), and a relay node (R). Basically, the relay node receives and process the information from the source node and, then, this one forwards the information to the destination node according to a specific relaying mode or protocol. Two kinds of configurations can be deployed: serial and parallel relaying. Serial configuration is also called multi-hop transmission, which is usually employed to extend the coverage area not providing a significant diversity gain, as demonstrated in [105]. In [106], Safari and Uysal proposed an artificial broadcasting through the use of multiple transmitters directed to relay nodes in the context of parallel and serial configurations. It was concluded that multi-hop transmissions can achieve a good performance in terms of the diversity gain when shorter distance among hops are exploited. Parallel relaying can also be deployed where the source node and the relay take part in the cooperative strategy, creating a virtual or distributed MIMO FSO system. One of the disadvantages of FSO technology is the need for LOS, i.e., transmitter and receiver must see each other. In this way, the broadcast nature of RF systems is not present in FSO technology and, hence, there must be another transmitter (laser source) at the source node for sending the signal from the transmitter to the relay node, which means extra hardware in comparison with RF systems [107]. For instance, one laser is pointing to the destination node and the other one is pointing to the relay node. Anyway, both relaying schemes are strongly dependent on the number of relays [106].

Generally speaking, cooperative relaying not only is able to achieve spatial diversity by creating a virtual MIMO FSO system, but also to increase the coverage area. The employment of cooperative technology is well justified since an FSO node may not be able to support multiple lasers or receiver apertures due to size, hardware limitations or even cost with the goal of improving the performance. In this way, this virtual MIMO FSO system can be created using transceivers available at the other nodes of the network. While MIMO FSO systems can even suffer from channel correlation in some cases, this problem is naturally alleviated in relaying systems given the large distances separating the different nodes in the network. The impact of MIMO relay channel on cooperative FSO system has also been analyzed [108, 109]. Cooperative communication for FSO systems have been recognized as a very promising solution for future wireless networks.

There are different relaying modes to forward the information to the destination node. These relaying modes can be classified into two main categories: non-regenerative and regenerative relaying modes. AF relaying is considered the most famous non-regenerative relaying mode due to its simplicity, and DF is the most famous regenerative relaying mode due to the fact that this one is able to achieve an optimum performance. Next, a brief description of these protocols is drawn from [110]:

**Amplify-and-forward** In AF, the received information is amplified at the relay node by using an amplifier and, then, the information is again forwarded to the destination

node. It is said that AF is non-regenerative relaying mode since the relay node does not modify the information.

**Decode-and-forward** DF is just the opposite of AF relaying mode. Before forwarding the information to the destination node, the relay detects, decodes and re-encodes the information. In case there is no coding, the relay node just detects.

Importantly, AF relaying presents an important advantage in relation to DF relaying. This advantage is related to the hardware requirements in DF relaying to be able to achieve an optimum performance. DF relaying needs high-speed electronic circuits at the order of GHz at the relay node. On the contrary, AF can avoid that requirement but the obtained performance in terms of the BER and capacity is limited [110].

Taking into account the advances proposed in RF systems with regard to cooperative communications where more attention has been paid to the concept of user cooperation as a new form of diversity for future wireless communication systems [111–113], different authors have studied the employment of cooperative transmission in FSO communication systems, and a considerable number of research articles have been reported. Parallel relaying as a 3-way or N-way communications setup has been studied in terms of the BER and outage performance in the literature [89, 107, 114–125].

### 3.6.2 System Model

Let us consider a three-node cooperative system based on three separate FSO links, as shown in Fig. 3.12, where the ergodic capacity is analyzed for two different DF relaying strategies. The bit detect-and-forward (BDF) cooperative strategy and the adaptive detect-and-forward (ADF) cooperative strategy are proposed and discussed as solutions to improve the ergodic capacity of cooperative FSO systems. In the following, the subscript  $m$  is used to represent the different FSO links considered here, i.e., S-D, S-R and R-D. Furthermore, we assume that  $I_{SD}$ ,  $I_{SR}$  and  $I_{RD}$  are statistically independent. Next, both cooperative strategies are explained in detail.

#### BDF Cooperative Strategy

The BDF cooperative protocol works in two stages as in [114, 117], which is reproduced here for convenience. In the first stage, the source node sends its own data to the destination node and the relay node, i.e., the source node transmits the same information to the relay node and destination node. In the second stage, the relay node sends the received data from the source node in the first stage to the destination node. The relay node detects each code bit of the cooperative signal individually and forwards it to the destination node, regardless of the channel coding. In this fashion, the relay node detects each code bit and sends the bit

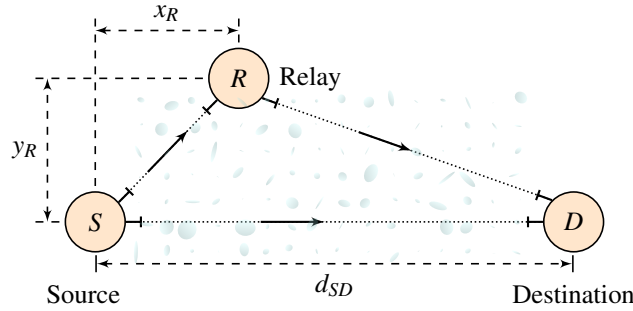


Figure 3.12: Block diagram of the considered 3-way FSO communication system, where  $d_{SD}$  is the S-D link distance and  $(x_R, y_R)$  represents the location of the relay node.

with the new power to the destination node. Finally, the received signals from the source node and the relay node are combined by using EGC reception at destination node. Then, the combined output is detected.

### ADF Cooperative Strategy

The ADF cooperative strategy is similar to the BDF cooperative strategy. This strategy selects between direct transmission or BDF on the basis of the value of the fading gain. When the irradiance of the S-D link ( $I_{SD}$ ) is greater than the irradiance of the R-D link ( $I_{RD}$ ), the cooperative FSO system is only based on the direct transmission to the destination node, obviating the cooperative mode. On the contrary, the source node performs cooperation using the relay node if the irradiance of the R-D link is greater than the irradiance of the S-D link.

It should be noted that the selection criterion is based on the value of the irradiance instead of its square magnitude, as usually assumed in the literature [89, 118, 126, 127], not being required the square magnitude due to the fact that the fading gain in FSO systems is always positive when IM/DD is assumed. Moreover, it is taking into consideration that CSI is known not only at the receiver side but also at the transmitter side. The knowledge of CSI at the transmitter side is feasible for FSO links given that scintillation is a slow time varying process relative to the large symbol rate. This has also been considered for FSO links from the point of view of information theory [79, 128]. The CSI can be acquired by using the training sequence at the receiver side and feedback the CSI back to transmitter. An interesting approach to acquire the CSI at the transmitter was proposed in [129], wherein the CSI is estimated at the receiver side and feed this channel estimate back to the transmitter using an RF feedback channel. At the same time, it would also be sufficient to send only one feedback bit from the destination to the source node highlighting what cooperative protocol should be activated, i.e, the BDF cooperative protocol or the direct transmission.

Due to the fact that atmospheric turbulence changes slowly with correlation time ranging from 10  $\mu$ s to 10 ms, this is a plausible scenario for FSO channels with data rates on the order of Gbps, implementing a continuous feedback from the receiver to maintain a specific performance level. In this sense, the receiver always knows if the cooperative protocol is being used.

Note that the same information rate is obtained for BDF and ADF at destination node in comparison with the direct transmission or the direct path link without using a cooperative strategy. For the sake of simplicity and an easier practical implementation, it should be emphasized that all the bits detected at the relay node are always forwarded with the new power to the destination node regardless of these bits are detected correctly or incorrectly as in BER and outage performance [121, 124, 125].

### 3.6.3 Performance Analysis

In this section, we analyze the ergodic capacity of the cooperative FSO system under study for two different cooperative strategies.

#### Ergodic Capacity of the BDF Cooperative Protocol

Firstly, we study the corresponding ergodic capacity of the BDF cooperative strategy, depending on the fact that the bit is detected correctly or incorrectly at the relay node. Assuming a statistical channel model as follows

$$Y_{\text{BDF}} = \frac{1}{2}X I_{SD} + Z_{SD} + X^* I_{RD} + Z_{RD}, \quad Z_{SD}, Z_{RD} \sim N(0, N_0/2) \quad (3.43)$$

where  $X^*$  represents the RV of the information detected at the relay node and, hence,  $X^* = X$  when the bit has been detected correctly and,  $X^* = d_E - X$  when the bit has been detected incorrectly. Note that  $I_{SD}$  and  $I_{RD}$  are the irradiances of the S-D link and the R-D link, respectively, and  $Z_{SD}$  and  $Z_{RD}$  are the corresponding AWGNs of the S-D link and the R-D link, respectively. The division by 2 is considered in Eq. (3.43) to maintain the average optical power in the air at a constant level of  $P_t$ , being transmitted by each laser at the source node an average optical power of  $P_t/2$ , as in previous sections. A power normalization factor of 1/2 has been used at the source node since the selected criterion for this cooperative system is that each node transmits an average optical power of  $P_t$ . As expected, there are other ones, such as the whole cooperative FSO system transmits an average optical power  $P_t$ , among others. In this case, the power normalization factor would be 1/3. The expression of  $Y_{\text{BDF}}$  in Eq. (3.43) can also be expressed as follows

$$Y_{\text{BDF}} = \frac{X}{2} (I_{SD} + 2I_{RD}) + Z_{SD} + Z_{RD}, \quad X^* = X \quad (3.44a)$$

$$Y_{\text{BDF}} = \frac{X}{2} (I_{SD} - 2I_{RD}) + d_E \cdot I_{RD} + Z_{SD} + Z_{RD}, \quad X^* = d_E - X \quad (3.44b)$$



Note that the term  $d_E \cdot I_{RD}$  becomes irrelevant to the detection process. Hence, the resulting received electrical SNR at the destination node is written as

$$\gamma_{\text{BDF}} = \frac{\gamma}{2} (I_{SD} + 2I_{RD})^2, \quad X^* = X \quad (3.45a)$$

$$\gamma_{\text{BDF}} = \frac{\gamma}{2} (I_{SD} - 2I_{RD})^2 \quad X^* = d_E - X \quad (3.45b)$$

Now, assuming instantaneous CSI at the receiver, the corresponding ergodic capacity of the BDF cooperative protocol is given by

$$C_{\text{BDF}} = C_0 \cdot (1 - P_b^{SR}) + C_1 \cdot P_b^{SR} = C_0 - (C_0 - C_1) \cdot P_b^{SR}, \quad (3.46)$$

where  $P_b^{SR}$  denotes the BER of the S-R link, and  $C_0$  and  $C_1$  are the ergodic capacities when the bit is detected correctly and incorrectly at the relay node, respectively. The above expression can be accurately approximated as follows

$$C_{\text{BDF}} \approx C_0 = \frac{B}{2 \ln(2)} \int_0^\infty \int_0^\infty \ln \left( 1 + \frac{\gamma}{2} (i_1 + 2i_2)^2 \right) f_{I_{SD}}(i_1) f_{I_{RD}}(i_2) di_1 di_2, \quad (3.47)$$

where  $f_{I_m}(i)$  is the PDF of atmospheric turbulence and pointing errors, i.e., GG atmospheric turbulence with zero boresight pointing errors as given in Eq. (2.34). It must be noted that this approximation is completely valid as SNR increases since the term  $P_b^{SR}$  tends to zero as SNR increases. In addition, the expression in Eq. (3.47) does not depend on the modulation scheme due to the fact that the term  $P_b^{SR}$  tends to zero fast when the simplest modulation scheme is implemented, i.e., OOK signaling. Moreover, this approximation has been numerically corroborated by Monte Carlo simulation, and it will be checked in the following subsection. Hence, the ergodic capacity of BDF cooperative protocol can be written as

$$C_{\text{BDF}}/B \approx \frac{1}{\ln(4)} \int_0^\infty \ln \left( 1 + \frac{\gamma}{2} i^2 \right) f_{I_T}(i) di, \quad (3.48)$$

where  $I_T = I_{SD} + 2I_{RD}$ . It should be noted that obtaining the corresponding PDF of  $I_T$  is remarkably tedious and not easily tractable due to the difficulty in finding its statistics.

As previous step, we can solve the integral in Eq. (3.48) by approximating the PDF of  $I_T$  by the  $\alpha$ - $\mu$  PDF as proposed in [87]. In this way,  $f_{I_T}(i)$  is approximated as follows

$$f_{I_T}(i) \approx \frac{\alpha \mu^\mu \hat{i}^{\alpha\mu-1}}{\hat{i}^{\alpha\mu} \Gamma(\mu)} \exp \left( -\mu \frac{i^\alpha}{\hat{i}^\alpha} \right). \quad (3.49)$$

The  $\alpha$ - $\mu$  distribution is characterized by the  $\alpha$  and  $\mu$  parameters as well as the  $\alpha$ -root mean value  $\hat{i}$  of the RV  $I_T$ . Note that  $\alpha$  is the parameter of the  $\alpha$ - $\mu$  distribution and this one cannot be confused with  $\alpha_{SD}$ ,  $\alpha_{RD}$  and  $\alpha_{SR}$  since these ones are related to GG atmospheric turbulence. The use of this approximate PDF is suitable in order to study the ergodic capacity of cooperative FSO systems due to the fact that this PDF contains information regarding the mean, the variance, and the fourth moment of  $I_T$ . These parameters are

obtained as the solution of the system of transcendental equations derived in [87, eqn. (24) and (25)]:

$$\frac{\Gamma(\mu + 1/\alpha)^2}{\Gamma(\mu)\Gamma(\mu + 2/\alpha) - \Gamma(\mu + 1/\alpha)^2} = \frac{\mathbb{E}[I_T]^2}{\mathbb{E}[I_T^2] - \mathbb{E}[I_T]^2}, \quad (3.50a)$$

$$\frac{\Gamma(\mu + 2/\alpha)^2}{\Gamma(\mu)\Gamma(\mu + 4/\alpha) - \Gamma(\mu + 2/\alpha)^2} = \frac{\mathbb{E}[I_T^2]^2}{\mathbb{E}[I_T^4] - \mathbb{E}[I_T^2]^2}. \quad (3.50b)$$

The solution for the system of transcendental equations has numerically been solved in an efficient manner. The parameter  $\hat{i}$  can be obtained as  $\hat{i} = \mu^{1/\alpha}\Gamma(\mu)\mathbb{E}[I_T]/\Gamma(\mu + 1/\alpha)$ . The required  $n$ th moment of  $I_T$  can be determined as follows

$$\mathbb{E}[I_T^n] = \int_0^\infty \int_0^\infty (i_1 + 2i_2)^n f_{I_{SD}}(i_1)f_{I_{RD}}(i_2)di_1di_2. \quad (3.51)$$

According to the binomial theorem, it is possible to expand the power  $(i_1 + 2i_2)^n$  into a sum and, after performing some straightforward manipulations in Eq. (3.51), we can express  $\mathbb{E}[I_T^n]$  as

$$\mathbb{E}[I_T^n] = \sum_{k=0}^n \frac{n!2^k}{k!(n-k)!} \int_0^\infty i_1^{n-k} f_{I_{SD}}(i_1)di_1 \cdot \int_0^\infty i_2^k f_{I_{RD}}(i_2)di_2. \quad (3.52)$$

Both integrals in Eq. (3.52) can be solved with the help of [58, eqn. (07.34.21.0009.01)] (See Appendix A.3.2) and, performing some algebraic manipulations, the corresponding closed-form solution for the  $n$ th moment of  $I_T$  can be written as

$$\begin{aligned} \mathbb{E}[I_T^n] &= \varphi_{SD}^2 \varphi_{RD}^2 \sum_{k=0}^n \frac{n!2^k}{k!(n-k)!} \left( \frac{\alpha_{SD}\beta_{SD}}{A_{0SD}L_{SD}} \right)^{k-n} \frac{\Gamma(n-k+\alpha_{SD})\Gamma(n-k+\beta_{SD})}{\Gamma(\alpha_{SD})\Gamma(\beta_{SD})(n-k+\varphi_{SD}^2)} \\ &\times \left( \frac{\alpha_{RD}\beta_{RD}}{A_{0RD}L_{RD}} \right)^{-k} \frac{\Gamma(k+\alpha_{RD})\Gamma(k+\beta_{RD})}{\Gamma(\alpha_{RD})\Gamma(\beta_{RD})(k+\varphi_{RD}^2)}. \end{aligned} \quad (3.53)$$

For  $n = 1$ , we can obtain the mean of  $I_T$ , i.e.,  $\mathbb{E}[I_T]$ . Substituting Eq. (3.49) into Eq. (3.48) and, after making the change of variables  $i' = i^\alpha/\hat{i}^\alpha$ , the ergodic capacity for BDF relaying scheme can be accurately approximated as follows

$$C_{\text{BDF}/B} \approx \frac{\mu^\mu}{\ln(4)\Gamma(\mu)} \int_0^\infty \ln \left( 1 + \frac{\hat{i}\gamma_0}{2} i'^{2/\alpha} \right) \frac{i'^\mu}{i'} \exp(-\mu i') di'. \quad (3.54)$$

The above integral can be solved by using [59, eqn. (8.4.6.5)] and [59, eqn. (8.4.3.1)] in order to express the natural logarithm in terms of the Meijer's G-function, and the exponential in terms of the Meijer's G-function, respectively (See Appendix A.3.1). Then, we can obtain the approximate closed-form solution for the ergodic capacity of the BDF cooperative protocol by using [58, eqn. (07.34.21.0012.01)] (See Appendix A.3.2) as follows

$$C_{\text{BDF}/B} \approx \frac{1}{\ln(4)\Gamma(\mu)} H_{1,3}^{3,2} \left( \frac{\gamma\Gamma(\mu)^2\mathbb{E}[I_T]^2}{2\Gamma(\mu+1/\alpha)^2} \left| \begin{matrix} (1,1), (1,1), (1-\mu, 2/\alpha) \\ (1,1), (0,1) \end{matrix} \right. \right). \quad (3.55)$$

It is corroborated in [20] that the above expression is in good agreement with simulation results but this one is not expressed in terms of channel parameters such as atmospheric turbulence and pointing errors and, hence, the conclusions have to be derived from a numerical observation. More details about this procedure can be found in [20]. Thus, we can use another method to try to find out an approximate closed-form expression for the capacity of the BDF cooperative protocol as in previous sections. Hence, a lower bound for  $I_T$  can be obtained by using the inequality between AM and GM (as in Sections 3.4 and 3.5), i.e.  $AM \geq GM$ , where  $AM = (I_{SD} + 2I_{RD})/2$  and  $GM = \sqrt{I_{SD} \cdot 2I_{RD}}$  are the arithmetic and geometric means, respectively. Therefore, a lower bound for  $I_T$  can be obtained as

$$I_{SD} + 2I_{RD} \geq \sqrt{8 \cdot I_{SD} \cdot I_{RD}} = \sqrt{8 \cdot I_T^{LB}}. \quad (3.56)$$

From Eq. (3.56), it can be deduced that the mathematical expectation in both sides of the inequality take different values and, hence, a correcting factor  $F$  should be added to the inequality in order to maintain the same value in both sides as in previous sections. This correcting factor can be derived from Eq. (3.56) and be seen in greater detail in Appendix B.3. Substituting Eq. (3.56) into Eq. (3.48) and, after performing some algebraic manipulations, the ergodic capacity for BDF relaying scheme can be accurately approximated as follows

$$C_{\text{BDF}}/B \approx \frac{1}{\ln(4)} \int_0^\infty \ln(1 + 4\gamma F i) f_{I_T^{LB}}(i) di. \quad (3.57)$$

The PDF  $f_{I_T^{LB}}(i)$  can be derived in closed-form via inverse Mellin transform in a similar way to MISO FSO systems (See Appendix A.7). Due to the fact that the irradiances  $I_{SD}$  and  $I_{RD}$  are statistically independent, the Mellin transform of their product is equal to the product of the Mellin transforms of  $I_{SD}$  and  $I_{RD}$ . Hence, the closed-form expression for the PDF of  $I_T^{LB}$  can be expressed in terms of the Meijer's G-function by employing the definition of the Mellin transform (See Appendix A.7.2) as follows

$$\begin{aligned} & f_{I_T^{LB}}(i) \\ &= \frac{i^{-1} \varphi_{SD}^2 \varphi_{RD}^2 G_{2,6}^{6,0} \left( \frac{\alpha_{SD} \beta_{SD} \alpha_{RD} \beta_{RD}}{A_{0SD} L_{SD} A_{0RD} L_{RD}} i \middle| \begin{matrix} \varphi_{SD}^2 + 1, \varphi_{RD}^2 + 1 \\ \varphi_{SD}^2, \alpha_{SD}, \beta_{SD}, \varphi_{RD}^2, \alpha_{RD}, \beta_{RD} \end{matrix} \right)}{\Gamma(\alpha_{SD}) \Gamma(\beta_{SD}) \Gamma(\alpha_{RD}) \Gamma(\beta_{RD})}. \end{aligned} \quad (3.58)$$

The integral in Eq. (3.57) can be solved by using [59, eqn. (8.4.6.5)] in order to express the natural logarithm in terms of the Meijer's G-function (See Appendix A.3.1). Then, we can obtain the approximate closed-form expression for the ergodic capacity of the BDF cooperative protocol  $C_{\text{BDF}}$  by using [59, eqn. (2.24.1.2)] (See Appendix A.3.2) as

$$\begin{aligned} & C_{\text{BDF}}/B \\ & \approx \frac{\varphi_{SD}^2 \varphi_{RD}^2 G_{4,8}^{8,1} \left( \frac{\alpha_{SD} \beta_{SD} \alpha_{RD} \beta_{RD}}{\gamma^{4F} A_{0SD} L_{SD} A_{0RD} L_{RD}} \middle| \begin{matrix} 0, 1, \varphi_{SD}^2 + 1, \varphi_{RD}^2 + 1 \\ \varphi_{SD}^2, \alpha_{SD}, \beta_{SD}, \varphi_{RD}^2, \alpha_{RD}, \beta_{RD}, 0, 0 \end{matrix} \right)}{\ln(4) \Gamma(\alpha_{SD}) \Gamma(\beta_{SD}) \Gamma(\alpha_{RD}) \Gamma(\beta_{RD})}. \end{aligned} \quad (3.59)$$

To provide a much deeper insight into this ergodic capacity, an asymptotic expression for this capacity at high SNR can be readily and accurately lower-bounded due to the fact that  $\ln(1+z) \approx \ln(z)$  when  $z \rightarrow \infty$  as follows

$$C_{\text{BDF}}/B \doteq \frac{\ln(4\gamma F)}{\ln(4)} + \frac{1}{\ln(4)} \int_0^\infty \ln(i) f_{I_T^{LB}}(i) di. \quad (3.60)$$

The above integral can be rewritten in a much easier way by using the definition of  $I_T^{LB} = I_{SD}I_{RD}$  as

$$C_{\text{BDF}}/B \doteq \frac{\ln(4\gamma F)}{\ln(4)} + \frac{1}{\ln(4)} \int_0^\infty \ln(i_1) f_{I_{SD}}(i_1) di_1 + \frac{1}{\ln(4)} \int_0^\infty \ln(i_2) f_{I_{RD}}(i_2) di_2. \quad (3.61)$$

Each of the integrals in Eq. (3.61) was solved in Eq. (2.55) for GG atmospheric turbulence channels with zero boresight pointing errors. Hence, the corresponding asymptotic ergodic capacity expression of the BDF cooperative protocol can be seen in

$$\begin{aligned} C_{\text{BDF}}^H/B &\doteq \frac{\ln(\gamma 4F)}{\ln(4)} + \frac{1}{\ln(4)} \left( -\frac{1}{\varphi_{SD}^2} - \frac{1}{\varphi_{RD}^2} \right) \\ &+ \frac{1}{\ln(4)} \left( \psi(\alpha_{SD}) + \psi(\beta_{SD}) + \psi(\alpha_{RD}) + \psi(\beta_{RD}) + \ln \left( \frac{A_{0SD} L_{SD} A_{0RD} L_{RD}}{\alpha_{SD} \beta_{SD} \alpha_{RD} \beta_{RD}} \right) \right). \end{aligned} \quad (3.62)$$

### Ergodic Capacity of the ADF Cooperative Protocol

Next, we analyze the corresponding ergodic capacity of the ADF cooperative strategy. The statistical channel model can be written as

$$Y_{\text{BDF}} = \frac{1}{2} X I_{SD} + X^* I_{RD} + Z_{SD} + Z_{RD}, \quad I_{RD} > I_{SD} \quad (3.63a)$$

$$Y_{\text{DT}} = X I_{SD} + Z_{SD}, \quad I_{RD} < I_{SD} \quad (3.63b)$$

The corresponding ergodic capacity of the ADF cooperative protocol is given by

$$C_{\text{ADF}} = C_{\text{BDF}} \cdot P(I_{RD} > I_{SD}) + C_{\text{DT}} \cdot P(I_{RD} < I_{SD}), \quad (3.64)$$

where  $C_{\text{BDF}}$  is the ergodic capacity of the BDF cooperative protocol,  $C_{\text{DT}}$  is the ergodic capacity of the direct transmission,  $P(I_{RD} > I_{SD})$  is the probability of  $I_{RD} > I_{SD}$ , and  $P(I_{RD} < I_{SD})$  is the probability of  $I_{RD} < I_{SD}$ . In this way, assuming instantaneous CSI at the receiver, the ergodic capacity of the ADF cooperative protocol is computed as follows

$$\begin{aligned} C_{\text{ADF}} &\approx \frac{B}{2 \ln(2)} \int_0^\infty \int_0^{i_2} \ln \left( 1 + \frac{\gamma}{2} (i_1 + 2i_2)^2 \right) f_{I_{SD}}(i_1) f_{I_{RD}}(i_2) di_1 di_2 \\ &+ \frac{B}{2 \ln(2)} \int_0^\infty \ln(1 + 4\gamma i^2) F_{I_{RD}}(i) f_{I_{SD}}(i) di. \end{aligned} \quad (3.65)$$

where  $P(I_{RD} > I_{SD})$  is computed by solving the inner integral ( $i_1 = I_{SD}$ ) corresponding to the first integral in Eq. (3.65) in the interval of integration from 0 to  $i_2$  ( $i_2 = I_{RD}$ ),

and  $P(I_{RD} < I_{SD})$  is computed by using  $F_{I_{RD}}(i)$  ( $i = I_{SD}$ ) since both RVs are statistically independent. Similar to the BDF cooperative protocol, the inequality between AM and GM is also used. Hence, the expression in Eq. (3.65) is re-written as follows

$$\begin{aligned} C_{\text{ADF}/B} &\approx \frac{1}{\ln(4)} \int_0^\infty \int_0^{i_2} \ln(1 + 4\gamma F' i_1 i_2) f_{I_{SD}}(i_1) f_{I_{RD}}(i_2) di_1 di_2 \\ &+ \frac{1}{\ln(4)} \int_0^\infty \ln(1 + 4\gamma i^2) F_{I_{RD}}(i) f_{I_{SD}}(i) di = C'_{\text{BDF}} + C_{\text{DT}}, \end{aligned} \quad (3.66)$$

where  $F'$  is another correcting factor that is derived in a similar way to  $F$  (See Appendix B.4). Unfortunately, an approximate closed-form solution for  $C'_{\text{BDF}}$  is not available and, hence, a numerical integration must be used. On the contrary, the term  $C_{\text{DT}}$  can be expressed in closed-form in terms of GBMGF (See Appendix A.6). Nevertheless, an approximate closed-form expression for  $C_{\text{ADF}}$  cannot be found. In this way, an asymptotic analysis is carried out at high SNR as in Eq. (3.60). Thus, after performing some algebraic manipulations in Eq. (3.66), we obtain

$$\begin{aligned} C_{\text{ADF}/B}^H &\doteq \underbrace{\frac{\ln(4\gamma F')}{\ln(4)} \int_0^\infty F_{I_{SD}}(i) f_{I_{RD}}(i) di + \frac{1}{\ln(4)} \int_0^\infty \int_0^{i_2} \ln(i_1 i_2) f_{I_{SD}}(i_1) f_{I_{RD}}(i_2) di_1 di_2}_{C_{\text{BDF}}^{H'}} \\ &+ \underbrace{\frac{\ln(4\gamma)}{\ln(4)} \int_0^\infty F_{I_{RD}}(i) f_{I_{SD}}(i) di + \frac{2}{\ln(4)} \int_0^\infty \ln(i) F_{I_{RD}}(i) f_{I_{SD}}(i) di}_{C_{\text{DT}}^H} = C_{\text{BDF}}^{H'} + C_{\text{DT}}^H. \end{aligned} \quad (3.67)$$

It is noteworthy to mention that the average probability when the source node selects cooperative transmission instead of direct transmission is defined as follows

$$P = \int_0^\infty F_{I_{SD}}(i) f_{I_{RD}}(i) di. \quad (3.68)$$

On the contrary, the average probability when the source node selects direct transmission instead of cooperative transmission is defined as follows

$$1 - P = \int_0^\infty F_{I_{RD}}(i) f_{I_{SD}}(i) di. \quad (3.69)$$

Note that  $P$  is independent of the SNR  $\gamma$ , resulting in a positive value that is upper bounded by 1. To evaluate Eq. (3.68), we can use [59, eqn. (2.24.1.2)] in order to transform the integral expression in terms of the Meijer's G-function (See Appendix A.3.2). Hence, a closed-form solution is obtained as can be seen in

$$P = \frac{\varphi_{RD}^2 \varphi_{SD}^2 G_{5,5}^{4,3} \left( \begin{array}{c} \frac{\alpha_{RD} \beta_{RD} A_{0SD} L_{SD}}{\alpha_{SD} \beta_{SD} A_{0RD} L_{RD}} \left| 1 - \varphi_{SD}^2, 1 - \alpha_{SD}, 1 - \beta_{SD}, 1, \varphi_{RD}^2 + 1 \right. \\ \varphi_{RD}^2, \alpha_{RD}, \beta_{RD}, 0, -\varphi_{SD}^2 \end{array} \right)}{\Gamma(\alpha_{RD}) \Gamma(\alpha_{SD}) \Gamma(\beta_{RD}) \Gamma(\beta_{SD})}. \quad (3.70)$$

Finally, the asymptotic expression for the ergodic capacity expression of the ADF cooperative protocol  $C_{\text{ADF}}^H$  is given by

$$C_{\text{ADF}}^H/B \doteq \frac{\ln(4\gamma) + P \ln(F') + I_1 + 2I_2}{\ln(4)}, \quad (3.71)$$

where

$$I_1 = \int_0^\infty \int_0^{i_2} \ln(i_1 i_2) f_{I_{SD}}(i_1) f_{I_{RD}}(i_2) di_1 di_2, \quad (3.72a)$$

$$I_2 = \int_0^\infty \ln(i) f_{I_{RD}}(i) f_{I_{SD}}(i) di. \quad (3.72b)$$

Unfortunately, the corresponding closed-form solution of the integral  $I_1$  cannot be determined and a numerical integration should be also used. However, the integral  $I_2$  can be expressed in closed-form. Note that  $I_2$  involves the product of the three independent Meijer's G-functions which can be expressed in terms of the GBMGF (See Appendix A.6). Hence, the expression of  $I_2$  is given by

$$I_2 = \frac{\varphi_{SD}^2 \varphi_{RD}^2}{\Gamma(\alpha_{SD})\Gamma(\beta_{SD})\Gamma(\alpha_{RD})\Gamma(\beta_{RD})} \times G_{2,2:2,3,1:3,0}^{2,2:2,4:1,3} \left( \begin{array}{c|c|c|c} 1, 1 & 1, \varphi_{RD}^2 + 1 & \varphi_{SD}^2 + 1 & \frac{\alpha_{RD}\beta_{RD}}{A_{0RD}L_{RD}}, \frac{\alpha_{SD}\beta_{SD}}{A_{0SD}L_{SD}} \end{array} \right). \quad (3.73)$$

To the best of our knowledge, the GBMGF is not available in standard mathematical packages such as Mathematica<sup>TM</sup>, Maple<sup>TM</sup> or Matlab<sup>TM</sup>. However, the GBMGF in Eq. (3.73) can be computed in an efficient manner by using the two-fold Mellin-Barnes representation of the Meijer's G-function. Similar to [130, Table II] and [131, appendix], the GBMGF was implemented using a Mathematica<sup>TM</sup> implementation for the numerical evaluation of Eq. (3.73). Both  $I_1$  and  $I_2$  are independent of the SNR  $\gamma$ .

### 3.6.4 Numerical Results and Discussion

From this ergodic capacity analysis, it can be deduced that the main aspect to consider in order to optimize the ergodic capacity is the relay location as well as channel parameters. Both aspects play an important role in ergodic capacity analysis for cooperative FSO systems.

The corresponding results of this ergodic capacity analysis are depicted in Fig. 3.13 when different relay locations of  $y_R = \{0.5 \text{ km}, 2 \text{ km}\}$  are considered for a S-D link distance of  $d_{SD} = 3 \text{ km}$ . Different weather conditions are adopted as shown in Table 3.1. Pointing errors are present assuming a normalized beam width value of  $\omega_z/a = 5$  and different normalized jitter values of  $\sigma_s/a = \{1, 3\}$  for each FSO link. A remarkable improvement in performance can be observed at high SNR in both DF relaying strategies, when comparing

to the direct transmission without cooperative communication. Monte Carlo simulation results are furthermore included as a reference (Eq. (3.46) for BDF cooperative protocol, Eq. (3.65) for ADF cooperative protocol and Eq. (2.52) for the direct transmission), confirming the accuracy of the proposed approximation, and usefulness of the derived results. In addition, this figure shows a high accuracy of the asymptotic results based on the logarithm approximation given in Eqs. (3.62), (3.71) and (2.59) at high SNR.

This ergodic capacity analysis can be extended in order to obtain a point where the asymptotic ergodic capacity intersects with the  $\gamma$ -axis, as in previous sections. In this way, from Eq. (3.62) we can obtain the corresponding expression of  $\gamma_{\text{BDF}}^{\text{th}}$  in terms of the channel parameters as follows

$$\begin{aligned} \gamma_{\text{BDF}}^{\text{th}}[dB] = & -\frac{10 \ln(4F)}{\ln(10)} + \frac{10}{\ln(10)} \left( \frac{1}{\varphi_{SD}^2} + \frac{1}{\varphi_{RD}^2} \right) \\ & + \frac{10}{\ln(10)} \left( \ln \left( \frac{\alpha_{SD} \beta_{SD} \alpha_{RD} \beta_{RD}}{A_{0SD} L_{SD} A_{0RD} L_{RD}} \right) - \psi(\alpha_{SD}) - \psi(\beta_{SD}) - \psi(\alpha_{RD}) - \psi(\beta_{RD}) \right). \end{aligned} \quad (3.74)$$

Similar to Eq. (3.74), from Eq. (3.71) we can also obtain the corresponding SNR threshold of  $\gamma_{\text{ADF}}^{\text{th}}$  in terms of the channel parameters as follows

$$\gamma_{\text{ADF}}^{\text{th}}[dB] = -\frac{10}{\ln(10)} (I_1 + 2I_2 + P \ln(F') + \ln(4)). \quad (3.75)$$

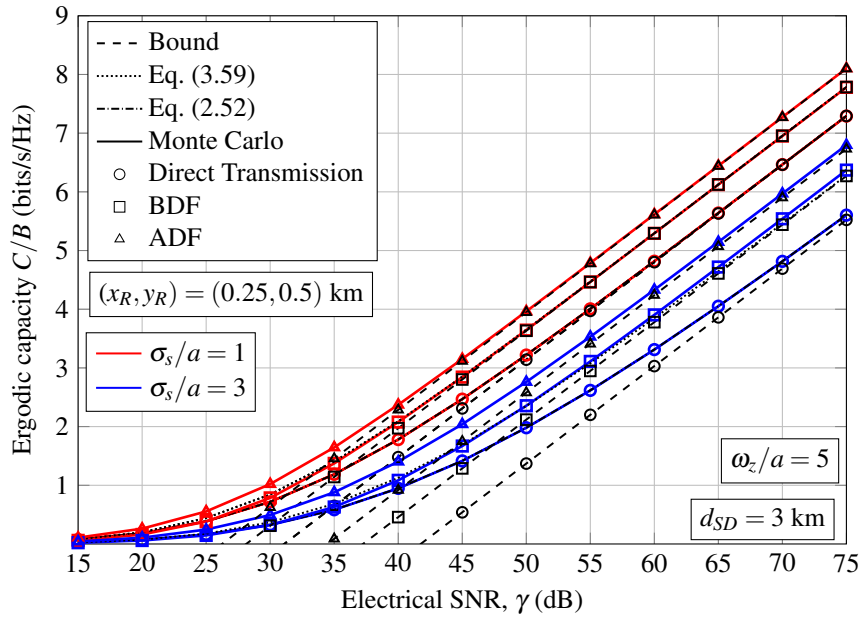
From Eqs. (3.74) and (3.13), we can obtain this improvement or gain of the BDF cooperative protocol in relation to the direct transmission, i.e.  $G_{\text{BDF}}[dB]$ , as follows

$$G_{\text{BDF}}[dB] = \gamma_{\text{DT}}^{\text{th}}[dB] - \gamma_{\text{BDF}}^{\text{th}}[dB]. \quad (3.76)$$

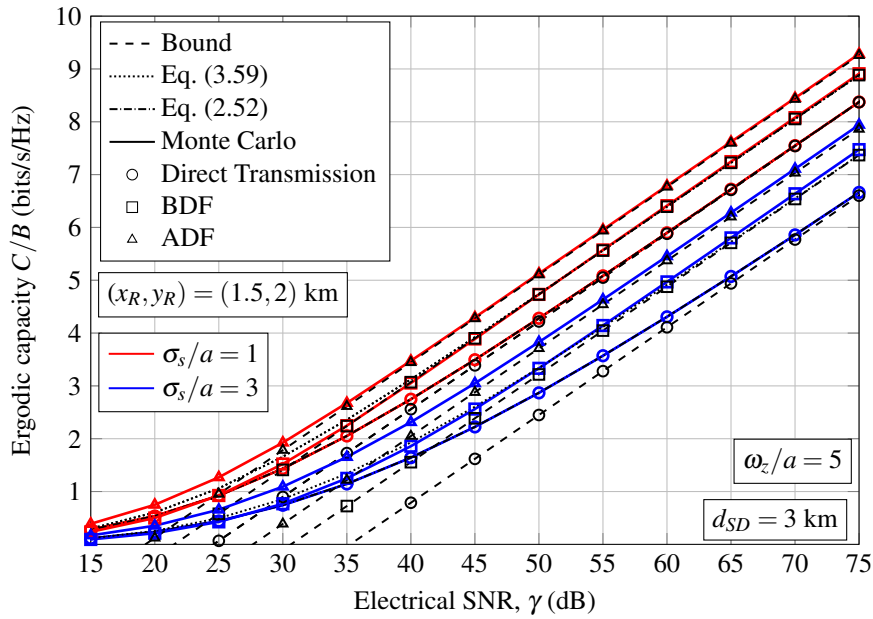
At the same time, from Eqs. (3.75) and (3.13), we can also obtain the improvement or gain of the ADF cooperative protocol in relation to the direct transmission, i.e.  $G_{\text{ADF}}[dB]$ , as follows

$$G_{\text{ADF}}[dB] = \gamma_{\text{DT}}^{\text{th}}[dB] - \gamma_{\text{ADF}}^{\text{th}}[dB]. \quad (3.77)$$

For a better understanding of the impact of the three-node cooperative FSO system under study, these gains, i.e.,  $G_{\text{BDF}}[dB]$  in Eq. (3.76) and  $G_{\text{ADF}}[dB]$  in Eq. (3.77) are plotted in Fig. 3.14 as a function of the horizontal displacement of the relay node  $x_R$  for a S-D link distance of  $d_{SD} = 3$  km when different relay locations of  $y_R = \{0.5 \text{ km}, 1 \text{ km}, 1.5 \text{ km}, 2 \text{ km}\}$  are assumed. In order to show the effect of pointing errors on the ergodic capacity, different normalized beam width and normalized jitter values of  $(\omega_z/a, \sigma_s/a) = (5, 1)$  and  $(\omega_z/a, \sigma_s/a) = (5, 3)$  are considered. Moreover, it can be observed that cooperative communications can be used in order to achieve a greater robustness against pointing errors since the obtained performance is much better with respect to the direct transmission when more severe pointing errors are considered. It should be also noted that ergodic capacity is severely degraded as normalized jitter increases.



(a) Moderate turbulence.



(b) Strong turbulence.

Figure 3.13: Ergodic capacity for a S-D link distance of  $d_{SD} = 3$  km when different weather condition and different normalized beam width and normalized jitter values of  $(\omega_z/a, \sigma_s/a) = (5, 1)$  and  $(\omega_z/a, \sigma_s/a) = (5, 3)$  are assumed.



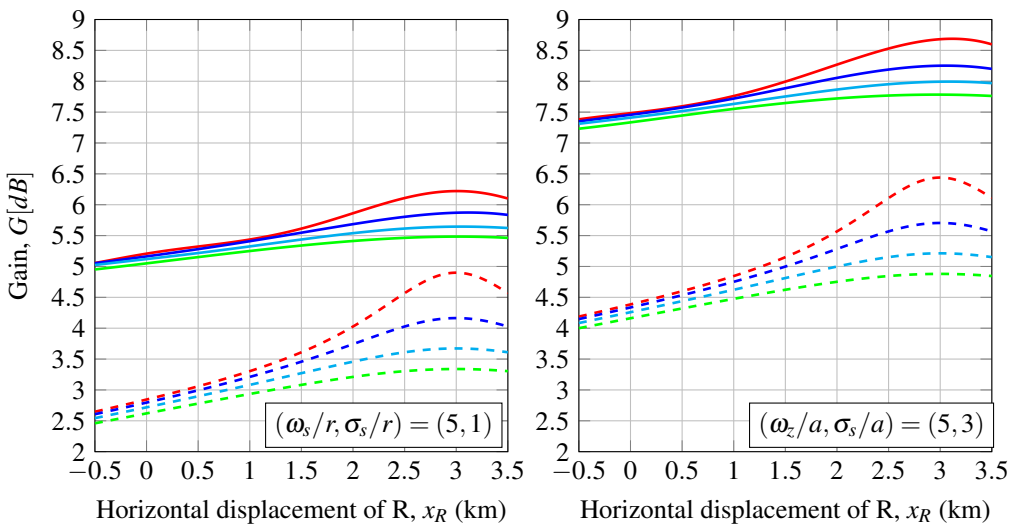
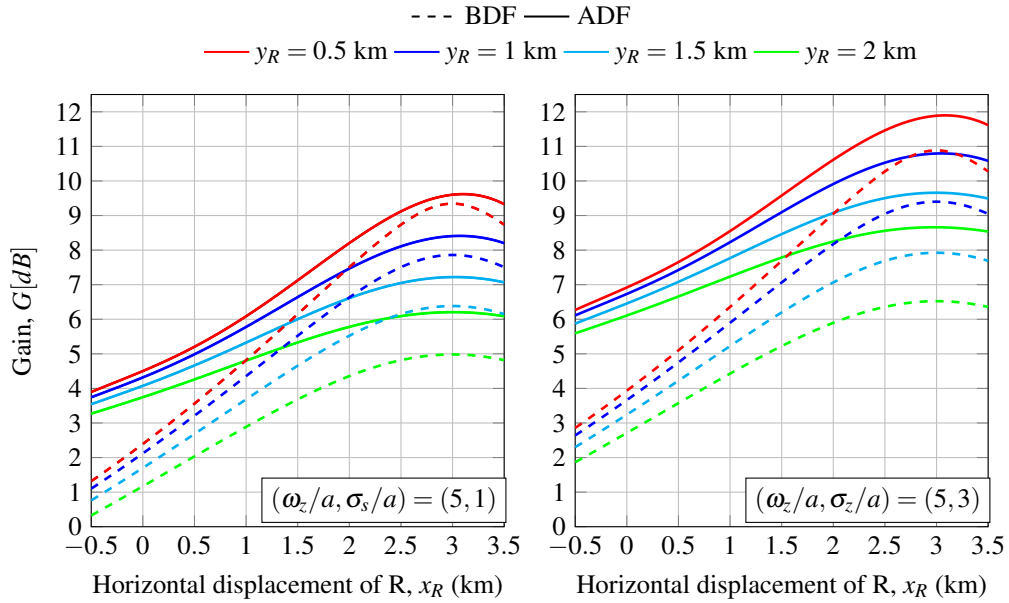


Figure 3.14: Gain,  $G[dB]$ , for a S-D link distance of  $d_{SD} = 3$  km when different weather conditions and different normalized beam width and normalized jitter values of  $(\omega_z/a, \sigma_s/a) = (5, 1)$  and  $(\omega_z/a, \sigma_s/a) = (5, 3)$  are assumed.

As expected, the ergodic capacity is strongly dependent on the relay location regardless of the cooperative protocol adopted. It must be highlighted that the ergodic capacity shows one maximum value when the horizontal displacement of the relay node is equal to the S-D link distance regardless of the atmospheric turbulence and pointing errors. This maximum gain is related to the minimum R-D link distance due to the fact that the relation  $x_R = d_{SD}$  holds and, hence, the received SNR at the destination node is maximum. On the one hand, it can be seen that ADF cooperative protocol always presents a better and robust performance than BDF cooperative protocol due to the fact that ADF is based on the selection of the optical path with a greater value of irradiance. On the other hand, the BDF cooperative protocol is only able to achieve a better performance than the direct transmission for specific relay locations. In other words, BDF cooperative protocol does not improve the ergodic capacity for longer R-D link distances.

Finally, it can be seen in Fig. 3.13 that gains of 4.83 dB and 7.26 dB for ADF in contrast to gains of 2.96 dB and 4.05 dB for BDF under moderate turbulence when normalized beam width and normalized jitter values of  $(\omega_z/a, \sigma_s/a) = (5, 1)$  and  $(\omega_z/a, \sigma_s/a) = (5, 3)$  are considered, respectively. Analogously, it can be also seen in Fig. 3.13 that gains of 5.1 dB and 7.38 dB for ADF in contrast to gains of 3.08 dB and 4.62 dB for BDF under strong turbulence when normalized beam width and normalized jitter values of  $(\omega_z/a, \sigma_s/a) = (5, 1)$  and  $(\omega_z/a, \sigma_s/a) = (5, 3)$  are considered, respectively.

### 3.7 Summary

Ergodic capacity analysis in terms of approximate closed-form expressions is presented along with some simulation results to validate these analytical expressions. This ergodic capacity analysis is carried out in the context of advanced FSO communication techniques such as MISO, SIMO, MIMO and cooperative communication over atmospheric turbulence channels with pointing errors.

To the best of our knowledge, the study of the ergodic capacity of MISO FSO systems was never taken into account in the literature. In this way, this research problem is addressed in this thesis, presenting new results for the optics community. The ergodic capacity is analyzed over GG atmospheric turbulence channels with zero boresight pointing errors when IM/DD and EGC reception are implemented. [18]. The key contribution of this study are summarized as follows

- A novel closed-form expression is obtained for the ergodic capacity over GG fading channels with pointing errors which allows us to compute the capacity from low to high SNR.
- The closed-form expression is derived in terms of H-Fox function by using the well-known inequality between arithmetic and geometric means of positive RVs in order

to obtain an approximate closed-form expression of the distribution of the sum of  $M$  GG with pointing errors variates.

- An asymptotic closed-form expression at high SNR for the ergodic capacity of MISO FSO systems is also derived to study other effects such as the impact of pointing errors at high SNR, the impact of number of lasers, among others.

With the goal of generalizing the results obtained in the previous study, the ergodic capacity analysis is extended to MIMO FSO systems in [17] over different atmospheric turbulence models and under the presence of nonzero boresight pointing errors when IM/DD and EGC reception are implemented. The effect of nonzero boresight is a new feature in this analysis and in the open literature. To the best of our knowledge, there are no reported works that take into consideration the effect of nonzero boresight on the performance of MIMO FSO systems. Such effect was only considered for FSO links, i.e. SISO FSO systems, in [50, 72, 101]. In this way, the key contributions of this study are summarized as follows

- A new methodology has been proposed in order to generate different receiver configurations from the juxtaposition of equilateral triangles which guarantees a notable reduction of the effect of the inherent boresight displacement against other geometric arrangements at the receiver.
- Asymptotic closed-form expressions at high SNR for the ergodic capacity of MIMO FSO systems are derived over GG atmospheric turbulence channels when different geometric arrangements of the receive apertures are considered.
- This analysis can be extended to other atmospheric turbulence models such as LN and EW, among others, in order to analyze the ergodic capacity over weak turbulence or under aperture averaging conditions.

Finally, the ergodic capacity is also studied for cooperative FSO systems [19]. The purpose of this analysis is to study and comprehend the ergodic capacity in the context of cooperative FSO systems for different DF relaying schemes and when LOS is available. In this way, the key contributions of this study are summarized as follows

- Two different cooperative strategies are analyzed in terms of the capacity for a 3-way communications setup: BDF cooperative protocol where the source node and the relay node take part jointly in the cooperation, and ADF cooperative protocol where the source node selects between cooperative communication and direct transmission according to the CSI.
- Approximate closed-form expressions are obtained for the ergodic capacity of a DF-based cooperative FSO system over GG fading channels with pointing errors.

- The closed-form expressions are derived in terms of Meijer's G-function by using the well-known inequality between arithmetic and geometric means of positive RVs.
- An asymptotic analysis at high SNR for the ergodic capacity of these relaying schemes are also included in order to study the impact of the relay location on the ergodic capacity.

## Chapter 4

# Generalized Misalignment Fading Model

The impact of generalized misalignment fading on performance of FSO communication systems is carefully analyzed over atmospheric turbulence channels, presenting new results for the optics community. Besides, a new accurate and useful tool is proposed to model generalized pointing errors.

### 4.1 Motivation and Related Work

As commented in Section 2.3.2, FSO communication systems are mainly affected by atmospheric turbulence and pointing errors. An accurate alignment between transmitter and receiver is required [10, 22, 53]. Pointing accuracy is a critical issue in determining link performance and reliability, and they might arise due to many different factors such as building sway and mechanical errors, among others. Adding the effect of pointing errors to performance of FSO communication systems makes the analysis more difficult and, for that reason, many authors ignore such effect. It is obvious that pointing errors play an important role in channel fading characteristics and, hence, this damaging effect must always be taken into account in FSO system design.

The study of pointing errors from a statistical point of view has been a matter of interest over the past decade. Many authors have proposed some statistical models to describe and analyze its impact on performance [53, 56, 132]. These models present one thing in common: all of them are obtained under the assumption that building sway is well-described according to an independent Gaussian distribution for the elevation and the horizontal displacement. The radial displacement  $r$  at the receiver is modeled as a sum of two independent squared normal Gaussian RVs.



In [53], a pointing error model was proposed, where the effect of beam width, detector size and independent identical Gaussian distributions for the elevation and the horizontal displacement were considered. This model continues to be used in a great deal of research articles due to its relative simplicity from a mathematical point of view, where the radial displacement at the receiver is determined by a Rayleigh distribution, as well as due to its realistic assumptions. This statistical model is considered as a cornerstone of all the pointing error models. The effect of nonzero boresight is not taken into account in this model, and neither the effect of different jitters for the elevation and the horizontal displacement. This model was used to study the outage capacity over LN fading channels in that work. A few years later, the analysis carried out in [53] was extended in [132] to assume different jitters for the elevation and the horizontal displacement, i.e., the radial displacement  $r$  at the receiver follows a Hoyt distribution. This model was used to study the BER performance over LN fading channels. Three years ago, a pointing error model once again based on [53] was proposed in [56] to consider a nonzero boresight error at the receiver for independent identical Gaussian distributions for the elevation and the horizontal displacement, i.e., the radial displacement  $r$  at the receiver follows a lognormal-Rician distribution. This model was used to study the BER and outage performance over LN and GG atmospheric turbulence. In the case of GG fading channels, obtained results are only valid when atmospheric turbulence is the dominant effect in relation to pointing errors and, hence, they do not analyze the performance when pointing error is the dominant effect. Unlike satellite FSO communication systems, where is generally accepted to assume the same jitter variance for the elevation and the horizontal displacement as assumed in [56], a more realistic approach was assumed in [132] for terrestrial FSO links since physical impacts such as dynamic wind loads, thermal expansion and weak earthquakes have different impact on horizontal and vertical axes of constructions.

It is evident that there is quite an important need for considering a much more realistic pointing error model where the effect of different jitters for the elevation and the horizontal displacement and nonzero boresight errors at the receiver are assumed. In that model, the radial displacement  $r$  at the receiver is determined by the Beckmann distribution [34], which is a versatile statistical model that includes many distributions as special cases such as Rayleigh, Hoyt and lognormal-Rician, among others. This generalized approach was considered in [133] to evaluate the asymptotic ergodic capacity of FSO links over LN and GG atmospheric turbulence channels. It must be noted that neither a closed-form expression nor an approximate expression for the composite PDF of atmospheric turbulence and pointing errors were obtained.

## 4.2 Statistical Background

Let us to reproduce again some parameters and concepts related to pointing errors as explained in Section 2.3.2. The attenuation due to geometric spread and pointing errors is

approximated as follows

$$I_p(r; z) \approx A_0 \exp\left(\frac{-2r^2}{\omega_{zeq}^2}\right), \quad (4.1)$$

where  $v = \sqrt{\pi}a/\sqrt{2}\omega_z$ ,  $A_0 = [\text{erf}(v)]^2$  is the fraction of the collected power at  $r = 0$ , and  $\omega_{zeq}^2 = \omega_z^2 \sqrt{\pi} \text{erf}(v) / 2v \exp(-v^2)$  is the equivalent beam width. The radial displacement  $r$  at the receiver plane can be expressed as  $r^2 = x^2 + y^2$ , where  $x$  and  $y$  represent the horizontal displacement and the elevation, respectively. Both  $x$  and  $y$  are modeled as independent Gaussian RVs with different jitters for the horizontal displacement ( $\sigma_x > 0$ ) and the elevation ( $\sigma_y > 0$ ), and different boresight errors in each axis of the receiver plane ( $\mu_x$  and  $\mu_y$ ) i.e.,  $x \sim N(\mu_x, \sigma_x)$  and  $y \sim N(\mu_y, \sigma_y)$ . We can define  $\varphi_x = \omega_{zeq}/2\sigma_x$  and  $\varphi_y = \omega_{zeq}/2\sigma_y$  as the ratios between the equivalent beam radius at the receiver and the corresponding pointing error displacement standard deviation (jitter) at the receiver. It must be noted that a circular detection aperture of radius  $a = D/2$  is assumed at the receiver. The beam footprint with generalized misalignment on the detector plane is illustrated in Fig. 4.1.

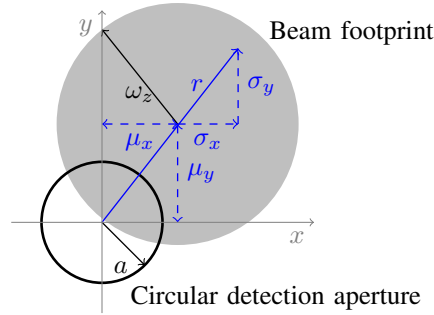


Figure 4.1: Beam footprint with generalized pointing errors on the receiver aperture plane.

In the general case, the radial displacement  $r$  at the receiver follows a Beckmann distribution whose integral-form PDF can be found in [34, eqn. (31)] as follows

$$f_r(r) = \frac{r}{2\pi\sigma_x\sigma_y} \int_0^{2\pi} \exp\left(-\frac{(r \cos \theta - \mu_x)^2}{2\sigma_x^2} - \frac{(r \sin \theta - \mu_y)^2}{2\sigma_y^2}\right) d\theta, \quad r \geq 0. \quad (4.2)$$

It must be mentioned that finding the combined effect of atmospheric turbulence and generalized pointing errors might be mathematically intractable due to the fact that the Beckmann distribution presents certain impediments from a practical point of view since a closed-form solution for its integral in Eq. (4.2) is unknown.

One of the statistical tools that can be used to mathematically treat the Beckmann distribution is the moment generating function (MGF) of the squared Beckmann distribution ( $r^2$ ). In probability theory, the MGF of a RV  $\chi$  is defined as the expectation of the RV  $\exp(t\chi)$  as

$$M_\chi(t) = \mathbb{E}[\exp(t\chi)] = \int_{-\infty}^{\infty} \exp(tx) f_\chi(x) dx. \quad (4.3)$$

Therefore, the corresponding MGF of the squared Beckmann distribution can easily be derived from the sum of two independent squared normal RVs [73, eqn. (2.37)] as

$$M_{r,2}(t) = \mathbb{E}[e^{t \cdot r^2}] = \frac{\exp\left(\frac{\mu_x^2 t}{1-2t\sigma_x^2} + \frac{\mu_y^2 t}{1-2t\sigma_y^2}\right)}{\sqrt{(1-2t\sigma_x^2)(1-2t\sigma_y^2)}}. \quad (4.4)$$

Note that  $M_{r,2}(\cdot)$  is always greater than zero, i.e.,  $\forall t \ M_{r,2}(t) \geq 0$ .

### 4.3 Structure

The remainder of this chapter is organized as follows. In Section 4.4, the impact of generalized pointing errors on the outage performance is evaluated over EW atmospheric turbulence channels where the results are only valid when atmospheric turbulence is the dominant effect. Next, an approximation of the well-known Beckmann distribution is proposed to model generalized pointing errors in Section 4.5. This approximation is used to evaluate the BER and outage performance over GG atmospheric turbulence channels not only when atmospheric turbulence is the dominant effect, but also when pointing errors is the dominant effect. In addition, this tool is used to find optimum beam widths that minimize the impact of pointing error effects in a variety of atmospheric turbulence conditions. In Section 4.6, the approximation previously presented is used to add the effect of correlated sways to the FSO system. Finally, this chapter is concluded in Section 4.7.

### 4.4 An MGF-Based Approach to Analyze Generalized Pointing Errors

This analysis can be considered as a first step into the performance analysis of FSO systems under the effect of generalized pointing errors, resulting in two more works that will be presented in the next sections. These results are only valid when atmospheric turbulence is the dominant effect in relation to pointing errors.

This analysis focuses on the asymptotic outage performance of FSO links over EW atmospheric turbulence channels with generalized pointing errors (following a Beckmann distribution) by using an MGF-based approach as given in Eq. (4.4). It must be noted that there are no reported works that investigate the outage performance of FSO systems over EW atmospheric turbulence with generalized pointing errors.



#### 4.4.1 System and Channel Models

Let us consider a SISO FSO system that is based on IM/DD and OOK modulation. The statistical channel model for a SISO FSO system is given in Eq. (2.3) as

$$Y = IX + Z, \quad Z \sim N(0, N_0/2), \quad (4.5)$$

where  $I$  represents the equivalent irradiance through the optical channel between the transmit aperture and the photodetector. The received electrical SNR is also given in Eq. (2.47) as  $\gamma_T(i) = 4\gamma i^2$ , where  $\gamma = P_t^2 T_b / N_0$  represents the electrical SNR in absence of turbulence. In this analysis, atmospheric turbulence is modeled by the EW distribution in order to consider a wide range of turbulence conditions (weak-to-strong) and aperture averaging conditions, i.e., when the condition  $D \geq \rho_c$  holds. The PDF of EW atmospheric turbulence was presented in Eq. (2.22), and it is given by

$$f_{I_a}(i) = \frac{m_1 m_2}{m_3} \left( \frac{i}{m_3} \right)^{m_2-1} \times \exp \left( - \left( \frac{i}{m_3} \right)^{m_2} \right) \left\{ 1 - \exp \left( - \left( \frac{i}{m_3} \right)^{m_2} \right) \right\}^{m_1-1}, \quad i \geq 0 \quad (4.6)$$

where  $m_2 > 0$  is a shape parameter related to the SI,  $m_3 > 0$  is a scale parameter related to the mean value of the irradiance, and  $m_1 > 0$  is an extra shape parameter that is strongly dependent on the receiver aperture size. Pointing errors are modeled by the Beckmann distribution as given in Eq. (4.2).

Determining the combined effect of atmospheric turbulence and generalized pointing errors might be mathematically intractable due to the reasons as commented before. As a first step into the analysis of generalized pointing errors, an asymptotic analysis at high SNR is investigated in order to study how generalized pointing errors and atmospheric turbulence impact on outage performance when atmospheric turbulence is the dominant effect in relation to pointing errors. In this way, an asymptotic expression for atmospheric turbulence is adopted. Hence, the corresponding asymptotic expression of  $f_{I_a}(i)$  is given by Eq. (2.37) as

$$f_{I_a}(i) \doteq a i^{b-1}, \quad i \geq 0 \quad (4.7)$$

based on the fact that the asymptotic behavior of the system performance is dominated by the behavior of the PDF near the origin, i.e.  $f_{I_a}(i)$  at  $i \rightarrow 0$  determines high SNR performance. In this case, we obtain the corresponding asymptotic behavior of atmospheric turbulence due to the fact that the combined PDF of atmospheric turbulence and pointing errors is unknown regardless of the considered atmospheric turbulence model. At the end of this subsection, the EW atmospheric turbulence model will be assumed, and the corresponding parameters  $a$  and  $b$  will be computed.

In this chapter  $f_I(i)$  represents the combined PDF of atmospheric turbulence and generalized pointing errors and, hence, the PDF of  $I = L \cdot I_a \cdot I_p$  can also be obtained as

$$f_I(i) = \int_0^{A_0} f_{I|I_p}(i|L \cdot i_p) f_{I_p}(i_p) di_p, \quad (4.8)$$

where  $f_{I|I_p}(i|L \cdot i_p)$  is the conditional probability given a pointing error state  $I_p$  and  $L$  acts as a scaling factor. Hence, the resulting conditional distribution can be written as

$$f_{I|I_p}(i|L \cdot i_p) = \frac{1}{L \cdot i_p} f_{I_a} \left( \frac{i}{L \cdot i_p} \right). \quad (4.9)$$

Now, substituting Eq. (4.7) into Eq. (4.9) gives

$$f_{I|I_p}(i|L \cdot i_p) = \frac{a}{L \cdot i_p} f_{I_a} \left( \frac{i}{L \cdot i_p} \right) \doteq \frac{a}{L \cdot i_p} \left( \frac{i}{L \cdot i_p} \right)^{b-1}. \quad (4.10)$$

The asymptotic behavior of the PDF of  $I$ , i.e. combined effect of atmospheric turbulence and generalized pointing errors, can be expressed as follows

$$f_I(i) \doteq \frac{a}{L} \int_0^{A_0} \frac{1}{i_p} \left( \frac{i}{L \cdot i_p} \right)^{b-1} f_{I_p}(i_p) di_p = \frac{a}{L^b} i^{b-1} \underbrace{\int_0^{A_0} i_p^{-b} f_{I_p}(i_p) di_p}_{\mathbb{E}[I_p^{-b}]}. \quad (4.11)$$

In order to avoid computing the PDF of the generalized pointing error  $f_{I_p}(i)$ , we use an MGF-based approach. In this way, the above integral can be interpreted as  $\mathbb{E}[I_p^{-b}]$  since  $I_p$  is defined from 0 to  $A_0$ . Hence, taking into account that  $I_p(r; z) \approx A_0 \exp\left(\frac{-2r^2}{\omega_{z_{eq}}^2}\right)$ , we can rewrite  $\mathbb{E}[I_p^{-b}]$  as follows

$$\mathbb{E}[I_p^{-b}] = \mathbb{E} \left[ \left( A_0 \exp \left( \frac{-2r^2}{\omega_{z_{eq}}^2} \right) \right)^{-b} \right] = A_0^{-b} \cdot \mathbb{E} \left[ \exp \left( \frac{2br^2}{\omega_{z_{eq}}^2} \right) \right]. \quad (4.12)$$

Knowing that the MGF of a RV  $\chi$  is defined as the expectation of the RV  $\exp(t\chi)$ , the above equation is computed as the corresponding MGF of the RV  $r^2$  as

$$\mathbb{E}[I_p^{-b}] = A_0^{-b} \cdot \mathbb{E} \left[ \exp \left( \frac{2br^2}{\omega_{z_{eq}}^2} \right) \right] = A_0^{-b} M_{r^2} \left( \frac{2b}{\omega_{z_{eq}}^2} \right). \quad (4.13)$$

Hence, substituting Eq. (4.13) into Eq. (4.11), the asymptotic behavior of the PDF of  $I$  is finally expressed as

$$f_I(i) \doteq \frac{a}{(LA_0)^b} i^{b-1} \mathbb{E} \left[ e^{\frac{2br^2}{\omega_{z_{eq}}^2}} \right] = \frac{a M_{r^2} \left( \frac{2b}{\omega_{z_{eq}}^2} \right)}{(LA_0)^b} i^{b-1}, \quad i \geq 0. \quad (4.14)$$

Taking into account that  $\omega_{zeq}^2 = 4\sigma_x\sigma_y\varphi_x\varphi_y$ ,  $M_{r,2}\left(\frac{2b}{\omega_{zeq}^2}\right)$  yields

$$M_{r,2}\left(\frac{2b}{\omega_{zeq}^2}\right) = M_{r,2}\left(\frac{b}{2\sigma_x\sigma_y\varphi_x\varphi_y}\right) = \frac{\varphi_x\varphi_y \exp\left(\frac{b\mu_x^2}{2\sigma_x^2(\varphi_x^2-b)} + \frac{b\mu_y^2}{2\sigma_y^2(\varphi_y^2-b)}\right)}{\sqrt{(\varphi_x^2-b)(\varphi_y^2-b)}}. \quad (4.15)$$

Note that both  $\varphi_x^2$  and  $\varphi_y^2$  must be greater than  $b$  since  $\forall t M_{r,2}(t) \geq 0$ .

#### 4.4.2 Performance Analysis

As explained in Subsection 2.4.2, the outage probability  $P_{\text{out}}$  is defined as the probability that the received electrical SNR  $\gamma_T(i) = 4\gamma i^2$  falls below a certain specified threshold  $\gamma_{th}$ , i.e. ( $\gamma_T(i) \leq \gamma_{th}$ ), and, hence, this metric is computed as

$$P_{\text{out}} = P(4\gamma i^2 \leq \gamma_{th}) = \int_0^{\sqrt{\gamma_{th}/4\gamma}} f_I(i) di. \quad (4.16)$$

In this way, the asymptotic closed-form expression for the outage probability of the considered SISO FSO system can readily be obtained with the help of Eq. (4.14) as follows

$$\begin{aligned} P_{\text{out}} &= \int_0^{\sqrt{\gamma_{th}/4\gamma}} f_I(i) di \doteq \frac{aM_{r,2}\left(\frac{2b}{\omega_{zeq}^2}\right)}{(LA_0)^b} \int_0^{\sqrt{\gamma_{th}/4\gamma}} i^{b-1} di \\ &= \frac{aM_{r,2}\left(\frac{b}{2\sigma_x\sigma_y\varphi_x\varphi_y}\right)}{b(2LA_0)^b} \left(\frac{\gamma_{th}}{\gamma}\right)^{\frac{b}{2}} \\ &= \left[ \left( \frac{aM_{r,2}\left(\frac{b}{2\sigma_x\sigma_y\varphi_x\varphi_y}\right)}{b(2LA_0)^b} \right)^{-\frac{2}{b}} \cdot \frac{\gamma}{\gamma_{th}} \right]^{-\frac{b}{2}}, \end{aligned} \quad (4.17)$$

It is straightforward to show that the outage probability behaves asymptotically as  $P_{\text{out}} \doteq (O_c\gamma)^{-O_d}$ , where  $O_d$  and  $O_c$  denote outage diversity and coding gain, as commented in Subsection 2.4.2. Note that the outage diversity only depends on atmospheric turbulence, i.e.,  $O_d = b/2$  and, for that reason, this result is only valid when atmospheric turbulence is the dominant effect.

Now, we can particularize the asymptotic expression of the outage performance for EW atmospheric turbulence. In this way, the corresponding asymptotic expression of  $f_{I_a}(i)$ , where  $I_a$  is distributed according to the EW dsitribution, can easily be obtained from the

corresponding series expansion of the exponential function in Eq. (4.6) as follows

$$\begin{aligned}
f_{I_a}(i) &\doteq ai^{b-1} \\
&= \frac{m_1 m_2}{m_3} \left( \frac{i}{m_3} \right)^{m_2-1} \left\{ 1 - 1 + \frac{i^{m_2}}{m_3^{m_2}} \right\}^{m_1-1} \\
&= \frac{m_1 m_2}{m_3} \left( \frac{i}{m_3} \right)^{m_2-1} \frac{i^{m_1 m_2 - m_2}}{m_3^{m_1 m_2 - m_2}} = \frac{m_1 m_2}{m_3^{m_1 m_2}} i^{m_1 m_2 - 1}, \quad i \geq 0.
\end{aligned} \tag{4.18}$$

For the sake of clarity,  $a = m_1 m_2 / m_3^{m_1 m_2}$  and  $b = m_1 m_2$ . In order to provide more insights into Eq. (4.17) when EW atmospheric turbulence has been evaluated, we can say that the outage diversity is  $O_d = m_1 m_2 / 2$  when the effect of EW atmospheric turbulence is the dominant effect in relation to generalized pointing errors at high SNR, i.e, when  $m_1 m_2 < \{\varphi_x^2, \varphi_y^2\}$  according to Eq. (4.15) and, hence, the asymptotic expression is only valid when atmospheric turbulence is the dominant effect. In other words, the outage diversity only depends on atmospheric turbulence when larger amounts of misalignment are not assumed. By other hand, it is conjectured that outage diversity will depend on  $\varphi_x^2, \varphi_y^2$  and nonzero boresight errors when pointing errors dominate. However, this case is difficult to derive due to the Beckmann distribution. This case will be studied in the next sections. It can be shown that most practical terrestrial FSO systems operate under the condition of atmospheric turbulence is the dominant effect. This will be verified numerically in the next subsection. It must also be mentioned that a much higher outage diversity can be achieved under this condition and, hence, a much better performance is obtained. As a result, the adoption of the transmitter with accurate control of their beam width is especially important here to satisfy this desired FSO scenario in order to maximize the outage diversity.

It can be convenient to compare with the outage performance obtained here in a similar context without considering generalized pointing errors. Knowing that the impact of pointing errors in this analysis can be suppressed by assuming  $A_0 \rightarrow 1$ ,  $\mu_x = \mu_y = 0$ ,  $\varphi_x^2 \rightarrow \infty$  and  $\varphi_y^2 \rightarrow \infty$ , the corresponding asymptotic expression can easily be derived from Eq. (4.17) as follows

$$P_{\text{out}}^{npe} \doteq \left[ \left( \frac{a}{b(2L)^b} \right)^{-\frac{2}{b}} \cdot \frac{\gamma}{\gamma_{th}} \right]^{-\frac{b}{2}} = \left[ \underbrace{\left( \frac{1}{(2L m_3)^{m_1 m_2}} \right)^{-\frac{2}{m_1 m_2}}}_{O_c^{npe}} \cdot \frac{\gamma}{\gamma_{th}} \right]^{-\frac{m_1 m_2}{2}}. \tag{4.19}$$

Note that the above expression is the corresponding asymptotic behavior of the outage probability over EW atmospheric turbulence when generalized pointing errors are not considered, which allows us to easily obtain once again the outage diversity, i.e., the slope of the outage probability versus SNR. It is noteworthy to mention that the outage diversity  $O_d = m_1 m_2 / 2$  of the EW atmospheric turbulence had not been derived in any earlier work [44, 45, 47–51], which not only depends on channel parameters but also on aperture averaging.

Table 4.1: SISO FSO system configuration.

Parameter	Symbol	Value
S-D link distance	$d_{SD}$	3 km
Wavelength	$\lambda$	1550 nm
Receiver aperture diameter	$D = 2a$	10 cm
Transmit divergence at $1/e^2$	$\theta_z$	0.66 mrad
Beam width at 3 km	$\omega_z$	$\approx 200$ cm
Jitter angle at $1/e^2$	$\theta_s$	0.11 mrad
Maximum jitter at 3 km	$\sigma_x, \sigma_y$	$\approx 35$ cm
Boresight angle at $1/e^2$	$\theta_b$	0.06 mrad
Maximum boresight at 3 km	$\mu_x, \mu_y$	$\approx 20$ cm

Table 4.2: Weather conditions for EW atmospheric turbulence.

Weather	Visibility (km)	$C_n^2 \times 10^{-14} m^{-2/3}$
Haze	4	2 (Moderate turb.)
Clear	16	8 (Strong turb.)

#### 4.4.3 Numerical Results and Discussion

As an illustration of the asymptotic expression for the outage probability obtained in Eq. (4.17), some numerical results over EW atmospheric turbulence channels with generalized pointing errors are analyzed in this subsection. It must be noted that the system configuration adopted in this study is used in most practical terrestrial FSO communication systems as in [22, 53, 56, 134] as shown in Table 4.1. Different weather conditions are also adopted as shown in Table 4.2. Rytov variance values of  $\sigma_R^2 = \{3, 12\}$  are derived for a S-D link distance of  $d_{SD} = 3$  km corresponding to moderate and strong turbulence, respectively. Additionally, the optical beam width is relatively wide of 2-10 mrad of divergence at  $1/e^2$  that is equivalent to a beam spread of 6-30 m at 3 km (the S-D link distance considered here). Nevertheless, a narrower beam width should be used to avoid a high geometric loss when link distances greater than one kilometer are assumed. In this case, the use of automatic pointing and tracking systems is required in order to reduce pointing error effects, typically between 0.05-1 mrad of divergence at  $1/e^2$  that is equivalent to a beam spread of 15-300 cm at 3 km [22, 134]. Pointing errors are present assuming different

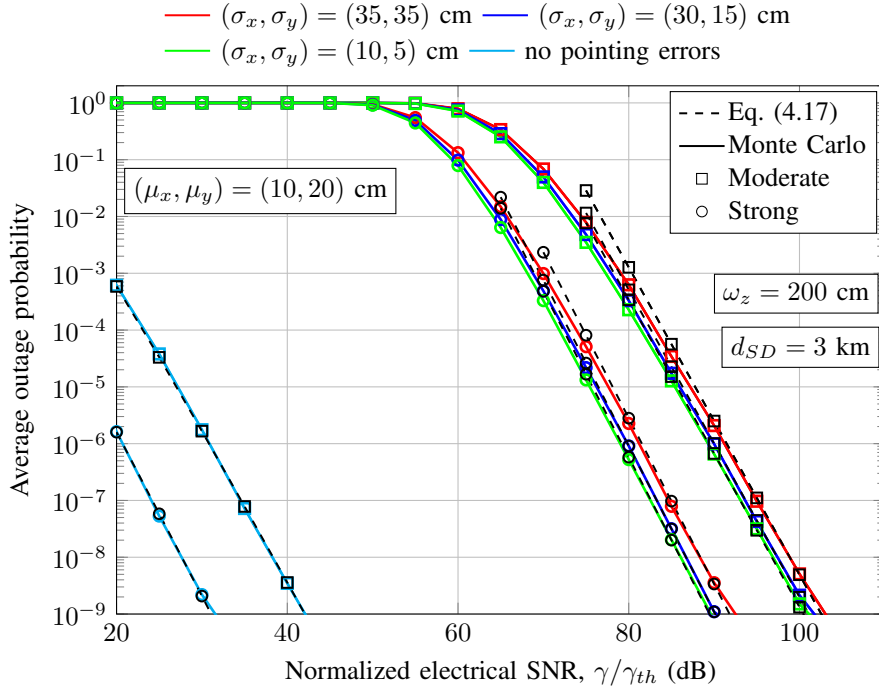


Figure 4.2: Outage performance for a 10 cm receiver aperture together with a beam width value of  $\omega_z = 200$  cm when different jitter values of  $(\sigma_x, \sigma_y) = \{(35, 35), (30, 15), (10, 5)\}$  cm are assumed under different atmospheric turbulence conditions.

jitters values and nonzero boresight errors, which can take values up to 0.1 mrad or even much smaller [55]. Parameters  $m_1$ ,  $m_2$  and  $m_3$  are calculated from Eq. (2.23), obtaining values of  $(m_1, m_2, m_3) = (4.57, 1.18, 0.52)$  and  $(m_1, m_2, m_3) = (4.31, 1.35, 0.58)$  corresponding to moderate and strong turbulence, respectively, for a S-D link distance of  $d_{SD} = 3$  km and a 10 cm receiver aperture.

### Outage Probability

The corresponding results of this asymptotic outage performance analysis are depicted in Fig. 4.2 as a function of the inverse normalized threshold SNR  $\gamma/\gamma_{th}$  when a  $D = 10$  cm receiver aperture is used. This aperture size has been selected according to the technical specifications for commercial FSO applications given in [11]. A beam width value of  $\omega_z = 200$  cm is considered corresponding to a 0.66 mrad of divergence at 3 km approximately. It can be shown that a value of  $\varphi^2 = 6.25$  greater than the product of  $m_1 m_2$  is computed when a beam width value of  $\omega_z = 200$  cm and a jitter angle of 0.13 mrad at  $1/e^2$  that is equivalent to a jitter value of 40 cm at 3 km are assumed. Hence, atmospheric turbulence is the dominant effect even when the greatest jitter value is considered. At

the same time, different jitters values of  $(\sigma_x, \sigma_y) = \{(35, 35), (30, 15), (10, 5)\}$  cm together with boresight error values of  $(\mu_x, \mu_y) = (10, 20)$  cm are considered in order to evaluate how generalized pointing errors impact on the FSO communications system under different atmospheric turbulence and aperture averaging conditions. In order to confirm the accuracy and usefulness of the derived expression, Monte Carlo simulation results are included as usual. Although the typical outage performance target is set to  $10^{-6}$  for most practical FSO systems, Monte Carlo simulation results only up to  $10^{-9}$  (due to long time involved) are included in this analysis due to the fact that targets as low as  $10^{-9}$  are typically aimed to achieve. As can be seen in Fig. 4.2, the derived expression for the outage probability is in good agreement with these simulation results. Furthermore, simulation results corroborate that the obtained asymptotic expression leads to a simple bound on the outage probability that get tighter over a wide range of SNR. Outage performance without pointing errors is also displayed by using Eq. (4.19). As commented before, a higher diversity order is achieved, which is determined by the product of  $m_1 m_2 / 2$ , when atmospheric turbulence is the dominant effect in relation to generalized pointing errors. This assumption is widely adopted in most practical terrestrial FSO communication systems. Furthermore, it can be observed that the outage probability decreases as generalized pointing errors increase. In other words, jitters values of  $(\sigma_x, \sigma_y) = \{(35, 35), (30, 15)\}$  cm significantly reduce much more the outage performance than jitters values of  $(\sigma_x, \sigma_y) = (10, 5)$  cm in both atmospheric turbulence scenarios. It should be highlighted that the 10 cm receiver aperture is considered as an aperture-averaged receiver under moderate-to-strong turbulence due to the fact that this diameter is greater than the correlation length  $\rho_c = \{12.6, 5.5\}$  mm under moderate and strong turbulence, respectively. As expected, aperture averaging can significantly improve the performance under moderate and strong atmospheric turbulence regardless of generalized pointing errors. A very interesting point is that the outage diversity is smaller in moderate turbulence than strong turbulence for this receiver aperture. This point might be confusing since we use a larger aperture receiver to mitigate the effect of atmospheric turbulence. But this one can be explained from the SI point of view. In moderate turbulence, the SI is at the beginning of the saturation regime and, hence, the effect of aperture averaging is less efficient. At the same time, in strong turbulence, we are in a well-established saturation regime as commented in Chapter 2. This phenomenon has been investigated by different authors in the literature [135, 136] where pointing error effects were not considered.

On the one hand, outage diversities of 2.7 and 2.92 are obtained over moderate and strong turbulence, respectively. On the other hand, a coding gain of 8.3 dB is achieved over strong turbulence channels in relation to moderate turbulence channels when a different visibility is considered. Although, a coding gain of approximately 1 dB is also achieved over strong turbulence when the same visibility is assumed for both turbulence regimes. It can also be observed that aperture averaging can take place even for relatively small apertures, i.e.  $D = 10$  cm, particularly under strong turbulence conditions as concluded in [135].

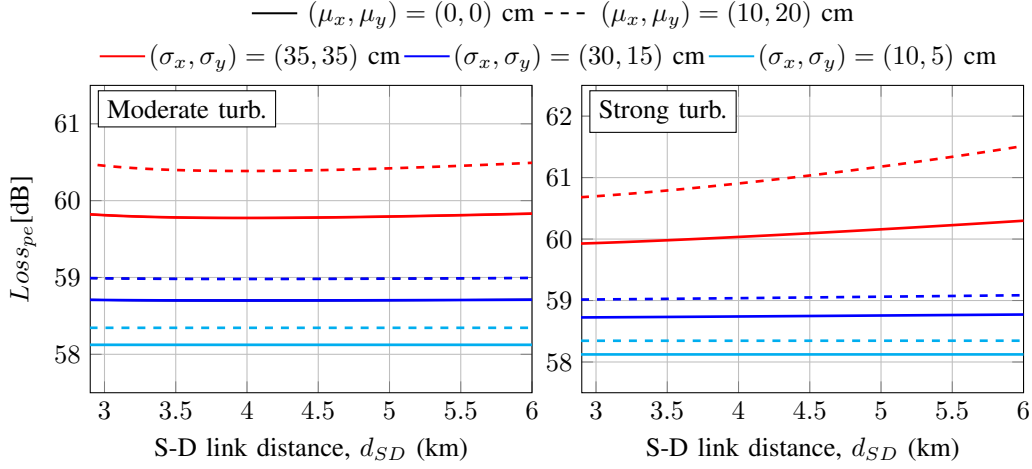


Figure 4.3:  $Loss_{pe}$  [dB] for moderate atmospheric turbulence and strong atmospheric turbulence when a 10 cm receiver aperture together with a beam width value of  $\omega_z = 200$  cm are considered under different nonzero boresight error values.

### Impact of generalized pointing errors

Taking into account the coding gain  $O_c$  in Eq. (4.17), the impact of generalized pointing errors translates into a loss,  $Loss_{pe}$  [dB], relative to a generic atmospheric turbulence without generalized misalignment fading in Eq. (4.19) given by

$$\begin{aligned}
 Loss_{pe} [dB] &\triangleq 10 \log \left( \frac{O_c^{npe}}{O_c} \right) \\
 &= -\frac{20}{b} \log \left( \frac{a/b(2L)^b}{aM_{r,2} \left( \frac{b}{2\sigma_x\sigma_y\varphi_x\varphi_y} \right) / b(2LA_0)^b} \right) \\
 &= \frac{20}{b} \log_{10} \left( A_0^{-b} M_{r,2} \left( \frac{b}{2\sigma_x\sigma_y\varphi_x\varphi_y} \right) \right).
 \end{aligned} \tag{4.20}$$

Now, we can particularize the above expression for EW atmospheric turbulence as

$$Loss_{pe} [dB] \triangleq \frac{20}{m_1 m_2} \log_{10} \left( A_0^{-m_1 m_2} M_{r,2} \left( \frac{m_1 m_2}{2\sigma_x\sigma_y\varphi_x\varphi_y} \right) \right). \tag{4.21}$$

The above expression computes the additional power needed to obtain a given outage performance when there is pointing error versus no pointing error.  $Loss_{pe}$  [dB] is plotted in Fig. 4.3 for a 10 cm receiver aperture as a function of the S-D link distance when different jitter values and boresight errors are considered as well as different turbulence conditions. It can be observed in Fig. 4.3 that the loss generally remains at a constant level as S-D link distance increases. However, it can also be seen in this figure that the loss slightly increases as the S-D link distance increases under strong turbulence conditions due to the fact



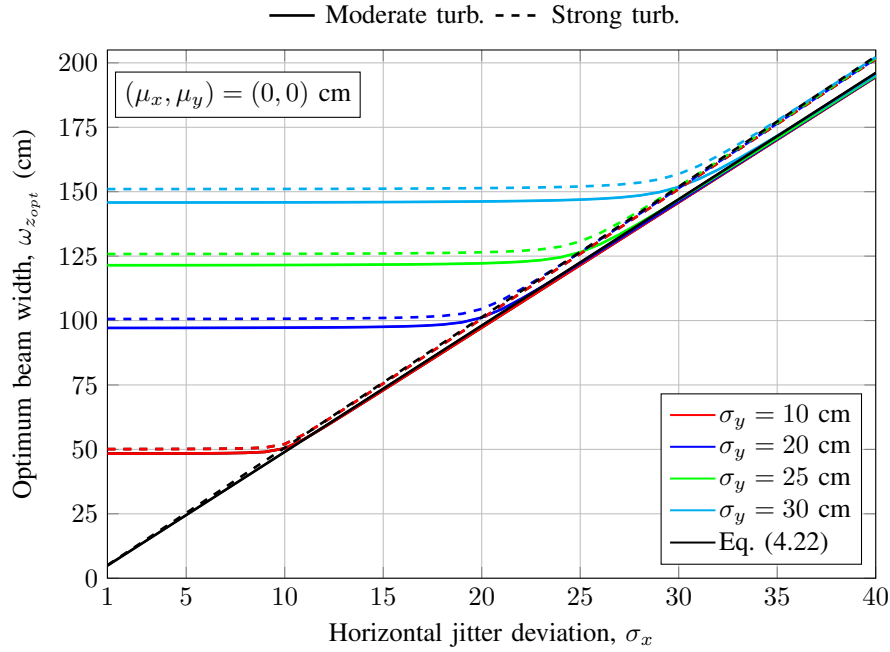


Figure 4.4: Optimum beam width,  $\omega_{z_{opt}}$ , versus horizontal jitter,  $\sigma_x$ , when different vertical jitter values,  $\sigma_y$ , are assumed in FSO links over EW atmospheric turbulence together with a S-D link distance of  $d_{SD} = 3$  km for a 10 cm receiver aperture.

that the product of  $m_1 m_2$  also increases as the S-D link distance increases for this aperture size ( $D = 10$  cm). Additionally, the loss increases considerably as nonzero boresight errors increase, i.e., as the impact of pointing errors is more severe.

### Beam Width Optimization

In order to minimize the effect of generalized pointing errors, the beam width  $\omega_z$  is chosen to minimize the outage probability in Fig. 4.4. Note that the beam width is an important parameter to consider in FSO communications link design. In this way, the optimization procedure is finished by finding the optimum beam width  $\omega_{z_{opt}}$  that gives the minimum loss in Eq. (4.21). This optimum beam width is achieved by using numerical observation methods for different jitter values and an aperture size of  $D = 10$  cm. The optimum value is obtained with the help of software packages such as Mathematica<sup>TM</sup> (version 10.4.1.0) by using a derivative-based method, which was found through a sweep of the beam width subject to constraints such as  $\omega_z > 6a$ ,  $\omega_z > \{\sigma_x, \sigma_y\}$  and  $m_1 m_2 < \{\varphi_x^2, \varphi_y^2\}$ . It can be seen in Fig. 4.4 that numerical results for the optimum beam width are plotted as a function of the horizontal jitter when different vertical jitter values of  $\sigma_y = \{10, 20, 25, 30\}$  cm are assumed. From this figure, it can be deduced that the outage performance optimization provides

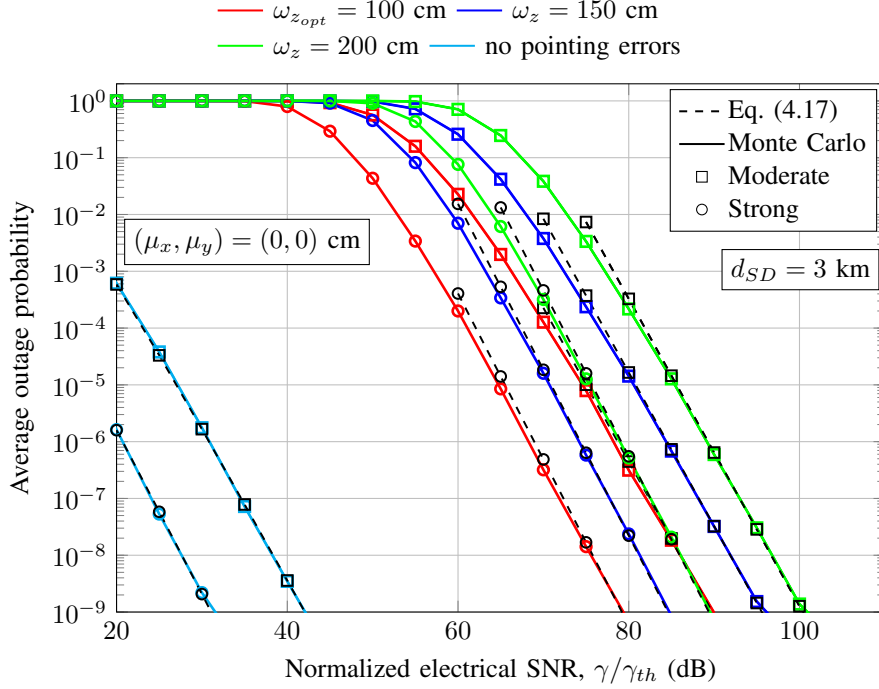


Figure 4.5: Outage performance for a 10 cm receiver aperture together with jitter values of  $(\sigma_x, \sigma_y) = (5, 20)$  cm when different beam width values of  $\omega_z = \{100, 150, 200\}$  cm are assumed under different atmospheric turbulence conditions.

numerical results (red, blue, green and cyan colors) tending to a linear performance for each value of  $\sigma_y$  (black color), where the corresponding slope only depends on EW atmospheric turbulence. Note that the optimum beam width depends on the maximum value between  $\sigma_x$  and  $\sigma_y$ . This linear behavior leads to easily obtain a first-degree polynomial, which is derived from the optimum beam width values through polynomial interpolation given by

$$\omega_{z_{opt}} \approx (-0.036(m_1 m_2)^2 + 0.77 m_1 m_2 + 1.76) \sigma_x, \quad \sigma_y < \sigma_x \quad (4.22)$$

where the slope follows a quadratic form in  $m_1 m_2$ . In the light of the expression obtained in Eq. (4.22), it can be observed that the optimum beam width is strongly dependent on the outage diversity,  $O_d = m_1 m_2 / 2$ . In other words, this optimum beam width depends on the aperture averaging and the receiver aperture diameter due to the fact that  $m_1$  and  $m_2$  are related to these parameters through the scintillation index as can be seen in Eqs. (2.13) and (2.23). As can be seen in Fig. 4.4, it is clearly depicted that the approximation remains very close to numerical results. Interestingly, it can also be seen in this figure that different slopes are derived for the optimum beam width when the product of  $m_1 m_2$  is equal to 5.41 and 5.84 for moderate and strong turbulence, respectively. Note that the expression in Eq. (4.22) can only be used when the relation  $\sigma_y < \sigma_x$  holds. It is noteworthy to mention that a slightly greater optimum beam width is required for strong turbulence in comparison

with moderate turbulence due to the fact that the product of  $m_1 m_2$  is greater under strong turbulence than moderate turbulence. It should be noted that the above expression can be used to estimate the optimum beam width when the boresight error takes small values up to 0.03 mrad, as reported in [55].

Numerical results for the optimum beam width are used in Fig. 4.5 for a 10 cm receiver aperture when jitter values of  $(\sigma_x, \sigma_y) = (5, 20)$  cm are assumed under different turbulence conditions. According to Eq. (4.21), it can be observed in Fig. 4.5 that losses of 48, 53.2 and 57.2 decibels are achieved for beam width values of  $\omega_z = \{100, 150, 200\}$  cm under moderate turbulence conditions. Analogously, losses of 48, 53.2 and 57.2 decibels are also achieved for beam width values of  $\omega_z = \{100, 150, 200\}$  cm under strong turbulence conditions. Note that the minimum achievable loss for jitter values of  $(\sigma_x, \sigma_y) = (5, 20)$  cm is 48 dB for an optimum beam width of  $\omega_{z_{opt}} = 100$  cm in this case.

## 4.5 Approximation of Generalized Pointing Errors

The second step into the analysis of generalized pointing errors is stated as follows. Due to the fact that finding a closed-form expression of the combined PDF of atmospheric turbulence and generalized pointing errors is mathematically intractable, we introduce an efficient and accurate approximation of the Beckmann distribution in this section, which is used to model generalized pointing errors with high precision over GG atmospheric turbulence channels. In this way, we derive an approximate closed-form PDF for the composite GG atmospheric turbulence with pointing errors by using the proposed approximation of the Beckmann distribution, which is valid for typical values in terrestrial FSO links and more extreme FSO scenarios. The performance of FSO communication links is analyzed in terms of the BER and outage probability. Moreover, the accuracy of the method is measured both visually and quantitatively using curve-fitting metrics.

The key contribution of this study in relation to the study performed in the previous section is that this novel approximation allows us to obtain its asymptotic behavior and delimit two different FSO scenarios. The first of them is when atmospheric turbulence is the dominant effect in relation to generalized pointing errors, and the second one when generalized pointing error is the dominant effect in relation to atmospheric turbulence (this scenario was unknown in the previous study and in the literature). Unfortunately, delimiting these two FSO scenarios has not been analyzed in-depth in the literature when the radial displacement  $r$  is not determined by a Rayleigh distribution, as in [56, 132]. In [132], obtained expressions for the BER over GG fading channels when the radial displacement  $r$  is determined by a Hoyt distribution are not valid for larger amounts of misalignment, i.e., when pointing errors become dominant in relation to atmospheric turbulence. Hence, we do not know when pointing errors begin to be dominant from a mathematical point of view. At the same time, in [56], the diversity order gain is given as a function of atmospheric turbulence

parameters, not being valid the obtained asymptotic expressions for the BER over GG fading channels when pointing error is the dominant effect, and, hence, as in [132], not knowing when pointing errors begin to be dominant. This study pretends to fill this gap with the proposed approximation of the Beckmann distribution.

#### 4.5.1 System and Channel Models

As in the previous section, the statistical channel model for a SISO FSO system is given in Eq. (2.3) as

$$Y = IX + Z, \quad Z \sim N(0, N_0/2). \quad (4.23)$$

Now, a novel approximation of the Beckmann distribution is presented and analyzed. As a result, the PDF in Eq. (4.2), i.e. the Beckmann distribution, is approximated by a modified Rayleigh distribution of parameter  $\sigma_{\text{mod}}$ . The advantage of approximating the Beckmann distribution by a modified Rayleigh distribution is twofold:

- (1) The corresponding PDF of  $I_p$  can easily be obtained as in [53, eqn. (11)] when the radial displacement  $r$  at the receiver is determined by a Rayleigh distribution.
- (2) The combined effect of GG atmospheric turbulence and pointing errors based on a modified Rayleigh distribution allows us to asymptotically analyze the performance of FSO communication systems and, hence, we can study how basic parameters impact on the FSO systems and optimize some of them such as beam width for potential FSO applications.

Quite interesting conclusions have been drawn from the asymptotic behavior in different FSO topics such as MIMO FSO systems, cooperative FSO systems and space-time codes in [17, 109, 137, 138], among others.

For convenience, let us consider  $u = r^2$  and, hence, it can be demonstrated that the squared radial displacement  $r^2$  follows an exponential distribution when  $r$  follows a modified Rayleigh distribution given by

$$f_{r^2}(u) = \frac{1}{2\sigma_{\text{mod}}^2} \exp\left(-\frac{u}{2\sigma_{\text{mod}}^2}\right), \quad u \geq 0. \quad (4.24)$$

Thus,  $\sigma_{\text{mod}}$  is used to estimate the diversity order gain when pointing error is the dominant effect in relation to atmospheric turbulence and delimit the two FSO scenarios previously commented. By using the method of central moments, we can obtain the expression of  $\sigma_{\text{mod}}$  from the third-order central moment. This method is quite simple and yields consistent estimators under not very strong assumptions. We observed through numerical observations that the diversity order gain when pointing error is the dominant effect can accurately be approximated from the third-order central moment, not deriving a relevant improvement

for higher-order central moments. The main idea behind this is to balance between the corresponding third-order central moment of the squared radial displacement ( $r$  follows a Beckmann distribution) and the corresponding third-order central moment of the exponential distribution given in Eq. (4.24). A central moment can be defined as the expected value of a specified integer power of the deviation of the RV from the mean, and it is defined as  $\Omega_n^X = \mathbb{E}[(\chi - \mathbb{E}[\chi])^n]$ . Hence, the corresponding third-order central moment of the squared radial displacement, where  $r$  follows a Beckmann distribution, can easily be expressed from the corresponding third-order central moment of the distribution of the sum of two squared normal RVs as

$$\Omega_3^{r^2} = 8\sigma_x^4 (3\mu_x^2 + \sigma_x^2) + 8\sigma_y^4 (3\mu_y^2 + \sigma_y^2), \quad (4.25)$$

and the third-order central moment of the exponential distribution is derived as

$$\Omega_3^u = 16\sigma_{\text{mod}}^6. \quad (4.26)$$

Now, matching Eq. (4.25) and Eq. (4.26), we can derive the corresponding expression of  $\sigma_{\text{mod}}^2$  as follows

$$\sigma_{\text{mod}}^2 = \left( \frac{3\mu_x^2\sigma_x^4 + 3\mu_y^2\sigma_y^4 + \sigma_x^6 + \sigma_y^6}{2} \right)^{1/3}. \quad (4.27)$$

As can be observed in Eq. (4.27), this expression reduces to the simplest case, i.e., the Rayleigh distribution, when same jitters and zero boresight errors are considered. Finally, the Beckmann distribution can accurately be approximated by a modified Rayleigh distribution as follows

$$f_r(r) \approx \frac{r}{\sigma_{\text{mod}}^2} \exp\left(-\frac{r^2}{2\sigma_{\text{mod}}^2}\right), \quad r \geq 0. \quad (4.28)$$

Similar to [53], combining Eq. (2.28) and Eq. (4.28), the PDF of  $I_p$  is approximated by

$$f_{I_p}(i) \approx \frac{\varphi_{\text{mod}}^2}{(A_0G)\varphi_{\text{mod}}^2} i^{\varphi_{\text{mod}}^2-1}, \quad 0 \leq i \leq A_0G \quad (4.29)$$

where  $\varphi_{\text{mod}} = \omega_{z_{\text{eq}}}/2\sigma_{\text{mod}}$ . We have derived an approximation of the PDF of  $I_p$  whose radial displacement  $r$  follows a Beckmann distribution of four parameters:  $\mu_x$ ,  $\mu_y$ ,  $\sigma_x$  and  $\sigma_y$ , by a PDF whose radial displacement  $r$  follows a modified Rayleigh distribution of one parameter:  $\sigma_{\text{mod}}$ . As can be deduced from Eq. (4.24), only one degree of freedom can be used to estimate the PDF of  $I_p$ . This degree of freedom has been used to balance the third-order central moment which have a strong impact on the obtained diversity order gain when pointing error is the dominant effect in relation to atmospheric turbulence. At the same time, to balance the mismatch between expectations, a new parameter  $G$  is added to the PDF in Eq. (4.29) to get a better fit.

Next,  $G$  is derived as follows. Taking as reference the method published in [139] for approximating the log-normal variates sum by Schwartz and Yeh, which is quite accurate for estimating the CDF for small values of its argument, we match the moment in the log-domain, i.e., we equate the first moment or expectation of  $\ln(I_p)$  when  $r$  is determined by

a Beckmann distribution with  $\ln(I_p)$  when  $r$  is determined by a modified Rayleigh distribution. Knowing that  $I_p$  is approximated as in Eq. (2.28), the logarithm of  $I_p$  can be expressed as  $\ln(I_p) = \ln(A_0) - 2r^2/\omega_{z_{eq}}^2$ . Hence, the expectation of  $\ln(I_p)$  is given by

$$\mathbb{E}[\ln(I_p)] = \ln(A_0) - (2/\omega_{z_{eq}}^2)\mathbb{E}[r^2]. \quad (4.30)$$

In this way, the expectation of  $\ln(I_p)$  is easily obtained from the MGF of the squared Beckmann distribution  $r^2$ . Hence, making use of that MGF, we can compute the expectation of  $\ln(I_p)$  when  $r$  is determined by a Beckmann distribution as follows

$$\mathbb{E}[\ln(I_p)] = \ln(A_0) - \frac{2(\mu_x^2 + \mu_y^2 + \sigma_x^2 + \sigma_y^2)}{\omega_{z_{eq}}^2} = \ln(A_0) - \frac{\mu_x^2 + \mu_y^2 + \sigma_x^2 + \sigma_y^2}{2\sigma_x\sigma_y\varphi_x\varphi_y}. \quad (4.31)$$

It must be noted that the above expression also represents the impact of generalized pointing errors on the asymptotic ergodic capacity of SISO FSO systems. From the above expression, we can obtain the corresponding impact of pointing errors on ergodic capacity for the rest pointing error models as derived in Appendix A.10. When  $r$  is determined by a modified Rayleigh distribution, the expectation of  $\ln(I_p)$  is easily obtained as

$$\mathbb{E}[\ln(I_p)] = \ln(A_0) + \ln(G) - 1/\varphi_{\text{mod}}^2. \quad (4.32)$$

Now, matching Eq. (4.31) and Eq. (4.32), we derive the corresponding expression of  $G$  as

$$G = \exp\left(\frac{1}{\varphi_{\text{mod}}^2} - \frac{1}{2\varphi_x^2} - \frac{1}{2\varphi_y^2} - \frac{\mu_x^2}{2\sigma_x^2\varphi_x^2} - \frac{\mu_y^2}{2\sigma_y^2\varphi_y^2}\right). \quad (4.33)$$

Note that a new parameter  $A_{\text{mod}}$  is defined as  $A_{\text{mod}} = A_0G$ .

### Combined Effect of GG Fading and Generalized Pointing Errors

The PDF in Eq. (2.34) which computes the combined effect of GG atmospheric turbulence and misalignment fading modeled by a Rayleigh distribution can be used to compute the combined effect of GG atmospheric turbulence and generalized pointing errors in this study. We only have to substitute the corresponding parameters  $A_0$  and  $\varphi^2$  by the corresponding parameters derived in this subsection  $A_{\text{mod}}$  and  $\varphi_{\text{mod}}^2$  as

$$f_I(i) \approx \frac{\alpha\beta\varphi_{\text{mod}}^2 i^{-1}}{A_{\text{mod}}L\Gamma(\alpha)\Gamma(\beta)} G_{1,3}^{3,0} \left( \frac{\alpha\beta}{A_{\text{mod}}L} i \left| \begin{array}{c} \varphi_{\text{mod}}^2 + 1 \\ \varphi_{\text{mod}}^2, \alpha, \beta \end{array} \right. \right), \quad i \geq 0. \quad (4.34)$$

The corresponding CDF was also derived in Eq. (2.36). Hence, this CDF can also be used to compute the combined effect of GG atmospheric turbulence and generalized pointing errors by repeating the same operation as in Eq. (4.34) as follows

$$F_I(i) \approx \frac{\varphi_{\text{mod}}^2}{\Gamma(\alpha)\Gamma(\beta)} G_{2,4}^{3,1} \left( \frac{\alpha\beta}{A_{\text{mod}}L} i \left| \begin{array}{c} 1, \varphi_{\text{mod}}^2 + 1 \\ \varphi_{\text{mod}}^2, \alpha, \beta, 0 \end{array} \right. \right), \quad i \geq 0. \quad (4.35)$$

As commented before, the PDF in Eq. (4.34) is approximated by its corresponding asymptotic behavior as follows

$$f_I(i) \approx a_M i^{b_M-1} = \begin{cases} \frac{\varphi_{\text{mod}}^2 (\alpha\beta)^\beta \Gamma(\alpha-\beta)}{(A_{\text{mod}}L)^\beta \Gamma(\alpha)\Gamma(\beta)(\varphi_{\text{mod}}^2-\beta)} i^{\beta-1}, & \varphi_{\text{mod}}^2 > \beta \\ \frac{\varphi_{\text{mod}}^2 (\alpha\beta)^{\varphi_{\text{mod}}^2} \Gamma(\alpha-\varphi_{\text{mod}}^2) \Gamma(\beta-\varphi_{\text{mod}}^2)}{(A_{\text{mod}}L)^{\varphi_{\text{mod}}^2} \Gamma(\alpha)\Gamma(\beta)} i^{\varphi_{\text{mod}}^2-1}. & \varphi_{\text{mod}}^2 < \beta \end{cases} \quad (4.36)$$

Note that different expressions for  $a_M$  and  $b_M$  were derived in Eq. (4.36) depending on the relation between  $\varphi_{\text{mod}}^2$  and  $\beta$  since plane wave propagation is assumed. Let us recall the parameters  $a$  and  $b$  as  $a_M$  and  $b_M$  in order to differentiate from the parameters obtained in Eq. (2.38).

#### 4.5.2 Performance Analysis

According to Eq. (2.48), the outage probability can be written as

$$\begin{aligned} P_{\text{out}} &= P(4\gamma i^2 \leq \gamma_{\text{th}}) \\ &= \int_0^{\sqrt{\gamma_{\text{th}}/4\gamma}} f_I(i) di = F_I\left(\sqrt{\frac{\gamma_{\text{th}}}{4\gamma}}\right) \\ &= \frac{\varphi_{\text{mod}}^2}{\Gamma(\alpha)\Gamma(\beta)} G_{2,4}^{3,1}\left(\frac{\alpha\beta}{A_{\text{mod}}L} \sqrt{\frac{\gamma_{\text{th}}}{4\gamma}} \middle| \begin{matrix} 1, \varphi_{\text{mod}}^2 + 1 \\ \varphi_{\text{mod}}^2, \alpha, \beta, 0 \end{matrix}\right). \end{aligned} \quad (4.37)$$

At the same time, the asymptotic BER was also obtained in Eq. (2.44), and it is given by

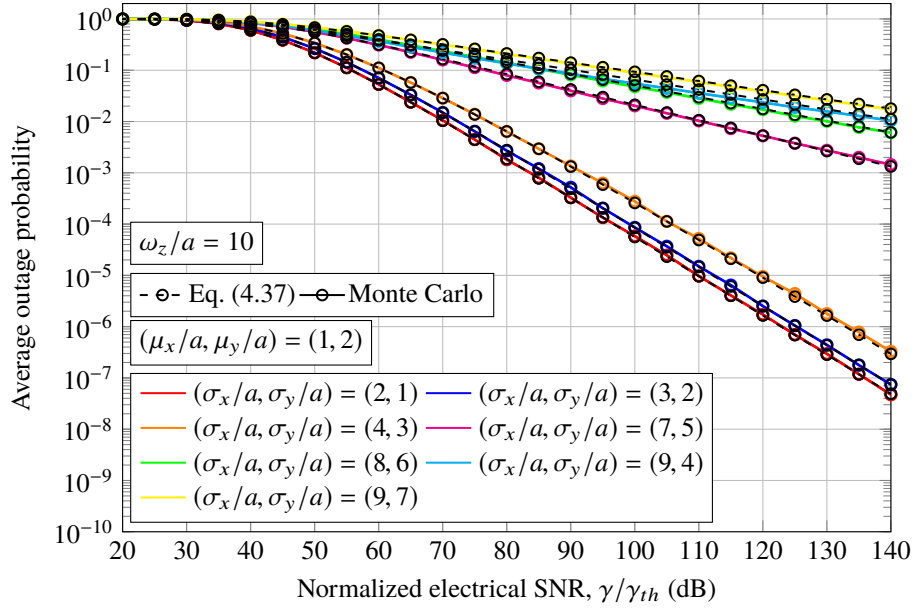
$$P_b \doteq \left[ \left( \frac{a_M \Gamma((b_M + 1)/2)}{2b_M \sqrt{\pi}} \right)^{-\frac{2}{b_M}} \cdot \gamma \right]^{-\frac{b_M}{2}}. \quad (4.38)$$

#### 4.5.3 Numerical Results and Discussion

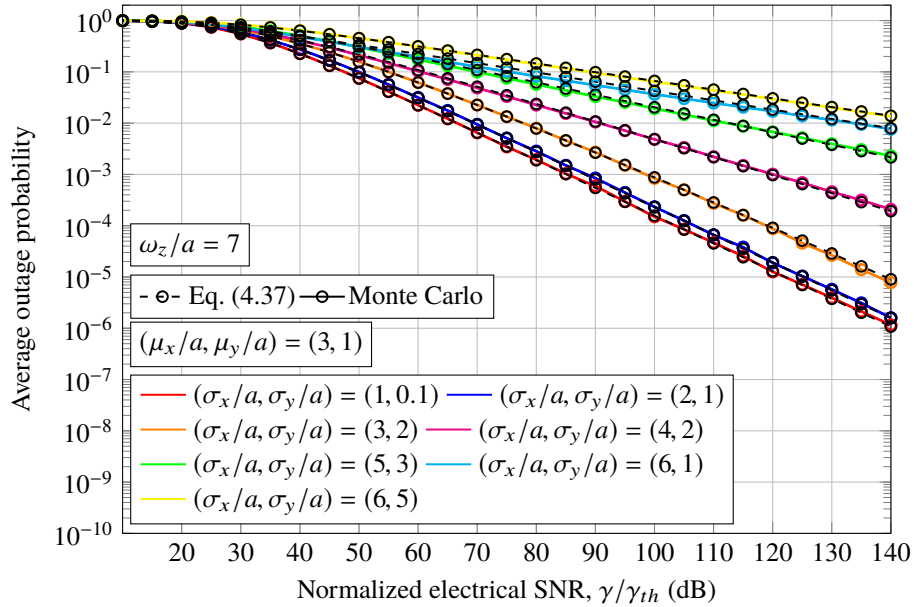
In this section, the proposed approximation for modeling the effect of generalized pointing errors on FSO links is evaluated over GG atmospheric turbulence channels, different misalignment error values, and different weather conditions as shown in Table 4.2. A value of wavelength of  $\lambda = 1550$  nm is assumed together with a S-D link distance of  $d_{SD} = 3$  km. Here,  $\alpha$  and  $\beta$  are calculated from Eq. (2.20) for GG atmospheric turbulence. Pointing errors are present assuming normalized beam width values of  $\omega_z/a = \{7, 10\}$  as well as different normalized jitter values and nonzero boresight errors.

#### BER and Outage Performance

Firstly, the corresponding results of the outage performance are illustrated in Fig. 4.6(a) for moderate turbulence and Fig. 4.6(b) for strong turbulence as a function of the inverse



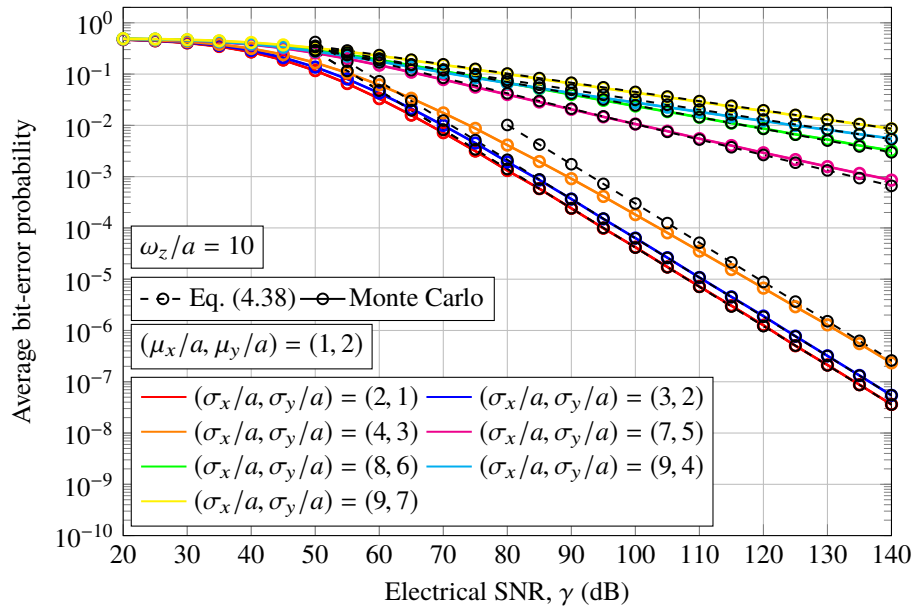
(a) Moderate turbulence.



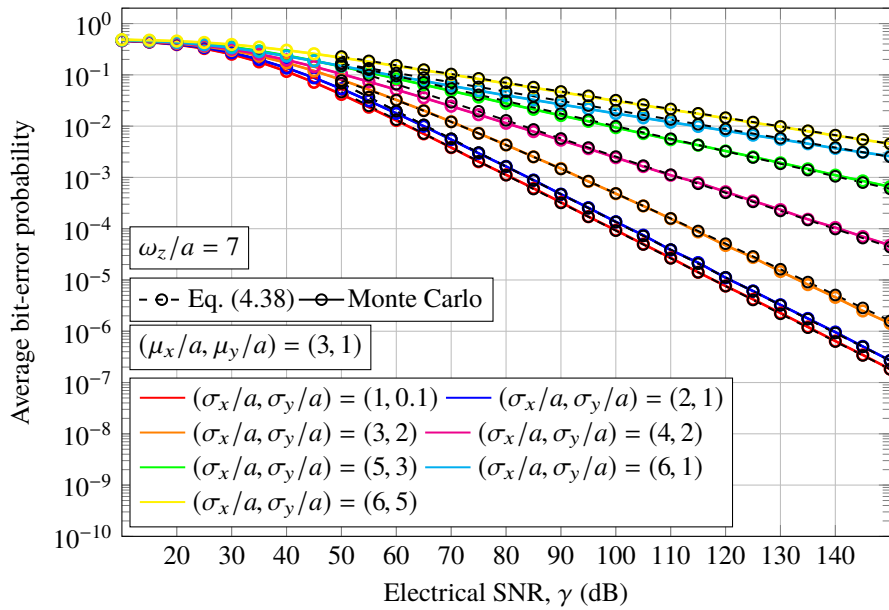
(b) Strong turbulence.

Figure 4.6: Outage performance over GG atmospheric turbulence and generalized misalignment fading channels when different weather conditions (a)  $C_n^2 = 1.7 \times 10^{-14} \text{ m}^{-2/3}$  and (b)  $C_n^2 = 8 \times 10^{-14} \text{ m}^{-2/3}$  are assumed for a S-D link distance of  $d_{SD} = 3 \text{ km}$ .





(a) Moderate turbulence.



(b) Strong turbulence.

Figure 4.7: BER performance over GG atmospheric turbulence and generalized misalignment fading channels when different weather conditions (a)  $C_n^2 = 1.7 \times 10^{-14} \text{ m}^{-2/3}$  and (b)  $C_n^2 = 8 \times 10^{-14} \text{ m}^{-2/3}$  are assumed for a S-D link distance of  $d_{SD} = 3 \text{ km}$ .

normalized threshold SNR,  $\gamma/\gamma_{th}$ . Analogously, the corresponding results of the asymptotic BER performance are illustrated in Fig. 4.7(a) for moderate turbulence and Fig. 4.7(b) for strong turbulence by assuming the same FSO scenario as in Fig. 4.6. Different normalized jitter values for the elevation and the horizontal displacement as well as different normalized nonzero boresight errors for each axes are assumed in Figs. 4.6 and 4.7 in order to carefully analyze how terrestrial FSO links are affected by generalized pointing errors.

Taking into account the proposed approximation in this study, two different FSO scenarios are analyzed depending on the relation  $\beta < \varphi_{\text{mod}}^2$  is satisfied or not. In this way, when this condition is satisfied, different normalized jitter values of  $(\sigma_x/a, \sigma_y/a) = \{(2, 1), (3, 2), (4, 3)\}$  together with normalized boresight error values of  $(\mu_x/a, \mu_y/a) = (1, 2)$  are considered in Figs. 4.6(a) and 4.7(a) for moderate turbulence conditions. Based on this, a higher diversity order, which is determined by  $\beta$ , is achieved when atmospheric turbulence is the dominant effect. In other words, the diversity order only depends on atmospheric turbulence, while the coding gain is affected by the degradation effect induced by generalized pointing errors. Analogously, different normalized jitter values of  $(\sigma_x/a, \sigma_y/a) = \{(1, 0.1), (2, 1), (3, 2)\}$  together with normalized boresight error values of  $(\mu_x/a, \mu_y/a) = (3, 1)$  are considered in Figs. 4.6(b) and 4.7(b) for strong turbulence conditions. These results are quite similar to those commented previously so that same conclusions can be drawn.

At the same time, the performance is also evaluated for larger amounts of generalized misalignment, showing that the proposed approximation is in good agreement with extreme FSO scenarios, i.e., when atmospheric turbulence is not the dominant effect. In other words, when the condition  $\beta < \varphi_{\text{mod}}^2$  is not satisfied and, hence, the diversity order is determined by  $\varphi_{\text{mod}}^2$ , which depends on the normalized beam width, normalized jitters and normalized boresight errors. As expected, the obtained performance in both outage probability and BER is notably decreased as a result of assuming much more severe pointing errors, i.e., normalized jitter values of  $(\sigma_x/a, \sigma_y/a) = \{(7, 5), (8, 6), (9, 4), (9, 7)\}$  together with normalized boresight error values of  $(\mu_x/a, \mu_y/a) = (1, 2)$  for moderate turbulence in Figs. 4.6(a) and 4.7(a), and normalized jitter values of  $(\sigma_x/a, \sigma_y/a) = \{(4, 2), (5, 3), (6, 1), (6, 5)\}$  together with normalized boresight error values of  $(\mu_x/a, \mu_y/a) = (3, 1)$  for strong turbulence in Figs. 4.6(b) and 4.7(b). In order to confirm the accuracy and usefulness of the proposed approximation, Monte Carlo simulation results are furthermore included by using solid line.

Due to the long simulation time involved, simulation results only up to  $10^{-9}$  are included in Figs. 4.6 and 4.7. It is noteworthy to mention that these results provide quite a good match between the analytical and the respective Monte Carlo simulation results and, hence, not only a high accuracy of the proposed approximation is verified over the outage probability, but also over the asymptotic BER performance. Moreover, the accuracy of the proposed approximation not only is measured visually, but also quantitatively using curve-fitting metrics defined over a region of interest.

Now, we quantitatively measure the accuracy of the proposed approximation in a specific

region of interest, in which the accuracy must be emphasized, taking as reference the FSO scenario illustrated in Fig. 4.6. Let  $\hat{F}_{OP}(\cdot)$  denote the approximate outage probability expression derived in Eq. (4.37) and  $F_{OP}(\cdot)$  the exact outage probability expression obtained by Monte Carlo simulation. Let  $\gamma_1, \dots, \gamma_N$  also denote  $N$  reference points in the region of interest. The accuracy metric for the outage probability is defined, as in [140, eqn. (25)], as follows

$$M_{OP} = \sum_{k=0}^N e_k \frac{|F_{OP}(\gamma_k) - \hat{F}_{OP}(\gamma_k)|}{F_{OP}(\gamma_k)}, \quad (4.39)$$

where  $e_k$  represents the relative error weight to emphasize different accuracies in tracking different reference points. Note that the following sum  $\sum_{k=1}^N e_k = 1$  must be satisfied. Let us assume that the relative error weights  $e_k$  are equal to  $1/N$  for all  $k$ . At the same time, the region of interest is defined to be from  $\gamma_1 = 20$  dB to  $\gamma_N = 120$  dB, with the reference points spaced 5 dB apart, i.e.,  $N = 21$ . Let us define  $q$  as the relation between  $\sigma_y/a$  and  $\sigma_x/a$ , where  $q \in (0, 1]$ , i.e.,  $\sigma_y/a = q\sigma_x/a$ . In this way, the accuracy metric  $M_{OP}$  is depicted in Fig. 4.8(a) as a function of  $q$ , considering the same FSO scenario as in Fig. 4.6. It can be observed that a much higher achievable accuracy is obtained when small normalized jitter values are adopted, obtaining values of the order of  $10^{-3}$ . Even when larger normalized jitter values are assumed, an achievable accuracy of the order of  $10^{-2}$  is obtained. In addition, the achievable accuracy is even much better as  $q$  increases. Analogously, it is depicted another accuracy metric in Fig. 4.8(b) as a practical example but considering another S-D link distance of  $d_{SD} = 5$  km in order to demonstrate the reliability of the proposed approximation in this study.

### Impact of Pointing Errors

Next, the impact of different jitters for the elevation and the horizontal displacement on asymptotic BER performance of FSO systems is studied. Hence, once the condition  $\beta < \varphi_{\text{mod}}^2$  is satisfied and taking into account the asymptotic analysis carried out in Subsection 4.5.2, we can obtain the loss in decibels between considering and not considering pointing errors. Knowing that the impact of pointing errors in our analysis can be suppressed by assuming  $A_{\text{mod}} \rightarrow 1$  and  $\varphi_{\text{mod}}^2 \rightarrow \infty$ , and considering the expression given in Eq. (4.38), the impact of the generalized pointing error effects translates into a loss,  $Loss_{pe}[dB]$ , relative to GG atmospheric turbulence without generalized misalignment fading given by

$$Loss_{pe}[dB] \triangleq \frac{20}{\beta} \log_{10} \left( \frac{\varphi_{\text{mod}}^2}{(A_{\text{mod}})^\beta (\varphi_{\text{mod}}^2 - \beta)} \right). \quad (4.40)$$

The above expression is obtained in a similar way to Eq. (4.20) since  $M_{r,2} \left( \frac{b}{2\sigma_x\sigma_y\varphi_x\varphi_y} \right)$  reduces to  $\varphi^2/(\varphi^2 - b)$  when pointing errors are modeled by a Rayleigh distribution. In this case, generalized pointing errors are modeled by a modified Rayleigh distribution and, hence,  $M_{r,2}(\cdot)$  reduces to  $\varphi_{\text{mod}}^2/(\varphi_{\text{mod}}^2 - \beta)$  where  $b = \beta$  in GG atmospheric turbulence. For

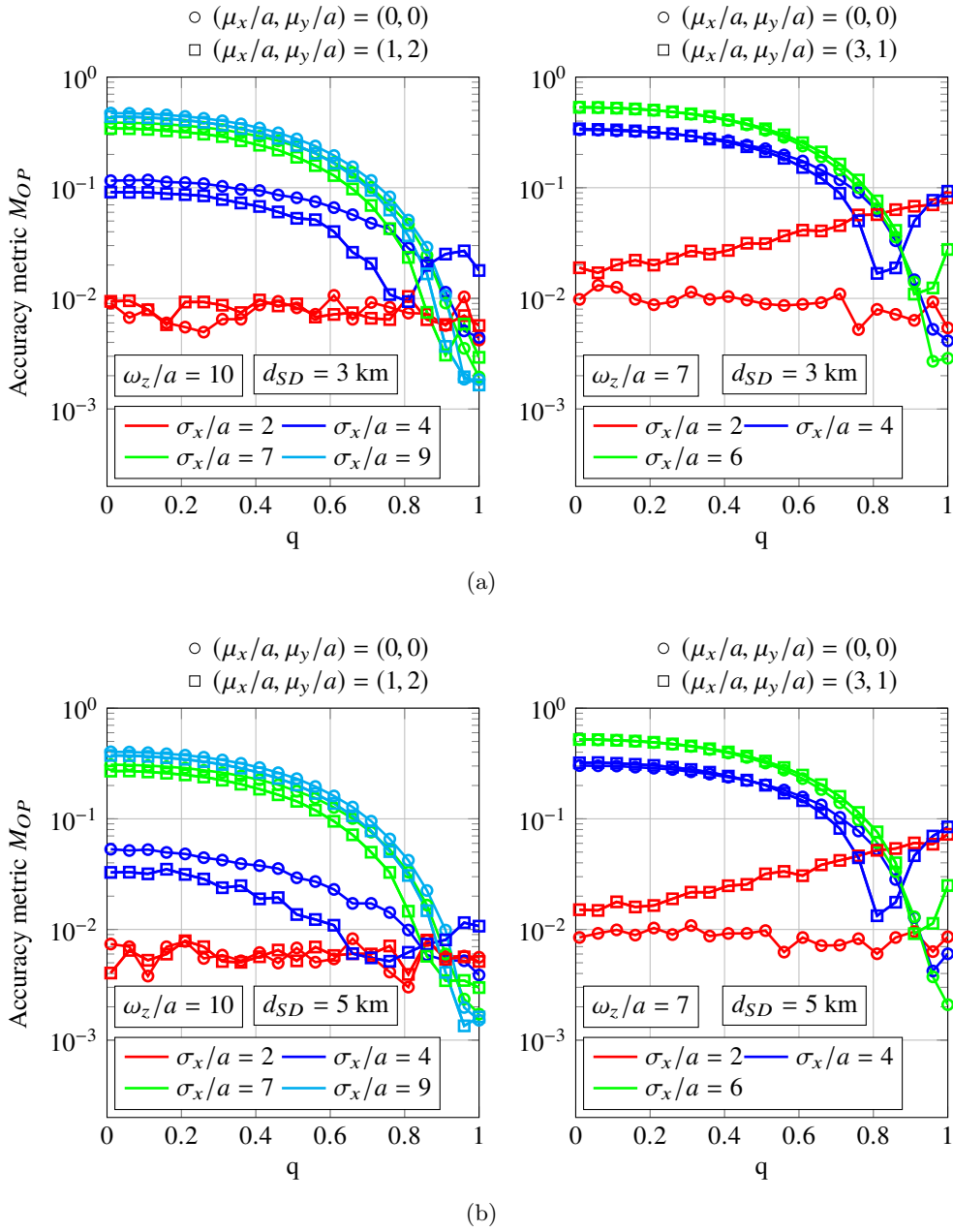


Figure 4.8: Accuracy metric  $M_{OP}$  as a function of  $q$  for the outage probability when (a) a S-D link distance of  $d_{SD} = 3$  km is assumed, and when (b) a S-D link distance of  $d_{SD} = 5$  km is assumed.

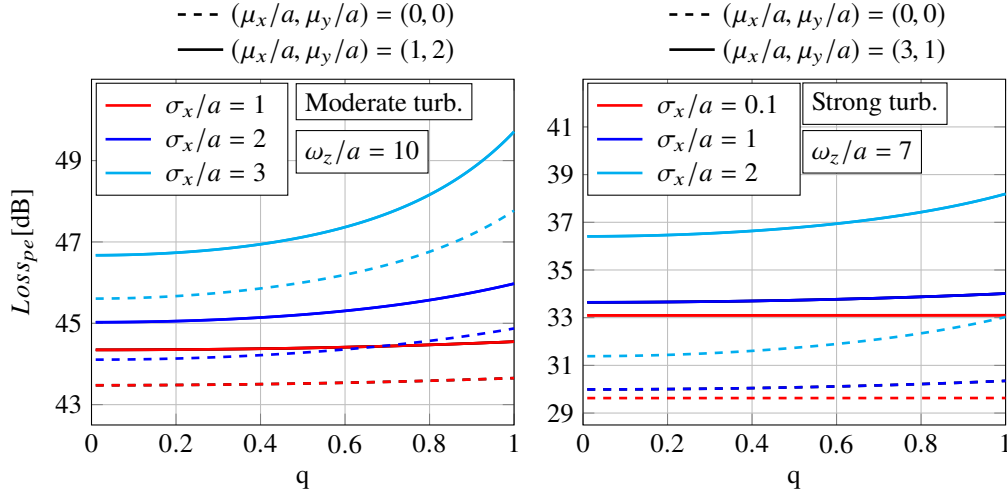


Figure 4.9:  $Loss_{pe}$  [dB] as a function of  $q$  for a S-D link distance of  $d_{SD} = 3$  km and different normalized boresight error values.

a better understanding of the impact of considering different jitters for the elevation and the horizontal displacement,  $Loss_{pe}$  [dB] is depicted in Fig. 4.9 as a function of  $q$  when different normalized boresight error values are assumed. From this figure, it can be deduced that the losses increase as the normalized jitter  $\sigma_x/a$  increases. However, this loss keeps practically constant when normalized jitter values much smaller than the normalized beam width are adopted. Equivalently, the same results and conclusions can be drawn when  $q$  is defined as  $\sigma_x/a = q\sigma_y/a$ . At the same time, the impact of nonzero boresight error is also studied in Fig. 4.10 as a function of the normalized horizontal boresight error when different normalized vertical boresight error values are assumed. As expected, the effect of nonzero boresight error can dramatically reduce the performance of FSO communication systems, increasing its effect as normalized jitter values increase. Equivalently, the same results and conclusions can be drawn when the impact of nonzero boresight is depicted as a function of the normalized vertical boresight error.

Finally, it should be commented that the adoption of the transmitter with accurate control of their beam width is especially important in order to maximize the diversity order gain and minimize both outage and BER under different atmospheric turbulence conditions. Therefore, a study of the required minimum normalized beam width is also included to guarantee that the relation  $\beta < \varphi_{\text{mod}}^2$  is always satisfied. We have to equate the corresponding expression of  $\varphi_{\text{mod}}^2 = \omega_{z_{eq}}^2 / 4\sigma_{\text{mod}}^2$  with  $\beta$  in order to know what the minimum normalized beam width value makes the condition  $\beta = \varphi_{\text{mod}}^2$  holds. For that, the equivalent beam width  $\omega_{z_{eq}}^2$  can be approximated by a parabola with sufficient accuracy as follows

$$\omega_{z_{eq}}^2 = \frac{\omega_z^2 \sqrt{\pi} \text{erf}(v)}{2v \exp(-v^2)} \approx \omega_z^2 + \frac{3}{2\sqrt{2}}. \quad (4.41)$$

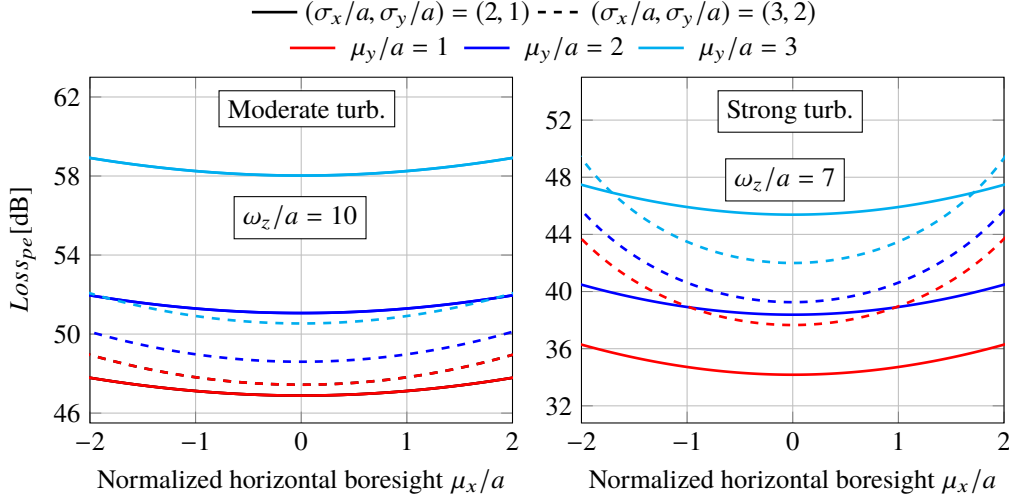


Figure 4.10: Impact of nonzero boresight error as a function of the normalized horizontal boresight error  $\mu_x/a$  for a S-D link distance of  $d_{SD} = 3$  km under different normalized vertical boresight error values of  $\mu_y/a = \{1, 2, 3\}$ .

The above expression is quite simple and favors mathematical treatment. It can be deduced that the corresponding expression of  $\varphi_{\text{mod}}^2$  can be approximated by

$$\varphi_{\text{mod}}^2 = \frac{\omega_{z_{eq}}^2}{4\sigma_{\text{mod}}^2} \approx \frac{2\sqrt{2}\omega_z^2 + 3}{8\sqrt{2}\sigma_{\text{mod}}^2}. \quad (4.42)$$

Now, we equate the expression in Eq. (4.42) with  $\beta$  and, after doing some easy algebraic manipulations, we obtain the required minimum normalized beam width to satisfy the relation  $\beta < \varphi_{\text{mod}}^2$  as follows

$$\omega_{z_{\min}}/a \approx 2^{-3/4} \left( 2^{1/6} 8\beta (3\mu_x^2 \sigma_x^4 + 3\mu_y^2 \sigma_y^4 + \sigma_x^6 + \sigma_y^6)^{1/3} - 3 \right)^{1/2}. \quad (4.43)$$

The above expression is plotted in Fig. 4.11 as a function of  $q$  when different normalized boresight error values are assumed. It can be observed in that figure that the minimum value of the normalized beam width slowly increases as  $q$  increases, being the worst case when  $q$  equals 1. It can be concluded that a greater severity of pointing error effects could be corrected with an increase in beam width in order to satisfy the condition  $\beta < \varphi_{\text{mod}}^2$ , i.e., to achieve a much higher diversity order gain. It is noteworthy to mention that increasing the beam footprint also reduces the incident power on a fixed-size receiver and, hence, it is important to not significantly overestimate the necessary receiver beam size.

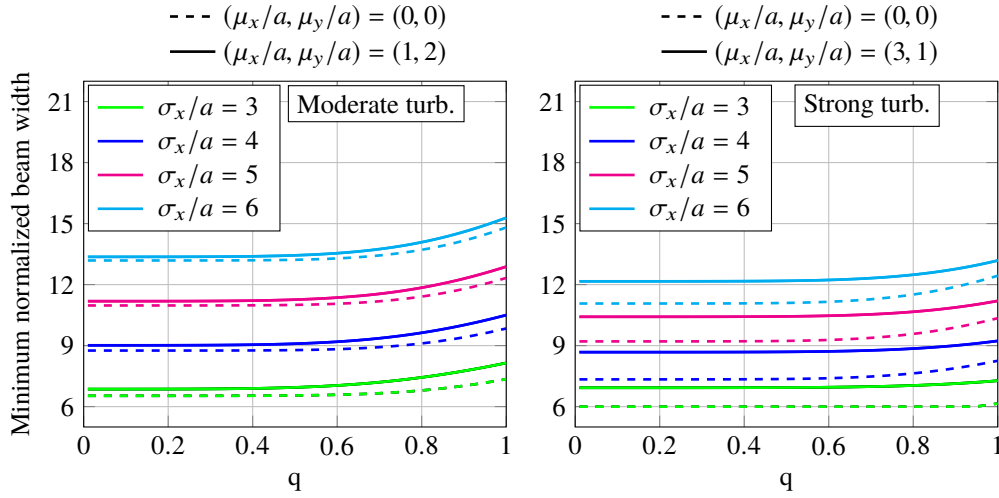


Figure 4.11: Minimum normalized beam width as a function of  $q$  for a S-D link distance of  $d_{SD} = 3$  km and different normalized boresight error values.

## 4.6 Impact of Correlated Sways on Pointing Errors

The third and last step into the analysis of generalized pointing errors is to add the effect of correlated sways to the FSO system design. In this section, the impact of correlated sways on generalized misalignment fading channels is evaluated. Generally, the radial displacement at the FSO receiver follows a Beckmann distribution as well as in other fields or applications. Hence, it seems much more reasonable to assume the effect of correlation between the horizontal displacement and the elevation since both of sways are not necessarily uncorrelated RVs in potential FSO applications. So far, the effect of correlated sways has only been assumed in satellite optical transmission when the radial displacement is distributed according to a Rayleigh distribution [141, 142].

Now, we characterize for the first time, the outage performance over GG atmospheric turbulence channels under the presence of generalized pointing errors with correlated sways. In this way, we propose a new statistical model to describe the effect of correlated sways on pointing errors that is used to analyze the outage performance of FSO links. It must be noted that there are no reported works that address this challenging research problem. An approximate closed-form PDF based on the previous results is derived that serves as an analytical tool to evaluate the performance of any kind of FSO communications system with a higher degree of sophistication and realism.

### 4.6.1 Statistical Background

The main idea behind this is to use the same expressions for the PDF and the CDF in Section 4.5 but including the effect of correlated sways. Hence, the approximate PDF of generalized pointing errors obtained in Eq. (4.29) will be modified to include the effect of correlated sways.

Next, a statistical model to include the effect of correlated sways on misalignment fading will be established and analyzed in greater detail. As commented before,  $x$  and  $y$  are not necessarily uncorrelated RVs in terrestrial FSO applications. Both  $x$  and  $y$  can be modeled as correlated Gaussian RVs with different jitters for the horizontal displacement ( $\sigma_x > 0$ ) and the elevation ( $\sigma_y > 0$ ), and different boresight errors in each axis of the receiver plane ( $\mu_x$  and  $\mu_y$ ), i.e.  $x \sim N(\mu_x, \sigma_x)$  and  $y \sim N(\mu_y, \sigma_y)$ , and Pearson correlation coefficient  $\rho \in [-1, 1]$ . Then, the random vector  $(x, y)$  follows a bivariate normal distribution with mean vector  $(\mu_x, \mu_y)$  and covariance matrix

$$\begin{pmatrix} x \\ y \end{pmatrix} \sim N \left[ \begin{pmatrix} \mu_x \\ \mu_y \end{pmatrix}, \begin{pmatrix} \sigma_x^2 & \rho\sigma_x\sigma_y \\ \rho\sigma_x\sigma_y & \sigma_y^2 \end{pmatrix} \right]. \quad (4.44)$$

It must be mentioned that zero correlation implies independence, for bivariate normal distribution. This is, of course, not so in general. The bivariate normal distribution for two related, normally distributed variables is defined by the following PDF

$$\begin{aligned} f_{XY}(x, y) &= \frac{1}{2\pi\sigma_x\sigma_y\sqrt{1-\rho^2}} \\ &\times \exp \left[ -\frac{1}{2(1-\rho^2)} \left[ \left( \frac{x-\mu_x}{\sigma_x} \right)^2 + \left( \frac{y-\mu_y}{\sigma_y} \right)^2 - 2\rho \left( \frac{x-\mu_x}{\sigma_x} \right) \left( \frac{y-\mu_y}{\sigma_y} \right) \right] \right]. \end{aligned} \quad (4.45)$$

The above PDF has a maximum at the mean vector  $(\mu_x, \mu_y)$ . The contours of equal density of bivariate normal distribution are ellipses at  $(\mu_x, \mu_y)$ . The major axes of these ellipses have a positive slope when  $\rho$  is positive, and a negative slope when  $\rho$  is negative. If  $\rho = 0$ , these contours are circles.

Knowing that  $x$  and  $y$  can be written in polar coordinates as  $x = r \cos \phi$  and  $y = r \sin \phi$ , where  $r$  is the non-negative RV that represents the radial displacement, and  $\phi$  is an angle in the interval  $(-\frac{\pi}{2}, \frac{\pi}{2})$ . In order to include the effect of correlated sways in this analysis, we define two new RVs:  $x'$  and  $y'$ . Both RVs are statistically independent whose statistics, i.e. mean and variance, will be expressed as a function of the correlation coefficient  $\rho$  between  $x$  and  $y$ . In this way, let us also define these new RVs in polar coordinates as  $x = r \cos \phi'$  and  $y = r \sin \phi'$ , where  $\phi_0 = \phi - \phi'$ . It must be noted that the relation  $x^2 + y^2 = x'^2 + y'^2 = r^2$  always holds, as in [34]. Now, we obtain the value of  $\phi_0$  that makes the covariance between  $x'$  and  $y'$  equals zero since both of them are statistically independent. Note that  $x = x'$  and  $y = y'$  when  $\phi = \phi'$ . Hence, we can write the covariance between  $x'$  and  $y'$  as

$$\text{Cov}[x', y'] = \text{Cov}[r \cos(\phi - \phi_0), r \sin(\phi - \phi_0)]. \quad (4.46)$$



Table 4.3: Expressions for pointing error parameters with correlated sways.

Parameter	Symbol	Expression
Horizontal mean	$\mu'_x$	$\mu_x \cos \phi_0 + \mu_y \sin \phi_0$
Vertical mean	$\mu'_y$	$\mu_y \cos \phi_0 - \mu_x \sin \phi_0$
Horizontal variance	$\sigma_x'^2$	$\sigma_x^2 \cos^2 \phi_0 + \sigma_y^2 \sin^2 \phi_0 + 2\rho\sigma_x\sigma_y \sin \phi_0 \cos \phi_0$
Vertical variance	$\sigma_y'^2$	$\sigma_y^2 \cos^2 \phi_0 + \sigma_x^2 \sin^2 \phi_0 - 2\rho\sigma_x\sigma_y \sin \phi_0 \cos \phi_0$

Taking into account the properties of the covariance under linear transformations whose intermediate steps have been omitted in this thesis, we can rewrite the above covariance as follows

$$Cov[x', y'] = 2\rho\sigma_x\sigma_y \cos^2 \phi_0 + (\sigma_y^2 - \sigma_x^2) \sin \phi_0 \cos \phi_0 - \rho\sigma_x\sigma_y. \quad (4.47)$$

Next, we have to find the values of  $\phi_0$  that make the covariance equals zero. Then, if  $Cov[x', y'] = 0$ , we obtain

$$\frac{2 \sin \phi_0 \cos \phi_0}{2 \cos^2 \phi_0 - 1} = \frac{2\rho\sigma_x\sigma_y}{\sigma_x^2 - \sigma_y^2}. \quad (4.48)$$

Now, we can rewrite the above expression with the help of [62, eqn. (1.313.9)] (See Appendix A.8), obtaining

$$\tan 2\phi_0 = \frac{2\rho\sigma_x\sigma_y}{\sigma_x^2 - \sigma_y^2}. \quad (4.49)$$

Finally, the values of  $\phi_0$  that make the covariance equals zero are computed as follows

$$\phi_0 = \begin{cases} \frac{\pi}{4}, & \sigma_x = \sigma_y \\ \frac{1}{2} \arctan\left(\frac{2\rho\sigma_x\sigma_y}{\sigma_x^2 - \sigma_y^2}\right), & \sigma_x \neq \sigma_y \end{cases} \quad (4.50)$$

At this time, we can derive the corresponding means and variances of  $x'$  and  $y'$  that are shown as a summary in Table 4.3 (See Appendix C). Similar to Eq. (4.44), we can express both  $x'$  and  $y'$  in a matrix form as follows

$$\begin{pmatrix} x' \\ y' \end{pmatrix} \sim N \left[ \begin{pmatrix} \mu'_x \\ \mu'_y \end{pmatrix}, \begin{pmatrix} \sigma_x'^2 & 0 \\ 0 & \sigma_y'^2 \end{pmatrix} \right]. \quad (4.51)$$

Finally, it must be noted that the radial displacement  $r$  at the receiver plane is expressed as  $r^2 = x'^2 + y'^2$ , where  $x'$  and  $y'$  represent the equivalent horizontal displacement and the equivalent elevation, respectively. Both  $x'$  and  $y'$  are modeled as independent Gaussian RVs with unequal means and unequal variances.

### Linear Correlation Analysis

In the light of expressions obtained in Table 4.3, different conclusions can be drawn from the transformation of Gaussian RVs performed here in order to add the effect of correlated

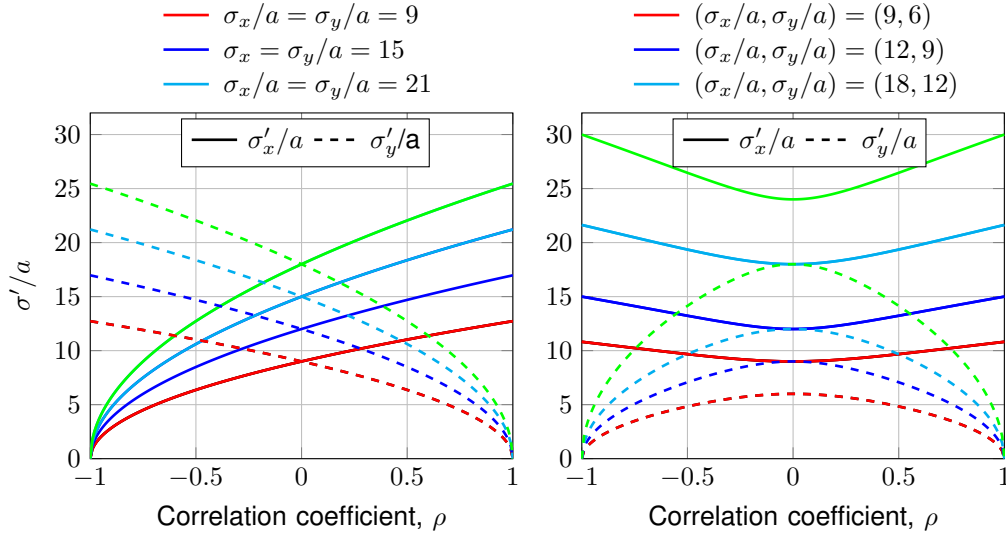


Figure 4.12: Effect of correlation on normalized jitters as a function of the correlation coefficient  $\rho$  for a S-D link distance of  $d_{SD} = 3$  km.

sways to the generalized misalignment fading. It must be noted that both boresight errors and pointing error deviations corresponding to the horizontal displacement and the elevation strongly depend on the correlation coefficient. This fact makes a transformation in PDFs that needs to be commented.

On the one hand, when the radial displacement follows a Rayleigh distribution, i.e.  $\mu_x = \mu_y = 0$  and  $\sigma_x = \sigma_y$ , the effect of correlated sways turns a Rayleigh distribution into a Hoyt distribution. The effect of correlation makes different jitters in each axis. At the same time, when the radial displacement follows a lognormal-Rice distribution, i.e.  $\mu_x \neq \mu_y \neq 0$  and  $\sigma_x = \sigma_y$ , the effect of correlated sways turns a lognormal-Rice distribution into a Beckmann distribution, i.e. the most general case, where each of parameters can take different values.

On the other hand, this phenomenon does not occur in the rest of distributions such as Hoyt and Beckmann, i.e.  $\sigma_x \neq \sigma_y$ , due to the fact that both of them assume different jitters and, hence, the effect of correlation keeps making the same PDF. According to Table 4.3, the corresponding expressions of jitter variances are plotted in Fig. 4.12 in order to see how these variances are affected by the effect of correlation when both jitter variances start taking the same value and, when, they start taking different values. The most relevant thing here is that when one axis increases, the another one does the opposite, increasing the dispersion between both axes as well as the symmetry with respect to  $\rho = 0$ .

### 4.6.2 System and Channel Models

As in previous sections, the statistical channel model for a SISO FSO system is given by

$$Y = IX + Z, \quad Z \sim N(0, N_0/2). \quad (4.52)$$

As presented in Section 4.5, we take full advantage of this approximation due to its mathematical simplicity to include the effect of correlated sways. On the one hand, the corresponding PDF of  $I_p$  is approximated as in Eq. (4.29) where the parameters  $\varphi_{\text{mod}}$  and  $A_{\text{mod}}$  both include the effect of correlated sways as obtained in this section and summarized in Table 4.3. In fact, the corresponding expression of  $\sigma_{\text{mod}}^2$  is redefined as

$$\sigma_{\text{mod}}^2 = \left( \frac{3\mu_x'^2 \sigma_x'^4 + 3\mu_y'^2 \sigma_y'^4 + \sigma_x'^6 + \sigma_y'^6}{2} \right)^{1/3}, \quad (4.53)$$

where  $\varphi_{\text{mod}} = \omega_{z_{eq}}/2\sigma_{\text{mod}}$ . Also, the corresponding expression of  $A_{\text{mod}}$  is redefined as

$$A_{\text{mod}} = A_0 \exp \left( \frac{1}{\varphi_{\text{mod}}^2} - \frac{1}{2\varphi_x'^2} - \frac{1}{2\varphi_y'^2} - \frac{\mu_x'^2}{2\sigma_x'^2 \varphi_x'^2} - \frac{\mu_y'^2}{2\sigma_y'^2 \varphi_y'^2} \right). \quad (4.54)$$

On the other hand, both the PDF and the CDF obtained in Eq. (4.34) and Eq. (4.35), respectively, can be used here but taking into account the effect of correlated sways, i.e., the new expressions of  $\varphi_{\text{mod}}$  and  $A_{\text{mod}}$ . In this sense, an asymptotic expression for the PDF was obtained in Eq. (2.38) as follows

$$\begin{aligned} f_I(i) &\approx a_M i^{b_M-1} \\ &= \begin{cases} \frac{\varphi_{\text{mod}}^2 (\alpha\beta)^{\min(\alpha,\beta)} \Gamma(|\alpha-\beta|)}{(A_{\text{mod}}L)^{\min(\alpha,\beta)} \Gamma(\alpha)\Gamma(\beta) (\varphi_{\text{mod}}^2 - \min(\alpha,\beta))} i^{\min(\alpha,\beta)-1}, & \varphi_{\text{mod}}^2 > \min(\alpha,\beta) \\ \frac{\varphi_{\text{mod}}^2 (\alpha\beta)^{\varphi_{\text{mod}}^2} \Gamma(\alpha - \varphi_{\text{mod}}^2) \Gamma(\beta - \varphi_{\text{mod}}^2)}{(A_{\text{mod}}L)^{\varphi_{\text{mod}}^2} \Gamma(\alpha)\Gamma(\beta)} i^{\varphi_{\text{mod}}^2-1}. & \varphi_{\text{mod}}^2 < \min(\alpha,\beta) \end{cases} \end{aligned} \quad (4.55)$$

### 4.6.3 Performance Analysis

According to Eq. (2.48), the outage probability can be written as

$$\begin{aligned} P_{\text{out}} &= P(4\gamma i^2 \leq \gamma_{th}) = \int_0^{\sqrt{\gamma_{th}/4\gamma}} f_I(i) di = F_I \left( \sqrt{\frac{\gamma_{th}}{4\gamma}} \right) \\ &= \frac{\varphi_{\text{mod}}^2}{\Gamma(\alpha)\Gamma(\beta)} G_{2,4}^{3,1} \left( \frac{\alpha\beta}{A_{\text{mod}}L} \sqrt{\frac{\gamma_{th}}{4\gamma}} \left| \begin{array}{l} 1, \varphi_{\text{mod}}^2 + 1 \\ \varphi_{\text{mod}}^2, \alpha, \beta, 0 \end{array} \right. \right). \end{aligned} \quad (4.56)$$

Unlike Eq. (4.37), the parameters  $A_{\text{mod}}$  and  $\varphi_{\text{mod}}^2$  both include the effect of correlated sways. To provide more insight into this analysis, we can obtain the corresponding asymptotic

Table 4.4: FSO communication system settings.

Parameter	Symbol	Value
S-D link distance	$d_{SD}$	3 km
Wavelength	$\lambda$	1550 nm
Receiver aperture diameter	$D = 2a$	10 cm
Transmit divergence	$\theta_z$	1 mrad
Normalized beam width	$\omega_z/a$	$\simeq 60$
Maximum jitter angle	$(\theta_{sx}, \theta_{sy})$	0.4 mrad
Maximum normalized jitter	$(\sigma_x/a, \sigma_y/a)$	$\simeq 24$
Maximum boresight angle	$(\theta_{bx}, \theta_{by})$	0.3 mrad
Maximum normalized boresight error	$(\mu_x/a, \mu_y/a)$	$\simeq 18$

behavior of Eq. (4.56). Note that an asymptotic expression for the outage probability was derived in Eq. (2.49) as

$$P_{\text{out}} \doteq \left[ \left( \frac{a'_M}{b'_M (2L)^{b'_M}} \right)^{-\frac{2}{b'_M}} \cdot \frac{\gamma}{\gamma_{th}} \right]^{-\frac{b'_M}{2}}, \quad (4.57)$$

The above expression serves to analyze the impact of correlated sways on coding gain and outage diversity. Finally, the outage diversity is obtained as

$$O_d = b'_M/2 = \min(\alpha, \beta, \varphi_{\text{mod}}^2) / 2, \quad (4.58)$$

where the effect of correlated sways appears to be implicitly in the  $\varphi_{\text{mod}}^2$  parameter.

#### 4.6.4 Numerical Results and Discussion

In this section, the effect of correlated sways is evaluated over GG atmospheric turbulence channels with generalized pointing errors. The system configuration adopted in this study is shown in Table E.3, and weather conditions in Table 4.2.

##### Outage Diversity Analysis

For a better understanding of the impact of correlated sways on outage performance of FSO links, the outage diversity is depicted in Fig. 4.13 as a function of the linear correlation

coefficient  $\rho$  for different normalized jitter values as well as different normalized boresight error values. Pointing error values are obtained according to Table E.3. A normalized beam width value of  $\omega_z/a = 60$  is derived according to the S-D link distance considered in this analysis. In the light of Eq. (4.58), we can know what issue, i.e., atmospheric turbulence or pointing errors, the dominant effect is. From Fig. 4.13, it can be observed that the outage diversity is strongly dependent on the correlation coefficient. As expected, when atmospheric turbulence is the dominant effect, i.e. when normalized jitter values of  $\sigma_x/a = \sigma_y/a = 6$  are considered, the outage diversity keeps at a constant level due to the fact that atmospheric turbulence does not depend on the correlation coefficient. On the contrary, when pointing error is the dominant effect, i.e. when normalized jitter values of  $\sigma_x/a = \sigma_y/a = \{15, 18, 21\}$  are considered, the outage diversity strongly depends on the correlation coefficient. In other words, the relation  $\varphi_{\text{mod}}^2 > \min(\alpha, \beta)$  does not hold when larger amounts of misalignment are assumed such as  $\sigma_x/a = \sigma_y/a = \{15, 18, 21\}$ .

Note that the pointing error values used in Fig. 4.13, i.e. pointing error values that are used as described in the legend to Fig. 4.13, are the input parameters in the FSO system together with other ones such as FSO link distance, wavelength, among others. As previously commented, the effect of correlated sways turns an initial PDF into another one. This fact, for instance, can be observed in Fig. 4.13 where normalized jitter values for the horizontal displacement and the elevation start taking the same value but the effect of correlation makes different jitters in each axis as corroborated in Fig. 4.12. This phenomenon is more pronounced under high correlation conditions. More specifically, we can see in Fig. 4.13(a) how the effect of correlated sways turns a Rayleigh distribution into a Hoyt distribution and, hence, the outage diversity decreases as the correlation coefficient increases since the dispersion between both sigma values increase. At the same time, we can also see a similar behavior in Figs. 4.13(b) and 4.13(c) where a lognormal-Rice distribution turns into a Beckmann distribution but taking into account the effect of boresight errors. In this case, the outage diversity degrades more rapidly with larger amounts of misalignment.

More importantly, generalized pointing errors with correlated sways can make a change in the dominant effect, mainly under strong turbulence conditions. For instance, it can be observed in Fig. 4.13(b) under strong turbulence that the outage diversity is flat for normalized jitter values of  $\sigma_x/a = \sigma_y/a = 6$ , which means that this one is determined by atmospheric turbulence. But, the outage diversity is also flat up to a correlation coefficient value of  $\rho \approx 0.75$  for normalized jitter values of  $\sigma_x/a = \sigma_y/a = 15$ , which means that the outage diversity is determined by atmospheric turbulence up to that value. The outage diversity starts to be determined by pointing errors for correlation coefficient values greater than  $\approx 0.75$ . This is a clear example of how the effect of correlated sways can make a change in the dominant effect. The same conclusions can also be drawn from Figs. 4.13(a) and 4.13(c). This phenomenon happens much more frequently under strong turbulence than moderate turbulence due to the fact that the atmospheric turbulence parameters such as  $\alpha$  and  $\beta$  take smaller values.

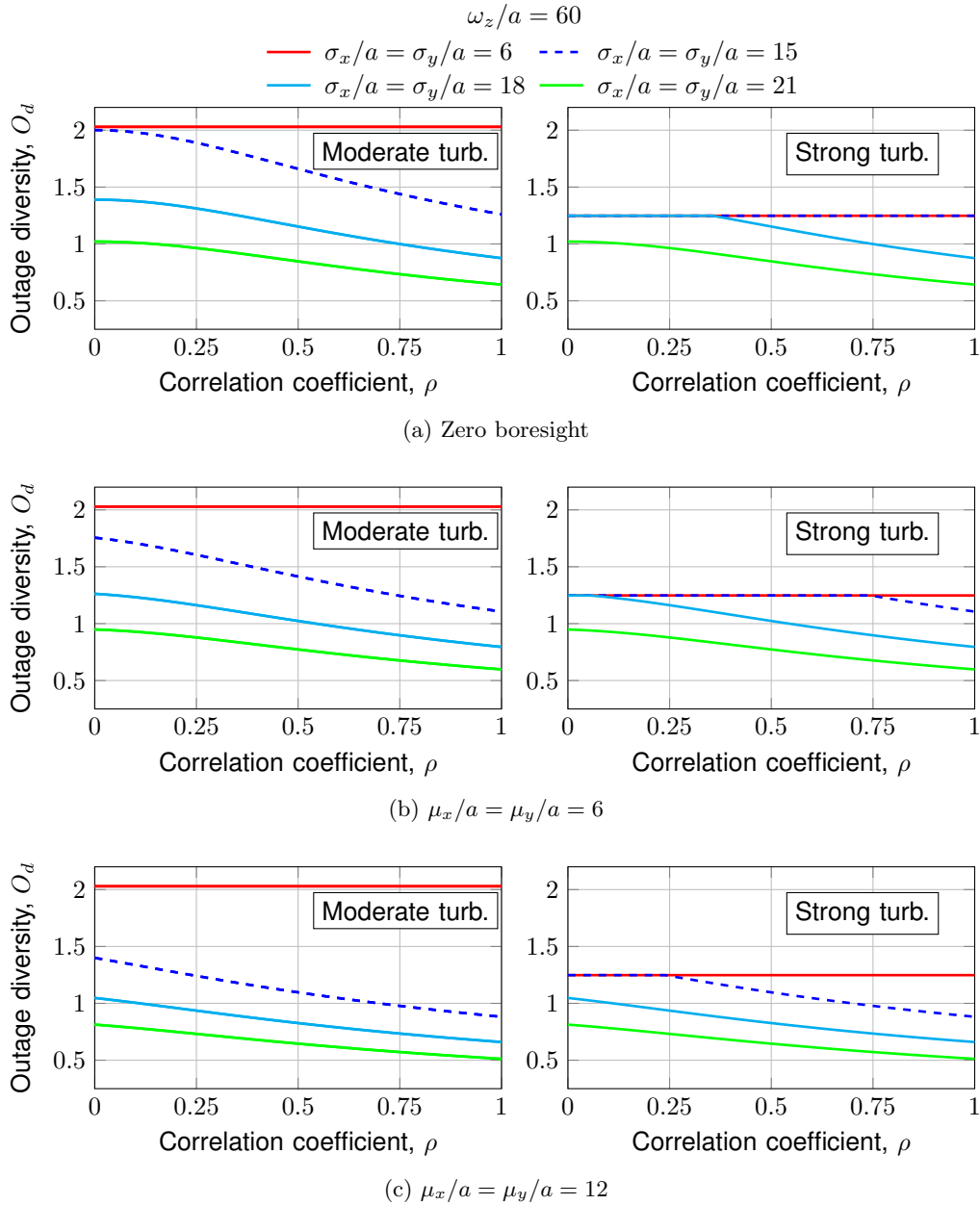


Figure 4.13: Outage diversity  $O_d$  as a function of the correlation coefficient  $\rho$  for a S-D link distance of  $d_{SD} = 3$  km and different normalized boresight error values when a normalized beam width value of  $\omega_z/a = 60$  is assumed.

### Outage Performance Analysis

The corresponding results of this outage performance analysis are illustrated in Fig. 4.14(a) for moderate turbulence and Fig. 4.14(b) for strong turbulence as a function of the inverse normalized threshold SNR,  $\gamma/\gamma_{th}$ . Monte Carlo simulation results are further included by using solid line. Due to the long simulation time involved, simulation results only up to  $10^{-8}$  are included in Fig. 4.14. It is noteworthy to mention that the results obtained by using the proposed approximate expression provide quite a good match between the analytical and the respective Monte Carlo simulation results.

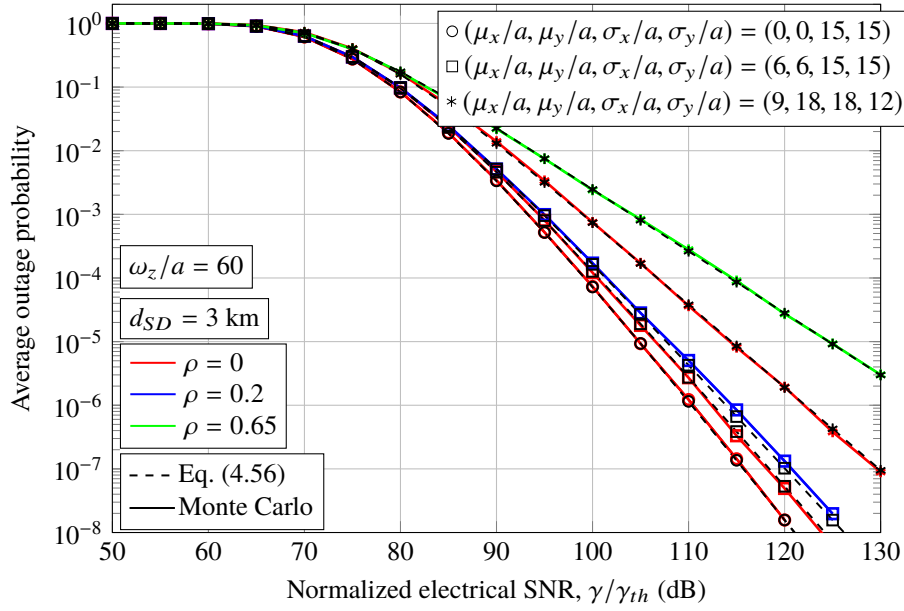
With the goal of analyzing the effect of correlated sways on outage performance, different correlation coefficient values are considered in Fig. 4.14 such as  $\rho = \{0, 0.2, 0.65\}$  and  $\rho = \{0, 0.2, 0.5\}$  for moderate and strong turbulence conditions, respectively. Additionally, the uncorrelated case, i.e. uncorrelated sways, is also included in Fig. 4.14 as a reference. As in Fig. 4.13, the pointing error values used in Fig. 4.14, i.e. pointing error values that are used as described in the legend to Fig. 4.14, are the input parameters in the FSO system. In this way, simulation and analytical results that are illustrated by using red color and different marks represent the uncorrelated cases when the radial displacement is distributed according to the Rayleigh, lognormal-Rice and Beckmann distributions. At the same time, two different correlated cases are depicted. On the one hand, when the radial displacement follows a lognormal-Rice distribution, the effect of correlated sways makes this PDF turns into a Beckmann distribution, which is illustrated by using blue color. On the other hand, when the radial displacement follows a Beckmann distribution, the effect of correlated sways keeps making the same distribution but the statistical parameters take different values, which is illustrated by using green color. As expected, the obtained outage performance is strongly dependent on the effect of correlated sways. It should be mentioned that the effect of correlation has an impact not only on the outage diversity when pointing error is the dominant effect, as shown in the previous figure, but also on the coding gain when atmospheric turbulence is the dominant effect.

### Impact of Correlation on Coding Gain

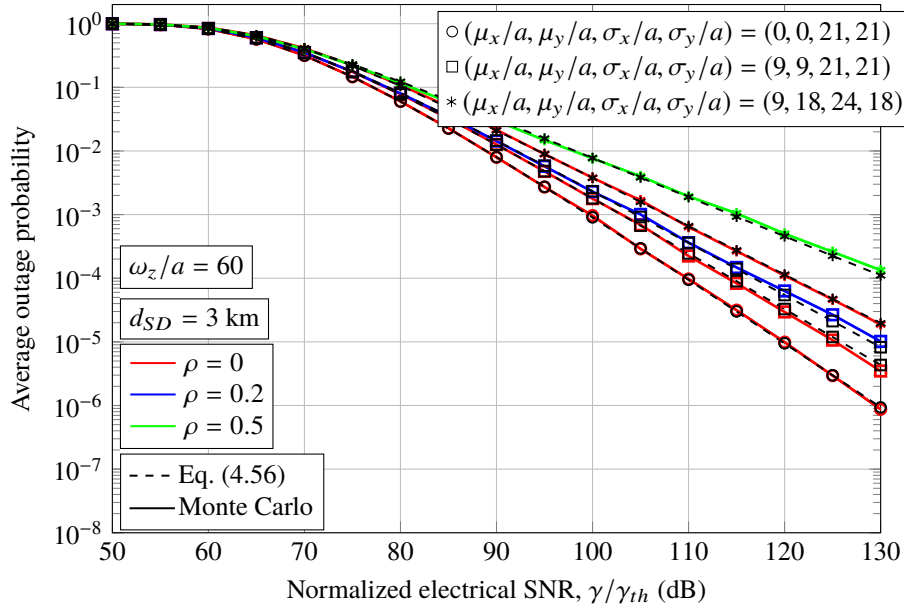
Taking into account the coding gain  $O_c$  in Eq. (4.57), the impact of correlated sways translates into a loss,  $Loss[dB]$ , relative to GG atmospheric turbulence without considering correlated sways given by

$$Loss[dB] \triangleq O_c^{\rho \neq 0}[dB] - O_c^{\rho = 0}[dB]. \quad (4.59)$$

The above expression computes the additional power needed to obtain a given outage performance when there is correlation versus no correlation. The above expression is plotted in Fig. 4.15 as a function of the correlation coefficient for a S-D link distance of  $d_{SD} = 3$  km and a normalized beam width value of  $\omega_z/a = 60$  under the condition that atmospheric turbulence is the dominant effect, i.e., the outage diversity is only determined by atmospheric



(a) Moderate turbulence.



(b) Strong turbulence.

Figure 4.14: Outage performance over GG atmospheric turbulence and generalized misalignment fading channels with correlated sways, when different weather conditions (a)  $C_n^2 = 2 \times 10^{-14} \text{ m}^{-2/3}$  and (b)  $C_n^2 = 8 \times 10^{-14} \text{ m}^{-2/3}$  are assumed for a S-D link distance of  $d_{SD} = 3$  km and different correlation values.



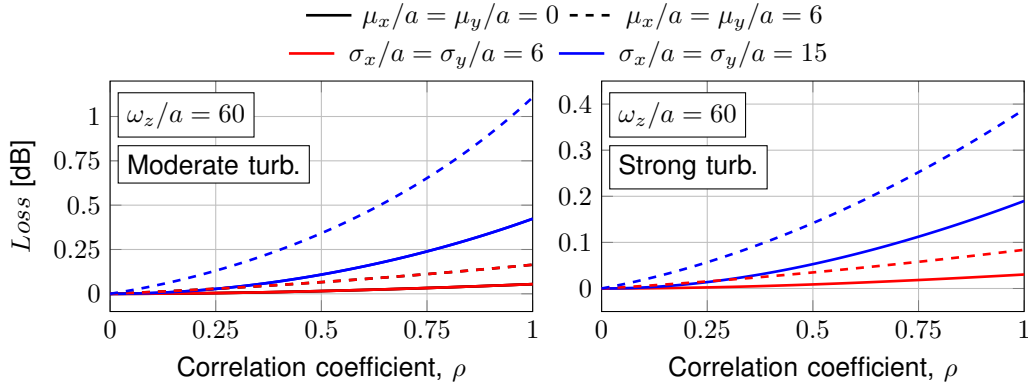


Figure 4.15:  $Loss$ [dB] as a function of the correlation coefficient for a S-D link distance of  $d_{SD} = 3$  km and different jitter variances and normalized boresight error values.

turbulence. It can be observed that the losses slightly increase as the correlation coefficient does regardless of the severity of atmospheric turbulence. Nevertheless, the impact of correlation on coding gain is more remarkable for moderate turbulence than strong turbulence. As expected, a greater loss is obtained when nonzero boresight errors are considered.

## 4.7 Summary

The impact of generalized pointing errors on the performance of FSO communication systems has been analyzed over atmospheric turbulence channels, presenting new results for the optics community. The analysis of generalized pointing errors has been divided into three case studies.

The first case study is when atmospheric turbulence is the dominant effect and, hence, pointing errors only presents an impact on the coding gain since the diversity order is fully dependent on atmospheric turbulence. In this way, the key contributions of this study are summarized as follows

- An asymptotic closed-form expression is obtained for the outage probability over EW atmospheric turbulence with generalized pointing errors, considering the effect of aperture averaging. This expression is derived by using an MGF-based approach due to the difficulty of mathematically treating the Beckmann distribution.
- These results are valid only when atmospheric turbulence is the dominant effect in relation to pointing errors.

- The developed expression is used to find the optimum beam width value that minimizes the impact of pointing errors on the coding gain over EW atmospheric turbulence channels.
- The asymptotic expression is validated through Monte Carlo simulation results.

In the second case study, a deep analysis of the performance of FSO links over GG atmospheric turbulence channels with generalized pointing errors was carried out. In this analysis, the effect of pointing error as dominant effect is analyzed in detail. In this way, the key contributions of this study are summarized as follows

- An efficient and accurate approximation of the Beckmann distribution is presented which is used to model generalized pointing errors with high precision.
- An approximate closed-form PDF for the composite GG atmospheric turbulence with pointing errors is derived by using the proposed approximation of the Beckmann distribution which is valid not only for typical values in terrestrial FSO links, but also for more extreme FSO scenarios.
- The performance of FSO communication links is analyzed in terms of BER and outage probability.
- These results are valid not only when atmospheric turbulence is the dominant effect in relation to pointing errors, but also when pointing error is the dominant effect in relation to atmospheric turbulence.
- The accuracy of the approximation is measured both visually and quantitatively using curve-fitting metrics.
- The obtained expression is used to find the optimum beam width value that minimize the effect of pointing errors. This expression is valid for any atmospheric turbulence channels as long as this one can be expanded into Maclaurin series.
- The results are validated through Monte Carlo simulation results.

From this analysis, we can conclude that a much higher diversity order is achieved when atmospheric turbulence is the dominant effect in relation to generalized pointing errors whose diversity gain is determined by  $\min(\alpha, \beta)$  in GG atmospheric turbulence. In addition, the beam width can be optimized in order to improve the performance of FSO links in presence of both atmospheric turbulence and generalized pointing errors. It can also be concluded that the optimum beam width is a feasible method for reducing pointing error losses in terrestrial FSO links.

Finally, the effect of correlated sways is analyzed in the third case study. This analysis is performed by taking full advantage of the proposed approximation in the second case study.

The effect of correlated sways on FSO link design was never taken into account, i.e., both the horizontal displacement and the elevation have always been modeled as uncorrelated RVs. In this way, the key contributions of this study are summarized as follows

- A new statistical model to describe the effect of correlated sways on pointing errors is proposed to analyze the outage performance of FSO links.
- An approximate closed-form PDF for the composite GG atmospheric turbulence with generalized pointing errors is derived that serves as an analytical tool to evaluate the performance of any kind of FSO communications system with a higher degree of sophistication and realism.
- The obtained expression is validated through Monte Carlo simulation results.

From this study, we can conclude that the impact of correlated sways on the outage performance cannot be ignored in terrestrial FSO applications since the horizontal displacement and the elevation are not necessarily uncorrelated RVs.



UNIVERSIDAD  
DE MÁLAGA

## Chapter 5

# Conclusions and Future Work

This chapter summarizes the main conclusions of the work developed in this thesis. Besides, new directions for future research are suggested.

### 5.1 Conclusions

In this thesis, the performance analysis of advanced FSO communication systems over atmospheric turbulence channels with pointing errors has been addressed. The conclusions drawn from this thesis can be divided into two major areas: ergodic capacity analysis and modeling of generalized pointing errors. The motivation behind this is that the study of ergodic capacity has been carried out to know what the limits are in terms of the capacity of advanced FSO communication systems such as MISO, SIMO and MIMO communication FSO systems. At the same time, the ergodic capacity of a three-way communications setup has also been studied as an interesting solution to FSO systems based on spatial diversity. Finally, a generalized pointing error model has been proposed as a fairly useful and handy tool to include pointing errors in the analysis of any kind of FSO communication systems. In general, the performance of FSO systems has been evaluated over GG atmospheric turbulence channels and, furthermore, IM/DD and OOK modulation have been considered in each of FSO links involved in each FSO system.

A comprehensive ergodic capacity analysis was performed in Chapter 3 over GG atmospheric turbulence channels with zero boresight pointing errors in the case of MISO FSO systems and DF strategies, and with nonzero boresight pointing errors in the case of SIMO and MIMO FSO systems. Thus, novel approximate closed-form expressions for the ergodic capacity were obtained as well as their asymptotic behavior at high SNR. Obtained closed-form expressions for the ergodic capacity were expressed in terms of the Meiger's G-function and H-Fox function to estimate the ergodic capacity from low to high SNR.

On the one hand, it was concluded that finding an exact closed-form expression for the ergodic capacity of MIMO FSO systems over atmospheric turbulence channels (GG, LN and EW models) with nonzero boresight pointing errors is not possible and, hence, an asymptotic analysis had to be carried out in this regard. Here, it was also concluded that MISO FSO systems presents a better performance than SIMO and MIMO FSO systems in terms of the ergodic capacity due to the fact that only one laser can be aligned with only one receiver aperture, and the rest ones present a nonzero boresight error that must be taken into consideration. In addition to this, a new methodology was proposed to generate optimum receiver configurations and, hence, to minimize the effect of nonzero boresight. Unlike RF systems, it is more convenient to deploy MISO systems than SIMO and MIMO systems in FSO technology due to the effect of nonzero boresight. Moreover, the effect of aperture averaging was considered by using the EW model, demonstrating that we can mitigate the effect of atmospheric turbulence even in strong turbulence regime when smaller aperture diameters are used.

On the other hand, it was demonstrated that cooperative strategies based on DF relaying can improve the performance in terms of the capacity and even achieve a greater capacity than MISO FSO systems for some relay locations. As expected, relay placement is also really important to maximize the ergodic capacity in cooperative FSO systems.

Accurate channel modeling for FSO communication systems is one of the key challenge in system design. In this thesis, a generalized statistical pointing error model has been developed in Chapter 4 that is based on the pointing error model proposed in [53]. This generalized pointing error model considers not only the beam width and detector size, but also the effect of different jitters for the elevation and the horizontal displacement, the effect of nonzero boresight errors and the effect of correlated sways. This generalized statistical model enables the system designer to use more degrees of freedom to optimally design FSO systems. The developed model is used to study the BER and outage performance and provide fundamental limits on the system performance.

In the light of results derived from Chapter 4, we provide some tool to add the effect of generalized pointing errors to the FSO system and study the two different FSO scenarios, i.e., when atmospheric turbulence is the dominant effect and when pointing error is the dominant effect. Both FSO scenarios had not been considered in the literature due to the difficulty of studying it. Hence, this research problem has been a great challenge during the development of this thesis.

Finally, the effect of correlation turns a PDF into another one. In other words, the effect of correlation makes that the statistical distribution corresponding to the radial displacement at the receiver turns to another one when the correlation coefficient takes nonzero values. This phenomenon is really interesting since two pointing error models might be assumed taking into account the effect of correlated sways such as Rayleigh (zero boresight case) and lognormal-Rice (nonzero boresight case) distributions. The correlation makes that both

statistical distributions turn to other ones more real when the correlation coefficient does not equal zero, obtaining a Hoyt distribution and a Beckmann distribution, respectively.

## 5.2 Future Work

In this thesis, some challenging problems have been addressed as suggested in Chapter 1. Hence, some research issues may be developed in the context of OWC systems as future work from the relevant results obtained here. The following future directions are proposed:

- Imperfect CSI and synchronization errors.
- Distributed space-time coding (DSTC).
- Performance analysis of MIMO FSO systems under generalized pointing errors.
- Experimental work and practical measurements.
- VLC and UOC systems.

The study of ergodic capacity of cooperative FSO systems was addressed by assuming perfect CSI at the transmitter side to make the selection. Then, the best possible performance was obtained from a CSI point of view. An interesting research topic is to assume imperfect CSI or outdated CSI in order to study how performance is deteriorated as a result of using an imperfect CSI to make the selection in cooperative FSO systems. At the same time, the effect of small synchronization errors at the receiver can lead to performance deterioration.

Another research topic that may be interesting is to employ DSTC in cooperative FSO systems in order to increase the average channel capacity. Taking into account advances in non-cooperative FSO systems by employing space-time block coding (STBC) and space-time trellis code (STTC) in FSO systems [138, 143], hopefully they may serve as an important tool to mitigate the combined effect of atmospheric turbulence and pointing errors in optical wireless relay networks. This kind of codes allows to obtain a much higher diversity order compared to repetition coding (RC) at the expense of a greater complexity. In this way, the study of performance of this kind of system in terms of the BER, outage probability and ergodic capacity would be of real interest for the optics community.

The performance analysis of MIMO FSO systems under the presence of generalized pointing errors continues being an open problem in the literature due to the difficulty of analyzing from a mathematical point of view. In this way, the approximation presented in Chapter 4 allows to efficiently study such research problem and evaluate the performance in terms of BER, outage probability and ergodic capacity. In addition, the effect of correlation among sways of different receiver apertures is another open problem since laser sources and/or

receiver apertures are located in the same physical plane and, hence, there is a correlation among jitters.

Finally, a very important step forward in FSO communications system design is to verify the theoretical results with experimental work and practical measurements. Besides the above future directions, there are other ones due to the wide range of OWC systems such as VLC and UOC systems, which are expected to grow further in the coming years.



# Appendix A

## Special Functions

### A.1 Gamma Function

The gamma function is considered as an extension of the factorial function. If  $n$  is a positive integer

$$\Gamma(n) = (n - 1)! \quad (\text{A.1.1})$$

The gamma function is defined for all complex numbers except the non-positive integers. In this case,  $\Gamma(z)$  is defined through the integral representation as in [62, eqn. (8.310)]

$$\Gamma(z) = \int_0^{\infty} x^{z-1} \exp(-x) dx. \quad (\text{A.1.2})$$

Note that  $\Gamma(z)$  satisfies the relation  $\Gamma(1) = 1$ . An interesting property is given by  $z\Gamma(z) = \Gamma(z + 1)$  [58, eqn. (06.05.17.0002.01)].

### A.2 Macdonald Function

The modified Bessel function of the second kind  $K_\nu(z)$  is also called the Macdonald function, and its integral representation is given by [62, eqn. (8.432.6)]

$$K_\nu(z) = \frac{1}{2} \left(\frac{z}{2}\right)^\nu \int_0^{\infty} \frac{\exp(-t - z^2/4t)}{t^{\nu+1}} dt. \quad (\text{A.2.1})$$

### A.3 Meijer's G-Function

A general definition of the Meijer's G-function  $G_{p,q}^{m,n}(\cdot)$  is given by the following line integral in the complex plane as in [62, eqn. (9.301)]

$$G_{p,q}^{m,n} \left( z \left| \begin{matrix} (a_p) \\ (b_q) \end{matrix} \right. \right) = \frac{1}{2\pi i} \int_L \frac{\prod_{j=1}^m \Gamma(b_j - s) \prod_{j=1}^n \Gamma(1 - a_j + s)}{\prod_{j=m+1}^q \Gamma(1 - b_j + s) \prod_{j=n+1}^p \Gamma(a_j - s)} z^s ds, \quad (\text{A.3.1})$$

where  $(a_p) = a_1, \dots, a_p$ ,  $(b_q) = b_1, \dots, b_q$ , and  $L$  denotes the path to be followed in the integration. For integers  $m, n, p, q$  such that  $0 \leq m \leq q$ ,  $0 \leq n \leq p$ , and the poles of  $\Gamma(b_j - s)$  must not coincide with the poles of  $\Gamma(1 - a_k + s)$  for any  $j$  and  $k$  where  $j = 1, \dots, m$  and  $k = 1, \dots, n$ . Moreover, the Meijer's G-function is a standard built-in function in most of the well-known mathematical software packages such as Maple<sup>TM</sup> and Wolfram Mathematica<sup>TM</sup>. The Meijer's G-function includes most of the special functions used in mathematics as particular cases.

#### A.3.1 Relation to Other Functions

The function  $K_\nu(\cdot)$  can be expressed in terms of the Meijer's G-function [62, eqn. (9.34.3)] as follows

$$K_\nu(z) = \frac{1}{2} G_{0,2}^{2,0} \left( z \left| \begin{matrix} - \\ \frac{\nu}{2}, -\frac{\nu}{2} \end{matrix} \right. \right). \quad (\text{A.3.2})$$

The natural logarithm  $\ln(\cdot)$  can be expressed in terms of the Meijer's G-function [59, eqn. (8.4.6.5)] as follows

$$\ln(1+z) = G_{2,2}^{1,2} \left( z \left| \begin{matrix} 1, 0 \\ 1, 1 \end{matrix} \right. \right). \quad (\text{A.3.3})$$

The exponential function  $\exp(\cdot)$  can be expressed in terms of the Meijer's G-function [59, eqn. (8.4.3.1)] as follows

$$\exp(x) = G_{0,1}^{1,0} \left( -x \left| \begin{matrix} - \\ 0 \end{matrix} \right. \right). \quad (\text{A.3.4})$$

#### A.3.2 Definite Integrals

1. The following integral can be found in [58, eqn. (07.34.21.0085.01)]:

$$\int_0^\infty t^{\alpha-1} (t-a)^{\beta-1} G_{p,q}^{m,n} \left( \omega t^{l/k} \left| \begin{matrix} a_1, \dots, a_p \\ b_1, \dots, b_q \end{matrix} \right. \right) dt = \frac{k^\mu l^{-\beta} \Gamma(\beta)}{(2\pi)^{c^*(k-1)} a^{1-\alpha-\beta}} G_{kp+l, kq+l}^{km+l, kn} \\ \times \left( \frac{\omega^k a^l}{k^k (q-p)} \left| \begin{matrix} \frac{a_1}{k}, \dots, \frac{a_1+k-1}{k}, \dots, \frac{a_p}{k}, \dots, \frac{a_p+k-1}{k}, \frac{1-\alpha}{l}, \dots, \frac{l-\alpha}{l} \\ \frac{1-\alpha-\beta}{l}, \dots, \frac{l-\alpha-\beta}{l}, \frac{b_1}{k}, \dots, \frac{b_1+k-1}{k}, \dots, \frac{b_q}{k}, \dots, \frac{b_q+k-1}{k} \end{matrix} \right. \right),$$

where  $k, l \in \mathbb{N}^+$ ,  $\gcd(k, l) = 1$ ,  $c^* = m + n - \frac{p+q}{2}$ , and  $\mu = \sum_{j=1}^q b_j - \sum_{j=1}^p a_j + \frac{p-q}{2} + 1$ .

2. The following integral can be found in [59, eqn. (1.16.2.1)]:

$$\int_0^x x^{\alpha-1} G_{p,q}^{m,n} \left( cx \left| \begin{matrix} a_1, \dots, a_p \\ b_1, \dots, b_q \end{matrix} \right. \right) dx = x^\alpha G_{p+1,q+1}^{m,n+1} \left( cx \left| \begin{matrix} 1-\alpha, a_1, \dots, a_p \\ b_1, \dots, b_q, -\alpha \end{matrix} \right. \right).$$

3. The following integral can be found in [58, eqn. (07.34.21.0012.01)] when  $r \in \mathbb{R}^+$ :

$$\int_0^\infty \tau^{\alpha-1} G_{u,v}^{s,t} \left( \sigma\tau \left| \begin{matrix} c_1, \dots, c_u \\ d_1, \dots, d_v \end{matrix} \right. \right) G_{p,q}^{m,n} \left( \omega\tau^r \left| \begin{matrix} a_1, \dots, a_p \\ b_1, \dots, b_q \end{matrix} \right. \right) d\tau = \sigma^{-\alpha} H_{p+v,q+u}^{m+t,n+s} \\ \times \left( \frac{\omega}{\sigma^r} \left| \begin{matrix} (a_1, 1), \dots, (a_n, 1), (1-\alpha-d_1, r), \dots, (1-\alpha-d_v, r), (a_{n+1}, 1), \dots, (a_p, 1) \\ (b_1, 1), \dots, (b_m, 1), (1-\alpha-c_1, r), \dots, (1-\alpha-c_u, r), (b_{m+1}, 1), \dots, (b_q, 1) \end{matrix} \right. \right).$$

4. The following integral can be found in [59, eqn. (2.24.1.2)]:

$$\int_0^\infty G_{u,v}^{s,t} \left( \sigma x \left| \begin{matrix} c_1, \dots, c_u \\ d_1, \dots, d_v \end{matrix} \right. \right) G_{p,q}^{m,n} \left( \omega x \left| \begin{matrix} a_1, \dots, a_p \\ b_1, \dots, b_q \end{matrix} \right. \right) dx \\ = \sigma^{-1} G_{p+v,q+u}^{m+t,n+s} \left( \frac{\omega}{\sigma} \left| \begin{matrix} a_1, \dots, a_n, -d_1, \dots, -d_v, a_{n+1}, \dots, a_p \\ b_1, \dots, b_m, -c_1, \dots, -c_u, b_{m+1}, \dots, b_q \end{matrix} \right. \right).$$

5. The following integral can be found in [58, eqn. (07.34.21.0009.01)]:

$$\int_0^\infty t^\alpha G_{p,q}^{m,n} \left( tz \left| \begin{matrix} a_1, \dots, a_p \\ b_1, \dots, b_q \end{matrix} \right. \right) dt = \frac{\prod_{k=1}^m \Gamma(\alpha + b_k) \prod_{k=1}^n \Gamma(1 - \alpha - a_k)}{\prod_{k=n+1}^p \Gamma(\alpha + a_k) \prod_{k=m+1}^q \Gamma(1 - \alpha - b_k)} z^{-\alpha}.$$

All these integrals must satisfy some restrictions that have been omitted here.

## A.4 Digamma Function

The psi (digamma) function is defined as in [62, eqn. (8.360.1)]

$$\psi(x) = \frac{d}{dx} \ln \Gamma(x). \quad (\text{A.4.1})$$

## A.5 H-Fox Function

The H-Fox function  $H_{p,q}^{m,n}[\cdot]$  is a generalization of the Meijer's G-function and is defined via a Mellin Barnes type integral [100, eqn. (1.1)] as follows

$$\begin{aligned} H_{p,q}^{m,n} \left( z \left| \begin{array}{c} (a_p, A_p) \\ (b_q, B_q) \end{array} \right. \right) & \\ = \frac{1}{2\pi i} \int_L \frac{\prod_{j=1}^m \Gamma(b_j + B_j s) \prod_{j=1}^n \Gamma(1 - a_j - A_j s)}{\prod_{j=m+1}^q \Gamma(1 - b_j - B_j s) \prod_{j=n+1}^p \Gamma(a_j + A_j s)} z^s ds, & \end{aligned} \quad (\text{A.5.1})$$

where  $(a_p, A_p) = (a_1, A_1), \dots, (a_p, A_p)$ ,  $(b_q, B_q) = (b_1, B_1), \dots, (b_q, B_q)$ , and  $L$  denotes the path to be followed in the integration. The special case for which the H-Fox function reduces to the Meijer's G-function is  $A_j = B_k = C$ ,  $C > 0$  for  $j = 1, \dots, p$  and  $k = 1, \dots, q$ .

$$H_{p,q}^{m,n} \left( z \left| \begin{array}{c} (a_1, C), \dots, (a_p, C) \\ (b_1, C), \dots, (b_q, C) \end{array} \right. \right) = \frac{1}{C} G_{p,q}^{m,n} \left( z^{1/C} \left| \begin{array}{c} a_1, \dots, a_p \\ b_1, \dots, b_q \end{array} \right. \right). \quad (\text{A.5.2})$$

## A.6 Generalized Bivariate Meijer's G-Function

The integral from three different Meijer's G-functions can be expressed in closed-form by using [58, eqn. (07.34.21.0081.01)]. The result is called generalized bivariate Meijer's G-function (GBMGF) that involves the product of three Meijer's G-functions as follows

$$\begin{aligned} & \int_0^\infty x^{\alpha-1} G_{p,q}^{m,n} \left( zx \left| \begin{array}{c} a_1, \dots, a_p \\ b_1, \dots, b_q \end{array} \right. \right) \\ & \times G_{p_1,q_1}^{m_1,n_1} \left( tx \left| \begin{array}{c} a_{11}, \dots, a_{1p_1} \\ b_{11}, \dots, b_{1q_1} \end{array} \right. \right) G_{p_2,q_2}^{m_2,n_2} \left( yx \left| \begin{array}{c} a_{21}, \dots, a_{2p_1} \\ b_{21}, \dots, b_{2q_1} \end{array} \right. \right) dx \\ & = z^{-\alpha} G_{q,p:p_1,q_1:p_2,q_2}^{n,m:m_1:n_1:n_2,m_2} \\ & \times \left( \begin{array}{c} 1 - \alpha - b_1, \dots, 1 - \alpha - b_q \\ 1 - \alpha - a_1, \dots, 1 - \alpha - a_p \end{array} \left| \begin{array}{c} a_{11}, \dots, a_{1p_1} \\ b_{11}, \dots, b_{1q_1} \end{array} \right| \begin{array}{c} a_{21}, \dots, a_{2p_2} \\ b_{21}, \dots, b_{2q_2} \end{array} \left| \begin{array}{c} t \\ z \end{array}, \begin{array}{c} y \\ z \end{array} \right). \end{aligned} \quad (\text{A.6.1})$$

Note that this relationship only holds true when the parameters satisfy certain specific restrictions as can be seen in greater detail in [58, eqn. (07.34.21.0081.01)].

## A.7 Mellin Transform

The Mellin transform is the operation mapping the function  $f(x)$  into the function  $F(s)$  defined on the complex plane by the following relation [62, eqn. (17.41)]

$$\{\mathcal{M}f\}(s) = F(s) = \int_0^\infty x^{s-1} f(x) dx. \quad (\text{A.7.1})$$

Generally speaking, the Mellin transform is an integral transform that may be regarded as the multiplicative version of the two-sided Laplace transform. This integral transform is used in number theory, mathematical statistics, among other fields. The inverse Mellin transform is expressed as follows

$$\{\mathcal{M}^{-1}F\}(x) = f(x) = \frac{1}{2\pi i} \int_{c-i\infty}^{c+i\infty} x^{-s} F(s) ds. \quad (\text{A.7.2})$$

The importance of the Mellin transform in probability theory lies in the fact that if  $X$  and  $Y$  are two independent RVs, then the Mellin transform of their product is equal to the product of the Mellin transforms of  $X$  and  $Y$  as follows [98]

$$\mathcal{M}_{XY}(s) = \mathcal{M}_X(s)\mathcal{M}_Y(s), \quad (\text{A.7.3})$$

where  $\mathcal{M}_X(s)$  and  $\mathcal{M}_Y(s)$  are the corresponding Mellin transforms of  $X$  and  $Y$ , respectively. Hence, the PDF of  $X$  and  $Y$  is obtained via inverse Mellin transform.

### A.7.1 Derivation of $I_{LB} = \prod_{k=1}^M I_k$ in Ergodic Capacity Analysis of MISO FSO Systems

The Mellin transform of a Meijer's G-function is obtained by using [58, eqn. (07.34.21.0009.01)] as

$$\int_0^\infty x^{s-1} G_{p,q}^{m,n} \left( \eta x \left| \begin{matrix} (a_p) \\ (b_q) \end{matrix} \right. \right) = \eta^{-s} \frac{\prod_{j=1}^m \Gamma(b_j + s) \prod_{j=1}^n \Gamma(1 - a_j - s)}{\prod_{j=m+1}^q \Gamma(1 - b_j - s) \prod_{j=n+1}^p \Gamma(a_j + s)}. \quad (\text{A.7.4})$$

Taking into account that the PDF of GG atmospheric turbulence with zero boresight pointing errors  $f_I(i)$  is expressed in terms of a Meijer's G-function in Eq. (2.34), its corresponding Mellin transform is derived from the above result as follows

$$\begin{aligned} & \{\mathcal{M}f_I(i)\}(s) \\ &= \frac{\alpha\beta\varphi^2}{(A_0L)\Gamma(\alpha)\Gamma(\beta)} \left( \frac{\alpha\beta}{A_0L} \right)^{-s} \frac{\Gamma(s + \alpha - 1)\Gamma(s + \beta - 1)\Gamma(\varphi^2 + s - 1)}{\Gamma(s + \varphi^2)}. \end{aligned} \quad (\text{A.7.5})$$

Hence, the PDF of the product of  $M$  GG with zero boresight pointing errors variates is obtained via inverse Mellin transform as follows

$$\begin{aligned} f_{I_{LB}}(i) &= \frac{1}{2\pi i} \int_{c-i\infty}^{c+i\infty} i^{-s} \prod_{k=1}^M \frac{\alpha_k \beta_k \varphi_k^2}{(A_{0k} L_k) \Gamma(\alpha_k) \Gamma(\beta_k)} \\ &\times \left( \frac{\alpha_k \beta_k}{A_{0k} L_k} \right)^{-s} \frac{\Gamma(s + \alpha_k - 1) \Gamma(s + \beta_k - 1) \Gamma(\varphi_k^2 + s - 1)}{\Gamma(s + \varphi_k^2)} ds. \end{aligned} \quad (\text{A.7.6})$$

Due to the similarity with the Mellin transform of the Meijer's G-function, the PDF of  $I_{LB}$  can be expressed in terms of the Meijer's G-function as follows

$$f_{I_{LB}}(i) = \frac{i^{-1} \prod_{k=1}^M \varphi_k^2 G_{M,3M}^{3M,0} \left( \prod_{k=1}^M \frac{\alpha_k \beta_k}{A_{0k} L_k} i \left| \begin{matrix} \varphi_1^2 + 1, \dots, \varphi_M^2 + 1 \\ \varphi_1^2, \alpha_1, \beta_1, \dots, \varphi_M^2, \alpha_M, \beta_M \end{matrix} \right. \right)}{\prod_{k=1}^M \Gamma(\alpha_k) \Gamma(\beta_k)}. \quad (\text{A.7.7})$$

### A.7.2 Derivation of $I_T^{LB} = I_{SD}I_{RD}$ in Ergodic Capacity Analysis of Cooperative FSO Systems

The PDF of  $I_T^{LB}$  is a particular case of Eq. (A.7.7) for two RVs, i.e.,  $I_{SD}$  and  $I_{RD}$ . Hence, the PDF of  $I_T^{LB}$  can easily be derived from Eq. (A.7.7) as follows

$$f_{I_T^{LB}}(i) = \frac{i^{-1} \varphi_{SD}^2 \varphi_{RD}^2 G_{2,6}^{6,0} \left( \frac{\alpha_{SD} \beta_{SD} \alpha_{RD} \beta_{RD}}{A_{0SD} L_{SD} A_{0RD} L_{RD}} i \mid \begin{matrix} \varphi_{SD}^2 + 1, \varphi_{RD}^2 + 1 \\ \varphi_{SD}^2, \alpha_{SD}, \beta_{SD}, \varphi_{RD}^2, \alpha_{RD}, \beta_{RD} \end{matrix} \right)}{\Gamma(\alpha_{SD}) \Gamma(\beta_{SD}) \Gamma(\alpha_{RD}) \Gamma(\beta_{RD})}. \quad (\text{A.7.8})$$

## A.8 Other Relations

The modified Bessel function of the second kind  $K_\nu(z)$  is related to the Bessel function of the first kind  $J_\nu(\cdot)$  by using [58, eqn. (03.04.27.0001.01)] as follows

$$K_\nu(z) = \frac{\pi}{2} \csc(\pi\nu) (I_{-\nu}(z) - I_\nu(z)). \quad (\text{A.8.1})$$

The Bessel function of the first kind  $J_\nu(\cdot)$  is related to the modified Bessel function of the first kind  $I_\nu(\cdot)$  by using [58, eqn. (03.02.27.0001.01)] as follows

$$I_\nu(z) = \frac{z^\nu}{(iz)^\nu} J_\nu(iz). \quad (\text{A.8.2})$$

Another basic relation is given in [62, eqn. (1.313.9)] as follows

$$\tan(x \pm y) = \frac{\tan x \pm \tan y}{1 \mp \tan x \tan y}. \quad (\text{A.8.3})$$

## A.9 Other Definite Integrals

1.  $\int_0^\infty \operatorname{erfc}(x) x^{a-1} dx = \frac{\Gamma((1+a)/2)}{(\pi^{1/2} a)} [62, \text{eqn. (6.281)}].$
2.  $\int_0^\infty x^{\mu+\frac{1}{2}} \ln(x) J_\nu(ax) dx = \frac{2^{\mu-\frac{1}{2}} \Gamma(\frac{\mu+\nu+\frac{3}{4}}{2})}{\Gamma(\frac{\nu-\mu+\frac{1}{4}}{2}) a^{\mu+\frac{3}{4}}} \left[ \psi\left(\frac{\mu+\nu}{2} + \frac{3}{4}\right) + \psi\left(\frac{\nu-\mu}{2} + \frac{1}{4}\right) + \ln\left(\frac{a^2}{4}\right) \right]$   
when  $a > 0$ ,  $-\operatorname{Re} \nu - \frac{3}{2} < \operatorname{Re} \mu < 0$  [62, eqn. (6.771)].
3.  $\int_0^\infty x^{\nu-1} e^{-\mu x} \ln(x) dx = \frac{\Gamma(\nu)}{\mu^\nu} [\psi(\nu) - \ln(\mu)]$  when  $\operatorname{Re} \mu > 0$  and  $\operatorname{Re} \nu > 0$  [62, eqn. (4.352.1)].
4.  $\int_0^1 [\ln(1-x)]^n (1-x)^r dx = (-1)^n \frac{n!}{(r+1)^{n+1}}$  when  $r > -1$  [62, eqn. (4.294.10)].

## A.10 Impact of Pointing Errors on Ergodic Capacity

In this section, the solution for the integral in Eq. (2.58) is derived. Furthermore, this integral can also be interpreted as the expectation of  $\ln(I_p)$ , i.e.,  $\mathbb{E}[\ln(I_p)]$ . Substituting Eq. (3.21) into Eq. (3.33), we obtain

$$\frac{\varphi^2 \exp\left(-\frac{s^2}{2\sigma_s^2}\right)}{A\varphi^2} \int_0^{A_0} \ln(x)x^{\varphi^2-1} I_0\left(\frac{s}{\sigma_s} \sqrt{-2\varphi^2 \ln\left(\frac{x}{A_0}\right)}\right) dx. \quad (\text{A.10.1})$$

By using the Maclaurin series expansion of  $I_0(\cdot)$  [62, eqn. (8.445)], we have

$$\frac{\varphi^2 \exp\left(-\frac{s^2}{2\sigma_s^2}\right)}{A\varphi^2} \int_0^{A_0} \ln(x)x^{\varphi^2-1} \sum_{k=0}^{\infty} \frac{(-2\varphi^2)^k \left(\frac{s}{2\sigma_s}\right)^{2k}}{k!\Gamma(k+1)} \ln(x/A_0)^k dx. \quad (\text{A.10.2})$$

Since each term of the series is non-negative and the infinite series uniformly converges to  $I_0\left(\frac{s}{\sigma_s} \sqrt{-2\varphi^2 \ln\left(\frac{x}{A_0}\right)}\right)$ , we can swap the integral and infinite summation and write Eq. (A.10.1) as follows

$$\begin{aligned} & \frac{\varphi^2 \exp\left(-\frac{s^2}{2\sigma_s^2}\right)}{A\varphi^2} \sum_{k=0}^{\infty} \frac{(-2\varphi^2)^k \left(\frac{s}{2\sigma_s}\right)^{2k}}{k!\Gamma(k+1)} \int_0^{A_0} \ln(x)x^{\varphi^2-1} \ln(x/A_0)^k dx \\ &= \varphi^2 \exp\left(-\frac{s^2}{2\sigma_s^2}\right) \sum_{k=0}^{\infty} \frac{(-2\varphi^2)^k \left(\frac{s}{2\sigma_s}\right)^{2k}}{k!\Gamma(k+1)} \int_0^1 \ln(xA_0)x^{\varphi^2-1} \ln(x)^k dx. \end{aligned} \quad (\text{A.10.3})$$

The integral in Eq. (A.10.3) can be expressed as a sum of two integrals as follows

$$\int_0^1 \ln(xA_0)x^{\varphi^2-1} \ln(x)^k dx = \ln(A_0) \int_0^1 x^{\varphi^2-1} \ln(x)^k dx + \int_0^1 x^{\varphi^2-1} \ln(x)^{k+1} dx. \quad (\text{A.10.4})$$

Both integrals in Eq. (A.10.4) can be solved with the help of [62, eqn. (4.294.10)] (See Appendix A.9) and making a change of variable  $t = x - 1$ . Then, performing some straightforward algebraic manipulations, the expression in Eq. (A.10.3) can be written as

$$\begin{aligned} & \exp\left(-\frac{s^2}{2\sigma_s^2}\right) \sum_{k=0}^{\infty} \frac{\left(\frac{s^2}{2\sigma_s^2}\right)^k}{k!} \left(\frac{\ln(A_0) - 1 - k}{\varphi^2}\right) \\ &= \exp\left(-\frac{s^2}{2\sigma_s^2}\right) \left\{ \left(\ln(A_0) - \frac{1}{\varphi^2}\right) \sum_{k=0}^{\infty} \frac{\left(\frac{s^2}{2\sigma_s^2}\right)^k}{k!} - \sum_{k=0}^{\infty} \frac{k \left(\frac{s^2}{2\sigma_s^2}\right)^k}{\varphi^2 k!} \right\} \\ &= \exp\left(-\frac{s^2}{2\sigma_s^2}\right) \left\{ \left(\ln(A_0) - \frac{1}{\varphi^2}\right) \sum_{k=0}^{\infty} \frac{\left(\frac{s^2}{2\sigma_s^2}\right)^k}{k!} - \frac{s^2}{2\varphi^2 \sigma_s^2} \sum_{k=1}^{\infty} \frac{\left(\frac{s^2}{2\sigma_s^2}\right)^{k-1}}{(k-1)!} \right\}. \end{aligned} \quad (\text{A.10.5})$$

Knowing that  $e^x = \sum_{k=0}^{\infty} \frac{x^k}{k!}$  [62, eqn. (1.211.1)], the impact of nonzero boresight pointing error on the ergodic capacity of FSO systems can be written as

$$\begin{aligned} & \exp\left(-\frac{s^2}{2\sigma_s^2}\right) \left\{ \left(\ln(A_0) - \frac{1}{\varphi^2}\right) \exp\left(\frac{s^2}{2\sigma_s^2}\right) - \frac{s^2}{2\varphi^2\sigma_s^2} \exp\left(\frac{s^2}{2\sigma_s^2}\right) \right\} \\ & = \ln(A_0) - \frac{1}{\varphi^2} - \frac{s^2}{2\sigma_s^2\varphi^2}. \end{aligned} \quad (\text{A.10.6})$$

Note that when the boresight error is set to zero, i.e.  $s = 0$ , the solution in Eq. (A.10.6) corresponds to the solution of the integral in Eq. (2.58).



## Appendix B

# Derivation of the Correcting Factors

### B.1 Correcting Factor for MISO FSO Systems

The corresponding correcting factor of MISO FSO systems is derived from the correcting factor of MIMO FSO systems when the parameter  $s$  is equal to 0, i.e. zero boresight pointing errors, and the number of receiver apertures is equal to 1. Hence, it is possible to use the same expression of the correcting factor of MIMO FSO systems depending on the setting system as can be seen in the following section.

### B.2 Correcting Factor for MIMO FSO Systems

We can express the correcting factor  $F$  as follows

$$\begin{aligned} F &= \frac{\mathbb{E} \left[ \sum_{k=1}^M \sum_{l=1}^N I_{kl} \right]^{MN}}{(MN)^{MN} \cdot \mathbb{E} \left[ \sqrt[MN]{\prod_{k=1}^M \prod_{l=1}^N I_{kl}} \right]^{MN}} \\ &= \frac{\left( \sum_{k=1}^M \sum_{l=1}^N \mathbb{E} [I_{kl}] \right)^{MN}}{(MN)^{MN} \cdot \left( \prod_{k=1}^M \prod_{l=1}^N \mathbb{E} \left[ \sqrt[MN]{I_{kl}} \right] \right)^{MN}}. \end{aligned} \tag{B.2.1}$$

In order to compute the correcting factor  $F$  given in Eq. (B.2.1), we have to obtain the  $n$ th moment of  $I$ , i.e.,  $I = L \cdot I_a \cdot I_p$  knowing that  $I_a$  and  $I_p$  and statistically independent

as follows

$$\mathbb{E}[I^n] = \mathbb{E}[(L \cdot I_a \cdot I_p)^n] = L^n \cdot \mathbb{E}[I_a^n] \cdot \mathbb{E}[I_p^n] = L^n \cdot \int_0^\infty x^n f_{I_a}(x) dx \cdot \int_0^{A_0} y^n f_{I_p}(y) dy, \quad (\text{B.2.2})$$

where  $f_{I_a}(i)$  depends on atmospheric turbulence model, and  $f_{I_p}(i)$  is the PDF of nonzero boresight pointing error model given in Eq. (3.21). Firstly, we derive the  $n$ th moment of the nonzero boresight pointing error, which was derived in [56, appendix B] as follows

$$\mathbb{E}[(I_p)^n] = \frac{A_0 \varphi^2}{n + \varphi^2} \exp\left(-\frac{ns^2}{(n + \varphi^2)2\sigma_s^2}\right). \quad (\text{B.2.3})$$

Secondly, we derive the  $n$ th moment of LN atmospheric turbulence as

$$\mathbb{E}[(I_a^{LN})^n] = \exp\left(\frac{n\sigma_R^2}{2}(n-1)\right). \quad (\text{B.2.4})$$

Next, the  $n$ th moment of GG atmospheric turbulence can be written as

$$\mathbb{E}[(I_a^{GG})^n] = \left(\frac{1}{\alpha\beta}\right)^n \frac{\Gamma(n+\alpha)\Gamma(n+\beta)}{\Gamma(\alpha)\Gamma(\beta)}. \quad (\text{B.2.5})$$

Finally, the  $n$ th moment of EW atmospheric turbulence was derived for any  $m_1$  (both real and integer) in [144] as

$$\mathbb{E}[(I_a^{EW})^n] = m_1 m_2^n \Gamma\left(1 + \frac{n}{m_2}\right) g_n(m_1, m_2). \quad (\text{B.2.6})$$

As in Eq. (3.39), the summation in Eq. (B.2.6) can easily be computed as the series converges fast, and usually as much as 20 terms or less are sufficient for the series to converge. Finally, the correcting factor  $F$  is obtained by substituting Eq. (B.2.3) into Eq. (B.2.1), and by substituting Eq. (B.2.4), Eq. (B.2.5) or Eq. (B.2.6) into Eq. (B.2.1) depending on the considered atmospheric turbulence model.

### B.3 Correcting Factor for the BDF Cooperative Protocol

The correcting factor  $F$  for the BDF cooperative protocol is obtained for GG atmospheric turbulence with zero boresight pointing errors. We can express this correcting factor as follows

$$F = \frac{\mathbb{E}[I_T]^2}{8 \cdot \mathbb{E}\left[\sqrt{I_T^{LB}}\right]^2}. \quad (\text{B.3.1})$$

Before evaluating the parameter  $F$ , we obtain the mean of  $I_T$  as  $\mathbb{E}[I_T] = \mathbb{E}[I_{SD}] + 2\mathbb{E}[I_{RD}]$  since  $I_{SD}$  and  $I_{RD}$  are statistically independent. Therefore, the mean of a generic RV  $I_m$  for  $m = \{SD, RD\}$  is given by

$$\mathbb{E}[I_m] = \int_0^\infty i f_{I_m}(i) di, \quad (\text{B.3.2})$$

where  $f_{I_m}(i)$  is given by Eq. (2.34). The integral in Eq. (B.3.2) can be evaluated as in Eq. (B.2.2) particularizing for GG atmospheric turbulence channels with zero boresight pointing errors and  $n = 1$  as follows

$$\mathbb{E}[I_m] = \frac{A_{0m} L_m \varphi_m^2}{1 + \varphi_m^2}. \quad (\text{B.3.3})$$

The expectation of  $I_T$  is given by

$$\mathbb{E}[I_T] = \frac{A_{0SD} L_{SD} \varphi_{SD}^2}{1 + \varphi_{SD}^2} + 2 \frac{A_{0RD} L_{RD} \varphi_{RD}^2}{1 + \varphi_{RD}^2}. \quad (\text{B.3.4})$$

Secondly, we obtain the expectation of positive square root of  $I_T^{LB}$  as

$$\mathbb{E} \left[ \sqrt{I_T^{LB}} \right] = \int_0^\infty i^{1/2} f_{I_T^{LB}}(i) di. \quad (\text{B.3.5})$$

The above integral can be evaluated as in Eq. (B.2.2) particularizing for GG atmospheric turbulence channels with zero boresight pointing errors and  $n = 1/2$  as follows

$$\begin{aligned} \mathbb{E} \left[ \sqrt{I_T^{LB}} \right] &= \sqrt{\frac{A_{0SD} A_{0RD} L_{SD} L_{RD}}{\alpha_{SD} \beta_{SD} \alpha_{RD} \beta_{RD}}} \\ &\times \frac{4 \varphi_{SD}^2 \Gamma(\alpha_{SD} + 1/2) \Gamma(\beta_{SD} + 1/2) \varphi_{RD}^2 \Gamma(\alpha_{RD} + 1/2) \Gamma(\beta_{RD} + 1/2)}{(1 + 2\varphi_{SD}^2) \Gamma(\alpha_{SD}) \Gamma(\beta_{SD}) (1 + 2\varphi_{RD}^2) \Gamma(\alpha_{RD}) \Gamma(\beta_{RD})}. \end{aligned} \quad (\text{B.3.6})$$

Finally, the correcting factor  $F$  is easily derived from Eqs. (B.3.4) and (B.3.6) as follows

$$\begin{aligned} F &= \left( \frac{A_{0SD} L_{SD} \varphi_{SD}^2}{1 + \varphi_{SD}^2} + \frac{2A_{0RD} L_{RD} \varphi_{RD}^2}{1 + \varphi_{RD}^2} \right)^2 \\ &\times \frac{\alpha_{SD} \beta_{SD} (1 + 2\varphi_{SD}^2)^2 \Gamma(\alpha_{SD})^2 \Gamma(\beta_{SD})^2}{128 A_{0SD} L_{SD} \varphi_{SD}^4 \Gamma(\alpha_{SD} + 1/2)^2 \Gamma(\beta_{SD} + 1/2)^2} \\ &\times \frac{\alpha_{RD} \beta_{RD} (1 + 2\varphi_{RD}^2)^2 \Gamma(\alpha_{RD})^2 \Gamma(\beta_{RD})^2}{A_{0RD} L_{RD} \varphi_{RD}^4 \Gamma(\alpha_{RD} + 1/2)^2 \Gamma(\beta_{RD} + 1/2)^2}. \end{aligned} \quad (\text{B.3.7})$$

## B.4 Correcting Factor for the ADF Cooperative Protocol

The correcting factor  $F'$  for the ADF cooperative protocol is obtained for GG atmospheric turbulence with zero boresight pointing errors under the assumption that  $I_{RD} > I_{SD}$ . In this way, we can express this correcting factor as follows

$$F' = \frac{\mathbb{E}[I_{SD} + 2I_{RD}]^2}{8 \cdot \mathbb{E}[\sqrt{I_{SD} I_{RD}}]^2}, \quad I_{RD} > I_{SD}. \quad (\text{B.4.1})$$

Similar to the correcting factor obtained in Appendix B.3, we firstly obtain the expectation of  $\mathbb{E}[I_{SD} + 2I_{RD}]$  under the assumption that  $I_{RD} > I_{SD}$  as

$$\begin{aligned} \mathbb{E}[I_{SD} + 2I_{RD}] &= \int_0^\infty \int_0^{i_2} (i_1 + 2i_2) f_{I_{SD}}(i_1) f_{I_{RD}}(i_2) di_1 di_2 \\ &= \int_0^\infty \left[ \int_0^{i_2} i_1 f_{I_{SD}}(i_1) di_1 \right] f_{I_{RD}}(i_2) di_2 + 2 \int_0^\infty i_2 f_{I_{SD}}(i_2) f_{I_{RD}}(i_2) di_2 = A + 2B. \end{aligned} \quad (\text{B.4.2})$$

In order to evaluate the double integral in  $A$ , we have to evaluate the inner one first. In this way, we can obtain the corresponding closed-form expression of  $A$  with the help of [59, eqn. 1.16.2.1] and [59, eqn. 2.24.1.2] (See Appendix A.3.2) for the inner integral and the outer integral, respectively. Hence, the integral  $A$  can be expressed in terms of the Meijer's G-function as follows

$$A = \frac{\varphi_{RD}^2 \varphi_{SD}^2 A_{0SD} L_{SD} G_{5,5}^{4,3} \left( \frac{\alpha_{RD} \beta_{RD} A_{0SD} L_{SD}}{\alpha_{SD} \beta_{SD} A_{0RD} L_{RD}} \left| \begin{array}{l} -\varphi_{SD}^2, -\alpha_{SD}, -\beta_{SD}, 1, \varphi_{RD}^2 + 1 \\ \varphi_{RD}^2, \alpha_{RD}, \beta_{RD}, 0, -\varphi_{SD}^2 - 1 \end{array} \right. \right)}{\alpha_{SD} \beta_{SD} \Gamma(\alpha_{RD}) \Gamma(\alpha_{SD}) \Gamma(\beta_{RD}) \Gamma(\beta_{SD})}. \quad (\text{B.4.3})$$

Similar to  $A$ , we can obtain the corresponding closed-form expression of the integral  $B$  with the help of [59, eqn. 2.24.1.2] as

$$B = \frac{2\varphi_{RD}^2 \varphi_{SD}^2 A_{0SD} L_{SD} G_{5,5}^{4,3} \left( \frac{\alpha_{RD} \beta_{RD} A_{0SD} L_{SD}}{\alpha_{SD} \beta_{SD} A_{0RD} L_{RD}} \left| \begin{array}{l} -\varphi_{SD}^2, -\alpha_{SD}, -\beta_{SD}, 0, \varphi_{RD}^2 + 1 \\ \varphi_{RD}^2, \alpha_{RD}, \beta_{RD}, -1, -\varphi_{SD}^2 - 1 \end{array} \right. \right)}{\alpha_{SD} \beta_{SD} \Gamma(\alpha_{RD}) \Gamma(\alpha_{SD}) \Gamma(\beta_{RD}) \Gamma(\beta_{SD})}. \quad (\text{B.4.4})$$

Secondly, we obtain the expectation of positive square root of the product of  $I_{SD} I_{RD}$  under the assumption that  $I_{RD} > I_{SD}$  as follows

$$\begin{aligned} \mathbb{E}[\sqrt{I_{SD} I_{RD}}] &= \int_0^\infty \int_0^{i_2} \sqrt{i_1 i_2} f_{I_{SD}}(i_1) f_{I_{RD}}(i_2) di_1 di_2 \\ &= \int_0^\infty \sqrt{i_2} \left[ \int_0^{i_2} \sqrt{i_1} f_{I_{SD}}(i_1) di_1 \right] f_{I_{RD}}(i_2) di_2 = C. \end{aligned} \quad (\text{B.4.5})$$

Similar to  $A$ , we can obtain the expectation of positive square root of the product of  $I_{SD}$  and  $I_{RD}$  as

$$C = \frac{\varphi_{RD}^2 \varphi_{SD}^2 A_{0SD} L_{SD} G_{5,5}^{4,3} \left( \frac{\alpha_{RD} \beta_{RD} A_{0SD} L_{SD}}{\alpha_{SD} \beta_{SD} A_{0RD} L_{RD}} \left| \begin{array}{l} -\varphi_{SD}^2, -\alpha_{SD}, -\beta_{SD}, \frac{1}{2}, \varphi_{RD}^2 + 1 \\ \varphi_{RD}^2, \alpha_{RD}, \beta_{RD}, -\frac{1}{2}, -\varphi_{SD}^2 - 1 \end{array} \right. \right)}{\alpha_{SD} \beta_{SD} \Gamma(\alpha_{RD}) \Gamma(\alpha_{SD}) \Gamma(\beta_{RD}) \Gamma(\beta_{SD})}. \quad (\text{B.4.6})$$

Finally, the correcting factor  $F'$  is easily derived from Eqs. (B.4.3), (B.4.4) and (B.4.6) as follows

$$F' = \frac{(A + 2B)^2}{8 \cdot C^2}. \quad (\text{B.4.7})$$

## Appendix C

# Correlated Sways

In this Appendix, the corresponding means and variances of  $x'$  and  $y'$  are derived. In this way, the corresponding mean of  $x'$  can easily be obtained as follows

$$\begin{aligned}\mu'_x &= \mathbb{E}[x'] = \mathbb{E}[r \cos(\phi - \phi_0)] = \mathbb{E}[r \cos \phi \cos \phi_0 + r \sin \phi \sin \phi_0] \\ &= \cos \phi_0 \mathbb{E}[r \cos \phi] + \sin \phi_0 \mathbb{E}[r \sin \phi] = \mu_x \cos \phi_0 + \mu_y \sin \phi_0.\end{aligned}\quad (\text{C.0.1})$$

Similar to the above expression, the corresponding mean of  $y'$  is also obtained as follows

$$\begin{aligned}\mu'_y &= \mathbb{E}[y'] = \mathbb{E}[r \sin(\phi - \phi_0)] = \mathbb{E}[r \sin \phi \cos \phi_0 - r \cos \phi \sin \phi_0] \\ &= \cos \phi_0 \mathbb{E}[r \sin \phi] - \sin \phi_0 \mathbb{E}[r \cos \phi] = \mu_y \cos \phi_0 - \mu_x \sin \phi_0.\end{aligned}\quad (\text{C.0.2})$$

Finally, the corresponding variance of  $x'$  can be obtained by performing some easy algebraic manipulations as follows

$$\begin{aligned}\sigma_x'^2 &= \text{Var}[x'] = \text{Var}[r \cos(\phi - \phi_0)] = \text{Var}[r \cos \phi \cos \phi_0 + r \sin \phi \sin \phi_0] \\ &= \cos^2 \phi_0 \text{Var}[r \cos \phi] + \sin^2 \phi_0 \text{Var}[r \sin \phi] \\ &\quad + 2 \cos \phi_0 \sin \phi_0 \text{Cov}[r \cos \phi, r \sin \phi] \\ &= \sigma_x^2 \cos^2 \phi_0 + \sigma_y^2 \sin^2 \phi_0 + 2\rho\sigma_x\sigma_y \sin \phi_0 \cos \phi_0.\end{aligned}\quad (\text{C.0.3})$$

Similar to the above expression, the corresponding variance of  $y'$  is also obtained as follows

$$\begin{aligned}\sigma_y'^2 &= \text{Var}[y'] = \text{Var}[r \sin(\phi - \phi_0)] = \text{Var}[r \sin \phi \cos \phi_0 - r \cos \phi \sin \phi_0] \\ &= \cos^2 \phi_0 \text{Var}[r \sin \phi] + \sin^2 \phi_0 \text{Var}[r \cos \phi] \\ &\quad - 2 \cos \phi_0 \sin \phi_0 \text{Cov}[r \sin \phi, r \cos \phi] \\ &= \sigma_y^2 \cos^2 \phi_0 + \sigma_x^2 \sin^2 \phi_0 - 2\rho\sigma_x\sigma_y \sin \phi_0 \cos \phi_0.\end{aligned}\quad (\text{C.0.4})$$



UNIVERSIDAD  
DE MÁLAGA

# Appendix D

## Publications and Projects

### D.1 Publications

In this section, the publications derived during the development of this thesis are presented.

#### Book chapter

- R. Boluda-Ruiz, B. Castillo-Vázquez, C. Castillo-Vázquez, and A. García-Zambrana, "New Results in DF Relaying Schemes Using Time Diversity for Free-Space Optical Links," Dr. Narottam Das (Ed.), Chapter 8. InTech. pp.195-213, 2014. ISBN 978-953-51-1730-8.

#### Journal papers

- R. Boluda-Ruiz, A. García-Zambrana, B. Castillo-Vázquez, and C. Castillo-Vázquez, "On the effect of correlated sways on generalized misalignment fading for terrestrial FSO links," *Photonics Journal, IEEE*, **9**(3), 1–13, 2017 (Impact factor 2.177, 60/257 Engineering, Electrical and Electronic Q1 JCR 2015).
- R. Boluda-Ruiz, A. García-Zambrana, C. Castillo-Vázquez, B. Castillo-Vázquez, and Steve Hranilovic, "Outage Performance of Exponentiated Weibull FSO Links Under Generalized Pointing Errors," *J. of Lightwave Technol., IEEE/OSA*, vol. 35, no. 9, pp. 1605–1613, 2017 (Impact factor 2.567, 20/90 Optics Q1 JCR 2015).
- R. Boluda-Ruiz, A. García-Zambrana, C. Castillo-Vázquez, and B. Castillo-Vázquez, "Novel approximation of misalignment fading modeled by Beckmann distribution on free-space optical links," *Opt. Express* **24**(20), 22635–22649, 2016 (Impact factor 3.148, 14/90 Optics Q1 JCR 2015).

- R. Boluda-Ruiz, A. García-Zambrana, B. Castillo-Vázquez, and C. Castillo-Vázquez, "Impact of nonzero boresight pointing error on ergodic capacity of MIMO FSO communication systems," *Opt. Express* **24**(4), 3513–3534, 2016 (Impact factor 3.148, 14/90 Optics Q1 JCR 2015).
- R. Boluda-Ruiz, A. García-Zambrana, B. Castillo-Vázquez, and C. Castillo-Vázquez, "Ergodic capacity analysis of decode-and-forward relay-assisted FSO systems over alpha-mu fading channels considering pointing errors," *Photonics Journal, IEEE*, **8**(1), 1–11, 2016 (Impact factor 2.177, 60/257 Engineering, Electrical and Electronic Q1 JCR 2015).
- R. Boluda-Ruiz, A. García-Zambrana, B. Castillo-Vázquez, and C. Castillo-Vázquez, "MISO relay-assisted FSO systems over gamma-gamma fading channels with pointing errors," *Photonics Technology Letters, IEEE* **28**(3), 229–232, 2016 (Impact factor 1.945, 72/257 Engineering, Electrical and Electronic Q2 JCR 2015).
- A. García-Zambrana, R. Boluda-Ruiz, C. Castillo-Vázquez, and B. Castillo-Vázquez, "Novel space-time trellis codes for free-space optical communications using transmit laser selection," *Opt. Express* **23**(19), 24195–24211, 2015 (Impact factor 3.488, 9/86 Optics Q1 JCR 2013).
- R. Boluda-Ruiz, A. García-Zambrana, B. Castillo-Vázquez, and C. Castillo-Vázquez, "On the capacity of MISO FSO systems over gamma-gamma and misalignment fading channels," *Opt. Express* **23**(17), 22371–22385, 2015 (Impact factor 3.488, 9/86 Optics Q1 JCR 2013).
- R. Boluda-Ruiz, A. García-Zambrana, B. Castillo-Vázquez, and C. Castillo-Vázquez, "Ergodic capacity analysis for DF strategies in cooperative FSO systems," *Opt. Express* **23**(17), 21565–21584, 2015 (Impact factor 3.488, 9/86 Optics Q1 JCR 2013).
- C. Castillo-Vázquez, R. Boluda-Ruiz, B. del Castillo-Vázquez, and A. García-Zambrana, "Outage performance of DF relay assisted FSO communications using time-diversity," *Photonics Technology Letters, IEEE* **27**(11), 1149–1152, 2015 (Impact factor 2.110, 56/249 Engineering, Electrical and Electronic Q1 JCR 2013).
- R. Boluda-Ruiz, A. García-Zambrana, B. Castillo-Vázquez, and C. Castillo-Vázquez, "Impact of relay placement on diversity order in adaptive selective DF relay-assisted FSO communications," *Opt. Express* **23**(3), 2600–2617, 2015 (Impact factor 3.488, 9/86 Optics Q1 JCR 2013).
- A. García-Zambrana, R. Boluda-Ruiz, C. Castillo-Vázquez, and B. Castillo-Vázquez, "Transmit alternate laser selection with time diversity for FSO communications," *Opt. Express* **22**(20), 23,861–23,874, 2014 (Impact factor 3.488, 9/86 Optics Q1 JCR 2013).
- R. Boluda-Ruiz, A. García-Zambrana, C. Castillo-Vázquez, and B. Castillo-Vázquez, "Adaptive selective relaying in cooperative free-space optical systems over atmospheric



turbulence and misalignment fading channels,” *Opt. Express* **22**(13), 16,629–16,644, 2014 (Impact factor 3.488, 9/86 *Optics Q1 JCR* 2013).

### Conference papers

- R. Boluda-Ruiz, A. García-Zambrana, B. Castillo-Vázquez, and C. Castillo-Vázquez, “Rate-adaptive selective relaying using time diversity for relay-assisted FSO communications”, *IEEE Global Signal and Information Processing Conference (GlobalSIP’15)* December 14-16, 2015, Orlando, Florida, USA).
- C. Castillo-Vázquez, R. Boluda-Ruiz, B. Castillo-Vázquez, and A. García-Zambrana, “Outage Performance of DF Relay-Assisted FSO Communications Using Time-Diversity”, *IEEE International Photonics Conference (IPC)*, (28th Annual Conference of the IEEE Photonics Society, October 4-8, 2015, Reston, Virginia, USA).
- R. Boluda-Ruiz, A. García-Zambrana, B. Castillo-Vázquez, and C. Castillo-Vázquez, “Evaluating pointing errors on ergodic capacity of DF relay-assisted FSO communication systems”, *IEEE 82th Vehicular Technology Conference (VTC-Fall)* September 6-9, 2015, Boston, USA).
- R. Boluda-Ruiz, A. García-Zambrana, B. Castillo-Vázquez, and C. Castillo-Vázquez, “Análisis de la capacidad ergódica en sistemas cooperativos de comunicaciones ópticas no guiadas,” *XXX Symposium Nacional de la Unión Científica Internacional de Radio (URSI)* September 2-4, 2015, Pamplona, España).
- R. Boluda-Ruiz, A. García-Zambrana, B. Castillo-Vázquez, and C. Castillo-Vázquez, “Average channel capacity analysis of BDF relaying over alpha-mu fading channels”, *11th International Wireless Comunicaciones and Mobile Computing Conference (IWCMC)* August 24-28, 2015, Dubrovnik, Croatia).
- R. Boluda-Ruiz and A. García-Zambrana, “Protocolo de Cooperación Adaptativo para Sistemas de Comunicaciones Ópticas Atmosféricas,” *XXIX Symposium Nacional de la Unión Científica Internacional de Radio (URSI)* September 3-5, 2014, Valencia, España).

## D.2 Projects

This thesis has been founded by the Spanish Ministry of Economy and Competitiveness (MINECO) under FPI grant BES-2013-062689 and the research project TEC2012-32606, and the Junta de Andalucía (research group: TIC-0102).

### D.3 Research Fellowship

Finally, a research stay at McMaster University (Hamilton, Ontario, Canada) under the supervision of Prof. Steve Hranilovic was performed for 4 months in the context of FSO communication systems under mobility grant EEBB-I-16-11099.

# Appendix E

## Summary (Spanish)

### E.1 Introducción

#### E.1.1 Motivación

El uso de comunicaciones ópticas inalámbricas (OWC, *Optical Wireless Communication*) como solución a la escasez de recursos espectrales en la zona del espectro radioeléctrico ha atraído una considerable atención en años recientes como consecuencia del crecimiento del volumen de datos y la cantidad de usuarios, así como de la aparición de nuevas tecnologías tales como acceso a Internet de banda ancha ultra-rápido, *the Internet of Things* (IoT), servicios de alta definición para televisión, servicios de televisión en *streaming*, etc [1,2]. Esta tecnología puede ser aplicable a diferentes aplicaciones como: comunicaciones *chip-to-chip* para ultra-corto alcance, comunicaciones IR (*Infrared*), VLC (*Visible Light Communication*) y UOC (*Underwater Optical Communication*) para medio alcance, comunicaciones FSO (*Free-Space Optical*) para largo alcance, y enlaces tierra-satélite para ultra-largo alcance. En esta tesis, todo el estudio se realiza sobre enlaces terrestres FSO. Dichos enlaces utilizan longitudes de onda ubicadas en la zona del infrarrojo cercano, es decir, longitudes de ondas de 850 nm, 1300 nm y 1550 nm que se corresponden con la primera, segunda y tercera ventana de transmisión, respectivamente.

Tradicionalmente, los sistemas de comunicaciones FSO han sido propuestos como una alternativa a la tecnología de RF (*Radio-Frequency*) y como una interesante solución al conocido problema de la última milla, es decir, la distancia entre el usuario final y la infraestructura de fibra óptica. Este problema continua siendo el cuello de botella en las redes existentes debido a que la tecnología de RF limita la velocidad en el último tramo, obteniendo regímenes binarios del orden de 10-100 Mbps. La tecnología FSO permite a los diferentes usuarios conectarse a las redes de fibra óptica a una velocidad mucho mayor como consecuencia directa de su elevado ancho de banda disponible. El espectro óptico ofrece numerosas

ventajas tales como la posibilidad de utilizar un ancho de banda más elevado que el espectro radioeléctrico y, además, este carece de regulación por encima de los 300 GHz. Otra ventaja en relación a los sistemas de RF es que los sistemas FSO presentan una menor atenuación en lluvia e inmunidad frente a interferencias debido al uso de un haz muy estrecho entre transmisor y receptor. Por último, no solo son una más que interesante alternativa a los sistemas de RF, sino también a los sistemas guiados de fibra óptica. No cabe duda que los enlaces de fibra óptica son a día de hoy la mejor solución para garantizar una buena calidad de servicio, pero por temas relacionados con coste e instalación no siempre son una buena opción.

Como es de esperar, no todo son ventajas en el ámbito de la tecnología FSO donde algunos inconvenientes limitan el rango de viabilidad de estos sistemas. Los factores más delimitadores son: la turbulencia atmosférica, los errores por desapuntamiento entre transmisor y receptor, y la niebla espesa. La turbulencia atmosférica es provocada por microvariaciones de presión y temperatura que conllevan a fluctuaciones locales del índice de refracción en la atmósfera. Como resultado, la señal óptica que se propaga a través de la atmósfera sufre fluctuaciones aleatorias en intensidad y en fase. La turbulencia atmosférica puede ser descrita físicamente por la teoría de cascadas propuesta por Kolmogorov [13]. Según esta teoría, la masa de aire turbulento está compuesto por un conjunto de torbellinos de diferentes tamaños donde se asume que cada uno de ellos es homogéneo aunque con un índice de refracción diferente al de sus vecinos. La energía procedente del movimiento de las masas de aire será transportada a torbellinos cada vez más pequeños hasta que se termine disipando en calor. Respecto a los errores por desapuntamiento entre transmisor y receptor, estos son una consecuencia directa de la dificultad de conseguir un perfecto alineamiento entre ellos debido al estrecho haz de la fuente láser. Las causas del desapuntamiento pueden deberse a fenómenos meteorológicos como fuertes rachas de viento y pequeños terremotos, entre otras. Por último, los sistemas FSO son, en general, altamente vulnerables a condiciones meteorológicas adversas como la niebla espesa.

### E.1.2 Objetivos

Esta tesis está centrada en el estudio de las prestaciones de sistemas avanzados de comunicaciones ópticas atmosféricas o sistemas FSO. El estudio de las prestaciones, ya sea en términos de probabilidad de error de bit (BER, *Bit Error-Rate*), probabilidad de *outage* o capacidad ergódica, ha sido un tema de interés relevante para la comunidad científica desde hace varias décadas. En este sentido, dos grandes áreas o líneas de investigación son abordadas a lo largo de esta tesis, presentando nuevos e interesantes resultados relacionados con las comunicaciones ópticas. Estas dos grandes áreas son: análisis de la capacidad ergódica, y modelado de errores por desapuntamiento generalizado entre transmisor y receptor.

Por un lado, el estudio de la capacidad ergódica representa la primera línea de investigación de esta tesis en la cual no solo se analiza la capacidad ergódica correspondiente a sistemas

basados en diversidad espacial tales como sistemas MISO (*Multiple-Input/Single-Input*), SIMO (*Single-Input/Multiple-Output*) y MIMO (*Multiple-Input/Multiple-Input*) FSO, sino también de sistemas cooperativos FSO basados en retransmisión DF (*Detect-and-Forward*). La capacidad ergódica es una de las medidas de prestaciones más importante, la cual nos proporciona información sobre la máxima tasa de información libre de errores que puede lograrse cuando transmitimos información por un canal con desvanecimientos (*fading*) [73], es decir, sobre canales afectados por turbulencia atmosférica. Así pues, el objetivo de esta línea de investigación es doble: por un lado, desarrollar nuevas expresiones matemáticas que nos permitan computar la capacidad ergódica en todo el rango de valores de SNR (*Signal-to-Noise Ratio*), así como estudiar cómo esta se deteriora debido al efecto de la turbulencia atmosférica y, al mismo tiempo, cómo mejora con respecto a la capacidad ergódica obtenida por un sistema SISO FSO; por otro lado, incorporar el efecto del desapuntamiento Rayleigh (modelo más sencillo desde el punto de vista matemático) en el estudio de la capacidad ergódica (efecto que no ha sido tenido en cuenta en la literatura hasta ahora), así como incluir el efecto de los errores por puntería (*nonzero boresight error*) al desapuntamiento Rayleigh dando lugar a un desapuntamiento lognormal-Rice fundamentalmente en sistemas SIMO y MIMO FSO con más de una apertura receptora. El utilizar un modelo más sofisticado de desapuntamiento para el estudio de la capacidad de sistemas SIMO y MIMO FSO ha propiciado crear una segunda línea de investigación: modelado de errores por desapuntamiento generalizado entre transmisor y receptor.

Por otro lado, la segunda línea de investigación es el modelado de errores por desapuntamiento generalizado. En la última década se han propuesto diferentes modelos estadísticos con el fin de modelar dichos errores [53, 56, 132]. Los citados modelos se han usado en un elevado número de artículos de investigación con el objetivo de incorporar tal efecto en los diferentes estudios para dotarlos de un mayor grado de realismo. Incorporar el efecto del desapuntamiento conlleva una dificultad añadida a la hora de desarrollar nuevas expresiones matemáticas en forma cerrada que evalúen las prestaciones de los sistemas FSO. Por tanto, incluir el efecto de los errores por desapuntamiento en el análisis de las prestaciones no solo es dotar dicho análisis de un mayor grado de realismo, sino también supone un reto desde el punto de vista matemático. En el caso general, el efecto del desapuntamiento entre el transmisor y el receptor es modelado según la distribución Beckmann [34], cuya función densidad de probabilidad (PDF, *Probability Density Function*) presenta ciertos impedimentos desde el punto de vista práctico ya que está expresada en forma integral. En este sentido, se propone una aproximación a esta conocida PDF con el objetivo de incluir errores por desapuntamiento generalizado en el diseño de cualquier sistema FSO.

## E.2 El Canal Óptico Atmosférico

En esta sección se presenta el modelo de canal óptico atmosférico asumido a lo largo de esta tesis para cada uno de los enlaces FSO involucrados en cada sistema. Así pues, estos

enlaces están basados en modulación de intensidad y detección directa (IM/DD, *Intensity-Modulation and Direct-Detection*) con línea de visión directa (LOS, *Line-of-Sight*) entre transmisor y receptor. El sistema FSO está compuesto por un diodo láser emisor de infrarrojos y un fotodetector como transductor de señal óptica a señal eléctrica. El modelo matemático en banda base para dicho canal viene dado por

$$Y = IX + Z, \quad (\text{E.2.1})$$

donde  $Y$  es la corriente de salida del fotodetector,  $X$  es la potencia óptica instantánea transmitida al medio por el transmisor,  $I$  es la irradiancia del enlace óptico atmosférico entre el transmisor y el receptor, y  $Z$  es el ruido aditivo blanco y Gaussiano (AWGN, *Additive White Gaussian Noise*) de media cero y varianza  $\sigma_n^2 = N_0/2$  e independiente del estado on/off del bit recibido ( $Z \sim N(0, N_0/2)$ ). El sistema de modulación empleado es OOK (*On-Off Keying*) donde  $X$  es 0 o  $2P_t$ , siendo  $P_t$  la potencia óptica promedio enviada al aire. La irradiancia es considerada el producto de tres factores dada por  $I = L \cdot I_a \cdot I_p$ , donde  $L$  es la atenuación atmosférica (variable determinista),  $I_a$  es la turbulencia atmosférica, e  $I_p$  es la atenuación debida a los errores por desapuntamiento entre transmisor y receptor. Diferentes modelos estadísticos han sido propuestos para modelar la turbulencia atmosférica tales como los modelos log-normal (LN) y gamma-gamma (GG). Concretamente, LN es más adecuado para modelar escenarios de turbulencia débil, y GG es adecuado para escenarios de turbulencia moderada o fuerte. En esta tesis, se adopta principalmente el modelo GG.

## E.3 Análisis de la Capacidad Ergódica

### E.3.1 Motivación

En esta sección se realiza un estudio pormenorizado de la capacidad ergódica de sistemas MISO, SIMO, MIMO y cooperativos FSO sobre turbulencia atmosférica modelada con distribución GG y ante diferente severidad de errores por desapuntamiento entre transmisor y receptor. En este sentido, se obtienen nuevas expresiones matemáticas en forma cerrada las cuales nos sirven para estimar la capacidad ergódica del sistema bajo estudio.

En la última década, el estudio de la capacidad ergódica de los sistemas FSO sobre diferentes modelos estadísticos de turbulencia atmosférica y de desapuntamiento entre transmisor y receptor ha sido un tema de interés notable para la comunidad investigadora [65, 67–72].

### E.3.2 Capacidad Ergódica de Sistemas MISO FSO

En esta sección se obtienen nuevas expresiones matemáticas en forma cerrada para la capacidad ergódica de un sistema MISO FSO sobre canales atmosféricos modelados con distribución GG y ante diferente severidad de errores por desapuntamiento Rayleigh, es decir,

desapuntamiento con *zero boresight errors* entre transmisor y receptor. Hay que destacar que estas expresiones nunca antes se habían obtenido debido a que el efecto del desapuntamiento nunca se había tenido en cuenta en la literatura.

### Modelo de Sistema

Asumimos un sistema MISO FSO con  $M$  transmisores y un único receptor como el que se muestra en la Fig. E.1. Antes de comenzar con dicho análisis, algunas consideraciones

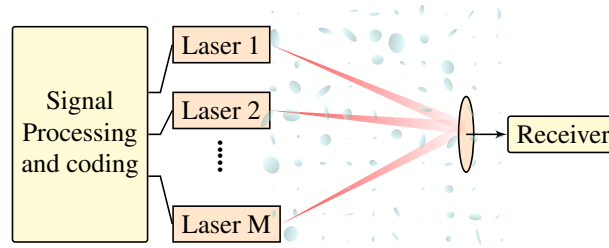


Figure E.1: Diagrama de bloques del sistema MISO FSO bajo estudio.

deben ser comentadas: en primer lugar, asumimos que el transmisor y el receptor están situados de forma que todas las fuentes láseres que forman el transmisor se encuentran en la línea de visión directa del receptor; en segundo lugar, todas las fuentes láseres se encuentran separadas una determinada distancia con el objetivo de considerar *fading* incorrelados y, por tanto, beneficiarnos de las ventajas que proporcionan las técnicas basadas en diversidad espacial. Esta distancia está relacionada con la longitud de coherencia atmosférica  $r_0$  (véase Capítulo 2). Si la distancia de separación entre las diferentes fuentes láseres es mayor que la longitud de coherencia atmosférica, entonces podemos considerar *fading* incorrelados. Esta situación suele ser habitual en la práctica [94, 95] y, al mismo tiempo, facilita el análisis matemático; y, en tercer lugar, asumimos también la técnica de combinación EGC (*Equal Gain Combining*) en el receptor como método de combinación de las diferentes réplicas que provienen de los diferentes láseres debido a su baja complejidad [96, 97].

### Análisis de la Capacidad

Asumiendo CSI (*Channel State Information*) instantáneo en el receptor, la capacidad ergódica de un sistema MISO FSO en bits/s/Hz puede ser escrita como

$$C_{\text{MISO}}/B = \frac{1}{2 \ln(2)} \int_0^\infty \ln \left( 1 + \frac{4\gamma}{M^2} i^2 \right) f_{I_T}(i) di, \quad (\text{E.3.1})$$

donde  $\gamma$  es la SNR en ausencia de turbulencia atmosférica y es definida como  $\gamma = P_t^2 T_b / N_0$  ( $T_b$  es el periodo de bit),  $I_T = I_1 + I_2 + \dots + I_M$  es la irradiancia total del canal MISO

FSO, y  $f_{I_T}(i)$  es la PDF de la suma de  $M$  variables aleatorias GG con desapuntamiento entre transmisor y receptor. Las  $M$  variables aleatorias involucradas en dicha suma son estadísticamente independientes pero no necesariamente idénticamente distribuidas. La división por  $M$  en la expresión de la SNR es para considerar la misma potencia óptica promedio en el aire que en el caso de un sistema SISO FSO con una única fuente láser, es decir, cada láser del sistema MISO FSO envía al aire una potencia óptica promedio de  $P_t/M$  debido a que estamos considerando  $M$  fuentes láseres.

Desafortunadamente, una expresión matemática en forma cerrada para la PDF combinada de la suma de  $M$  variables aleatorias GG con desapuntamiento Rayleigh entre transmisor y receptor no es posible obtener. Para solventar dicho problema recurrimos a realizar una aproximación basada en la desigualdad entre la media aritmética ( $AM$ ) y la media geométrica ( $GM$ ) dada por

$$AM \geq GM, \quad (\text{E.3.2})$$

donde  $AM = (1/M) \sum_{k=1}^M I_k$  y  $GM = \sqrt[M]{\prod_{k=1}^M I_k}$  son la AM y la GM, respectivamente. En este caso estamos obteniendo una cota inferior para dicha suma dada por

$$I_T = \sum_{k=1}^M I_k \geq M \sqrt[M]{F \cdot \prod_{k=1}^M I_k} = M \sqrt[M]{F \cdot I_{LB}}. \quad (\text{E.3.3})$$

Se puede advertir que la PDF de  $I_{LB}$  se presenta más tratable desde el punto de vista matemático que la PDF de  $I_T$ . Además, un factor de corrección  $F$  es añadido a la expresión de arriba con el fin de obtener una mayor precisión en el cómputo de la capacidad. Este factor de corrección está justificado desde el hecho de que la esperanza matemática (la media) en ambos lados de la desigualdad toma diferentes valores. Dicho factor de corrección convierte la desigualdad en aproximación. El factor de corrección  $F$  puede ser expresado como (véase Apéndice B.1)

$$F = \frac{\mathbb{E} \left[ \sum_{k=1}^M I_k \right]^M}{M^M \cdot \mathbb{E} \left[ \sqrt[M]{\prod_{k=1}^M I_k} \right]^M}. \quad (\text{E.3.4})$$

Ahora, substituyendo Eq. (E.3.3) en Eq. (E.3.1) y, realizando algunas simplificaciones matemáticas, se obtiene la siguiente expresión para la capacidad ergódica de un sistema MISO FSO

$$C_{\text{MISO}/B} \approx \frac{1}{\ln(4)} \int_0^\infty \ln \left( 1 + 4\gamma \left( i \cdot F \right)^{\frac{2}{M}} \right) f_{I_{LB}}(i) di. \quad (\text{E.3.5})$$

La PDF de  $f_{I_{LB}}(i)$  se obtiene vía transformada de Mellin (véase Apéndice A.7.1) cuyo resultado final es

$$f_{I_{LB}}(i) = \frac{i^{-1} \prod_{k=1}^M \varphi_k^2 G_{M,3M}^{3M,0} \left( \prod_{k=1}^M \frac{\alpha_k \beta_k}{A_{0k} L_k} i \mid \begin{array}{c} \varphi_1^2 + 1, \dots, \varphi_M^2 + 1 \\ \varphi_1^2, \alpha_1, \beta_1, \dots, \varphi_M^2, \alpha_M, \beta_M \end{array} \right)}{\prod_{k=1}^M \Gamma(\alpha_k) \Gamma(\beta_k)}. \quad (\text{E.3.6})$$



Table E.1: Condiciones climáticas del enlace FSO.

Clima	Visibilidad (km)	$C_n^2 \times 10^{-14} m^{-2/3}$
Neblina	4	1.7 (Turbulencia moderada.)
Cielo claro	16	8 (Turbulencia fuerte.)

La integral en Eq. (E.3.5) se puede resolver con la ayuda de [59, eqn. (8.4.6.5)] (véase Apéndice A.3.1) y [58, eqn. (07.34.21.0012.01)] (véase Apéndice A.3.2), obteniendo la siguiente expresión aproximada en forma cerrada para la capacidad de un sistema MISO FSO

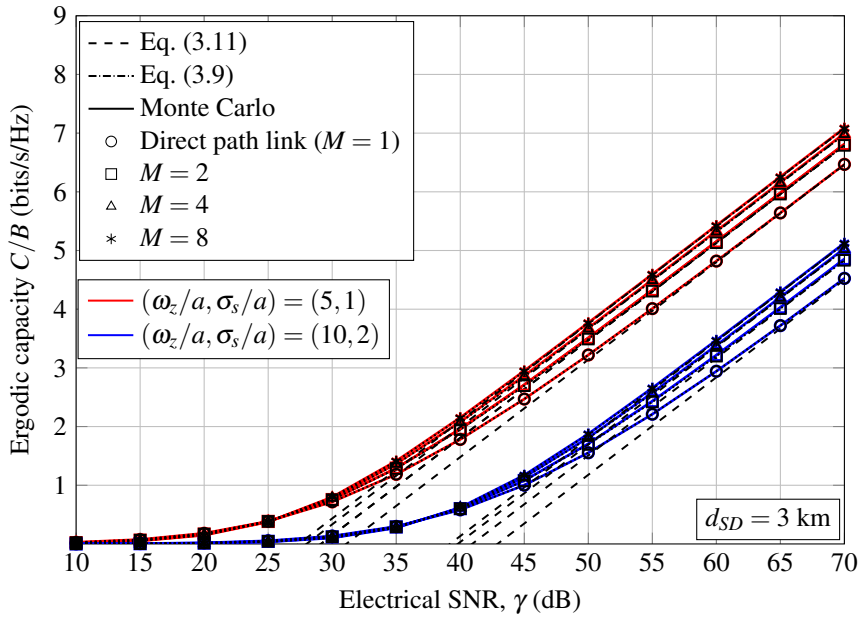
$$C_{\text{MISO}/B} \doteq \frac{\prod_{k=1}^M \varphi_k^2 H_{2+3M, 2+M}^{1, 2+3M} \left( 4\gamma \sqrt[M]{F} \left( \prod_{k=1}^M \frac{A_{0_k} L_k}{\alpha_k \beta_k} \right)^{\frac{2}{M}} \left| \begin{array}{l} (1, 1), (1, 1), \xi_1 \\ (1, 1), \xi_2, (0, 1) \end{array} \right. \right)}{\ln(4) \prod_{k=1}^M \Gamma(\alpha_k) \Gamma(\beta_k)}, \quad (\text{E.3.7})$$

donde  $\xi_1 = \{(1 - \varphi_1^2, \frac{2}{M}), (1 - \alpha_1, \frac{2}{M}), (1 - \beta_1, \frac{2}{M}), \dots, (1 - \varphi_M^2, \frac{2}{M}), (1 - \alpha_M, \frac{2}{M}), (1 - \beta_M, \frac{2}{M})\}$ ,  $\xi_2 = \{(-\varphi_1^2, \frac{2}{M}), \dots, (-\varphi_M^2, \frac{2}{M})\}$ , y  $H_{p,q}^{m,n}[\cdot]$  es la función H-Fox (véase Apéndice A.5).

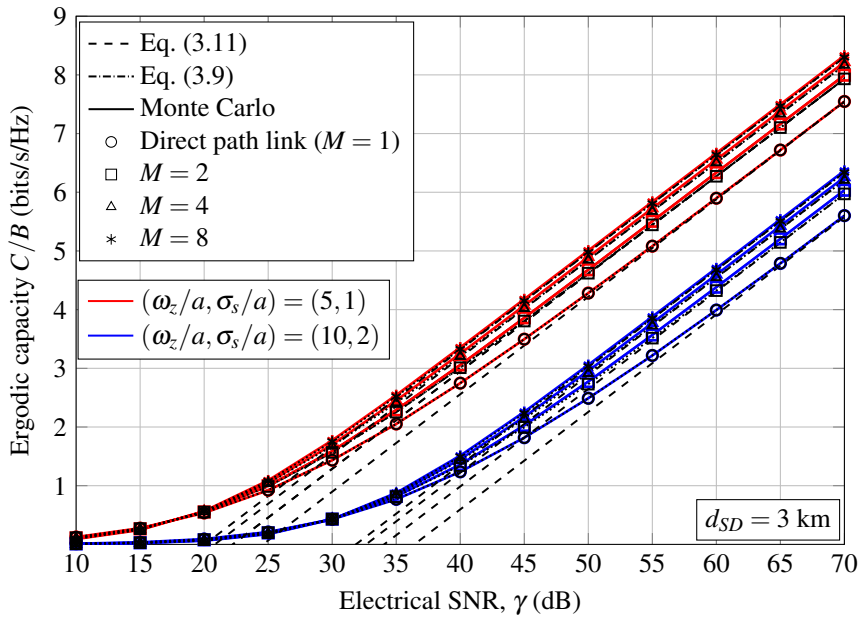
### Resultados Numéricos

A continuación se muestran algunos resultados numéricos con el fin de evaluar la expresión matemática obtenida para la capacidad ergódica en Eq. (E.3.7) correspondiente a un sistema MISO FSO. Además, se han incluido las correspondientes simulaciones de Monte Carlo con el objetivo de validar dicha expresión matemática. Estos resultados numéricos son mostrados en la Fig. E.2 para diferentes valores de  $M$ , y considerando una distancia típica de enlace FSO de 3 km. Diferentes condiciones climáticas también son consideradas para diferenciar entre turbulencia moderada y turbulencia fuerte como puede verse en la Tabla E.1. Con los valores que aparecen en la Tabla E.1 y considerando una distancia de enlace de 3 km, un espaciado mínimo entre láseres en transmisión de 2.94 cm y 1.16 cm para turbulencia moderada y fuerte, respectivamente, deben ser respetados para considerar *fading* incorrelados en ambos escenarios.

A la vista de los resultados numéricos, hay que destacar la precisión de la expresión analítica obtenida la cual nos permite computar la capacidad en todo el rango de valores de SNR. Al mismo tiempo, se puede observar que la capacidad en un sistema MISO FSO es proporcional al número de fuentes láseres usadas en el transmisor, no obteniendo una mejora apreciable cuando el número de fuentes láseres es superior a 4. A su vez, la capacidad en un sistema MISO FSO es disminuida como consecuencia directa de aumentar la severidad de los errores por desapuntamiento. Por último, hay que resaltar que la capacidad ergódica en un sistema



(a) Turbulencia moderada.



(b) Turbulencia fuerte.

Figure E.2: Capacidad ergódica para una distancia de enlace FSO de  $d_{SD} = 3$  km cuando se adoptan diferentes condiciones climáticas. También se asumen diferentes valores de ancho de haz normalizado y *jitter* normalizado de  $(\omega_z/a, \sigma_s/a) = (5, 1)$  y  $(\omega_z/a, \sigma_s/a) = (10, 2)$ .

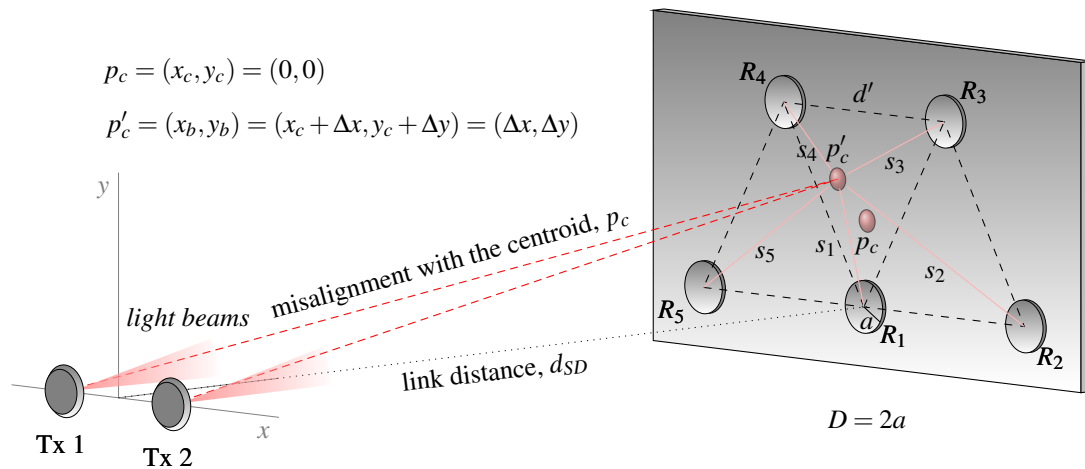


Figure E.3: Diagrama de bloques del sistema MIMO FSO bajo estudio.

MISO FSO es muy superior a la capacidad obtenida por un sistema SISO FSO con una única fuente láser.

### E.3.3 Capacidad Ergódica de Sistemas MIMO FSO

En esta sección se obtienen nuevas expresiones asintóticas en forma cerrada para la capacidad ergódica de un sistema MIMO FSO sobre canales atmosféricos modelados con distribución GG, y ante diferente severidad de errores por desapuntamiento lognormal-Rice, es decir, teniendo en cuenta el efecto de *nonzero boresight errors*.

#### Modelo de Sistema

Asumimos un sistema MIMO FSO con  $M$  transmisores y  $N$  aperturas receptoras tal como se muestra en la Fig. E.3, donde todas las fuentes láseres están alineadas con el centroide de la figura formada por las aperturas receptoras (trapezoido). El centroide es considerado el punto de alineación ( $p_c = (x_c, y_c) = (0, 0)$ ).

### Análisis de la Capacidad

Asumiendo CSI instantáneo en el receptor, la capacidad ergódica de un sistema MIMO FSO en bits/s/Hz puede ser escrita como

$$C_{\text{MIMO}/B} = \frac{1}{\ln(4)} \underbrace{\int_0^\infty \cdots \int_0^\infty}_{\text{MN-fold}} \ln \left( 1 + \frac{4\gamma}{M^2 N^2} \left( \sum_{k=1}^M \sum_{l=1}^N i_{kl} \right)^2 \right) \prod_{k=1}^M \prod_{l=1}^N f_{I_{kl}}(i_{kl}) di_{kl}, \quad (\text{E.3.8})$$

donde  $\gamma$  es la SNR en ausencia de turbulencia atmosférica, y  $f_{I_{kl}}(i_{kl})$  es la PDF combinada de turbulencia atmosférica y desapuntamiento con *nonzero boresight errors* entre la  $k$ -ésima fuente láser y la  $l$ -ésima apertura receptora. La división por  $M$  es debido al mismo razonamiento que en el caso de sistemas MISO FSO, y la división por  $N$  es para asegurar que el área de la apertura receptora de un sistema SISO FSO es equivalente a la suma de las  $N$  áreas de las aperturas receptoras en un sistema MIMO FSO.

Desafortunadamente, una expresión en forma cerrada para la PDF combinada de la suma de  $MN$  variables aleatorias que representan el efecto combinado de turbulencia atmosférica y desapuntamiento con *nonzero boresight errors* no es posible obtener. Por tanto, recurrimos al comportamiento asintótico para el cálculo de la capacidad ergódica en el caso de sistemas MIMO FSO. En este sentido, el comportamiento asintótico de la capacidad ergódica se obtiene aproximando  $\ln(1+z) \approx \ln(z)$  cuando  $z \rightarrow \infty$ , resultando

$$C_{\text{MIMO}/B} \doteq \frac{\ln(4\gamma_0)}{\ln(4)} + \frac{\ln(F)}{MN \ln(2)} + \frac{1}{MN \ln(2)} \sum_{k=1}^M \sum_{l=1}^N \underbrace{\int_0^\infty \ln(i_{kl}) f_{I_{kl}}(i_{kl}) di_{kl}}_{INT}. \quad (\text{E.3.9})$$

El factor de corrección  $F$  se obtiene de la misma forma que el factor de corrección para sistemas MISO FSO. Por tanto, el factor de corrección  $F$  para sistemas MIMO FSO se puede obtener a través de la siguiente expresión (véase Apéndice B.2)

$$F = \frac{\mathbb{E} \left[ \sum_{k=1}^M \sum_{l=1}^N I_{kl} \right]^{MN}}{(MN)^{MN} \cdot \mathbb{E} \left[ \sqrt[MN]{\prod_{k=1}^M \prod_{l=1}^N I_{kl}} \right]^{MN}}. \quad (\text{E.3.10})$$

Teniendo en cuenta que la turbulencia atmosférica y los errores por desapuntamiento son considerados estadísticamente independientes, la integral  $INT$  que aparece arriba puede ser

reescrita de una forma más sencilla como

$$\begin{aligned}
INT &= \int_0^\infty \ln(i_{kl}) f_{I_{kl}}(i_{kl}) di_{kl} \\
&= \int_0^\infty \int_0^{A_{0kl}} \ln(L_{kl} \cdot i_{kl}^a \cdot i_{kl}^p) f_{I_{kl}^a}(i_{kl}^a) f_{I_{kl}^p}(i_{kl}^p) di_{kl}^a di_{kl}^p \\
&= \ln(L_{kl}) + \underbrace{\int_0^\infty \ln(i_{kl}^a) f_{I_{kl}^a}(i_{kl}^a) di_{kl}^a}_{INT_1} + \underbrace{\int_0^{A_{0kl}} \ln(i_{kl}^p) f_{I_{kl}^p}(i_{kl}^p) di_{kl}^p}_{INT_2} \\
&= \ln(L_{kl}) + INT_1 + INT_2.
\end{aligned} \tag{E.3.11}$$

En primer lugar, obtenemos el resultado de la integral  $INT_2$  como (véase Apéndice A.10)

$$INT_2 = \int_0^{A_{0kl}} \ln(i_{kl}^p) f_{I_{kl}^p}(i_{kl}^p) di_{kl}^p = \ln(A_{0kl}) - \frac{1}{\varphi_{kl}^2} - \frac{s_{kl}^2}{2\sigma_{s_{kl}}^2 \varphi_{kl}^2}. \tag{E.3.12}$$

En segundo lugar, obtenemos el valor de la integral  $INT_1$  para turbulencia atmosférica GG la cual ya fue obtenida en Eq. (2.57), obteniendo la siguiente expresión en forma cerrada para el comportamiento asintótico de la capacidad ergódica de un sistema MIMO FSO

$$\begin{aligned}
C_{\text{MIMO}/B}^{\text{GG}} &\doteq \frac{\ln(4\gamma)}{\ln(4)} + \frac{\ln(F)}{MN \ln(2)} + \frac{1}{MN \ln(2)} \\
&\times \sum_{k=1}^M \sum_{l=1}^N \ln\left(\frac{L_{kl}}{\alpha_{kl}\beta_{kl}}\right) + \psi(\alpha_{kl}) + \psi(\beta_{kl}) + \ln(A_{0kl}) - \frac{1}{\varphi_{kl}^2} - \frac{s_{kl}^2}{2\sigma_{s_{kl}}^2 \varphi_{kl}^2}.
\end{aligned} \tag{E.3.13}$$

Se debe mencionar que este análisis también fue realizado para turbulencia atmosférica LN y EW (*Exponentiated Weibull*) con el objetivo de contemplar entornos de turbulencia débil y el efecto de *aperture averaging*, respectivamente. Más detalles sobre este análisis se pueden encontrar en el Capítulo 3.

## Resultados Numéricos

A continuación se muestran algunos resultados numéricos con el objetivo de evaluar la expresión matemática obtenida para la capacidad ergódica asintótica correspondiente a sistemas MIMO FSO. Para ello, se considera una distancia de enlace FSO de  $d_{SD} = 2$  km y un espaciado normalizado entre aperturas receptoras de  $d'/a = 6$  para turbulencia atmosférica GG. Además, se han incluido las correspondientes simulaciones de Monte Carlo con el objetivo de validar dicha expresión matemática.

Por un lado, podemos concluir que el sistema que mejores prestaciones obtiene en términos de capacidad es el sistema MISO FSO ya que el efecto de errores por desapuntamiento con *nonzero boresight error* puede ser despreciable al estar compuesto por un único receptor. Esto no ocurre en sistemas SIMO y MIMO FSO donde el efecto de *inherent nonzero boresight error* cobra mucha importancia como consecuencia directa de que cada láser solo puede estar

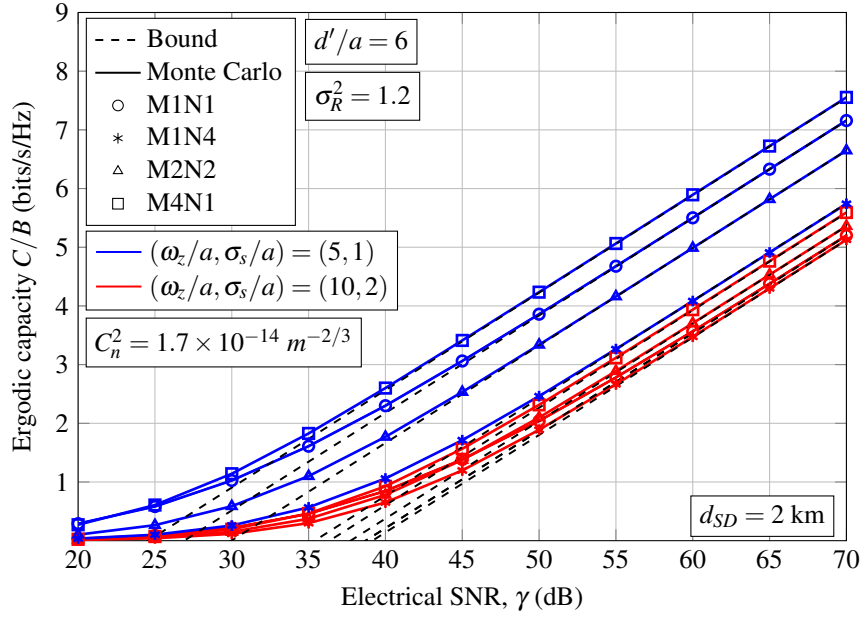


Figure E.4: Comportamiento asintótico de la capacidad ergódica de sistemas MIMO FSO para turbulencia atmosférica GG ante diferente severidad de errores por desapuntamiento.

perfectamente alineado con una única apertura receptora y, por tanto, el resto de aperturas receptoras presentan un *inherent nonzero boresight error* que no puede ser ignorado. Por otro lado, podemos también concluir que un sistema MISO FSO es una solución más interesante para aumentar la capacidad que los sistemas SIMO y MIMO FSO ya que las prestaciones de estos últimos dependen en mayor medida de la separación entre aperturas receptoras, la cual condiciona el aumento del efecto de *inherent nonzero boresight errors*.

### E.3.4 Capacidad Ergódica de Sistemas Cooperativos FSO

En esta sección se analiza la capacidad ergódica de un sistema cooperativo FSO formado por tres nodos donde la línea de visión directa entre el nodo fuente y el nodo destino se usa para aumentar la capacidad sobre canales con turbulencia atmosférica GG y teniendo en cuenta los errores por desapuntamiento Rayleigh, es decir, desapuntamiento con *zero boresight errors*.

### E.3.5 Comunicaciones Cooperativas

Tradicionalmente, las comunicaciones cooperativas fueron propuestas para conseguir diversidad espacial en el contexto de los sistemas de RF. Hoy en día, las comunicaciones cooperativas también son propuestas en el contexto de los sistemas FSO. En este sentido,

se presentan como una fuerte alternativa a los clásicos sistemas basados en diversidad espacial tales como MISO, SIMO y MIMO FSO con el objetivo de demostrar que existen otras vías para aumentar la capacidad en los sistemas de comunicaciones FSO cuando por razones de coste, tamaño o incluso hardware no es posible aumentar el número de fuentes láseres en transmisión y/o en recepción. Así pues, se propone usar otros nodos que puedan estar disponibles para su uso con el objetivo de crear un sistema MISO o MIMO virtual creando diferentes caminos ópticos para hacer llegar la información al nodo destino y aplicar algunos de los métodos de combinación existentes como por ejemplo EGC. En los últimos años, la comunidad científica ha demostrado un interés importante por las comunicaciones cooperativas en el contexto de los sistemas FSO concluyendo que esta propuesta es apta no solo para extender el área de cobertura y alcanzar mayores distancias, sino también como mecanismo para crear diversidad espacial y aumentar las prestaciones en términos de BER, probabilidad de *outage* y capacidad [88–93, 105–107, 114–120, 122–124].

**Amplify-and-forward (AF)** En AF, el nodo *relay* amplifica la señal recibida que proviene del nodo fuente y la reenvía hacia el nodo destino sin aplicar ningún tipo de detección y/o decodificación.

**Decode-and-forward (DF)** DF hace justo lo contrario que AF. El nodo *relay* previamente detecta y decodifica (en caso de ser necesario) la información recibida proveniente desde el nodo fuente y la reenvía con la nueva potencia hacia el nodo destino.

A pesar de que AF presenta una cierta ventaja desde el punto de vista de los requerimientos hardware necesarios con respecto a DF, DF obtiene mejores prestaciones que AF y, por este motivo, este método de retransmisión ha sido elegido para evaluar la capacidad de un sistema cooperativo formado por tres nodos [110].

## Modelo de Sistema

Asumimos un sistema cooperativo formado por tres nodos tal como se muestra en la Fig. E.5. Se va a analizar la capacidad ergódica para 2 protocolos de cooperación diferentes: BDF (*Bit Detect-and-Forward*) y ADF (*Adaptive Detect-and-Forward*).

## Protocolo Cooperativo BDF

El protocolo de cooperación BDF trabaja en dos etapas [114, 117]. En la primera etapa, el nodo fuente envía la misma información hacia el nodo *relay* y hacia el nodo destino. Al usar dos fuentes láseres, la potencia óptica promedio enviada al aire por cada fuente láser es  $P_t/2$ . En la segunda etapa, el nodo *relay* reenvía la información recibida en la etapa anterior por parte del nodo fuente hacia el nodo destino con la nueva potencia e independientemente de si la detección ha sido correcta o incorrecta. El nodo destino realiza la combinación de

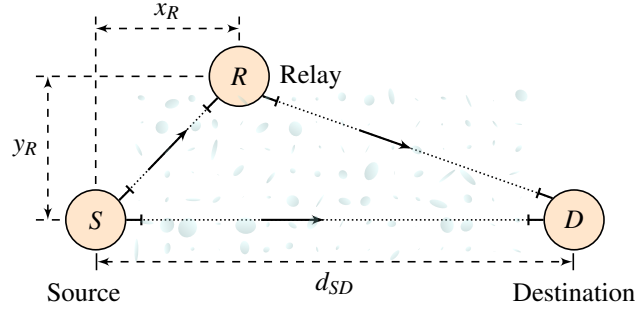


Figure E.5: Diagrama de bloques del sistema cooperativo FSO considerado en este estudio donde  $d_{SD}$  es la distancia fuente-destino (S-D), y  $(x_R, y_R)$  representa la ubicación del nodo *relay*.

ambas señales para realizar la detección, es decir, la combinación de la señal recibida por el enlace fuente-destino (S-D) y la señal recibida por el enlace *relay*-destino (R-D).

### Protocolo Cooperativo ADF

El protocolo de cooperación ADF es un protocolo selectivo que selecciona entre transmisión cooperativa vía protocolo cooperativo BDF o transmisión directa vía enlace S-D. La selección de una forma de transmisión u otra se hace en base al conocimiento del CSI del enlace R-D y del enlace S-D. Cuando la irradiancia del enlace S-D ( $I_{SD}$ ) es mayor que la irradiancia del enlace R-D ( $I_{RD}$ ) se realiza transmisión directa. En caso contrario se realiza transmisión cooperativa usando el protocolo cooperativo BDF.

### Análisis de la Capacidad

En primer lugar, obtenemos la expresión de la capacidad ergódica correspondiente al protocolo cooperativo BDF. En este sentido, la capacidad correspondiente a dicho protocolo cooperativo se puede calcular asumiendo CSI en el receptor como

$$C_{\text{BDF}} = C_0 \cdot (1 - P_b^{SR}) + C_1 \cdot P_b^{SR} = C_0 - (C_0 - C_1) \cdot P_b^{SR}, \quad (\text{E.3.14})$$

donde  $P_b^{SR}$  es la BER del enlace S-R, y  $C_0$  y  $C_1$  son las capacidades ergódicas cuando la detección en el nodo *relay* es correcta e incorrecta, respectivamente. La expresión de arriba se puede aproximar por

$$C_{\text{BDF}} \approx C_0 = \frac{B}{2 \ln(2)} \int_0^\infty \int_0^\infty \ln \left( 1 + \frac{\gamma}{2} (i_1 + 2i_2)^2 \right) f_{I_{SD}}(i_1) f_{I_{RD}}(i_2) di_1 di_2, \quad (\text{E.3.15})$$

donde  $f_{I_m}(i)$  es la PDF combinada de turbulencia atmosférica y desapuntamiento Rayleigh dada en Eq. (2.34). Sabiendo que la BER correspondiente al enlace S-R tiende a cero



conforme la SNR tiene a infinito, podemos aproximar la expresión de arriba por

$$C_{\text{BDF}}/B \approx \frac{1}{\ln(4)} \int_0^\infty \ln\left(1 + \frac{\gamma}{2}i^2\right) f_{I_T}(i) di, \quad (\text{E.3.16})$$

donde  $I_T = I_{SD} + 2I_{RD}$ . Teniendo en cuenta la relación entre la *AM* y *GM* dada por

$$I_{SD} + 2I_{RD} \geq \sqrt{8 \cdot I_{SD} \cdot I_{RD}} = \sqrt{8 \cdot I_T^{LB}}, \quad (\text{E.3.17})$$

la capacidad ergódica correspondiente al protocolo cooperativo BDF puede ser aproximada aún más como

$$C_{\text{BDF}}/B \approx \frac{1}{\ln(4)} \int_0^\infty \ln(1 + 4\gamma Fi) f_{I_T^{LB}}(i) di. \quad (\text{E.3.18})$$

La PDF de  $f_{I_T^{LB}}(i)$  se puede obtener vía transformada de Mellin (véase Apéndice A.7). Al igual que en sistemas MISO y MIMO FSO, el factor de corrección  $F$  se añade para obtener una mejor aproximación, y su correspondiente expresión se puede ver en Apéndice B.3. La integral que aparece en Eq. (3.57) se puede resolver con la ayuda de [59, eqn. (8.4.6.5)] con el fin de expresar la función logaritmo neperiano en términos de una función Meijer's G (véase Apéndice A.3.1) y, usando [59, eqn. (2.24.1.2)] (véase Apéndice A.3.2), podemos obtener la siguiente expresión aproximada en forma cerrada para evaluar la capacidad ergódica del protocolo cooperativo BDF en todo el rango de valores de SNR como

$$C_{\text{BDF}}/B \approx \frac{\varphi_{SD}^2 \varphi_{RD}^2 G_{4,8}^{8,1} \left( \frac{\alpha_{SD} \beta_{SD} \alpha_{RD} \beta_{RD}}{\gamma^4 F A_{SD} A_{RD} L_{SD} A_{RD} L_{RD}} \middle| \begin{matrix} 0, 1, \varphi_{SD}^2 + 1, \varphi_{RD}^2 + 1 \\ \varphi_{SD}^2, \alpha_{SD}, \beta_{SD}, \varphi_{RD}^2, \alpha_{RD}, \beta_{RD}, 0, 0 \end{matrix} \right)}{\ln(4) \Gamma(\alpha_{SD}) \Gamma(\beta_{SD}) \Gamma(\alpha_{RD}) \Gamma(\beta_{RD})}. \quad (\text{E.3.19})$$

En segundo lugar, analizamos la capacidad ergódica correspondiente al protocolo cooperativo ADF cuya expresión en forma integral viene dada por

$$C_{\text{ADF}}/B \approx \frac{1}{\ln(4)} \int_0^\infty \int_0^{i_2} \ln(1 + 4\gamma F' i_1 i_2) f_{I_{SD}}(i_1) f_{I_{RD}}(i_2) di_1 di_2 + \frac{1}{\ln(4)} \int_0^\infty \ln(1 + 4\gamma i^2) F_{I_{RD}}(i) f_{I_{SD}}(i) di = C'_{\text{BDF}} + C_{\text{DT}}, \quad (\text{E.3.20})$$

Debido a la imposibilidad de obtener una expresión matemática en forma cerrada para la integral anterior, recurrimos a realizar un análisis asintótico. En este caso, el comportamiento asintótico de la capacidad correspondiente al protocolo cooperativo ADF a alta SNR viene

dado por

$$\begin{aligned}
& C_{ADF}^H/B \\
& \doteq \underbrace{\frac{\ln(4\gamma F')}{\ln(4)} \int_0^\infty F_{ISD}(i) f_{IRD}(i) di + \frac{1}{\ln(4)} \int_0^\infty \int_0^{i_2} \ln(i_1 i_2) f_{ISD}(i_1) f_{IRD}(i_2) di_1 di_2}_{C_{BDF}^{H'}} \\
& + \underbrace{\frac{\ln(4\gamma)}{\ln(4)} \int_0^\infty F_{IRD}(i) f_{ISD}(i) di + \frac{2}{\ln(4)} \int_0^\infty \ln(i) F_{IRD}(i) f_{ISD}(i) di}_{C_{DT}^H} = C_{BDF}^{H'} + C_{DT}^H.
\end{aligned} \tag{E.3.21}$$

El resultado final se puede ver en mayor detalle en el Capítulo 3.

## Resultados Numéricos

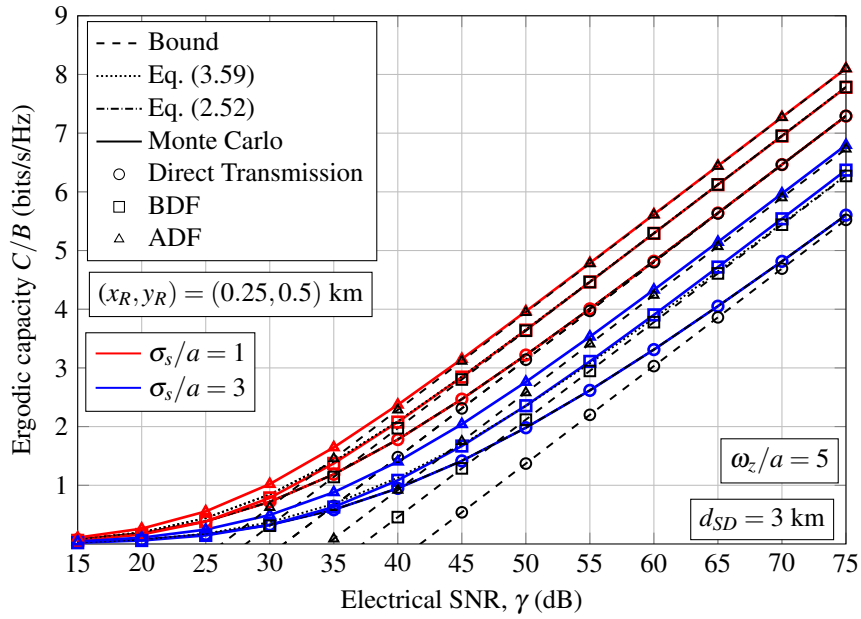
A continuación se muestran algunos resultados numéricos con el objetivo de evaluar las expresiones obtenidas para los diferentes protocolos cooperativos analizados. En la Fig. 3.13, se muestran resultados numéricos para diferentes posiciones del nodo *relay* cuando la distancia S-D es fijada a 3 km. Al mismo tiempo, se adoptan diferentes condiciones climáticas para diferenciar entre turbulencia moderada y fuerte según los valores mostrados en la Tabla E.1. También, las expresiones obtenidas se evalúan ante diferente severidad de errores por desapuntamiento usando valores de ancho de haz y *jitter* normalizado de  $(\omega_z/a, \sigma_s/a) = (5, 1)$  y  $(\omega_z/a, \sigma_s/a) = (5, 3)$ .

Por un lado, se puede observar cómo ambos protocolos cooperativos son capaces de obtener una mayor capacidad que una transmisión directa o sistema SISO FSO cuando no existe cooperación. Por otro lado, se puede apreciar cómo el protocolo ADF, el cual está basado en la selección de camino óptico con mayor valor de irradiancia, es capaz de mejorar aún más las prestaciones obtenidas por el protocolo cooperativo BDF. En este sentido, podemos afirmar que las técnicas basadas en selección son de gran utilidad para aumentar la capacidad.

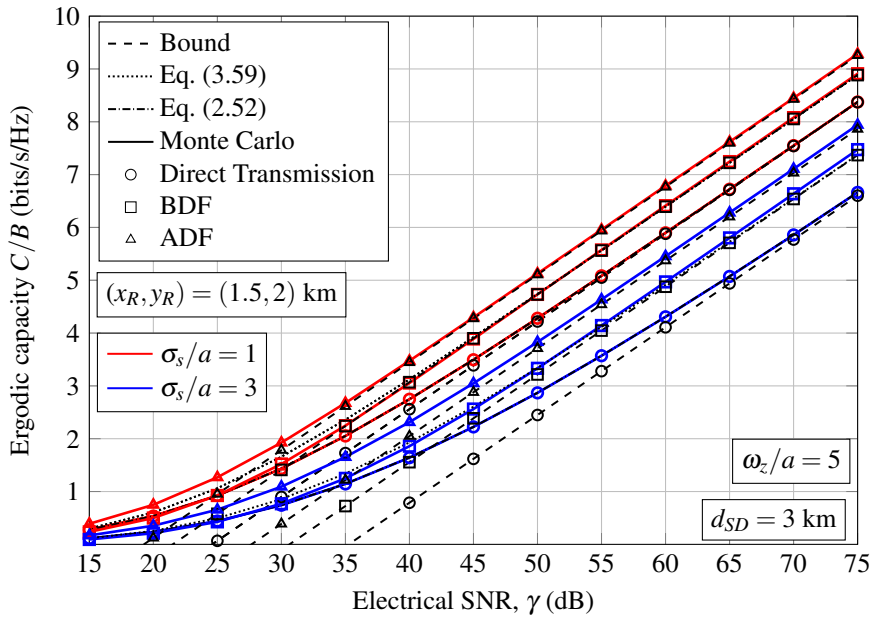
## E.4 Modelado de Errores por Desapuntamiento Generalizado

### E.4.1 Motivación

En esta sección, se propone un modelo para estudiar errores por desapuntamiento generalizado. A continuación se comentan brevemente cada uno de los modelos estadísticos propuestos en la literatura en la última década.



(a) Turbulencia moderada.



(b) Turbulencia fuerte.

Figure E.6: Capacidad ergódica para una distancia S-D de  $d_{SD} = 3$  km, y ante diferente severidad de errores por desapuntamiento usando valores de ancho de haz y jitter normalizado de  $(\omega_z/a, \sigma_s/a) = (5, 1)$  y  $(\omega_z/a, \sigma_s/a) = (5, 3)$ .

**Desapuntamiento Rayleigh** Este modelo es considerado la piedra angular entre los diferentes modelos existentes en la literatura [53], el cual ha sido usado y continúa usándose en un elevado número de artículos de investigación. En dicho modelo, el desplazamiento radial en el receptor  $r = \sqrt{x^2 + y^2}$ , es decir, la desviación con respecto al punto de alineamiento entre transmisor y receptor sigue una distribución Rayleigh. Dicho desplazamiento es modelado como la raíz cuadrada de la suma de dos variables aleatorias normales Gaussianas e independientes de media zero y misma varianza. El eje  $x$  representa el desplazamiento horizontal, y el eje  $y$  la elevación. En este modelo se asume que no hay errores por puntería de partida (*zero boresight error*) ya que la media tanto de  $x$  como de  $y$  es cero y, además, ambas variables aleatorias tienen la misma varianza de *jitter* ( $\sigma_s$ ). Este modelo fue usado en dicho artículo para el cálculo de la probabilidad de *outage* presentando nuevas expresiones en forma cerrada para la PDF combinada de turbulencia atmosférica LN y GG.

**Desapuntamiento Hoyt** Este modelo está basado en el modelo anterior y fue presentado en [132]. Dicho modelo incorpora un mayor grado de realismo al modelado de errores por desapuntamiento donde las varianzas de *jitter* de ambos ejes pueden tomar valores diferentes. Este supuesto es más realista que el anterior ya que la componente horizontal y la componente vertical no tienen por qué variar de la misma forma en un escenario real. Por tanto, el desplazamiento radial en el receptor sigue una distribución Hoyt. Este modelo fue usado en dicho artículo para el cálculo de la probabilidad de *outage* sobre turbulencia GG donde los resultados obtenidos son solamente válidos cuando la turbulencia atmosférica es el efecto dominante, es decir, cuando el orden de diversidad del sistema solo depende de la turbulencia y no del desapuntamiento entre transmisor y receptor. Además, no pudo ser determinado de forma analítica cuando las expresiones proporcionadas dejan de ser válidas, solamente mediante observación numérica.

**Desapuntamiento lognormal-Rice** Este modelo también está basado en [53], pero con la diferencia de que este contempla posibles errores por puntería de partida entre transmisor y receptor (*nonzero boresight error*) [56]. En este caso, el desplazamiento radial en el receptor sigue una distribución lognormal-Rice. Este modelo fue usado en dicho artículo para analizar las prestaciones en términos de BER y probabilidad de *outage* sobre turbulencia atmosférica LN y GG. Al igual que en el caso de desapuntamiento Hoyt, debido a la dificultad que representa obtener una expresión en forma cerrada para la PDF combinada de turbulencia atmosférica y desapuntamiento, las expresiones obtenidas en este caso solamente son válidas cuando la turbulencia atmosférica es el efecto dominante y, por tanto, no sabiendo cuando las expresiones analíticas obtenidas dejan de ser válidas.

**Desapuntamiento Beckmann** Este modelo, tal como se comentó en la introducción, representa el caso general y fue usado por primera vez en [133] para el cálculo de la capacidad ergódica asintótica, no proporcionando ninguna expresión en forma cerrada para

la PDF combinada de turbulencia atmosférica y de errores por desapuntamiento Beckmann. En dicho modelo, tanto el desplazamiento radial como la elevación presentan diferentes medias (*nonzero boresight error*) y diferentes varianzas de *jitter*.

En esta tesis, nos centramos en el estudio de este último modelo desarrollando una aproximación para el desplazamiento radial modelado con distribución Beckmann con el objetivo de obtener expresiones matemáticas en forma cerrada para la PDF combinada y ser capaces de evaluar las prestaciones de un sistema FSO en términos de BER y probabilidad de *outage*. Más importante, las expresiones que se obtienen en este sentido son válidas no solo cuando la turbulencia atmosférica es el efecto dominante, sino también cuando no lo es, es decir, cuando lo son los errores por desapuntamiento Beckmann. Además, detectar cuándo un efecto u otro dejar de ser dominante en el cómputo de las prestaciones. Finalmente, el efecto de ejes correlados también se tiene en cuenta.

#### E.4.2 Aproximación para Modelar Desapuntamiento Generalizado

En este apartado abordamos el problema que existe en la literatura a la hora de modelar errores por desapuntamiento generalizado, es decir, desapuntamiento Beckmann. La distribución Beckmann es una distribución estadística que presenta ciertos impedimentos desde el punto de vista práctico ya que no presenta un tratamiento matemático sencillo y, en ocasiones, es incluso imposible. Muchos autores han obtenido expresiones en forma cerrada para medir las prestaciones de los sistemas FSO que son solamente válidas cuando la turbulencia atmosférica es el efecto dominante. Esto quiere decir que el orden de diversidad del sistema tanto en BER como en probabilidad de *outage* depende única y exclusivamente de la turbulencia atmosférica y no de los errores por desapuntamiento. El efecto de los errores por desapuntamiento queda reducido a una disminución de la ganancia de codificación. Hay que destacar que este es el escenario que se busca en la práctica, es decir, un escenario donde la turbulencia atmosférica sea el efecto dominante ya que se pueden obtener mejores prestaciones. También hay que decir que es conveniente saber cuándo la turbulencia deja de ser dominante y bajo qué condiciones ocurre este cambio de efecto dominante. Este problema no está resuelto en la literatura, siendo su única solución la evaluación numérica con el fin de saber qué efecto es el dominante a alta SNR.

Una vez conocida la problemática, el objetivo principal es obtener una aproximación de la PDF combinada de turbulencia atmosférica y errores por desapuntamiento Beckmann. El siguiente objetivo es ser capaz de obtener el comportamiento asintótico de dicha PDF combinada. Una vez realizado el comportamiento asintótico, ya estaremos en condiciones de obtener el orden de diversidad del sistema y, por tanto, saber qué efecto es el dominante. Para ello, nos fijamos en el modelo de desapuntamiento Rayleigh y turbulencia atmosférica GG que sí permite obtener su comportamiento asintótico, y que fue analizado en el Capítulo 2. Utilizando este modelo de desapuntamiento, el orden de diversidad del

sistema viene determinado por  $G_d = \min(\alpha, \beta, \varphi^2)$  para el caso de turbulencia atmosférica GG. Esta sencilla expresión nos dice que el orden de diversidad del sistema será dependiente única y exclusivamente de la turbulencia atmosférica cuando  $\min(\alpha, \beta) < \varphi^2$ . Esto se puede hacer gracias a que la PDF del desplazamiento radial en el receptor sigue una distribución Rayleigh. Pero cuando el desplazamiento radial sigue una distribución Beckmann, el comportamiento asintótico no se puede realizar debido a la dificultad matemática que presenta esta PDF. En este sentido, nosotros proponemos aproximar el desplazamiento radial en el receptor por una distribución Rayleigh modificada de parámetro  $\sigma_{\text{mod}}$ . Se puede comprobar que cuando una variable aleatoria sigue una distribución Rayleigh, dicha variable aleatoria al cuadrado sigue una distribución exponencial. Si definimos  $u = r^2$ , podemos expresar la PDF de  $u$  como

$$f_{r^2}(u) = \frac{1}{2\sigma_{\text{mod}}^2} \exp\left(-\frac{u}{2\sigma_{\text{mod}}^2}\right), \quad u \geq 0. \quad (\text{E.4.1})$$

El parámetro  $\sigma_{\text{mod}}$  se usa para estimar el orden de diversidad del sistema cuando el desapuntamiento Beckmann es el efecto dominante. El citado parámetro se obtiene mediante la igualación del momento central de orden 3 de la variable aleatoria  $r^2$  cuando  $r$  sigue una distribución Beckmann al cuadrado, y cuando  $r$  sigue una distribución Rayleigh al cuadrado (distribución exponencial). El resultado que se obtiene al hacer dicha igualación viene dado por

$$\sigma_{\text{mod}}^2 = \left( \frac{3\mu_x^2\sigma_x^4 + 3\mu_y^2\sigma_y^4 + \sigma_x^6 + \sigma_y^6}{2} \right)^{1/3}. \quad (\text{E.4.2})$$

De una forma similar a [53], podemos obtener la PDF correspondiente al desapuntamiento Beckmann el cual es tratado como si fuese un desapuntamiento Rayleigh. Dicha PDF viene dada por

$$f_{I_p}(i) \approx \frac{\varphi_{\text{mod}}^2}{(A_0G)\varphi_{\text{mod}}^2} i^{\varphi_{\text{mod}}^2 - 1}, \quad 0 \leq i \leq A_0G \quad (\text{E.4.3})$$

donde  $\varphi_{\text{mod}} = \omega_{z_{\text{eq}}}/2\sigma_{\text{mod}}$ . Se añade el parámetro  $G$  para compensar la media de ambas variables aleatorias cuya expresión viene dada por

$$G = \exp\left( \frac{1}{\varphi_{\text{mod}}^2} - \frac{1}{2\varphi_x^2} - \frac{1}{2\varphi_y^2} - \frac{\mu_x^2}{2\sigma_x^2\varphi_x^2} - \frac{\mu_y^2}{2\sigma_y^2\varphi_y^2} \right). \quad (\text{E.4.4})$$

donde  $A_{\text{mod}} = A_0G$ .

### E.4.3 Impacto de Ejes Correlados

Un paso más hacia el modelo de errores por desapuntamiento generalizado es considerar que ambos ejes, es decir, tanto el eje horizontal como el eje vertical están correlados y no son variables aleatorias independientes. Es de esperar que ambas variables aleatorias estén correladas y no varíen de forman incorrelada. En este caso, los parámetros relacionados con

Table E.2: Expresiones para desapuntamiento con ejes correlados.

Parámetro	Símbolo	Expresión
Media horizontal	$\mu'_x$	$\mu_x \cos \phi_0 + \mu_y \sin \phi_0$
Media vertical	$\mu'_y$	$\mu_y \cos \phi_0 - \mu_x \sin \phi_0$
Varianza horizontal	$\sigma'^2_x$	$\sigma_x^2 \cos^2 \phi_0 + \sigma_y^2 \sin^2 \phi_0 + 2\rho\sigma_x\sigma_y \sin \phi_0 \cos \phi_0$
Varianza vertical	$\sigma'^2_y$	$\sigma_y^2 \cos^2 \phi_0 + \sigma_x^2 \sin^2 \phi_0 - 2\rho\sigma_x\sigma_y \sin \phi_0 \cos \phi_0$

el desapuntamiento Beckmann son modificados con el objetivo de considerar una correlación lineal de parámetro  $\rho$  entre el desplazamiento horizontal y la elevación en el receptor.

Para ello, definimos dos nuevas variables aleatorias Gaussianas  $x'$  e  $y'$  las cuales son estadísticamente independientes. En este caso, el desplazamiento radial en el receptor puede seguir siendo expresado como  $r^2 = x'^2 + y'^2 = x^2 + y^2$ . En la Tabla E.2 podemos ver un resumen de cómo los parámetros estadísticos correspondientes a  $x'$  y a  $y'$  son modificados para incluir el efecto de la correlación entre ejes y expresarlos en función de los parámetros estadísticos de  $x$  e  $y$ .

El efecto de la correlación produce un cambio de PDF cuando el coeficiente de correlación toma valores diferentes de cero fundamentalmente en aquellos modelos que de partida asumen misma varianza de *jitter* para ambos ejes, es decir, desapuntamiento Rayleigh y lognormal-Rice. En el caso de desapuntamiento Rayleigh, dicho modelo estadístico evoluciona hacia el modelo de desapuntamiento Hoyt cuando el coeficiente de correlación toma valores distintos de cero. Lo mismo ocurre cuando se asume un modelo de desapuntamiento lognormal-Rice, este evoluciona hacia el modelo más general, es decir, el modelo de desapuntamiento Beckmann. Este efecto no ocurre en el caso de desapuntamiento Hoyt y Beckmann porque asumen de partida diferentes varianzas de *jitter* en ambos ejes. El cambio de PDF ocurre en aquellos modelos que asumen de partida la misma varianza de *jitter* para ambos ejes.

### Análisis de Prestaciones: BER y Probabilidad de *outage*

Antes de analizar las prestaciones tenemos que calcular la PDF combinada de turbulencia atmosférica GG y de desapuntamiento Beckmann utilizando la aproximación propuesta. Realmente, las expresiones ya fueron obtenidas en el Capítulo 2, y son usadas aquí utilizando los nuevos parámetros:  $\varphi_{\text{mod}}^2$  y  $A_{\text{mod}}$ . En este sentido, la PDF combinada viene dada por

$$f_I(i) \approx \frac{\alpha\beta\varphi_{\text{mod}}^2 i^{-1}}{A_{\text{mod}}L\Gamma(\alpha)\Gamma(\beta)} G_{1,3}^{3,0} \left( \frac{\alpha\beta}{A_{\text{mod}}L} i \left| \begin{array}{c} \varphi_{\text{mod}}^2 + 1 \\ \varphi_{\text{mod}}^2, \alpha, \beta \end{array} \right. \right), \quad i \geq 0. \quad (\text{E.4.5})$$

Y la CDF viene dada por

$$F_I(i) \approx \frac{\varphi_{\text{mod}}^2}{\Gamma(\alpha)\Gamma(\beta)} G_{2,4}^{3,1} \left( \frac{\alpha\beta}{A_{\text{mod}}L} i \left| \begin{array}{c} 1, \varphi_{\text{mod}}^2 + 1 \\ \varphi_{\text{mod}}^2, \alpha, \beta, 0 \end{array} \right. \right). \quad i \geq 0. \quad (\text{E.4.6})$$

Con estas expresiones podemos obtener el correspondiente comportamiento asintótico como

$$f_I(i) \approx a_M i^{b_M-1} = \begin{cases} \frac{\varphi_{\text{mod}}^2 (\alpha\beta)^\beta \Gamma(\alpha-\beta)}{(A_{\text{mod}}L)^\beta \Gamma(\alpha)\Gamma(\beta) (\varphi_{\text{mod}}^2 - \beta)} i^{\beta-1}, & \varphi_{\text{mod}}^2 > \beta \\ \frac{\varphi_{\text{mod}}^2 (\alpha\beta) \varphi_{\text{mod}}^2 \Gamma(\alpha - \varphi_{\text{mod}}^2) \Gamma(\beta - \varphi_{\text{mod}}^2)}{(A_{\text{mod}}L)^{\varphi_{\text{mod}}^2} \Gamma(\alpha)\Gamma(\beta)} i^{\varphi_{\text{mod}}^2-1}. & \varphi_{\text{mod}}^2 < \beta \end{cases} \quad (\text{E.4.7})$$

La probabilidad de *outage* viene dada por

$$\begin{aligned} P_{\text{out}} &= P(4\gamma i^2 \leq \gamma_{\text{th}}) = \int_0^{\sqrt{\gamma_{\text{th}}/4\gamma}} f_I(i) di = F_I \left( \sqrt{\frac{\gamma_{\text{th}}}{4\gamma}} \right) \\ &= \frac{\varphi_{\text{mod}}^2}{\Gamma(\alpha)\Gamma(\beta)} G_{2,4}^{3,1} \left( \frac{\alpha\beta}{A_{\text{mod}}L} \sqrt{\frac{\gamma_{\text{th}}}{4\gamma}} \left| \begin{array}{c} 1, \varphi_{\text{mod}}^2 + 1 \\ \varphi_{\text{mod}}^2, \alpha, \beta, 0 \end{array} \right. \right). \end{aligned} \quad (\text{E.4.8})$$

Y el comportamiento asintótico de la BER viene dado por

$$P_b \doteq \frac{a_M \Gamma((b_M + 1)/2)}{2b_M \sqrt{\pi}} \gamma^{-b_M/2}. \quad (\text{E.4.9})$$

Se puede apreciar cómo el orden de diversidad del sistema tanto en BER como en *outage* viene determinado por  $\beta < \varphi_{\text{mod}}^2$  (asumiendo propagación de onda plana) donde  $\varphi_{\text{mod}}^2$  contiene información de todas las variables involucradas en el desapuntamiento Beckmann tales como  $\mu_x$ ,  $\mu_y$ ,  $\sigma_x$  y  $\sigma_y$ .

#### E.4.4 Resultados Numéricos

A continuación se muestran algunos resultados numéricos para la probabilidad de *outage* cuando se tiene o no en cuenta la correlación entre ejes sobre canales con turbulencia atmosférica GG. Diferentes valores de errores por desapuntamiento se han considerado con el fin de evaluar las expresiones obtenidas ante escenarios FSO más extremos desde el punto de vista de los errores por desapuntamiento tal como se muestra en la Tabla E.3.

Por un lado, puede ser concluido que esta herramienta es muy útil para detectar no solo qué efecto es el dominante, sino también para optimizar ciertos parámetros como el ancho de haz con el fin de asegurar el escenario en el cual la turbulencia atmosférica es dominante. En este sentido, la expresión del mínimo ancho de haz que asegura que la turbulencia atmosférica es el efecto dominante ( $\beta < \varphi_{\text{mod}}^2$ ) viene dada por

$$\omega_{z_{\text{min}}}/a \approx 2^{-3/4} \left( 2^{1/6} 8\beta (3\mu_x^2 \sigma_x^4 + 3\mu_y^2 \sigma_y^4 + \sigma_x^6 + \sigma_y^6)^{1/3} - 3 \right)^{1/2}. \quad (\text{E.4.10})$$

Por otro lado, podemos concluir también que el efecto de la correlación no puede ser ignorado en enlaces terrestres FSO ya que presenta un impacto importante no solo en el orden de diversidad, sino también en la ganancia de codificación.



Table E.3: Configuración del sistema FSO.

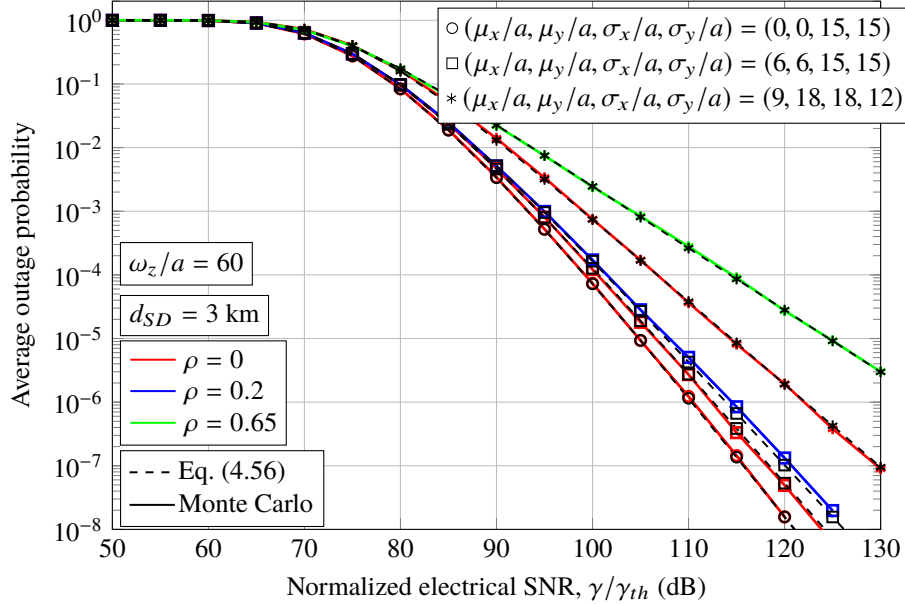
Parámetro	Símbolo	Valor
Distancia de enlace FSO	$d_{SD}$	3 km
Longitud de onda	$\lambda$	1550 nm
Diámetro de apertura receptora	$D = 2a$	10 cm
Divergencia en transmisión	$\theta_z$	1 mrad
Ancho de haz normalizado	$\omega_z/a$	$\simeq 60$
Máximo ángulo de <i>jitter</i>	$(\theta_{sx}, \theta_{sy})$	0.4 mrad
Máximo <i>jitter</i> normalizado	$(\sigma_x/a, \sigma_y/a)$	$\simeq 24$
Máximo ángulo de <i>boresight</i>	$(\theta_{bx}, \theta_{by})$	0.3 mrad
Máximo <i>boresight</i> normalizado	$(\mu_x/a, \mu_y/a)$	$\simeq 18$

## E.5 Conclusiones y Líneas Futuras

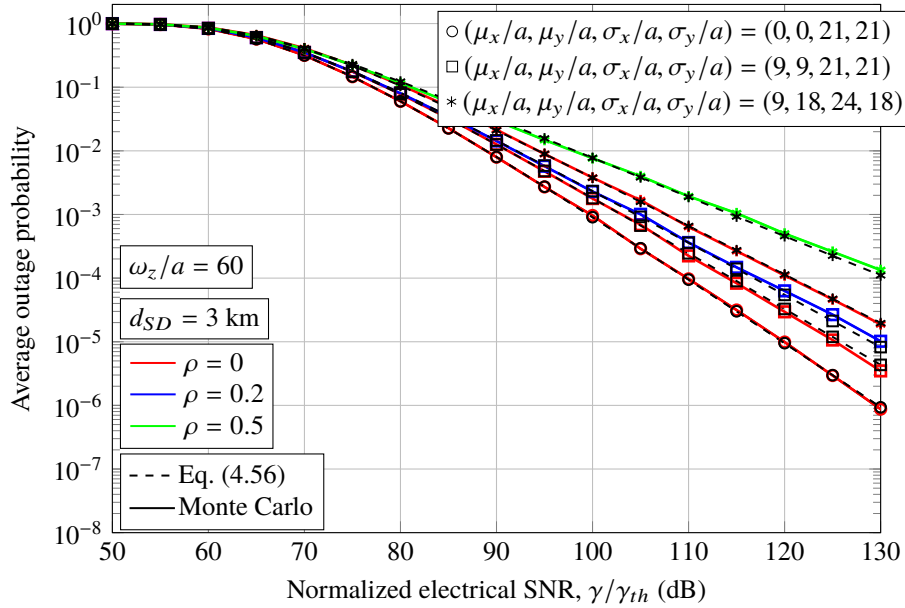
### E.5.1 Conclusiones

En esta tesis, el análisis de las prestaciones de los sistemas de comunicaciones ópticas atmosféricas o sistemas FSO ha sido abordado, presentando nuevos resultados para la comunidad científica e investigadora. Dicho análisis de prestaciones se ha dividido en dos grandes áreas de investigación: por un lado, el análisis de la capacidad ergódica de sistemas FSO avanzados basados en diversidad espacial como los sistemas MISO, SIMO y MIMO FSO, y de sistemas cooperativos basados en retransmisión DF como una solución interesante para aumentar la capacidad; por otro lado, el modelado de errores por desapuntamiento generalizado, donde no solo se tiene en cuenta el efecto de diferentes varianzas de *jitter* y *nonzero boresight errors*, sino también el efecto de ejes correlados. Estas dos grandes áreas de investigación han sido estudiadas principalmente sobre canales atmosféricos modelados con una distribución GG, asumiendo IM/DD y modulación OOK cuando la probabilidad de error de bit es estudiada.

Dentro del análisis de la capacidad ergódica se han obtenido nuevas expresiones matemáticas en forma cerrada que permiten computar la capacidad en todo el rango de valores de SNR en algunos casos como sistemas MISO y cooperativos FSO y, en el caso de sistemas MIMO FSO, solo ha sido posible obtener su comportamiento asintótico debido a la dificultad matemática que presentaba el análisis. A la luz de los resultados obtenidos, podemos concluir que los sistemas MISO FSO son probablemente la solución más interesante en comparación a los sistemas SIMO y MIMO FSO ya que el efecto de *nonzero boresight errors* es mucho



(a) Turbulencia moderada.



(b) Turbulencia fuerte.

Figure E.7: Probabilidad de *outage* sobre canales con turbulencia atmosférica GG para una distancia de enlace 3 km en dos escenarios diferentes: (a) turbulencia moderada  $C_n^2 = 2 \times 10^{-14} \text{ m}^{-2/3}$ , y (b) turbulencia fuerte  $C_n^2 = 8 \times 10^{-14} \text{ m}^{-2/3}$ .

menor en sistemas de una única apertura receptora. Esto último es debido a que una fuente láser solo puede estar alineada con una única apertura receptora. Sistemas MISO FSO son capaces de obtener mejores prestaciones, al menos en términos de capacidad, en comparación con sistemas con diversidad en recepción como los sistemas SIMO y MIMO FSO. Al mismo tiempo, los resultados obtenidos en comunicaciones cooperativas permiten concluir que los sistemas cooperativos basados en retransmisión DF son capaces de aumentar la capacidad e incluso mejorar a la capacidad obtenida por un sistema basado en diversidad espacial para determinadas posiciones del nodo *relay*.

Por último, el modelado de errores por desapuntamiento generalizado también ha dado lugar a diferentes aportaciones. Este análisis ha demostrado que para incluir el efecto de errores por desapuntamiento a cualquier sistema FSO se requiere de un modelo preciso y, a la vez, sencillo desde el punto de vista matemático con el fin de analizar las prestaciones de los sistemas FSO y poder obtener nuevas expresiones matemáticas en forma cerrada. La herramienta propuesta en esta tesis es válida para analizar cualquier sistema FSO y nos permite detectar qué efecto es dominante, es decir, si la turbulencia atmosférica o los errores por desapuntamiento. El efecto de la correlación también ha sido contemplado concluyendo que no puede ser ignorado. Las expresiones obtenidas cuando no existe correlación siguen siendo válidas cuando sí existe correlación pero utilizando los parámetros adecuados.

### E.5.2 Líneas Futuras

A continuación se muestran algunas líneas futuras de investigación dentro del ámbito de los sistemas FSO las cuales han sido derivadas de las investigaciones realizadas en esta tesis.

- Estudiar el efecto de CSI imperfecto a la hora de realizar la selección de camino óptico con mayor valor de irradiancia, así como contemplar errores de sincronización en el receptor dentro del estudio de la capacidad ergódica de sistemas cooperativos basados en retransmisión DF.
- Aplicar técnicas de codificación espacio-tiempo distribuidas (DSTC, *Distributed Space-Time Coding*) a sistemas cooperativos basados en retransmisión DF con el objetivo de conseguir unas prestaciones más robustas frente a la posición del nodo *relay*.
- Análisis de las prestaciones en términos de BER, probabilidad de *outage* y capacidad ergódica de sistemas MIMO FSO afectados por errores por desapuntamiento Beckmann.
- Análisis de las prestaciones en términos de BER, probabilidad de *outage* y capacidad ergódica de sistemas UOC con el objetivo de aplicar el conocimiento adquirido sobre el modelado de canal óptico atmosférico a canales ópticos subacuáticos.



UNIVERSIDAD  
DE MÁLAGA

# References

- [1] V. W. S. Chan, “Free-space optical communications,” *J. Lightwave Technol., IEEE/OSA*, vol. 24, no. 12, pp. 4750–4762, 2006.
- [2] M. A. Khalighi and M. Uysal, “Survey on free space optical communication: A communication theory perspective,” *Communications Surveys and Tutorials, IEEE*, vol. 16, no. 4, pp. 2231–2258, 2014.
- [3] R. Baldemair, E. Dahlman, G. Fodor, G. Mildh, S. Parkvall, Y. Selén, H. Tullberg, and K. Balachandran, “Evolving wireless communications: Addressing the challenges and expectations of the future,” *Vehicular Technology Magazine, IEEE*, vol. 8, no. 1, pp. 24–30, 2013.
- [4] Z. Ghassemlooy, S. Arnon, M. Uysal, Z. Xu, and J. Cheng, “Emerging optical wireless communications—advances and challenges,” *Journal on Selected Areas in Communications, IEEE*, vol. 33, no. 9, pp. 1738–1749, 2015.
- [5] Z. Pi, J. Choi, and R. Heath, “Millimeter-wave gigabit broadband evolution toward 5G: fixed access and backhaul,” *Communications Magazine, IEEE*, vol. 54, no. 4, pp. 138–144, 2016.
- [6] U. Siddique, H. Tabassum, E. Hossain, and D. I. Kim, “Wireless backhauling of 5G small cells: Challenges and solution approaches,” *Wireless Communications, IEEE*, vol. 22, no. 5, pp. 22–31, 2015.
- [7] C. Park and T. S. Rappaport, “Short-range wireless communications for next-generation networks: UWB, 60 GHz millimeter-wave WPAN, and zigbee,” *Wireless Communications, IEEE*, vol. 14, no. 4, 2007.
- [8] J. Zhang, J. Wang, Y. Xu, M. Xu, F. Lu, L. Cheng, J. Yu, and G.-k. Chang, “Fiber–wireless integrated mobile backhaul network based on a hybrid millimeter-wave and free-space-optics architecture with an adaptive diversity combining technique,” *Opt. Lett.*, vol. 41, no. 9, pp. 1909–1912, 2016.
- [9] LightPointe Communications, Inc. (1998). [Online]. Available: <http://http://www.lightpointe.com/>



- [10] S. Hranilovic, *Wireless Optical Communication Systems*. Springer, 2005.
- [11] The fSONA Networks, Inc. (2011). [Online]. Available: <http://www.fsona.com>
- [12] L. Andrews, R. Phillips, and C. Hopen, *Laser beam scintillation with applications*. SPIE press, 2001, vol. 99.
- [13] L. C. Andrews and R. L. Phillips, *Laser beam propagation through random media*. SPIE press Bellingham, WA, 2005, vol. 1.
- [14] R. Boluda-Ruiz, A. García-Zambrana, B. Castillo-Vázquez, and C. Castillo-Vázquez, “On the Effect of Correlated Sways on Generalized Misalignment Fading for Terrestrial FSO Links,” *Photonics Journal, IEEE*, vol. 9, no. 3, pp. 1–13, April 2017.
- [15] R. Boluda-Ruiz, A. García-Zambrana, C. del Castillo-Vázquez, B. del Castillo-Vázquez, and S. Hranilovic, “Outage Performance of Exponentiated Weibull FSO Links Under Generalized Pointing Errors,” *J. Lightwave Technol., IEEE/OSA*, vol. 35, no. 9, pp. 1605–1613, May 2017.
- [16] R. Boluda-Ruiz, A. García-Zambrana, C. Castillo-Vázquez, and B. Castillo-Vázquez, “Novel approximation of misalignment fading modeled by Beckmann distribution on free-space optical links,” *Opt. Express*, vol. 24, no. 20, pp. 22 635–22 649, Oct 2016.
- [17] R. Boluda-Ruiz, A. García-Zambrana, B. Castillo-Vázquez, and C. Castillo-Vázquez, “Impact of nonzero boresight pointing error on ergodic capacity of MIMO FSO communication systems,” *Opt. Express*, vol. 24, no. 4, pp. 3513–3534, Feb 2016.
- [18] —, “On the capacity of MISO FSO systems over gamma-gamma and misalignment fading channels,” *Opt. Express*, vol. 23, no. 17, pp. 22 371–22 385, Aug 2015.
- [19] —, “Ergodic capacity analysis for DF strategies in cooperative FSO systems,” *Opt. Express*, vol. 23, no. 17, pp. 21 565–21 584, Aug 2015.
- [20] R. Boluda-Ruiz, A. García-Zambrana, B. Castillo-Vázquez, and C. Castillo-Vázquez, “Ergodic Capacity Analysis of Decode-and-Forward Relay-Assisted FSO Systems over Alpha-Mu Fading Channels Considering Pointing Errors,” *Photonics Journal, IEEE*, vol. 8, no. 1, pp. 1–11, Feb 2016.
- [21] J. M. Kahn and J. R. Barry, “Wireless infrared communications,” *Proc. IEEE*, vol. 85, pp. 265–298, Feb. 1997.
- [22] S. Bloom, E. Korevaar, J. Schuster, and H. Willebrand, “Understanding the performance of free-space optics [invited],” *Journal of optical Networking*, vol. 2, no. 6, pp. 178–200, 2003.
- [23] L. F. Richardson, *Weather prediction by numerical process*. Cambridge University Press, 1922.

- [24] A. K. Majumdar and J. C. Ricklin, *Free-space laser communications: principles and advances*. Springer Science & Business Media, 2010, vol. 2.
- [25] H. Yuksel, S. Milner, and C. Davis, “Aperture averaging for optimizing receiver design and system performance on free-space optical communication links,” *Journal of Optical Networking*, vol. 4, no. 8, pp. 462–475, 2005.
- [26] L. C. Andrews, R. L. Phillips, C. Y. Hopen, and M. A. Al-Habash, “Theory of optical scintillation,” *J. Opt. Soc. Am. A*, vol. 16, no. 6, pp. 1417–1429, Jun 1999.
- [27] R. L. Phillips and L. C. Andrews, “Measured statistics of laser-light scattering in atmospheric turbulence,” *JOSA*, vol. 71, no. 12, pp. 1440–1445, 1981.
- [28] M. A. Al-Habash, L. C. Andrews, and R. L. Phillips, “Mathematical model for the irradiance probability density function of a laser beam propagating through turbulent media,” *Opt. Eng.*, vol. 40, p. 8, 2001.
- [29] E. Jakeman and P. Pusey, “A model for non-rayleigh sea echo,” *Transactions on antennas and propagation, IEEE*, vol. 24, no. 6, pp. 806–814, 1976.
- [30] —, “Significance of K distributions in scattering experiments,” *Physical Review Letters*, vol. 40, no. 9, p. 546, 1978.
- [31] L. Andrews and R. Phillips, “I-k distribution as a universal propagation model of laser beams in atmospheric turbulence,” *JOSA A*, vol. 2, no. 2, pp. 160–163, 1985.
- [32] J. H. Churnside and R. Hill, “Probability density of irradiance scintillations for strong path-integrated refractive turbulence,” *JOSA A*, vol. 4, no. 4, pp. 727–733, 1987.
- [33] J. H. Churnside and S. F. Clifford, “Log-normal rician probability-density function of optical scintillations in the turbulent atmosphere,” *JOSA A*, vol. 4, no. 10, pp. 1923–1930, 1987.
- [34] P. Beckmann, “Statistical distribution of the amplitude and phase of a multiply scattered field,” *J. Res. NBS D*, vol. 66, pp. 231–240, 1962.
- [35] F. S. Vetelino, C. Young, L. Andrews, and J. Rekolons, “Aperture averaging effects on the probability density of irradiance fluctuations in moderate-to-strong turbulence,” *Applied Optics*, vol. 46, no. 11, pp. 2099–2108, 2007.
- [36] S. D. Lyke, D. G. Voelz, and M. C. Roggemann, “Probability density of aperture-averaged irradiance fluctuations for long range free space optical communication links,” *Appl. Opt.*, vol. 48, no. 33, pp. 6511–6527, Nov 2009.
- [37] A. Jurado-Navas, J. M. Garrido-Balsells, J. F. Paris, and A. Puerta-Notario, “A unifying statistical model for atmospheric optical scintillation,” in *Numerical Simulations of Physical and Engineering Processes, Dr. J. Awrejcewicz(Ed.), Chapter 8*. Intech, 2011.



- [38] M. Kashani, M. Uysal, and M. Kavehrad, "A novel statistical model for turbulence-induced fading in free-space optical systems," in *Transparent Optical Networks (ICTON), 2013 15th International Conference on*. IEEE, 2013, pp. 1–5.
- [39] M. A. Kashani, M. Uysal, and M. Kavehrad, "On the performance of MIMO FSO communications over double generalized gamma fading channels," in *Communications (ICC), 2015 IEEE International Conference on*. IEEE, pp. 5144–5149, 2015.
- [40] R. Barrios and F. Dios, "Exponentiated weibull distribution family under aperture averaging for gaussian beam waves," *Opt. Express*, vol. 20, no. 12, pp. 13 055–13 064, 2012.
- [41] —, "Exponentiated weibull model for the irradiance probability density function of a laser beam propagating through atmospheric turbulence," *Optics & Laser Technology*, vol. 45, pp. 13–20, 2013.
- [42] H. Yura and T. Rose, "Exponentiated weibull distribution family under aperture averaging gaussian beam waves: comment," *Opt. Express*, vol. 20, no. 18, pp. 20 680–20 683, 2012.
- [43] R. Barrios and F. Dios, "Reply to comment on "the exponentiated weibull distribution family under aperture averaging for gaussian beam waves"," *Opt. Express*, vol. 20, no. 18, pp. 20 684–20 687, 2012.
- [44] X. Yi, Z. Liu, and P. Yue, "Average BER of free-space optical systems in turbulent atmosphere with exponentiated weibull distribution," *Opt. Letters*, vol. 37, no. 24, pp. 5142–5144, 2012.
- [45] P. Wang, L. Zhang, L. Guo, F. Huang, T. Shang, R. Wang, and Y. Yang, "Average BER of subcarrier intensity modulated free space optical systems over the exponentiated weibull fading channels," *Opt. Express*, vol. 22, no. 17, pp. 20 828–20 841, 2014.
- [46] M. Cheng, Y. Zhang, J. Gao, F. Wang, and F. Zhao, "Average capacity for optical wireless communication systems over exponentiated weibull distribution non-kolmogorov turbulent channels," *Applied Optics*, vol. 53, no. 18, pp. 4011–4017, 2014.
- [47] P. Wang, T. Cao, L. Guo, R. Wang, and Y. Yang, "Performance analysis of multi-hop parallel free-space optical systems over exponentiated weibull fading channels," *Photonics Journal, IEEE*, vol. 7, no. 1, pp. 1–17, Feb 2015.
- [48] P. Sharma, A. Bansal, P. Garg, T. Tsiftsis, and R. Barrios, "Performance of FSO links under exponentiated weibull turbulence fading with misalignment errors," in *Communications (ICC), 2015 IEEE International Conference on*. IEEE, pp. 5110–5114, 2015.



- [49] P. Wang, J. Zhang, L. Guo, T. Shang, T. Cao, R. Wang, and Y. Yang, "Performance analysis for relay-aided multihop BPPM FSO communication system over exponentiated weibull fading channels with pointing error impairments," *Photonics Journal, IEEE*, vol. 7, no. 4, pp. 1–20, Aug 2015.
- [50] X. Yi and M. Yao, "Free-space communications over exponentiated weibull turbulence channels with nonzero boresight pointing errors," *Opt. Express*, vol. 23, no. 3, pp. 2904–2917, 2015.
- [51] P. Wang, J. Qin, L. Guo, and Y. Yang, "Ber performance of FSO limited by shot and thermal noise over exponentiated weibull fading channels," *Photonics Technology Letters, IEEE*, vol. 28, no. 3, pp. 252–255, 2016.
- [52] I. I. Kim, B. McArthur, and E. J. Korevaar, "Comparison of laser beam propagation at 785 nm and 1550 nm in fog and haze for optical wireless communications," in *Information Technologies 2000* International Society for Optics and Photonics, pp. 26–37, 2001.
- [53] A. A. Farid and S. Hranilovic, "Outage capacity optimization for free-space optical links with pointing errors," *J. Lightwave Technol., IEEE/OSA*, vol. 25, no. 7, pp. 1702–1710, July 2007.
- [54] S. Arnon, "Effects of atmospheric turbulence and building sway on optical wireless-communication systems," *Opt. Letters*, vol. 28, no. 2, pp. 129–131, 2003.
- [55] D. K. Borah and D. G. Voelz, "Pointing error effects on free-space optical communication links in the presence of atmospheric turbulence," *J. Lightwave Technol., IEEE/OSA*, vol. 27, no. 18, pp. 3965–3973, 2009.
- [56] F. Yang, J. Cheng, and T. Tsiftsis, "Free-space optical communication with nonzero boresight pointing errors," *Transactions on Communications, IEEE*, vol. 62, no. 2, pp. 713–725, 2014.
- [57] H. G. Sandalidis, T. A. Tsiftsis, and G. K. Karagiannidis, "Optical wireless communications with heterodyne detection over turbulence channels with pointing errors," *J. Lightwave Technol., IEEE/OSA*, vol. 27, no. 20, pp. 4440–4445, 2009.
- [58] Wolfram Research, Inc. The Wolfram functions site. [Online]. Available: <http://functions.wolfram.com>
- [59] A. P. Prudnikov, Y. A. Brychkov, and O. I. Marichev, *Integrals and series Volume 3: More Special Functions*. Gordon and Breach Science Publishers, 1999, vol. 3.
- [60] Z. Wang and G. B. Giannakis, "A simple and general parameterization quantifying performance in fading channels," *Transactions on Communications, IEEE*, vol. 51, no. 8, pp. 1389–1398, 2003.

- [61] N. Wang and J. Cheng, "Moment-based estimation for the shape parameters of the gamma-gamma atmospheric turbulence model," *Opt. Express*, vol. 18, no. 12, pp. 12 824–12 831, Jun 2010.
- [62] I. S. Gradshteyn and I. M. Ryzhik, *Table of integrals, series and products*, 7th ed. Academic Press Inc., 2007.
- [63] C. E. Shannon, "A mathematical theory of communications," *Bell Sys. Tech. Journal*, vol. 27, pp. 379–423,623–656, 1948.
- [64] F. Yilmaz and M.-S. Alouini, "Novel asymptotic results on the high-order statistics of the channel capacity over generalized fading channels," in *Signal Processing Advances in Wireless Communications (SPAWC), 2012 IEEE 13th International Workshop on*. IEEE, pp. 389–393, 2012.
- [65] I. S. Ansari, F. Yilmaz, and M. S. Alouini, "Performance Analysis of FSO Links over Unified Gamma-Gamma Turbulence Channels," in *2015 IEEE 81st Vehicular Technology Conference (VTC Spring)*, pp. 1–5, May 2015.
- [66] M. C. Jeruchim, P. Balaban, and K. S. Shanmugan, *Simulation of communication systems*. Plenum Press, 1992.
- [67] H. E. Nistazakis, E. A. Karagianni, A. D. Tsigopoulos, M. E. Fafalios, and G. S. Tombras, "Average capacity of optical wireless communication systems over atmospheric turbulence channels," *J. of Lightwave Technol., IEEE/OSA*, vol. 27, no. 8, pp. 974–979, April 2009.
- [68] C. Liu, Y. Yao, Y. Sun, and X. Zhao, "Analysis of average capacity for free-space optical links with pointing errors over gamma-gamma turbulence channels," *Chinese Optics Letters*, vol. 8, no. 6, pp. 537–540, 2010.
- [69] J. M. Garrido-Balsells, A. Jurado-Navas, J. F. Paris, M. Castillo-Vázquez, and A. Puerta-Notario, "On the capacity of  $\mathcal{M}$ -distributed atmospheric optical channels," *Opt. Lett.*, vol. 38, no. 20, pp. 3984–3987, Oct 2013.
- [70] M. Z. Hassan, M. J. Hossain, and J. Cheng, "Ergodic capacity comparison of optical wireless communications using adaptive transmissions," *Opt. Express*, vol. 21, no. 17, pp. 20 346–20 362, Aug 2013.
- [71] F. Benkhelifa, Z. Rezki, and M. Alouini, "Low SNR capacity of FSO links over gamma-gamma atmospheric turbulence channels," *Communications Letters, IEEE*, vol. 17, no. 6, pp. 1264–1267, June 2013.
- [72] I. Ansari, M.-S. Alouini, and J. Cheng, "Ergodic capacity analysis of free-space optical links with nonzero boresight pointing errors," *Transactions on Wireless Communications, IEEE*, vol. 14, no. 8, pp. 4248–4264, Aug 2015.

- [73] M. K. Simon and M.-S. Alouini, *Digital communications over fading channels*, 2nd ed. New Jersey: Wiley-IEEE Press, 2005.
- [74] J. Anguita, I. Djordjevic, M. Neifeld, and B. Vasic, "Shannon capacities and error-correction codes for optical atmospheric turbulent channels," *J. Opt. Netw.*, vol. 4, no. 9, pp. 586–601, 2005.
- [75] M. Uysal, J. Li, and M. Yu, "Error rate performance analysis of coded free-space optical links over gamma-gamma atmospheric turbulence channels," *Transactions on Wireless Communications, IEEE*, vol. 5, no. 6, pp. 1229–1233, June 2006.
- [76] H. Sandalidis and T. Tsiftsis, "Outage probability and ergodic capacity of free-space optical links over strong turbulence," *Electronics Letters*, vol. 44, no. 1, pp. 46–47, 2008.
- [77] A. García-Zambrana, C. Castillo-Vázquez, and B. Castillo-Vázquez, "Space-time trellis coding with transmit laser selection for FSO links over strong atmospheric turbulence channels," *Opt. Express*, vol. 18, no. 6, pp. 5356–5366, 2010.
- [78] E. Biglieri, J. Proakis, and S. Shamai, "Fading channels: Information-theoretic and communications aspects," *Transactions on Information Theory, IEEE*, vol. 44, no. 6, pp. 2619–2692, 1998.
- [79] S. Z. Denic, I. Djordjevic, J. Anguita, B. Vasic, and M. A. Neifeld, "Information theoretic limits for free-space optical channels with and without memory," *J. of Lightwave Technol., IEEE/OSA*, vol. 26, no. 19, pp. 3376–3384, Oct. 2008.
- [80] A. Lapidoth, S. Moser, and M. Wigger, "On the capacity of free-space optical intensity channels," *Transactions on Information Theory, IEEE*, vol. 55, no. 10, pp. 4449–4461, Oct 2009.
- [81] D. A. Luong, T. C. Thang, and A. T. Pham, "Average capacity of MIMO/FSO systems with equal gain combining over log-normal channels," in *Ubiquitous and Future Networks (ICUFN), 2013 Fifth International Conference on.* IEEE, 2013, pp. 306–309.
- [82] P. Deng, M. Kavehrad, Z. Liu, Z. Zhou, and X. Yuan, "Capacity of MIMO free space optical communications using multiple partially coherent beams propagation through non-kolmogorov strong turbulence," *Opt. Express*, vol. 21, no. 13, pp. 15 213–15 229, Jul 2013.
- [83] D. A. Luong and A. T. Pham, "Average capacity of MIMO free-space optical gamma-gamma fading channel," in *Communications (ICC), 2014 IEEE International Conference on.* IEEE, 2014, pp. 3354–3358.

- [84] P. Kaur, V. K. Jain, and S. Kar, “Capacity of free space optical links with spatial diversity and aperture averaging,” in *Communications (QBSC), 27th Biennial Symposium on*. IEEE, pp. 14–18, 2014.
- [85] J. Zhang, L. Dai, Y. Han, Y. Zhang, and Z. Wang, “On the ergodic capacity of MIMO free-space optical systems over turbulence channels,” *Journal on Selected Areas in Communications, IEEE*, vol. 33, no. 9, pp. 1925–1934, Sept 2015.
- [86] N. D. Chatzidiamantis and G. K. Karagiannidis, “On the distribution of the sum of gamma-gamma variates and applications in rf and optical wireless communications,” *Transactions on Communications, IEEE*, vol. 59, no. 5, pp. 1298–1308, 2011.
- [87] M. D. Yacoub, “The  $\alpha$ - $\mu$  distribution: A general fading distribution,” in *Proc. IEEE International Symposium on Personal, Indoor and Mobile Radio Communications*, vol. 2, pp. 629–633, 2002.
- [88] K. P. Peppas, A. N. Stassinakis, H. E. Nistazakis, and G. S. Tombras, “Capacity analysis of dual amplify-and-forward relayed free-space optical communication systems over turbulence channels with pointing errors,” *Journal of Optical Communications and Networking*, vol. 5, no. 9, pp. 1032–1042, 2013.
- [89] L. Yang, X. Gao, and M.-S. Alouini, “Performance analysis of free-space optical communication systems with multiuser diversity over atmospheric turbulence channels,” *Photonics Journal, IEEE*, vol. 6, no. 2, April 2014.
- [90] S. Anees and M. R. Bhatnagar, “On the capacity of decode-and-forward dual-hop free space optical communication systems,” in *Wireless Communications and Networking Conference (WCNC), 2014 IEEE*. IEEE, pp. 18–23, 2014.
- [91] M. Aggarwal, P. Garg, and P. Puri, “Ergodic capacity of SIM based DF relayed optical wireless communication systems,” *Photonics Technology Letters, IEEE*, vol. 27, no. 10, pp. 1104–1107, 2015.
- [92] —, “Exact capacity of amplify-and-forward relayed optical wireless communication systems,” *Photonics Technology Letters, IEEE*, vol. 27, no. 8, pp. 903–906, 2015.
- [93] E. Zedini, I. S. Ansari, and M.-S. Alouini, “Performance analysis of mixed nakagami-and gamma-gamma dual-hop FSO transmission systems,” *Photonics Journal, IEEE*, vol. 7, no. 1, pp. 1–20, 2015.
- [94] J. A. Anguita, M. A. Neifeld, and B. V. Vasic, “Spatial correlation and irradiance statistics in a multiple-beam terrestrial free-space optical communication link,” *Appl. Opt.*, vol. 46, no. 26, pp. 6561–6571, Sep 2007.
- [95] J. A. Anguita and J. E. Cisternas, “Experimental evaluation of transmitter and receiver diversity in a terrestrial FSO link,” in *GLOBECOM Workshops (GC Wkshps), 2010 IEEE*. IEEE, pp. 1005–1009, 2010.

- [96] T. A. Tsiftsis, H. G. Sandalidis, G. K. Karagiannidis, and M. Uysal, "Optical wireless links with spatial diversity over strong atmospheric turbulence channels," *Transactions on Wireless Communications, IEEE*, vol. 8, no. 2, pp., 951–957, Feb. 2009.
- [97] E. Bayaki, R. Schober, and R. K. Mallik, "Performance analysis of MIMO free-space optical systems in gamma-gamma fading," *Transactions on Communications, IEEE*, vol. 57, no. 11, pp. 3415–3424, 2009.
- [98] J. Galambos and I. Simonelli, *Products of Random Variables: Applications to Problems of Physics and to Arithmetical Functions*. CRC Press, 2004.
- [99] F. Yilmaz and M.-S. Alouini, "Product of the powers of generalized nakagami-m variates and performance of cascaded fading channels," in *Global Telecommunications Conference, 2009. GLOBECOM 2009. IEEE*. IEEE, pp. 1–8, 2009.
- [100] A. A. Kilbas, *H-transforms: Theory and Applications*. CRC Press, 2004.
- [101] J.-Y. Wang, J.-B. Wang, M. Chen, Y. Tang, and Y. Zhang, "Outage analysis for relay-aided free-space optical communications over turbulence channels with nonzero boresight pointing errors," *Photonics Journal, IEEE*, vol. 6, no. 4, pp. 1–15, 2014.
- [102] S. M. Navidpour, M. Uysal, and M. Kavehrad, "Ber performance of free-space optical transmission with spatial diversity," *Transactions on Wireless Communications, IEEE*, vol. 6, no. 8, 2007.
- [103] E. J. Lee and V. W. S. Chan, "Part 1: optical communication over the clear turbulent atmospheric channel using diversity," *Journal on Selected Areas in Communications, IEEE*, vol. 22, no. 9, pp. 1896–1906, 2004.
- [104] Newport corporation. [Online]. Available: <http://www.newport.com>
- [105] G. K. Karagiannidis, T. A. Tsiftsis, and H. G. Sandalidis, "Outage probability of relayed free space optical communication systems," *Electronics Letters*, vol. 42, no. 17, pp. 994–995, August 17, 2006.
- [106] M. Safari and M. Uysal, "Relay-assisted free-space optical communication," *Transactions on Wireless Communications, IEEE*, vol. 7, no. 12, pp. 5441–5449, 2008.
- [107] C. Abou-Rjeily and A. Slim, "Cooperative diversity for free-space optical communications: transceiver design and performance analysis," *Transactions on Communications, IEEE*, vol. 59, no. 3, pp. 658–663, march 2011.
- [108] C. Abou-Rjeily, "Performance analysis of FSO communications with diversity methods: Add more relays or more apertures?" *Journal on Selected Areas in Communications, IEEE*, vol. 33, no. 9, pp. 1890–1902, 2015.



- [109] R. Boluda-Ruiz, A. García-Zambrana, B. Castillo-Vázquez, and C. Castillo-Vázquez, “MISO relay-assisted FSO systems over gamma-gamma fading channels with pointing errors,” *Photonics Technology Letters, IEEE*, vol. 28, no. 3, pp. 229–232, Feb 2016.
- [110] M. Dohler and Y. Li, *Cooperative communications: hardware, channel and PHY*. John Wiley & Sons, 2010.
- [111] A. Sendonaris, E. Erkip, and B. Aazhang, “User cooperation diversity. Part I: System description,” *Transactions on Communications, IEEE*, vol. 51, no. 11, pp. 1927–1938, nov. 2003.
- [112] —, “User cooperation diversity. Part II: Implementation aspects and performance analysis,” *Transactions on Communications, IEEE*, vol. 51, no. 11, pp. 1939 – 1948, nov. 2003.
- [113] J. Laneman, D. Tse, and G. Wornell, “Cooperative diversity in wireless networks: Efficient protocols and outage behavior,” *Transactions on Information Theory, IEEE*, vol. 50, no. 12, pp. 3062 – 3080, dec. 2004.
- [114] M. Karimi and M. Nasiri-Kenari, “BER analysis of cooperative systems in free-space optical networks,” *J. Lightwave Technol., IEEE/OSA*, vol. 27, no. 24, pp. 5639 –5647, dec.15, 2009.
- [115] —, “Outage analysis of relay-assisted free-space optical communications,” *IET Communications*, vol. 4, no. 12, pp. 1423 –1432, 2010.
- [116] M. Bhatnagar, “Performance analysis of decode-and-forward relaying in gamma-gamma fading channels,” *Photonics Technology Letters, IEEE*, vol. 24, no. 7, pp. 545 –547, april, 2012.
- [117] A. Garcia-Zambrana, C. Castillo-Vazquez, B. Castillo-Vazquez, and R. Boluda-Ruiz, “Bit detect and forward relaying for FSO links using equal gain combining over gamma-gamma atmospheric turbulence channels with pointing errors,” *Opt. Express*, vol. 20, no. 15, pp. 16 394–16 409, Jul 2012.
- [118] N. D. Chatzidiamantis, D. S. Michalopoulos, E. E. Kriezis, G. K. Karagiannidis, and R. Schober, “Relay selection protocols for relay-assisted free-space optical systems,” *Journal of Optical Communications and Networking*, vol. 5, no. 1, pp. 92–103, 2013.
- [119] M. A. Kashani, M. Safari, and M. Uysal, “Optimal relay placement and diversity analysis of relay-assisted free-space optical communication systems,” *Journal of Optical Communications and Networking*, vol. 5, no. 1, pp. 37–47, 2013.
- [120] C. Abou-Rjeily, “Performance analysis of selective relaying in cooperative free-space optical systems,” *J. Lightwave Technol., IEEE/OSA*, vol. 31, no. 18, pp. 2965–2973, 2013.

- [121] ———, “Achievable diversity orders of decode-and-forward cooperative protocols over gamma-gamma fading fso links,” *Transactions on Communications, IEEE*, vol. 61, no. 9, pp. 3919–3930, September 2013.
- [122] ———, “All-active and selective FSO relaying: Do we need inter-relay cooperation?” *J. of Lightwave Technol., IEEE/OSA*, vol. 32, no. 10, pp. 1899–1906, 2014.
- [123] P. K. Sharma, A. Bansal, and P. Garg, “Relay assisted Bi-directional communication in generalized turbulence fading,” *J. of Lightwave Technol., IEEE/OSA*, vol. 33, no. 1, pp. 133–139, 2015.
- [124] R. Boluda-Ruiz, A. García-Zambrana, B. Castillo-Vázquez, and C. Castillo-Vázquez, “Impact of relay placement on diversity order in adaptive selective df relay-assisted FSO communications,” *Opt. Express*, vol. 23, no. 3, pp. 2600–2617, 2015.
- [125] C. del Castillo-Vazquez, R. Boluda-Ruiz, B. del Castillo-Vazquez, and A. Garcia-Zambrana, “Outage performance of DF relay-assisted FSO communications using time-diversity,” *Photonics Technology Letters, IEEE*, vol. 27, no. 11, pp. 1149–1152, 2015.
- [126] S. I. Hussain, M. M. Abdallah, and K. A. Qaraqe, “Power optimization and kth-order selective relaying in free space optical networks,” in *GCC Conference and Exhibition (GCC), 2013 7th IEEE*. IEEE, pp. 330–333, 2013.
- [127] M. R. Bhatnagar, “Average BER analysis of relay selection based decode-and-forward cooperative communication over gamma-gamma fading FSO links,” in *Communications (ICC), 2013 IEEE International Conference on*. IEEE, pp. 3142–3147, 2013.
- [128] N. Letzepis and A. Guillen i Fabregas, “Outage probability of the Gaussian MIMO free-space optical channel with PPM,” *Transactions on Communications, IEEE*, vol. 57, no. 12, pp. 3682–3690, 2009.
- [129] I. B. Djordjevic and G. T. Djordjevic, “On the communication over strong atmospheric turbulence channels by adaptive modulation and coding,” *Opt. Express*, vol. 17, no. 20, pp. 18 250–18 262, 2009.
- [130] I. S. Ansari, S. Al-Ahmadi, F. Yilmaz, M.-S. Alouini, and H. Yanikomeroglu, “A new formula for the BER of binary modulations with dual-branch selection over generalized-K,” *Transactions on Communications, IEEE*, vol. 59, no. 10, pp. 2654–2658, 2011.
- [131] K. P. Peppas, “A new formula for the average bit error probability of dual-hop amplify-and-forward relaying systems over generalized shadowed fading channels,” *Wireless Communications Letters, IEEE*, vol. 1, no. 2, pp. 85–88, 2012.

- [132] W. Gappmair, S. Hranilovic, and E. Leitgeb, "OOK performance for terrestrial FSO links in turbulent atmosphere with pointing errors modeled by Hoyt distributions," *Communications Letters, IEEE*, vol. 15, no. 8, pp. 875–877, 2011.
- [133] H. AlQuwaiee, H. C. Yang, and M. Alouini, "On the asymptotic capacity of dual-aperture FSO systems with a generalized pointing error model," *Transactions on Wireless Communications, IEEE*, vol. PP, no. 99, pp. 1–1, 2016.
- [134] I. I. Kim, R. Stieger, J. A. Koontz, C. Moursund, M. Barclay, P. Adhikari, J. Schuster, E. Korevaar, R. Ruigrok, and C. DeCusatis, "Wireless optical transmission of fast ethernet, FDDI, ATM, and ESCON protocol data using the terralink laser communication system," *Optical Engineering*, vol. 37, no. 12, pp. 3143–3155, 1998.
- [135] L. C. Andrews, R. L. Phillips, and C. Y. Hopen, "Aperture averaging of optical scintillations: power fluctuations and the temporal spectrum," *Waves in Random Media*, vol. 10, no. 1, pp. 53–70, 2000.
- [136] M.-A. Khalighi, N. Schwartz, N. Aitamer, and S. Bourennane, "Fading reduction by aperture averaging and spatial diversity in optical wireless systems," *Journal of Optical Communications and Networking*, vol. 1, no. 6, pp. 580–593, 2009.
- [137] A. García-Zambrana, B. Castillo-Vázquez, and C. Castillo-Vázquez, "Asymptotic error-rate analysis of FSO links using transmit laser selection over gamma-gamma atmospheric turbulence channels with pointing errors," *Opt. Express*, vol. 19, no. 24, p. in press, Nov 2011.
- [138] A. García-Zambrana, R. Boluda-Ruiz, C. Castillo-Vázquez, and B. Castillo-Vázquez, "Novel space-time trellis codes for free-space optical communications using transmit laser selection," *Opt. Express*, vol. 23, no. 19, pp. 24 195–24 211, Sep 2015.
- [139] S. C. Schwartz and Y.-S. Yeh, "On the distribution function and moments of power sums with log-normal components," *Bell System Technical Journal*, vol. 61, no. 7, pp. 1441–1462, 1982.
- [140] N. B. Mehta, J. Wu, A. F. Molisch, and J. Zhang, "Approximating a sum of random variables with a lognormal," *Transactions on Wireless Communications, IEEE*, vol. 6, no. 7, pp. 2690–2699, 2007.
- [141] X. Liu, "Optimisation of satellite optical transmission with correlated sways," *IET Communications*, vol. 5, no. 8, pp. 1107–1112, 2011.
- [142] —, "Performance analysis of a multiple-input-single-output optical satellite communication system with correlated pointing errors," *IET Communications*, vol. 6, no. 15, pp. 2503–2511, 2012.



- [143] A. García-Zambrana, R. Boluda-Ruiz, C. Castillo-Vázquez, and B. Castillo-Vázquez, “Transmit alternate laser selection with time diversity for FSO communications,” *Opt. Express*, vol. 22, no. 20, pp. 23 861–23 874, 2014.
- [144] S. Nadarajah and A. K. Gupta, “On the moments of the exponentiated weibull distribution,” *Communications in Statistics-Theory and Methods*, vol. 34, no. 2, pp. 253–256, 2005.